



International
Biotechnology Congress

StartHUB

BIOSphere

9 - 11 September 2021

ABSTRACT BOOK



www.bioturkiye.org

OP-01

Construction of Anti-SARS-CoV-2 Phage Displayed Mouse ScFv Library From Hybridoma cells

Kübra Bilgiç^{1,2}, Oya Arı Uyar², Gamze Kılıç^{1,2}, Esin Akçael², Fatıma Yücel², Şaban Tekin^{2,3}, Aylin Özdemir Bahadır², Bertan Koray Balcıoğlu²

¹Gebze Technical University, Department of Molecular Biology and Genetics, Gebze, Kocaeli, Turkey

²TUBITAK Marmara Research Center (MAM), Genetic Engineering and Biotechnology Institute, Gebze, Kocaeli, Turkey

³University of Health Sciences, Department of Basic Medical Sciences, Istanbul, Turkey

Abstract

The new type of coronavirus SARS-CoV-2 is an arising pathogen that was first described in late December 2019. The outbreak of the novel coronavirus disease (COVID-19) in China rapidly spread worldwide causing serious respiratory infection in humans. Some of the existing drugs used in the treatment of SARS-COV-2 do not benefit, while others may be harmful. To date, no monoclonal antibodies, or peptides have been approved for the treatment of infections from coronavirus. Vaccination may provide a powerful and sustainable protection, however, development of vaccines is a long and challenging process, and vaccination is only useful in a preventive environment. However, immunotherapy is an effective method for treatment viral infections such as SARS-CoV. Phage display technology is a powerful in vitro selection technique that allows the rapid selection of recombinant antibodies with high affinity to the target antigen.

This study aims to obtain mouse single chain variable fragment (scFv) antibody candidates that specifically bind and potentially neutralize the SARS-CoV-2 Spike1 antigen by phage display technology.

For that purpose, polyclonal hybridoma cells developed from mice immunized with S antigen, were used as starting material. Total RNA from hybridoma cells was extracted and cDNA synthesis was performed. The mouse antibody variable region library and the scFv library was generated by PCR. The scFv library was then cloned into pCANTAB phagemid vector and transferred into *E.coli* TG1 strain. Transformed phagemid vector library was rescued with M13K07 helper phage. After two cycles of biopanning, colonies were picked and the diversity of the generated scFv were examined by PCR based DNA fingerprinting analysis.

In conclusion here we describe a fast an effective method for the construction of phage display mouse scFv library using polyclonal hybridoma cells. The use of polyclonal hybridoma cells increased the diversity of the generated scFv library derived from the mouse antibody heavy and light chain variable regions. Therefore, this diversity might increase the probability of obtaining neutralizing antibodies.

Keywords: SARS-CoV-2, Phage Display, scFv library, polyclonal hybridoma cells, Immunotherapy

Introduction

The outbreak of the novel coronavirus disease that caused acute infectious pneumonia in China spread worldwide, comes to be an urgently international concern (AminJafari & Ghasemi, 2020)(Zhai et al., 2020). There is no available approved specific treatment for COVID-19 (Ko et al., 2020). Immunotherapy (vaccines and monoclonal antibodies, mAbs) is an effective method for the treatment of viral infections such as SARS-CoV and MERS-CoV.(AminJafari & Ghasemi, 2020). Antibody therapy has taken over, during the past three decades, delivering a dramatic breakthroughs for the treatment of many diseases, particularly in oncology (Carter & Lazar, 2018) Scholler, 2010)(Erdag et al., 2011) and antitoxin treatment (Stanker et al., 2008)(Miethe et al., 2015). Antigen-binding fragments such as Fab (fragment antigen binding), scFv (single-chain variable fragment), nanobodies (VH/VL) have emerged as reliable alternatives to monoclonal antibodies (mAb) in many applications. (Vermeulen et al., 2018).

These recombinant antibody fragments (rAbFs) retain the target specificity and affinity of all mAbs. Phage display technology was first revealed in 1985 by Smith, who successfully incorporated foreign DNA into the M13 phage genome and expressed the foreign antigen as a fusion protein with the pIII coat protein of the M13 phage (Smith, 1985). The greatest advantage of phage display is based on the phenotype-genotype linkage of the relevant protein displayed on the phage surface with the encoding DNA packed in the phage particle. This allows selective enrichment of a library pools and efficient screening of the resulting clones (L. Sheng, M. Christopher, 2016). Since the COVID-19 outbreak was revealed in December 2019, phage display technology has been broadly used for the development of neutralizing antibodies. Many antibody libraries, immune, naive, synthetic human /mouse, have been screened for spike protein and receptor-binding domain (RBD), which play a role especially in the infection of the SARS-CoV-2 virus (Balcioglu et al., 2020). Some of the existing drugs used in the treatment of SARS-COV-2 do not present a great benefit, while others may be harmful. In this context, effective interventions for COVID-19 cases are urgently needed. This study aims to obtain mouse scFv antibody candidates that specifically bind and potentially neutralize SARS-CoV-2 Spike1 antigen with the use of phage display technology.

Material and Methods

Hybridoma polyclone cells from mice immunized against S antigen (TÜBİTAK-HADYEK ethics committee report no: 16563500-111-64). were collected and treated with TRI Reagent (Zymo, USA), total RNA was extracted with the Direct-zol RNA Miniprep Plus Kit (Zymo, USA). cDNA was generated from 1-5 µg of total RNA, using SuperScript III First-Strand Synthesis System for RT-PCR (Invitrogen, USA) 20µM random hexamer primer. The mouse antibody variable genes library was constructed by PCR with sets of specific primers (Zhou et al., 1994).

Variable heavy (VH), variable light kappa (VLk) and lambda (VLl) chain encoding genes were amplified by PCR. The PCR reactions were purified with Wizard® SV Gel and PCR Clean-Up System (Promega, USA), and used as a template for the generation of scFv. Therefore, the immune mouse antibody heavy and light chain and mouse scFv antibody libraries were

obtained. The generation of the scFv was performed in two steps. In the first step, 5 μ L Taq polymerase buffer (5 \times), 1 μ L MgCl₂ (25 mM), 0,5 μ L dNTP(10 mM), 300 ng VH PCR product, 300 ng VL PCR product, 75 ng linker primer and 0,25 μ L Taq polymerase (1 U) (Promega, USA) were combined in a 25 μ L reaction volume. The reaction was completed after eight cycles of a 1 min at 94° C and a 6 min at 63° C cycle. ScFv amplification reaction mix (3 μ L) was added to the second PCR reaction. The second PCR reaction was done as following, 30 cycles of a cycle of 94° C for 1 min, 55° C for 2 min, 72° C for 2 min.

The scFv library and the phagemid vector pCANTAB6 were digested with SfiI (New England Biolabs, USA) and NotI HF (New England Biolabs, USA) restriction enzymes. Digested and purified scFv library was ligated into pCANTAB6 vector with T4 DNA ligase (New England Biolabs, USA). The transformation was performed into *E.coli* TG1 strain by Calcium Chloride method. The transformed phagemid vector library was rescued with 10¹⁰ pfu M13K07 helper phage (New England Biolabs, USA) for selection and biopanning steps.

The scFv library was screened against SARS-COV-2 S1 antigen with two biopanning cycles. Randomly selected colonies from the 1st and 2nd biopanning cycles were examined by colony PCR. DNA fingerprinting with BstNI enzyme (NEB, USA) digestion was done to determine the sequence diversity of the clones.

Results and Discussion

In this work, antibodies heavy and light chain libraries were obtained from a mouse immunized against pandemic SARS-CoV-2 S1 antigen. Further, a scFv library was generated from the VH and VL libraries. Briefly total RNA was isolated from hybridoma polyclonal cells and transformed into cDNA. VH (400 bp) and VK/VL (350 bp) encoding genes were amplified by PCR from the cDNA template (**Figure 1**). The primers sets corresponding to the allelic variants of the light and heavy chains were selected from Zhou studies (Zhou et al., 1994). Then degenerated primer sets were created to reduce the PCR reaction number. The PCR products were then agarose gel purified and used for the generation of the scFv library.

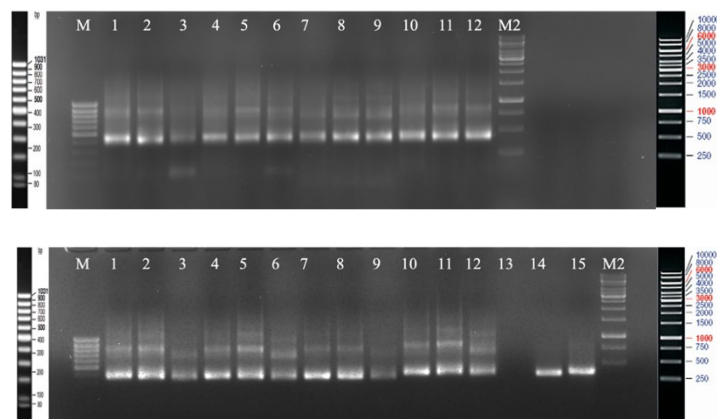


Figure 1. Generation of VH and VL libraries from anti-SARS-CoV-2 spike1 hybridoma cells. M1: MassRuler Low Range DNA Ladder, M2: 1 kb DNA Ladder (ThermoFisher Scientific,USA). **A.** VH PCR bands (400 bp), lane 1-3: MHV.For1- MHV.Back (1-3), lane 4-6: MHV.For2-MHV.Back(1-3), lane 7-9: MHV.For3-MHV.Back(1-3), lane 10-12: MHV.For4- MHV.Back(1-3). **B.** VL PCR bands (350 bp), lane 1-3: MKV.For1- MKV.Back

(1-3), lane 4-6: MKV.For2-MKV.Back(1-3), lane 7-9 : MKV.For3-MKV.Back(1-3), lane 10-12: MKC5For- MKV.Back(1-3), lane 14: MLV For1-MLV Back, lane 15: MLV For2-MLV Back.

A scFv is composed of one VH and one VL region fused together via a linker of 15 amino acids. For the production of the scFv library, a two-steps PCR reaction was done. The first one connects all the three genes to each other and the second one amplifies the generated scFv gene. The scFv was designed according to VH-Linker-VL structure. The assembly of the scFv fragments was checked with agarose gel electrophoresis. After several optimization steps regarding primers annealing temperature and the PCR cycles, a scFv library was obtained (**Figure 2**).

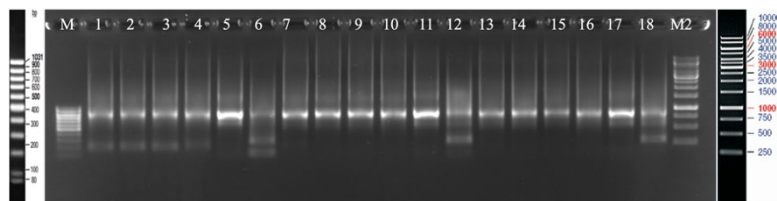


Figure 2. PCR amplifications the scFv constructs (750 bp), lane 1-6: MHV.Back1-MHV/MLV For (1-6), lane 7-12: MHV.Back2-MHV/MLV For(1-6), lane 12-18: MHV.Back3-MHV/MLV For (1-6).

The scFv library obtained from different allelic variants was mixed then digested with appropriate restriction enzymes. After the digestion process, the scFv library was inserted into the pCANTAB6 phagemid vector with T4 DNA ligase. The vector was then transferred into TG1 cells and phage displayed library was rescued with M13K07 helper phage. After two biopanning cycle against the SARS-COV-2 S1 antigen an enrichment of S1 binding phages was observed between the 1. and 2. biopanning steps (**Table 1**).

Table 1. Enrichment of SARS-CoV-2 S protein binding phages for each biopanning cycles

	Antigen	Phage input	Phage output	Output / input ratio
Cycle 1	5 µg	1 x 10 ¹¹ pfu	2,6 x 10 ⁴ pfu	2,6 x 10 ⁷
Cycle 2	2 µg	1 x 10 ¹¹ pfu	4,5 x 10 ⁴ pfu	4,5 x 10 ⁷

Randomly selected colonies from the 1st and 2nd biopanning cycle were examined by colony PCR for the presence of scFv. An amplicon of ~1100bp was observed with the use of primers specific to the vector (**Figure 3**). The DNA fingerprinting of the PCR amplicons with BstNI restriction enzyme digestion (**Figure 4**) revealed at least three different scFv clones.

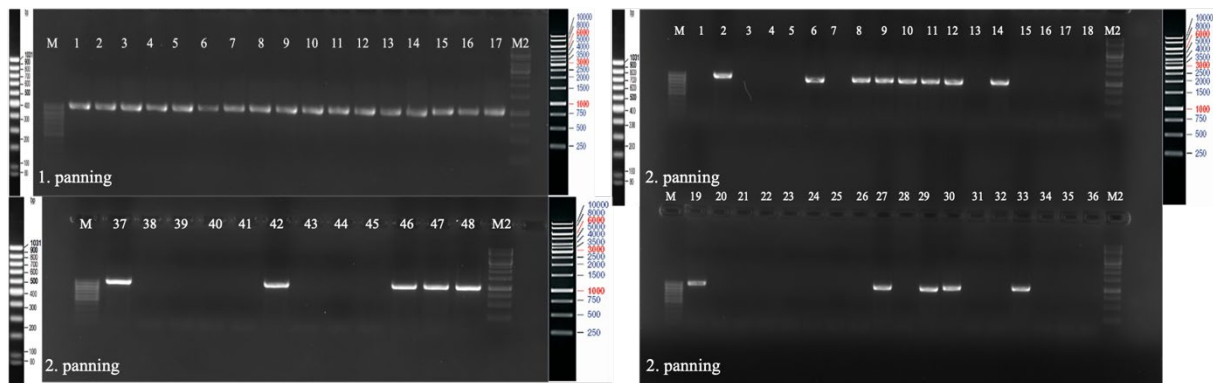


Figure 3. Colony PCR of selected colonies from 1st and 2nd round of biopanning. Markers are MassRuler Low Range DNA Ladder cat.SM0383 and 1kb DNA Ladder (ThermoFisher Scientific,USA), respectively.

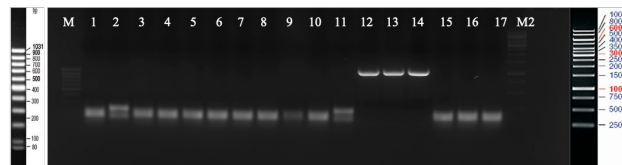


Figure 4. BstNI digestion analysis of selected colonies after 2nd round of biopanning. Markers are MassRuler Low Range DNA Ladder cat.SM0383 and 1kb DNA Ladder (ThermoFisher Scientific,USA), respectively.

Conclusion

Here we described the construction of a phage display mouse scFv library using hybridoma polyclonal cells derived from mice immunized with the SARS-CoV-2 S1 antigen. The use of polyclonal hybridoma cells in the study increased the chance of obtaining neutralizing antibodies by increasing the combinatorial variability of the generated scFv library. In this context, an effective method was achieved by combining hybridoma and phage display technologies.

Acknowledgments

This work was initiated with the support of the Scientific and Technological Research Council of Turkey (TÜBİTAK Grant T1004-18AG020).

References

- AminJafari, A., & Ghasemi, S. (2020). The possible of immunotherapy for COVID-19: A systematic review. *International Immunopharmacology*, 83(March), 106455. <https://doi.org/10.1016/j.intimp.2020.106455>
- Balcioğlu, B. K., Denizci Öncü, M., Öztürk, H. Ü., Yücel, F., Kaya, F., Serhatli, M., Ülbeği Polat, H., Tekin, Ş., & Özdemir Bahadır, A. (2020). SARS-CoV-2 neutralizing antibody development strategies. *Turkish Journal of Biology*, 44(Special issue 1), 203–214. <https://doi.org/10.3906/biy-2005-91>

- Carter, P. J., & Lazar, G. A. (2018). Next generation antibody drugs: Pursuit of the “high-hanging fruit.” *Nature Reviews Drug Discovery*, 17(3), 197–223.
<https://doi.org/10.1038/nrd.2017.227>
- Erdag, B., Koray Balcioglu, B., Ozdemir Bahadir, A., Serhatli, M., Kacar, O., Bahar, A., Seker, U. O. S., Akgun, E., Ozkan, A., Kilic, T., Tamerler, C., & Baysal, K. (2011). Identification of novel neutralizing single-chain antibodies against vascular endothelial growth factor receptor 2. *Biotechnology and Applied Biochemistry*, 58(6), 412–422.
<https://doi.org/10.1002/bab.61>
- Kazemi-Lomedasht, F., Yamabhai, M., Sabatier, J. M., Behdani, M., Zareinejad, M. R., & Shahbazzadeh, D. (2019). Development of a human scFv antibody targeting the lethal Iranian cobra (*Naja oxiana*) snake venom. *Toxicon*, 171(October), 78–85.
<https://doi.org/10.1016/j.toxicon.2019.10.006>
- Ko, W., Rolain, J., Lee, N., Chen, P., & Huang, C. (2020). *Since January 2020 Elsevier has created a COVID-19 resource centre with free information in English and Mandarin on the novel coronavirus COVID- 19 . The COVID-19 resource centre is hosted on Elsevier Connect , the company ’ s public news and information . January.*
- L. Sheng, M. Christopher, A. M. (2016). Protein and Antibody Engineering by Phage Display. *Physiology & Behavior*, 176(1), 100–106.
<https://doi.org/10.1016/j.gde.2016.03.011>
- Meulenberg, E. P. (2012). Antibodies Applications and New Developments. In E. P. Meulenberg (Ed.), *Antibodies Applications and New Development*. BENTHAM SCIENCE PUBLISHERS. <https://doi.org/10.2174/97816080526461120101>
- Miethe, S., Rasetti-Escargueil, C., Avril, A., Liu, Y., Chahboun, S., Korkeala, H., Mazuet, C., Popoff, M. R., Pelat, T., Thullier, P., Sesardic, D., & Hust, M. (2015). Development of human-like scFv-Fc neutralizing botulinum neurotoxin E. *PLoS ONE*, 10(10), 1–20.
<https://doi.org/10.1371/journal.pone.0139905>
- Scholler, N. (2010). Novel targeting strategies using recombinant antibodies for early diagnosis and therapy of ovarian cancer. *Therapy*, 7(3), 209–212.
<https://doi.org/10.2217/thy.10.19>
- Smith, G. P. (1985). Filamentous Fusion Phage : Novel Expression Vectors that Display Cloned Antigens on the Virion Surface Author (s): George P . Smith Reviewed work (s): Source : Science , New Series , Vol . 228 , No . 4705 (Jun . 14 , 1985), pp . 1315-1317 Published. *Science (New York, N.Y.)*, 228(4705), 1315–1317.
- Stanker, L. H., Merrill, P., Scotcher, M. C., & Cheng, L. W. (2008). Development and partial characterization of high-affinity monoclonal antibodies for botulinum toxin type A and their use in analysis of milk by sandwich ELISA. *Journal of Immunological Methods*, 336(1), 1–8. <https://doi.org/10.1016/j.jim.2008.03.003>
- Vermeulen, J. G., Burt, F., van Heerden, E., Cason, E., & Meiring, M. (2018). Evaluation of in vitro refolding vs cold shock expression: Production of a low yielding single chain variable fragment. *Protein Expression and Purification*, 151(June), 62–71.
<https://doi.org/10.1016/j.pep.2018.06.005>
- Zhai, P., Ding, Y., Wu, X., Long, J., Zhong, Y., & Li, Y. (2020). The epidemiology, diagnosis and treatment of COVID-19. *International Journal of Antimicrobial Agents*, 55(5).
<https://doi.org/10.1016/j.ijantimicag.2020.105955>
- Zhou, H., Fisher, R. J., Papasl, T. S., Biochemistry, C., & Dyncorp, P. R. I. (1994). Optimization of primer sequences for repertoire display library construction mouse scFv We thank the Advanced Scientific Computing Laboratory at. *Nucleic Acid Research*, 22(5), 1993–1994.

Genome analysis of a new potential probiotic strain *Lactiplantibacillus plantarum* DY46 isolated from fermented turnip

Fatih ORTAKCI¹, Ahmet E. YETİMAN², Seyfullah Enes KOTİL³

¹Abdullah Gül University, Faculty of Engineering, Nanotechnology Engineering, Kayseri, Turkey

²Erciyes University, Faculty of Engineering, Food Engineering Department, Kayseri, Turkey

³Department of Biophysics, Bahcesehir University Medical School, Kadikoy, Istanbul, Turkey

INTRODUCTION: *Lactiplantibacillus plantarum* is widely used as probiotic culture in dairy food applications such as milk, yogurt, yogurt drink etc. A new *Lb. plantarum* strain DY46 was isolated from a traditionally fermented liquid product called shalgam from the Southern region of Anatolia following incubation on MRS agar at 30°C for 5 days. **RESULTS:** DY46 is gram positive, short rod and catalase negative. This bacterium fermented 22 of the 50 substrates tested on API CH50 fermentation panels. To learn more about the metabolic capabilities of DY46, whole genome sequencing was performed using Illumina Miseq platform. The sequences were assembled into a 3.32 Mb draft genome using PATRIC 3.6.8. (<https://patricbrc.org/app/Assembly2>) consisting of 153 contigs, and preliminary genome annotation was performed using the RAST algorithm (rast.nmpdr.org). The DY46 genome consists of a single circular chromosome of 3,332,827 bp that is predicted to carry 3219 genes, including 61 tRNA genes, 2 rRNA operons. The genome has a GC content of 44.3% includes 98 predicted pseudogenes, 25 complete or partial transposases and 3 intact prophages. DY46 genome also predicted to carry genes of PlantaricinE, PlantaricinF and PlantaricinK showing antimicrobial potential of this bacterium which can be linked to in vitro antagonism tests that DY46 can inhibit dairy food pathogens of *Bacillus cereus* ATCC 33019, *Escherichia coli* ATCC 25922. Acid and bile tolerance of DY46 revealed this strain could potentially pass thru the stomach and reach into gut for providing probiotic therapeutic affects to health.

Keywords: Probiotic, fermented turnip, genome, antimicrobial

OP-03

Investigation of Protective and/or Therapeutic Effects of Cynara Scolymus Leaf on Diethylnitrosamine-Induced Cognitive Impairment Using Biochemical and Spatial Learning Data

Yesim Yeni¹, Sidika Genc¹, Betul Cicek², Mehmet Kuzucu³, Ahmet Cetin³, Muhammed Sait Ertugrul⁴, Ufuk Okay¹, Ahmet Hacimuftuoglu¹

¹Ataturk University, Faculty of Medicine, Department of Medical Pharmacology, Erzurum, Turkey

²Erzincan Binali Yildirim University, Faculty of Medicine, Department of Physiology, Erzincan, Turkey

³Department of Biology, Erzincan Binali Yildirim University, Faculty of Arts and Sciences, Erzincan, Turkey

⁴Agri Ibrahim Cecen University, Faculty of Pharmacy, Department of Pharmacology, Agri, Turkey

Abstract

The aim of the study was to determine the possible protective and/or therapeutic effects of Cynara scolymus leaf extract on diethylnitrosamine-induced cognitive impairment and oxidative damage in mice using learning measurement and biochemical approaches. 32 adult male BALB/c mice were divided into 4 groups with 8 mice in each group. Groups were formed as control, diethylnitrosamine, Cynara scolymus 0.8 and 1.6 g/mg. The treatment drug was administered by gavage for 15 days after administration of diethylnitrosamine. Diethylnitrosamine was administered to mice three times as a single dose intraperitoneally at a dose of 100 mg/kg body weight. After treatment, mice were subjected to the Morris water maze test. After the test, the mice were sacrificed and blood samples were taken. Glutathione reductase and lactate dehydrogenase levels in serum samples were determined by spectrophotometric methods. According to the data obtained, a decrease in glutathione reductase level was observed in the diethylnitrosamine group compared to the control, while it caused an increase in lactate dehydrogenase. In addition, learning and memory were found to be statistically significantly impaired in the Morris water maze test. We found that learning and memory improved, glutathione reductase level increased, lactate dehydrogenase decreased and approached the control group in a dose-dependent manner in the groups treated with Cynara scolymus. Considering the results of our study, it shows that Cynara scolymus may help prevent the development of cognitive impairment. In addition, based on its biochemical results, it shows that the therapeutic effect of Cynara scolymus is due to its antioxidant effect.

Keywords: Cynara scolymus, diethylnitrosamine, morris water maze.

Introduction

Nitrosamines and nitroso compounds are some of the most important chemicals and adversely affect human health. The dose, method of administration and frequency of exposure of these compounds may affect different organs, leading to tumorigenesis [1, 2]. Especially diethylnitrosamine (DEN) is a carcinogen that is widely used in experimental animal models. After DEN is administered to the body, it is hydroxylated by cytochrome P-450 isoenzymes in the liver and becomes bioactive by the alkylation mechanism [3]. Thus, DEN increases reactive oxygen species (ROS) and causes cell damage and oxidative stress [4, 5]. Increased intracellular ROS levels lead to mitochondrial damage, DNA modification and lipid peroxidation, causing

many diseases including cancer [4, 6]. There is empirical evidence that high doses of DEN cause cancer, while low doses cause cognitive impairment [7, 8, 9].

Many plants, vegetables and fruits naturally contain flavonoids, a group of compounds with various biological activities such as anti-oxidation, anti-inflammation, anti-bacterial, anti-viral and anti-cancer [10]. Artichoke *Cynara scolymus* L. from the Asteraceae family is a well-known staple food for the Mediterranean population [11, 12]. Today, it is widely cultivated all over the world. Artichoke heads and leaves contain bioactive components, monocaffeoylquinic and dicaffeoylquinic acids, and polyphenolic compounds such as flavonoids [13]. This vegetable is prepared for various products such as salads, jams, preserves, and its leaves are widely used for medicinal purposes. In previous studies, it has been shown that extracts obtained from artichoke flower leaves have antioxidant, anti-hypercholesterolemic, choleric, hypoglycemic, hepatoprotective, anti-cancer and anti-microbial effects [13, 14, 15].

The aim of the study was to determine the possible protective and/or therapeutic effects of *Cynara scolymus* L. extract on DEN-induced cognitive impairment and oxidative damage using learning measurement and biochemical approaches in mice.

Materials and Methods

Animals and experimental groups

A total of 32 adult male BALB/c mice 8 weeks old were obtained from Atatürk University Medical Experimental Application and Research Center. The experimental applications were conducted conveniently with the conditions for the care and use of laboratory animals (12 hours light; 12 hours darkness; $24\pm 1^\circ\text{C}$ humidity; $50 \pm 20\%$). During the experimental applications, the mice were provided the commercial feed and tap water ad libitum. The animals were randomly divided into four experimental groups, including eight mice in each. These groups were arranged as follows: control group (not treated), DEN group (a single dose of DEN was administered), CSL 0.8 and 1.6 g/kg groups (CSL doses were administered by gavage for 15 days after DEN was administered). CSL and DEN were dissolved in serum physiological (0.9% NaCl). In addition, a single intraperitoneal (i.p.) dose of DEN was administered to the animals at a dose of 100 mg/kg body weight three times.

DEN was obtained from Sigma-Aldrich Chemical Co., St. Louis, Mo. USA. Also, CSL was obtained from Solgar, Turkey.

Morris water maze test

Following treatment, all mice were subjected to the Morris water maze, an established test used to assess spatial learning and memory in rodents. The pool was filled with water to a depth of 30 cm ($22 \pm 1^\circ\text{C}$) 1 cm above the platform level. Visual cues were attached to the walls of the pool and to the walls of the test chamber to guide the animals to the position of the platform. Each mouse was positioned face-to-face against the wall and released from each of the four different quadrants of the maze to find the hidden platform. A time interval of 150 seconds was allowed for the animal to find the platform. If the animal could not find the platform, it was guided to the platform and allowed to remain on the platform for 15 seconds to orientate itself. This training session was repeated for 5 consecutive days. The time to reach the hidden platform was recorded and reported as the escape delay. On the sixth day, the platform was removed and memorization of the platform position was evaluated. Therefore, the time spent in the target quadrant was recorded. Behavioral assessments were scored manually during testing.

Biochemical analysis

Following the applications, mice were sacrificed samples were obtained from blood. Blood samples were collected in tubes containing anticoagulants and centrifuged for 10 min at 3000 rpm at $+4^\circ\text{C}$ to separate plasma. Glutathione reductase (GR) and lactate dehydrogenase (LDH)

(Elabsience, Teksas, USA) levels in serum samples were determined by spectrophotometric (ELISA reader (BioTek, USA)) methods.

Statistical analysis

The significance of the differences between groups was determined by one-way analysis of variance (ANOVA) test using SPSS 20 software for all calculations. $p < 0.05$ and $p < 0.01$ were accepted as the statistical threshold for each analysis.

Results

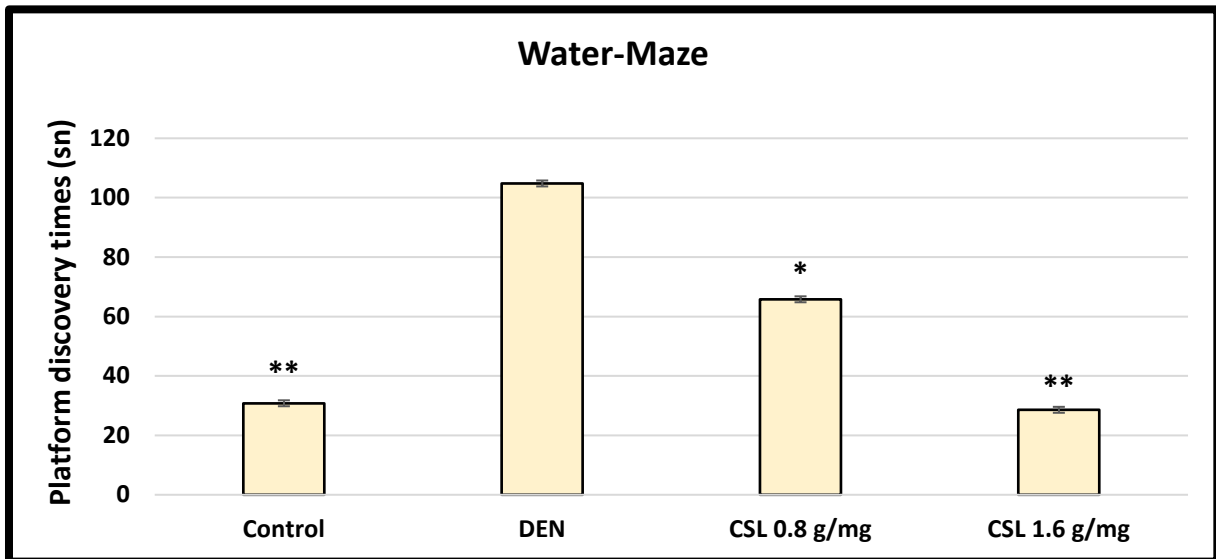


Figure 1.

The results of Morris' water tank test performed in our study are given as the time spent without the platform in the quadrant where the platform was in the previous days on the sixth day. CSL treatment significantly improved performance in the Morris water maze test in a dose-dependent manner. Performance was significantly impaired in the Morris water maze test of the DEN group (Fig.1).

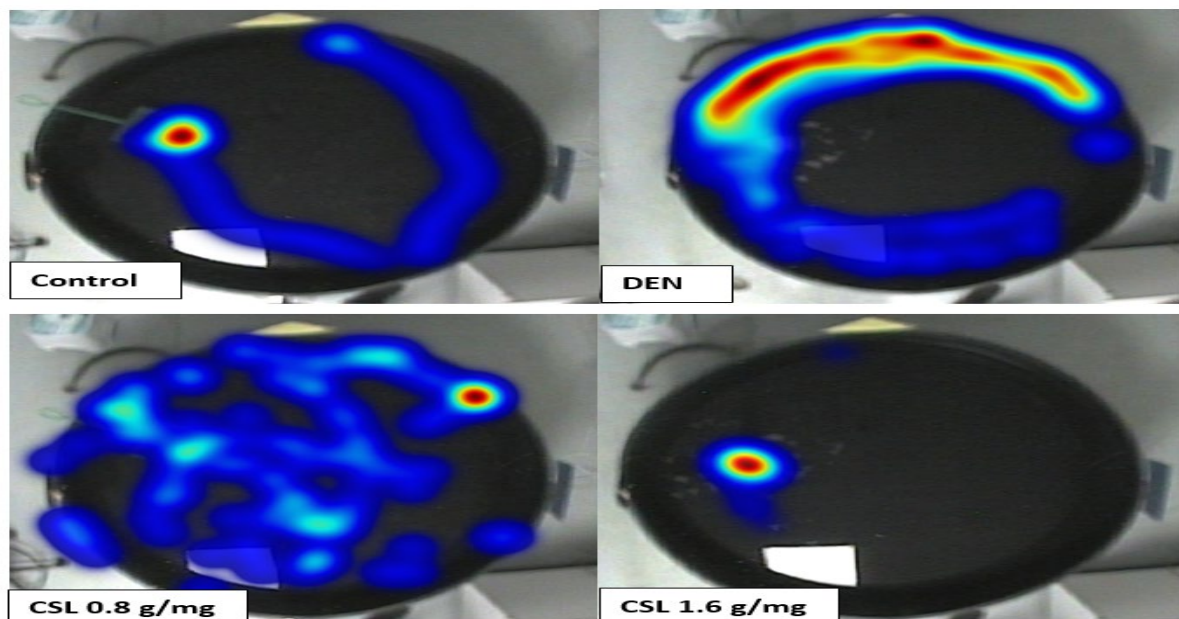


Figure 2.

Day six temperature maps showing the time spent by one animal from each group in the southwest region without a platform in the Morris water tank test.

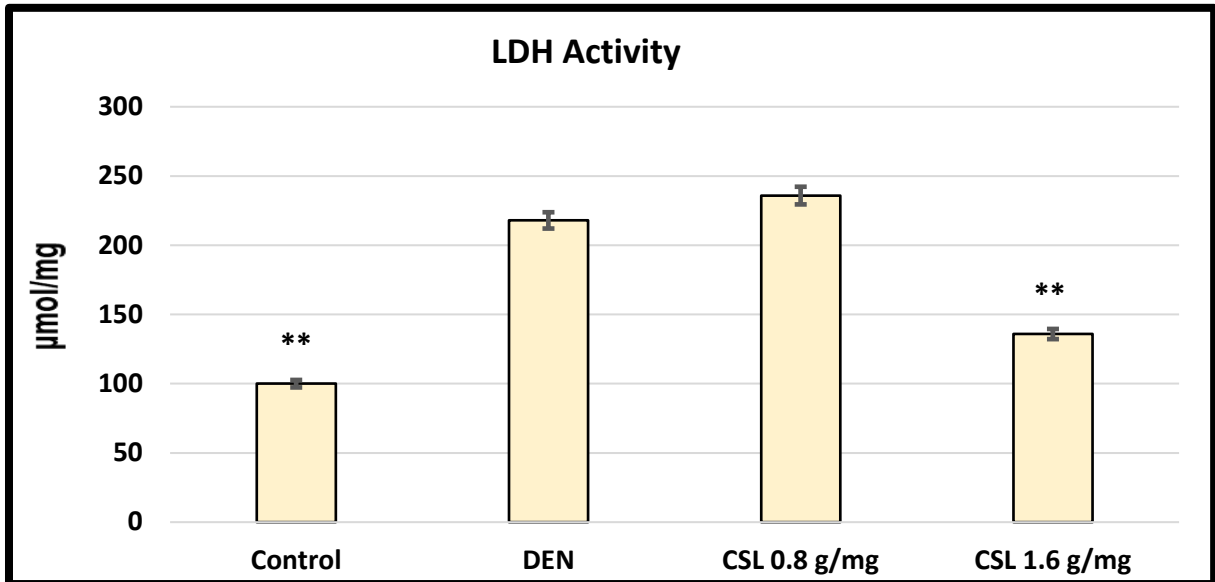


Figure 3.

We evaluated LDH activity according to $\mu\text{mol/mg}$ (Fig.3). According to this test, the LDH activity of the DEN group was found to be 217.93 $\mu\text{mol/mg}$ and the other groups were graded accordingly. LDH level of the control group decreased compared to DEN. Among the groups, the CSL (1.6 g/mg) group showed close LDH levels to the control. In addition, this group was found to be statistically significant compared to the DEN group ($p < 0.01$).

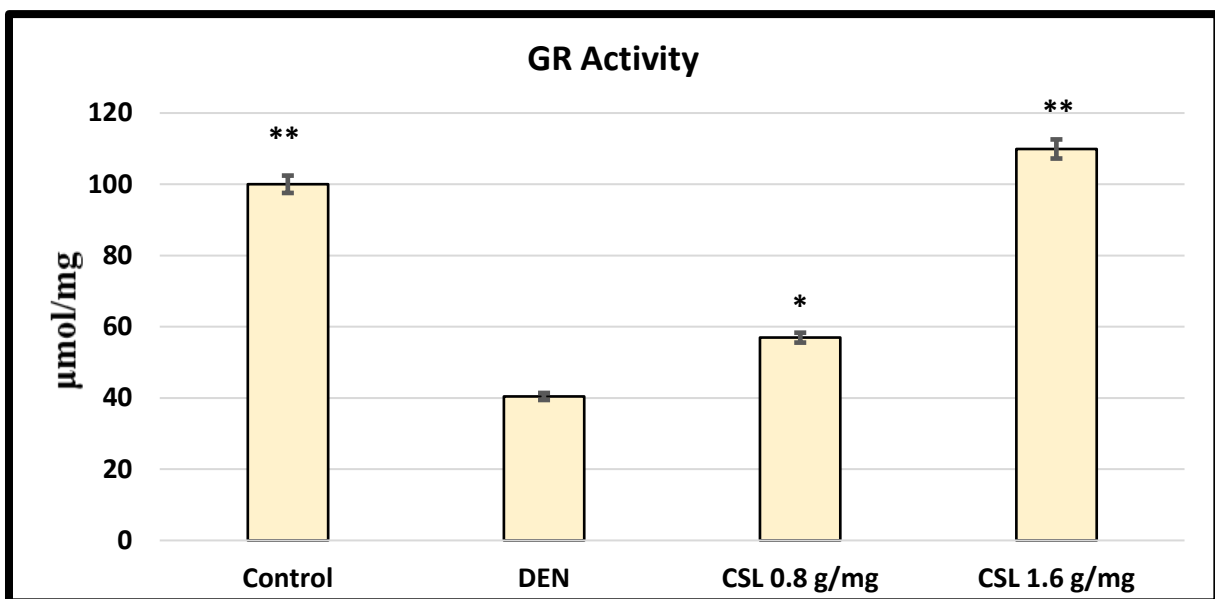


Figure 4.

We evaluated GR activity according to $\mu\text{mol}/\text{mg}$ (Fig.4). According to this test, the GR activity of the DEN group was found to be $40.42 \mu\text{mol}/\text{mg}$ and the other groups were graded accordingly. The GR level of the control group increased compared to DEN. However, the CSL groups increased the GR level in a dose-dependent manner. Among the groups, the CSL (1.6 g/mg) group had the highest GR activity and was statistically very significant compared to the DEN group ($p < 0.01$).

Discussion

Nitrosamines are known to cause neuronal damage, degeneration and death of the central nervous system in structures such as the cerebellum and temporal lobe [16, 17]. Spatial learning loss caused by nitrosamines has been demonstrated by Morris' water tank test and pathology in tau phosphorylation in rat brain as in Alzheimer's disease [18]. Tau protein and $A\beta$ in Alzheimer's disease; dementia, loss of cognitive function, neuropsychiatric changes and ultimately the death of neurons are the main pathological causes. Insulin-resistant brain state in animals given nitrosamine derivatives causes memory impairment, progressive cholinergic deficits, glucose hypometabolism, oxidative stress and neurodegeneration seen in Alzheimer's disease in humans. Studies have shown that nitrosamine derivatives exacerbate Alzheimer's disease-like changes, such as amyloid precursor protein formation, glucose metabolism disorder, synaptic dysfunction, protein kinase-related disorders, and apoptosis, similar to the triple transgenic mouse model [18, 19]. According to Morris' water tank test performed in our study, learning and memory were found to be significantly impaired in the DEN group compared to the control group. We found that learning and memory improved in a dose-dependent manner in the groups treated with CSL and approached the control group. These results show us that CSL can help prevent the development of cognitive impairment.

The reduction in GR activities due to DEN-induced oxidative stress may be due to the possible inhibitory effect of induced ROS on these enzymes and the reduced availability of GSH as a substrate, whereas GSH-Px catalyzes the conversion of lipid peroxide to hydroxy acids in the presence of GSH [20, 21]. GSH of GSH prevents peroxidation, protects cell membranes and ensures the removal of free radicals [20]. Kim et al. (1997), in a study using different nitrosamines in mice, reported that the combination of DEN (10 mg/kg i.p.) with other nitrosamines increased neoplasia and oxidative stress in the lungs of mice after 32 weeks. Pradeep et al. (2007) investigated the effects of silymarin on DEN-induced hepatotoxicity (200 mg/kg i.p.), and the authors reported an increase in some liver-specific enzymes, while a decrease in antioxidant enzyme levels in the DEN group. In this study, the decrease in GR levels observed in the blood serum of mice in the DEN group was attributed to the formation of conjugate with GR to facilitate the excretion of DEN or its metabolites from the body. In addition, CSL supplementation increases blood antioxidant activities and thus prevents the harmful effects of peroxidation products. In our LDH measurement, DEN administration significantly increased plasma LDH activity. This may be due to the rapid release of these enzymes from the cytoplasm into the bloodstream after plasma membrane breakage and cellular damage.

Conclusions

Considering the results of our study, it can be concluded that DEN-induced oxidative stress plays an important role in cognitive impairment. It also shows that *Cynara scolymus* may help prevent the development of cognitive impairment. In addition, based on its biochemical results, it shows that the therapeutic effect of *Cynara scolymus* is due to its antioxidant effect.

Reference

- [1] W. Lijinsky and R.M. Kovatch, "Carcinogenesis by nitrosamines and azoxyalkanes by different routes of administration to rats," *Biomed Environ Sci*, 1989, 2 (2), 154-159.
- [2] M.S. Jahan, G. Vani and C.S. Shyamaladevi, "Effect of *Solanum trilobatum* on hepatic drug metabolising enzymes during diethylnitrosamine- induced hepatocarcinogenesis promoted by Phenobarbital in rat," *Hepato Res*, 2007, 37 (1), 35-49.
- [3] L. Verna, J. Whysner and G.M. Williams, "N-nitrosodiethylamine mechanistic data and risk assessment: bioactivation, DNA-adduct formation, mutagenicity, and tumor initiation," *Pharmacol Ther*, 1996, 71(1-2), 57–81.
- [4] K. Yamada, I. Yamamiya and H. Utsumi, "In vivo detection of free radicals induced by diethylnitrosamine in rat liver tissue," *Free Radic Biol Med*, 2006, 40 (11), 2040-2046.
- [5] R. Gayathri, D.K. Priya, G.R. Gunassekaran, D. Sakthisekaran, "Ursolic acid attenuates oxidative stress-mediated hepatocellular carcinoma induction by diethylnitrosamine in male Wistar rats," *Asian Pac J Cancer Prev*, 2009, 10 (5), 933-938.
- [6] K. Pradeep, C.V.R. Mohan, K. Gobianand and S. Karthikeyan, "Silymarin modulates the oxidant-antioxidant imbalance during diethylnitrosamine induced oxidative stress in rats," *Euro J Pharmacol*, 2007, 560 (2-3), 110-116.
- [7] A.A. Rossini, A.A. Like, W.L. Chick, M.C. Appel, G.F. Cahill, "Jr Studies of streptozotocin-induced insulinitis and diabetes," *Proc Natl Acad Sci U S A*, 1977, 74, 2485–2489.
- [8] T. Szkudelski, "The mechanism of alloxan and streptozotocin action in B cells of the rat pancreas." *Physiol Res.*, 2001, 50, 537–546.
- [9] N. Lester-Coll et.al., "Intracerebral streptozotocin model of type 3 diabetes: relevance to sporadic Alzheimer's disease," *J Alzheimers Dis.*, 2006, 9,13–33.
- [10] A. Vijayalakshmi, K. Masilamani, E. Nagarajan and V. Ravichandiran, "In vitro antioxidant and anticancer activity of flavonoids from *Cassia tora* Linn. leaves against human breast carcinoma cell lines," *Der Pharma Chemica*, 2015, 7, 122–129.
- [11] V. Lattanzio, P.A. Kroon, V. Linsalata and A. Cardinali, "Globe artichoke: a functional food and source of nutraceutical ingredients," *J Funct Foods*, 2009, 1(2), 131–144.
- [12] D.I. Leskovar, C. Xu, S. Agehara, "Planting configuration and plasticulture effects on growth, physiology, and yield of globe Artichoke," *Hortic Sci*, 2013, 48, 1496–1501.
- [13] M. Ben Salem et.al., "Protective effects of *Cynara scolymus* leaves extract on metabolic disorders and oxidative stress in alloxan- diabetic rats," *BMC Complement Altern Med*, 2017, 17(328), 1–19.
- [14] M. El-Boshy et al., "Studies on the protective effect of the artichoke (*Cynara scolymus*) leaf extract against cadmium toxicity-induced oxidative stress, hepatorenal damage, and immunosuppressive and hematological disorders in rats," *Environ Sci Pollut Res Int*, 2017, 24, 12372–12383.
- [15] M. Ebrahimi-Mameghani, M. Asghari-Jafarabadi, K. Rezazadeh," TCF7L2-rs7903146 polymorphism modulates the effect of artichoke leaf extract supplementation on insulin resistance in metabolic syndrome: a randomized, double-blind, placebo-controlled trial, " *J Integr Med*, 2018, 16, 329–334.
- [16] S.M. de la Monte and J.R. Wands," Review of insulin and insulin-like growth factor expression, signaling, and malfunction in the central nervous system: relevance to Alzheimer's disease," *J Alzheimers Dis*, 2005, 7, 45–61.
- [17] S.M. de la Monte and J.R. Wands, "Alzheimer's Disease is Type 3 Diabetes: Evidence Reviewed," *J Diabetes Science Tech*. 2008, 2, 1101–1113.
- [18] C. Gao, Y. Liu, Y. Jiang, J. Ding and L. Li, "Geniposide ameliorates learning memory deficits, reduces tau phosphorylation and decreases apoptosis via GSK3beta pathway in streptozotocin-induced alzheimer rat model, " *Brain Pathol*, 2014, 24, 261-269.
- [19] S. Chen et al., "Glucagon-like peptide-1 protects hippocampal neurons against advanced glycation end product-induced tau hyperphosphorylation," *Neuroscience*, 2014, 256,137-146.
- [20] E.O. Farombi and A. Fakoya, "Free radical scavenging and antigenotoxic activities of natural phenolic compounds in dried flowers of *Hibiscus sabdariffa* L. *Mol Nutr Food Res*," 2005, 49 (12), 1120-1128.

- [21] B. Halliwell and J.M. Gutteridge, "Free Radicals in Biology and Medicine." Oxford University Press, 2015, USA.
- [22] D.J. Kim et al., "Chemoprevention by lycopene of mouse lung neoplasia after combined initiation treatment with DEN, MNU and DMH," *Cancer Lett*, 1997, 120 (1), 15-22.
- [23] K. Pradeep, C.V.R. Mohan, K. Gobianand and S. Karthikeyan, "Silymarin modulates the oxidant-antioxidant imbalance during diethylnitrosamine induced oxidative stress in rats," *Euro J Pharmacol*, 2007, 560 (2-3), 110-116.

Investigation of effects of the chitosan/ hyaluronic acid/ honey hydrogels on cell adhesion and proliferation

Ahmet Enes Akdağ¹, Emine Şalva², Sema Arısoy², Jülide Akbuğa³

¹Marmara University, Faculty of Pharmacy, Department of Pharmaceutical Biotechnology,

²Inonu University, Faculty of Pharmacy, Department of Pharmaceutical Biotechnology,

³Medipol University, Faculty of Pharmacy, Department of Pharmaceutical Technology

Abstract

In our work, it is aimed to prepare the optimal formulations of chitosan, honey and hyaluronic acid hydrogels and investigation of its effects on in vitro cell adhesion and proliferation and determining potential usage for tissue regeneration. Chitosan/Hyaluronic acid/Honey formulations prepared with different molecular weight chitosan and different proportions of ingredients. Viscosity, water content, water-holding capacities, porosity properties were compared and morphologies were investigated with SEM. The cell surface binding capabilities of hydrogels, their effects on cell viability and cell proliferation were investigated by cell culture studies. Our study reveals the optimization of hydrogel formulations and the potential use of this combination for tissue regeneration in combination of chitosan, honey, and hyaluronic acid. In the light of our study findings, we think that the combination of Chitosan/Hyaluronic acid/Honey hydrogel formulations can be potential therapeutic biomaterials for tissue regeneration.

Key words: chitosan, medical honey, hyaluronic acid, cell adhesion and proliferation

Introduction

The use of biomaterial preparations in wound treatment and tissue regeneration has recently gained importance. Medical honey, chitosan and hyaluronic acid are biomaterials that are used separately in various preparations, especially in wound-burn care. When preparing combination preparations in biomaterials, it is a challenging process to develop products with suitable formulation properties. In addition to protection against infection with appropriate pH, ambient humidity, antimicrobial environment in the regeneration microenvironment, the modulation of autocrine, paracrine, endocrine and intracrine signaling mechanisms can also be optimized with the right formulations, patient compliance and surface residence time can be adjusted with appropriate viscosity. Hydrogel formulations can be considered as the primary choice in wound care products in terms of both their physicochemical properties and the development of biocompatible combinations. In this study, we examined the in vitro characterization of hydrogels obtained by formulating the mentioned biomaterials, which have different mechanisms of action, and their effects on cell proliferation and adhesion, and their effects on fibroblast cells.

Material and Methods:

Preparation of Chitosan-Hyaluronic Acid-Honey Hydrogels

2% medium molecular weight chitosan (MMW) dissolved in 1% acetic acid (pH 3.5-4). While chitosan was mixed in a magnetic stirrer, 1 N NaOH was added dropwise, and the pH of the solution was brought to 8-9, allowing the chitosan to precipitate. Afterwards, it was centrifuged to remove excess NaOH from the formed hydrogel and washed 3 times with distilled water. High molecular weight hyaluronic acid (800 kDa) aqueous solutions at different concentrations (1%, 2%, 4% and 6%) were added to the precipitate and mixed for one hour on a magnetic stirrer (pH 7.5-8.0) to form the chitosan-hyaluronic acid hydrogel (Vignesh, 2018). Honey (1%, 2%, 4% and 6%) was added to this hydrogel in the same weight ratio as hyaluronic acid and mixing was continued (pH 6.5-7.0). When chitosan/hyaluronic acid/honey hydrogels were formulated in terms of w/w/w, formulations 1/0.5/0.5, 1/1/1, 1/2/2, 1/3/3 were prepared.

Controls on Chitosan-Hyaluronic Acid-Honey Hydrogels

Viscosity determination of Chitosan/Hyaluronic acid/Honey hydrogels, examination of surface properties with SEM, water holding capacity and swelling control, binding control with FT-IR, porosity measurements were conducted, and in vitro characterizations were analyzed.

Cell Culture Studies with Hydrogels

The cell line NIH-3T3 (mouse fibroblast cell) was used in in vitro cell culture studies of hydrogel formulations. Cells were cultured in DMEM medium containing 10% fetal bovine serum, 100 mM L-glutamine and 100 mM antibiotic solution. The hydrogels prepared under aseptic conditions for the adhesion of the cells to the hydrogels were placed in 12-well culture dishes in a laminar flow cabinet, sterilized under UV light and left to dry overnight. The next day, NIH 3T3 fibroblast cells were seeded on the hydrogels and the adhesion properties of the cells were examined. MTT test was performed to examine the effects of hydrogels on cell proliferation/cytotoxicity.

Results:

Analyzing In vitro Characterization Properties of Chitosan-Hyaluronic Acid-Honey Hydrogels

When the viscosity measurement results of the prepared hydrogel formulations were compared, it was observed that the viscosity values changed with the amount of hyaluronic acid added to the formulation. In formulations containing high molecular weight hyaluronic acid, the amount dependent viscosity increase is observed. However, the addition of honey caused a decrease in viscosity in high molecular weight hyaluronic acid hydrogel formulations containing honey (Fig.1).

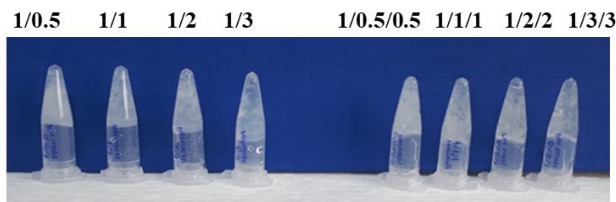


Figure 1. Viscosity measurements and gel structures of formulations

Formulations		Viscosity cp	Torq %
%2 Chitosan		1815,3	18,3
HMW HA		57051	57,5
Honey		11215	72
CS/HA	1/0.5	25301	25,5
	1/1	50106	50,5
	1/2	56753	57,2
	1/3	75804	76,4
CS/HA/Honey	1/0.5/0.5	49709	50,1
	1/1/1	42260	21,3
	1/2/2	11410	23,1
	1/3/3	10219	20,6

The microscopic morphology of the lyophilized hydrogels was examined by scanning electron microscope (SEM). While regular pore structure was observed in hydrogels containing only chitosan, irregular pore geometry was observed only in hyaluronic acid hydrogels (Fig.2.a-b). No regular pore structure was observed due to HA in hydrogels containing 1/0.5 chitosan/HA. Flat surface morphology was observed in Chitosan/HA/Bal hydrogels (Fig.2c-d). It was observed that the pore structure increased as the amount of hyaluronic acid increased in the hydrogels prepared at 1/2 and 1/2/2 ratios (Fig.2e-f).

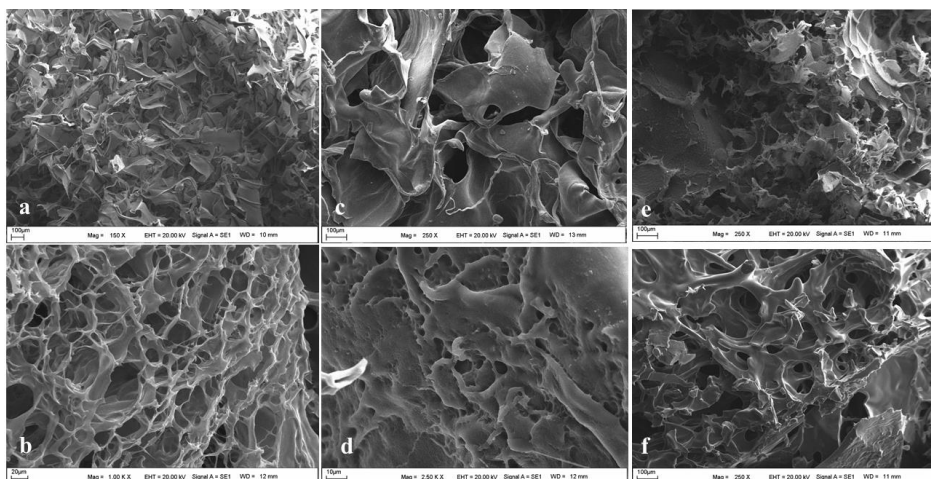


Figure 2. SEM images of the prepared hydrogels. a.HMW HA, b. MMW Chitosan, c. 1/0.5 CS/HA, d.1/0.5/0.5 CS/HA/Honey, e. 1/2 CS/HA, f. 1/2/2 CS/HA/Honey hydrogels.

Porosity was investigated depending on the volume of the pores present in the hydrogels. When porosity measurement of hydrogels was made, an increase in porosity was observed with the increase of hyaluronic acid concentration in the formulations. It has been determined that the porosity is low in formulas containing honey. The porosity increased due to the increase in the viscosity of the hydrogels (Fig 3A). When the water holding capacity and swelling degree of the hydrogels were evaluated, it was determined that the swelling percentage changed with the addition of honey to the formulation in the swelling study with chitosan/HA/honey hydrogel formulations. Addition of honey to the hydrogels caused a reduction in swelling percentages (Fig. 3B). The functional groups of chitosan, HA and prepared coacervate hydrogels were analyzed using FTIR. The FTIR spectrum of formulas containing honey showed similar patterns and band positions as honey (Fig. 3C).

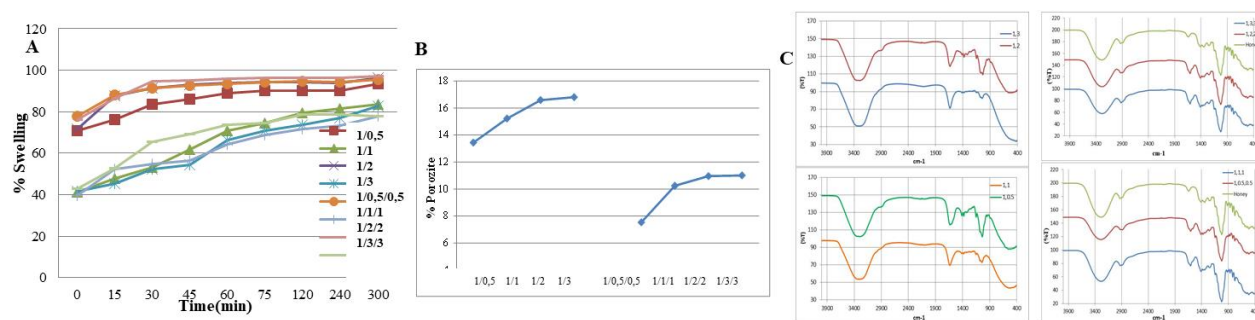


Figure 3. Investigation of A. Swelling, B. Porosity, C. FT-IR properties of hydrogels.

Cell Adhesion Properties and Effects of Hydrogels on Cell Viability and Proliferation

The effects of chitosan, HMW hyaluronic acid and honey used in the preparation of hydrogels on fibroblast cells were investigated. It was observed that fibroblast cells adhered to the hydrogel surface and increased cell proliferation in all groups.

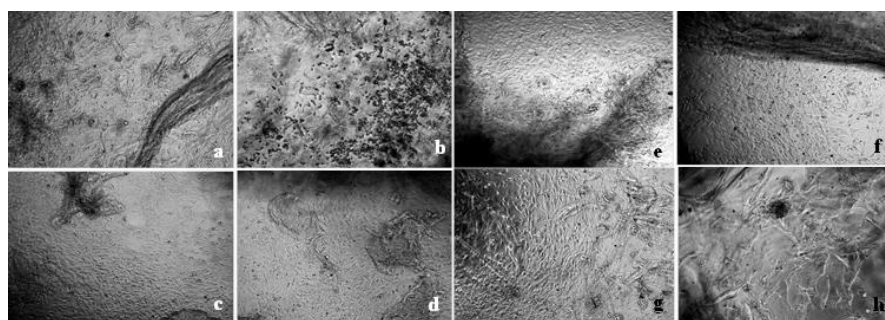


Figure 4. Morphological images after 48 hours (a-d) and 96. hours (e-h) after seeding NIH3T3 fibroblast cells on chitosan/HA/Honey hydrogels (a,e: 1/0.5/0.5, b,f:1/1/1, c,g:1/2/2, d,h:1/3/3).

Evaluating the effects of hydrogels on cell viability in all groups, no toxic properties observed for hydrogels. The viability values obtained in the cells in the groups to which Chitosan/HA/Honey hydrogels were applied were higher than the control group. Cell viability

was found to be the highest in formulations prepared with hone indicating hydrogels increase cell proliferation.

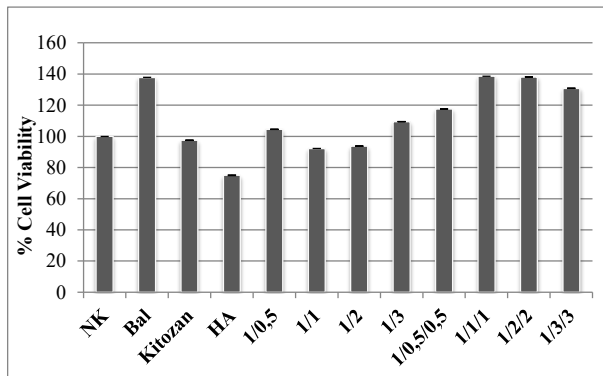


Figure 5. Demonstration of cell viability and proliferation after 72-hour exposure of NIH 3T3 cells to hydrogels with MTS

Our study reveals the optimization of hydrogel formulations and the potential use of this combination for tissue regeneration in combination of chitosan, honey, and hyaluronic acid. In the light of our study findings, we think that the combination of Chitosan-Honey-Hyaluronic acid hydrogel formulations can be a potential therapeutic for tissue regeneration.

References

S. Vignesh, A. Sivashanmugama, Annapoorna Mohandasa, R. Janarthanan, Subramania Iyer, Shantikumar V. Naira, R. Jayakumar. Injectable deferoxamine nanoparticles loaded chitosan-hyaluronic acid coacervate hydrogel for therapeutic angiogenesis *Colloids and Surfaces B: Biointerfaces* 161 (2018) 129–138

OP-08

Treating Neurotoxicity Developed in Triple Cocultures Created by Transwell Method with Graviola Plant

Sidika Genc^{1*}, Ali Taghizadehghalehjoughi², Yesim Yeni¹, Ahmet Hacimuftuoğlu¹

¹ Ataturk University, Faculty of Medicine, Department of Medical Pharmacology, Erzurum, Turkey

² Ataturk University, Faculty of Veterinary Medicine, Department of Pharmacology and Toxicology, Erzurum, Turkey

Abstract

Astrocytomas are the most common malignancy of the CNS, accounting for >60% of primary brain tumors. The most aggressive form of astrocytoma is glioblastoma. Glioblastoma cells, consisting of poorly differentiated neoplastic astrocytes, have properties similar to normal nerve precursor cells, including rapid cell proliferation, migration, and invasion. Despite efforts to improve treatment and advances in microsurgery, radiotherapy, and chemotherapy over the past two decades, the average survival of patients remains limited to 14 months after diagnosis.

The fruits, leaves, stems and roots of Graviola are known to be rich in flavonoids, isoquinoline alkaloids and annonaceous acetogens. Its bark, leaves, roots, fruits, seeds and flowers have been used for thousands of years to treat many diseases from arthritis to liver problems. It is also used to treat a wide variety of human ailments such as inflammation, rheumatism, diabetes, hypertension, insomnia, parasitic infections, and cancer.

The aim of our study is to reveal the anti-angiogenesis effect of the Graviola plant, which we will use for treatment, by creating neurotoxicity with the transwell co-culture method. For this purpose, firstly, primary neuron culture was made and planted in 24-well plates and left to incubate for three days. In the second step, HUVEC and U373 cell lines grown in the appropriate medium were removed from the medium with trypsin EDTA and cells were seeded on the lower base of the transwell membrane and U373 on the upper base of HUVEC. After 24 hours, the transwell membrane was added to the neuron culture and incubated for 48 hours in medium with Graviola plant at doses of 20, 40, 80, 160, 320 µg/ml. At the end of the study, MTT, GSH and LDH, TAK and TOS tests were performed and the results were compared with the control groups. The results were evaluated statistically.

According to our results, it was determined that Graviola 160 µg/ml is the most beneficial group in removing the damage caused by U373 cells on neurons via transwell. While the viability decreased up to 78% at low doses, this rate increased to 90% at 160 µg/ml concentration of Graviola. Similarly, LDH, HR, TAK and TOS results correlated with MTT.

Anahtar Kelime: Graviola, Transwell, MTT, LDH, GSH

1. Introduction

Glioblastoma (GBM) is the most common and aggressive primary brain tumor in adults. It is a disease that accounts for 45.6% of primary malignant brain tumors, but 3.1 annual cases per 100 000 are low compared to cancers originating from other organs such as the breast or prostate (1). Despite efforts to improve treatment and advances in microsurgery, radiotherapy, and chemotherapy in the last two decades, the average survival of patients remains limited to 14 months after diagnosis (2). It has been reported that GBMs are highly vascular tumors and tumor vasculature arises from the sprouting of pre-existing brain capillaries, and glioblastoma stem cells (GSCs) secrete angiogenic factors and trigger neovascularization formation. It has also been found that GSCs can differentiate into endothelial cells (ECs) to promote tumor vascularization. However, in randomized trials, antiangiogenic treatments did not show a significant survival benefit in GBMs (3).

Important characteristic features of cancer cells are their ability to proliferate, invade through the extra cellular matrix, and migrate to different parts of the body to form secondary tumors. The migration of cancerous cells is dependent on the tumor microenvironment, in which they are nourished and supported by forming a new vasculature (a process called angiogenesis) and allowing them to spread (4). Angiogenesis is an important marker of cancer metastasis. Therefore, anti-angiogenesis is defined as a therapeutic approach for the treatment of many cancers. When angiogenesis factors induce angiogenesis, tumors reach a vascularized state, recruit new blood vessels to supply nutrients and oxygen, and grow rapidly. (5). Tumor angiogenesis is mediated by various angiogenic factors and complex signaling networks. Among all known angiogenic factors, vascular endothelial growth factor (VEGF) and basic fibroblast growth factor (bFGF, FGF2) are the most important (6-7). The effects of VEGF are mediated through the binding and activation of its receptors (8). VEGF signaling plays the role of a 'critical rate-limiting step' in physiological angiogenesis and pathological angiogenesis. Interruption of the VEGF/VEGFR2 signaling pathway has been recognized as a therapeutic target in tumor angiogenesis (9). As another essential angiogenic factor, FGF2 is a heparin-binding protein with a range of pro-angiogenic effects (10). Studies show that FGF signaling is an important pathway in tumorigenesis and tumor angiogenesis (11). In line with the information given, anti-angiogenesis is emerging as an important strategy in cancer treatment.

Annona muricata, a plant of the Annonaceae family, is also known as Soursop or Graviola (12). It is known that the fruits, leaves, stems and roots of graviola are rich in flavonoids, isoquinoline alkaloids and annonaceous acetogens (13). Its bark, leaves, roots, fruits, seeds and flowers have been used for thousands of years to treat many diseases from arthritis to liver problems (12). It is also used to treat a wide variety of human diseases such as inflammation, rheumatism, diabetes, hypertension, insomnia, parasitic infections and cancer (14,15). Found only in the Annonaceae family, annonaceous acetogens kill malignant cells of 12 different types of cancer, including breast, ovarian, colon, prostate, liver, lung, pancreatic, and lymphoma (12). Despite their outstanding antiproliferative activity, the components of these annon-associated acetogens can easily cross the blood-brain barrier and even reduce side effects such as neurotoxicity, which are known to cause atypical Parkinson's disease and even limit their development as new drug entities (16). However, studies show that Graviola extract has a plausible chemotherapeutic role against cancer (17).

Traditional 2D cell cultures have long been used to evaluate the effects of drugs on tumor cell growth. However, the 2D culture medium does not provide information about the complex interactions between the physicochemical microenvironment that exists within viable tumors formed in human organs. More recently, more sophisticated transwell-based assays have been used to investigate cancer cell migration and invasion through their microscale pores (21).

Based on this information, we plan to use transwell co-culture in this study to determine the underlying mechanism that can illuminate the morphology of angiogenesis in vitro. In our study, a co-culture model will be made that allows direct interaction between human endothelial cell (HUVEC) and U373 cancer line, thus facilitating the study of signaling pathways that govern blood vessel formation in glioblastoma cancer, and increasing the tumorigenesis in neuron cells by increasing the spread of neuron cells. As a result, with the transwell system

Material Method

Cell culture

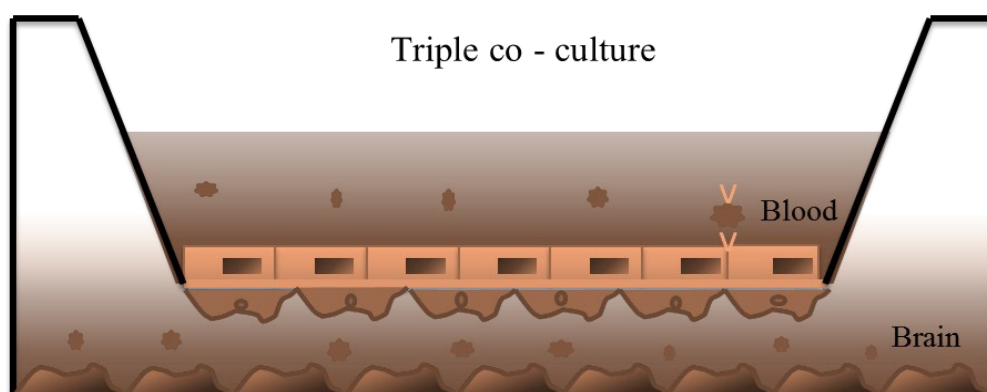
Primary Neuron Culture

In the study, a newborn Sprague Dawley rat that has not completed 24 hours was used to obtain cortex neurons. Briefly, after the rats were decapitated quickly, the removed cortices were transferred to 5 mL of Hanks' Balanced Salt solution (HBSS) solution, and macro fragmentation was performed with the help of a scalpel and then microfragmentation was performed with Trypsin-Ethylenediaminetetraacetic acid (EDTA) (0.25% Trypsin-0.02% EDTA). The cells were then centrifuged at 1200 rpm for 5 min. Cells sinking to the bottom are cellular medium (88% NBM (Neuro basal medium, Gibco, USA), 10% FBS (Fetal bovine solution, Gibco, USA), 2% B-27% (Supplement, Thermo Fisher, Germany), 0.1% antibiotic (Penicillin–Streptomycin) and amphotericin B (Thermo Fisher, Germany) were added. The cells were incubated for 10 days at 5% CO₂ and 37°C, changing the medium every 3 days.

HUVEC and U373 Cell Culture

For our study, HUVEC and U373 cell cultures were obtained from the medical pharmacology department of Atatürk University (Erzurum, Turkey). Briefly, the cell suspension was centrifuged at 1200 rpm for 5 minutes. Cells were resuspended in fresh medium (Dulbeco-modified eagle medium (DMEM), Fetal bovine serum (FBS) 10%, B27 2%, and antibiotic 1% (penicillin, streptomycin, and amphotricine B), and cells in a 25cm² flask). (Corning, USA) and stored in an incubator (5% CO₂; 37 °C) When 80% of the flask was covered with cells, it was centrifuged by removing Trypsin-Ethylene diaminetetraacetic acid (EDTA) (0.25% trypsin-0.02% EDTA) and Cells were seeded at the bottom of the transwell membrane and kept in matrigel medium for 24 hours.

Transwell



At the end of the experiment (after 24 hours of treatment), 10 µL of MTT solution is added to each well plate. Then the plates were incubating for 4 hours at 37 °C in a CO₂ incubator. 100 µL of DMSO solution was incorporated to all well to dissolve formazan crystals. The density of the Formazan crystals was read at a wavelength of 570 nm by the Multiskan TM GO Microplate Spectrophotometer reader

Oxidative Stress Analysis

Biochemical analyze of Total Antioxidant Capacity (TAC) and Total Oxidant Status (TOS) were performed accordingly to the manufacturers' instructions (Rel Assay Diagnostics, Gaziantep, Turkey) (13-14).

GSH and LDH Analysis

GSH and LDH activity were performed accordingly to the manufacturers' instructions (Elabscience, İstanbul, Turkey).

Statistical Analysis

Statistical calculations were carried out using SPSS 22.0 software. To determine the statistical significance of the results, the one-way ANOVA test was applied. The differences between the groups were considered significant at $P < 0.05$.

2. Result

When our results were examined, it was observed that the viability of neuron cells initially decreased up to 78%. This is because cancer cells interact with neuron cells, causing toxicity. It was determined that this toxicity was eliminated in the treatment groups created with graviola, especially at 160 μ g/ml concentration, with the highest viability rate. On the contrary, it was observed that the viability decreased again in the highest concentration of 320 μ g/ml group. This shows that Graviola is effective up to a certain concentration. Similar results were observed in other analyzes and all results correlated with MTT. The results of our study were statistically evaluated and found significant ($P < 0.05$)

Figure 1 MTT Results

Figure 2 LDH Results

Figure 3. GS Results

Figure 4. TAC Results

Figure 5. TOS Results

3. Discussion

The obstacle in the treatment of glioblastoma is tumor-induced angiogenesis, which leads to the formation of abnormal vessels and a dysfunctional blood-tumor barrier. The abnormal vascularization that occurs with glioblastoma metastasis disrupts the blood-brain barrier, preventing drug penetration. Therefore, identifying novel molecular targets that control GBM-induced angiogenesis will provide a new focus on more effective therapeutic strategies in GBM treatment. In the light of this information, it is aimed to co-culture with HUVEC endothelial, U373 cancer cell line and neuron cells using the transwell method and to determine the neurotoxicity of cancer cells and to investigate the treatment with Graviola plant at various doses. To achieve this goal, MTT, GSH and LDH tests were performed.

In current studies, it is reported that Graviola has a protective effect on various cancers. In an in vitro study, using A-549 lung cancer cell line, it was shown that Graviola leaf extract caused cell cycle arrest and induced apoptosis in G0/G1 phase. The underlying mechanism for this is that Graviola suppresses nuclear factor- κ B (NF- κ B) signaling, induces reactive oxygen species (ROS) production, and is mediated by the attenuation of mitochondrial membrane potential

(MMP), cytosolic cytochrome c, and caspase-3/9 activation of Bax. / Bcl-2 ratio was found to increase (18). In addition, a study on prostate reported antiproliferative effects of Graviola extract mediated by reducing HIF-1 α expression and inhibiting NADPH oxidase (NOX) activity (19). Specifically, the anti-proliferative activity of Graviola is attributed to its ability to inhibit the phosphoinositide-3-kinase/serine-threonine kinase (PI3K/Akt), protein kinases B/C, ERK1/2, Janus kinase, and p38 MAPK pathways, resulting in cell death (20).

5. References

- 1) Wirsching HG, Galanis E, Weller M. Glioblastoma. *Handb Clin Neurol*. 2016;134:381-97.
- 2) Huber RM, et al. Deltex-1 activates mitotic signaling and proliferation and increases the clonogenic and invasive potential of U373 and LN18 glioblastoma cells and correlates with patient survival. *PLoS One*. 2013;8(2):e57793.
- 3) Petropoulos C, et al. Functional invadopodia formed in glioblastoma stem cells are important regulators of tumor angiogenesis. *Oncotarget*. 2018 Apr 17;9(29):20640-20657.
- 4) Al-Asmari AK, et al. *Moringa oleifera* as an Anti-Cancer Agent against Breast and Colorectal Cancer Cell Lines. *PLoS One*. 2015;19;10(8):e0135814.
- 5) Carmeliet P, Jain R.K. Molecular mechanisms and clinical applications of angiogenesis *Nature*, 473 (7347) (2011), pp. 298-307.
- 6) Jayasinghe C, et al. The relevance of cell type- and tumor zone-specific VEGFR-2 activation in locally advanced colon cancer *J. Exp. Clin. Cancer Res.*, 34 (2015), p. 42.
- 7) Lieu C, et al. Beyond VEGF: inhibition of the fibroblast growth factor pathway and antiangiogenesis. *Clin. Cancer Res.*, 17 (19) (2011), pp. 6130-6139.
- 8) Garonna E, et al. Vascular endothelial growth factor receptor-2 couples cyclo-oxygenase-2 with pro-angiogenic actions of leptin on human endothelial cells *PLoS One*, 6 (4) (2011), p. e18823.
- 9) M. Shibuya. Vascular endothelial growth factor and its receptor system: physiological functions in angiogenesis and pathological roles in various diseases *J. Biochem.*, 153 (1) (2013), pp. 13-19.
- 10) Akl MR, et al. Molecular and clinical significance of fibroblast growth factor 2 (FGF2/bFGF) in malignancies of solid and hematological cancers for personalized therapies *Oncotarget*, 7 (28) (2016), pp. 44735-44762.
- 11) Wesche J, et al. Fibroblast growth factors and their receptors in cancer. *Biochem. J.*, 437 (2011), pp. 199-213.
- 12) Prabhakaran K, et al. Polyketide Natural Products, Acetogenins from *Graviola* (*Annona muricata* L), its Biochemical, Cytotoxic Activity and Various Analyses Through Computational and Bio-Programming Methods. *Curr Pharm Des*. 2016;22(34):5204-5210.
- 13) Zorofchian Moghadamtousi S, et al. *Annona muricata* leaves induce G₁ cell cycle arrest and apoptosis through mitochondria-mediated pathway in human HCT-116 and HT-29 colon cancer cells. *J. Ethnopharmacol.*, 2014;156:277–289.
- 14) Gavamukulya Y, et al. Phytochemical screening, anti-oxidant activity and in vitro anticancer potential of ethanolic and water leaves extracts of *Annona muricata* (*Graviola*). *Asian Pac. J. Trop. Med.*, 2014; 7S1:S355–S363.

- 15) Baskar R, et al. In vitro antioxidant studies in leaves of *Annona* species. *Indian J. Exp. Biol.*, 2007;45:480–485.
- 16) Torres MP, et al. Graviola: a novel promising natural-derived drug that inhibits tumorigenicity and metastasis of pancreatic cancer cells in vitro and in vivo through altering cell metabolism. *Cancer Lett.*, 2012;323:29–40.
- 17) Yang C, et al. Synergistic interactions among flavonoids and acetogenins in Graviola (*Annona muricata*) leaves confer protection against prostate cancer. *Carcinogenesis*. 2015 Jun;36(6):656-65.
- 18) Zhao GX, et al. Biologically active acetogenins from stem bark of *Asimina triloba*. *Phytochemistry*, 1993; 33:1065–1073.
- 19) Deep G, et al. Graviola inhibits hypoxia-induced NADPH oxidase activity in prostate cancer cells reducing their proliferation and clonogenicity. *Sci. Rep.*, 2016;6:23135.
- 20) Marengo B, et al. Redox homeostasis and cellular antioxidant systems: crucial players in cancer growth and therapy. *Oxid. Med. Cell. Longev*, 2016;2016:6235641.
- 21) Sontheimer-Phelps A, Hassell BA, Ingber DE. Modelling cancer in microfluidic human organs-on-chips. *Nature Reviews Cancer*, 2019. 19, 65–81.

OP-09

Evaluation of Anticancer Potential of a Cholesterol Lowering Drug and Its Synthetic Intermediates

Sefayi Merve Özdemir,^a Esen Bellur Atici^b and Ali Çağır^c

^a Izmir Institute of Technology, Biotechnology Graduate Program, 35430, Urla, Izmir, Turkey

^b DEVA Holding A.S. Cerkezkoy, 59500, Tekirdag, Turkey

^c Izmir Institute of Technology, Faculty of Science, Department of Chemistry, 35430, Urla, Izmir, Turkey

INTRODUCTION

Cancer is a disease underlying numerous molecular mechanisms of cell. It is resulted from abnormal cell division and growth[1]. Mutations in genes whose products plays role in cell cycle, proliferation and apoptosis cause the cancer formation and progression[2]. Cancer is second causing death in world with high incidence and mortality rates[3]. Thus, oncology researches for improving cancer treatment have been so important. Cancer treatments including surgery, radiation therapy and medicine have not been successful in completely curing disease, yet. In this point, the development of novel potential anticancer drugs became very important. Anticancer drugs can be classified into two groups as cytotoxic and cytostatic drugs. Cytotoxic drugs can cause cell death in cancer cells, whereas cytostatic drugs can block cell division and tumor growth[4]. These drugs have been commonly studied in clinical researches to establish their usage in cancer therapy. One of the strategies of anticancer drug treatment is the combinatory use of cytotoxic and cytostatic drugs[5].

MATERIALS & METHODS

MTT Assay:

The viability of MCF7, HeLa and LNCaP cells treated with compounds SM2-9 for 48 hours was analyzed by MTT assay. MCF7 and HeLa cells were inoculated at 3000 cells/well into 96-well plate, whereas LNCaP cells were seeded at 5000 cells/well into 96-well plate. Cells were incubated at 37 °C, 5% CO₂ for 24 hours. Then, compounds SM2-9 and the reference drug molecules such as pazopanib.HCl were added to wells at seven different concentrations. Plates

were incubated for 48 hours. Next treatment, 10 μ L of MTT dye (5 mg/1 mL) was added into each well, and plates were incubated with the dye for 4 hours. Then, the centrifugation of plates were performed at 1800 rpm for 10 minutes. Medium was removed and 100 μ L of DMSO was added to wells followed by absorbance measurements at 560 nm using spectrophotometer. All experiments performed as triplicate.

Caspases 3/7 Activity Assay:

As a result of MTT assay, compounds SM8 and SM9 were chosen to evaluate the apoptotic effects on LNCaP cells due to their strong anticancer activity. In this assay, idasanutlin was used as positive control. LNCaP cells were distributed at 5000 cells/well in 96-well plates, then cultured at 37 °C in 5% CO₂ for 24 hours. Next, the cells were exposed to 0.50, 2.95 and 12.00 μ M of SM8, or 0.10, 0.22 and 4.00 μ M of SM9, or 0.50, 2.00 and 8.00 μ M of idasanutlin for 24 hours. Then, 100 μ L of Apo-ONE Caspase 3/7 reagent was added to the wells and plate was mixed on shaker at 200 rpm for 30 seconds. Plate was incubated for 2 hours, followed by fluorescence intensity measurements via BioTek Synergy H1 instrument (Excitation: 428 nm and Emission: 520 nm). All molecules were examined three separate triplicates.

Annexin V-FITC Assay:

The apoptotic induction of SM8, SM9 and idasanutlin in LNCaP cells was examined by Annexin-V-FITC assay. LNCaP cells were seeded at 5×10^5 cell/well density and incubated in 24 hours at 37 °C CO₂ incubator. Then, the cells were exposed to 0.50, 2.95 and 12.00 μ M of SM8, or 0.10, 0.22 and 4.00 μ M of SM9, or 0.50, 2.00 and 8.00 μ M of idasanutlin for 24 hours. %1 DMSO was used as control. After 24 hours, the cells were harvested, washed two times with 1X PBS and then treated with 200 μ L of binding buffer. The stained of cells with 5 μ L of Annexin-V-FITC dye and 5 μ L of propidium iodide dye was performed for 15 minutes in darkness. Lastly, Flow Cytometry analysis was performed. All molecules were tested by two separate duplicates

Cell Cycle Analysis by PI Staining:

The effect of compound SM9 on cell cycle phases of LNCaP cells were analyzed by PI staining and Flow Cytometry. LNCaP cells were distributed at 4×10^5 cell/well density and incubated in 24 hours at 37 °C CO₂ incubator. Then, the cells were exposed to 0.10, 0.22 and 4.00

μM of SM9 for 24 hours. %1 DMSO was used as control. After 24 hours, the cells were harvested, washed two times with 1X PBS. Cells were fixed with 99 % ethanol overnight. Next, the cells was centrifuged at 800 rpm for 5 minutes. the cells were washed with 1X PBS. At last, the cells were dissolved with 200 μL of PBS containing 0.01% Triton-X-100. Then, 20 μL of RNase A (1 mg/mL) was added onto cells and incubated at 37 °C for 30 minutes. After incubation, the cells were stained with 20 μL of propidium iodide (PI, 1 mg/mL) and incubated in dark for 15 minutes at room temperature. The cell cycle analysis was performed by Flow Cytometry. All experiments were done by two separate duplicates.

RESULTS & DISCUSSIONS

The cytotoxic and cytostatic profiles of compounds SM2-9 were determined by MTT assay. All compounds were tested up to 100 μM concentration. For all compounds, GI_{50} values were calculated by GraphPad Prism 5 software. These values were demonstrated in Table 1. According to MTT results, compounds SM2, SM3, SM4 and SM6 exhibited cytotoxic effects whereas compounds SM5, SM8 and SM9 showed cytostatic effects in all cell lines, Compounds SM8 and SM9 were most potent compounds, so the apoptotic effects of these compounds were investigated. For this purpose, Caspases 3/7 activity assay and Annexin V-FITC assays was performed. As a results of these assays, compounds SM8 and SM9 had no activity on the apoptotic induction of LNCaP cells, as seen in Figure 1 and Figure 2. In Caspases 3/7 activity assay, compounds SM8 and SM9 slightly increased the levels of activated caspases 3 and 7 in LNCaP cells. Cell cycle analysis test demonstrated that compound SM9 have activity on G1 arrest in cell cycle of LNCaP cells, as seen in Figure 3.

CONCLUSIONS

Cancer is a major disease that have high incidence and mortality rates. There has been no permanent cure for cancer, up to date. The drug discovery and development is important for improving cancer treatment. Because cytotoxic and cytostatic drugs are most commonly used in cancer chemotherapy, discovery of new cytotoxic and cytostatic drugs is quite essential for the future of cancer treatment. In this study, the cytotoxic and cytostatic properties of a cholesterol-lowering drug and its synthetic intermediates (compounds SM2-9) were evaluated in MCF7, HeLa and LNCaP cancer cells. Among compounds, compounds SM8 and SM9 were found to be most

potent molecules with cytostatic effects. Compound SM9 demonstrated the induction of G1 arrest in LNCaP cancer cells. Thus, this study promises novel and potential compounds for drug discovery in cancer treatment.

REFERENCES

1. Fouad, Y.A. and C. Aanei, *Revisiting the hallmarks of cancer*. American journal of cancer research, 2017. **7**(5): p. 1016-1036.
2. Blackadar, C.B., *Historical review of the causes of cancer*. World J Clin Oncol, 2016. **7**(1): p. 54-86.
3. Sung, H., et al., *Global Cancer Statistics 2020: GLOBOCAN Estimates of Incidence and Mortality Worldwide for 36 Cancers in 185 Countries*. CA Cancer J Clin, 2021. **71**(3): p. 209-249.
4. Rixe, O. and T. Fojo, *Is Cell Death a Critical End Point for Anticancer Therapies or Is Cytostasis Sufficient?* Clinical Cancer Research, 2007. **13**(24): p. 7280-7287.
5. Kummar, S., et al., *Drug development in oncology: classical cytotoxics and molecularly targeted agents*. British Journal of Clinical Pharmacology, 2006. **62**(1): p. 15-26.

OP-10

Gold Nanoparticles Improve Locomotor Activity Rhythm and Alleviate Oxidative Stress in a Mice Model Nitrosamine–Mediated Degeneration

Sidika Genc^{1*}, Yesim Yeni¹, Betul Cicek², Mehmet Kuzucu³, Ahmet Cetin³, Kemal Volkan Ozdokur⁴, Ufuk Okkay¹, Ahmet Hacimuftuoğlu¹

¹ Ataturk University, Faculty of Medicine, Department of Medical Pharmacology, Erzurum, Turkey

² Erzincan Binali Yildirim University, Faculty of Medicine, Department of Physiology, Erzincan, Turkey

³ Department of Biology, Erzincan Binali Yildirim University, Faculty of Arts and Sciences, Erzincan, Turkey

⁴ Department of Chemistry, Faculty of Arts and Sciences, Erzincan Binali Yildirim University, Erzincan, Turkey

Abstract

Objective: Gold nanoparticles improve locomotor activity rhythm and attenuate oxidative stress in nitrosamine-mediated degeneration in a mouse model. However, nothing is known about the effect of Au-NP treatment on locomotor dysfunction caused by DEN, an important carcinogen in mice. We aim to test whether Au-NP can attenuate DEN-induced locomotor activity changes of mice by focusing on oxidative damage.

Material Method: Mature male BALB/c mice were housed in properly ventilated mouse cages and maintained at the appropriate ambient temperature ($24 \pm 1^\circ\text{C}$) under 12:12 light/dark phases. It was fed with standard laboratory chow and water. It was planned to divide them into four groups of six animals each. Group-I was determined as the control allowed to be fed with normal diet, Group II, III and IV mice were given three times intraperitoneal injection (i.p) of 0.1 ml of saline containing 100 mg/kg DEN. Group III and IV rats were given 5 $\mu\text{g/g/day}$ and 10 $\mu\text{g/g/day}$ of Au-NP's orally by gavage, respectively. It was tested for locomotor measurements followed by biochemistry analysis.

Results: According to the results we obtained, the resting time was 38% and the total distance was 4895,708 cm in the control group. In the + control group exposed to DEN, these values were found to be 65% and 2093,25%, respectively. In the Au-NP's groups, these values approached the control group depending on the dose. While 5 $\mu\text{g/g/day}$ was 56% and 3431,234, these values were found to be 43% and 4021,778 at 10 $\mu\text{g/g/day}$ doses. Similarly, the oxidation level was highest in the DEN group, while the antioxidant level was found to be significantly higher in the other groups. GSH and LDH results showed correlation the other results. All results were compared with the positive control group and were found to be statistically significant ($P < 0.05$).

Keywords: Au-NP's, BALB/c, DEN

Introduction

Nano chemistry is a rapidly growing field of research in the chemistry empire nowadays. Nanoparticles including noble metals such as gold (Au), platinum (Pt) and silver (Ag) are used for drug synthesis and as drug delivery systems (1). In particular, gold nanoparticles (AuNPs) have a number of physical properties that make them attractive for medical applications, such as being biocompatible and non-toxic (2). Also, AuNPs have been demonstrated to own important antioxidant properties. It was also declared AuNP alleviates oxidative damage, in part by decreasing the inducible nitric oxygen synthase expression and improvement of antioxidant enzymes activity (3-5). Together, the above-mentioned pharmacological properties of AuNP have greatly contributed to their success in the treatment of several different animal models of disease in which oxidative stress play major roles, such as, sepsis and Alzheimer's disease (3,6).

N-nitroso compounds are potent, broad-acting carcinogens. Nitrosamine-mediated injury and mutagenesis is severely affected by route of application, dose, chemical nature of the compound, and frequency of exposure (7). The parenteral or oral administration of the smallest quantities of diethylnitrosamine (DEN) targets the liver primarily and generates reactive oxygen species such as superoxide (O_2^-) and hydrogen peroxide (H_2O_2), and thereby increase oxidative stress, DNA damage, lipid peroxidation, and protein adduct formation (8). Liver failure affects brain function, leading to neurological behavioral alterations including disrupted locomotor activity rhythm (9). Recording locomotor activity patterns is a widely used method to analyze behavioral functions in experimental animals after treatment protocols have been implemented (10).

However, nothing is known regarding the effect of AuNP treatment in locomotor dysfunction caused by DEN, an important carcinogen in mice. We aim to test whether AuNP can alleviate the changes of locomotor activity caused by DEN of mice, with focus on oxidative damage

Material-Method

Nanoparticles

Gold nanoparticles were obtained by green synthesis method.

Animals and Treatments

Mature male BALB/c mice (aged 8 weeks; 27 ± 1.3 g) were acquired from Experimental Animal Laboratory of the Medicine and Experimental Application and Research Center of Ataturk University (Erzurum, Turkey). Animals were housed in properly aerated mice cages and maintained at environmental temperature ($24 \pm 1^\circ C$) under a regulated 12:12 light/dark phases. They were fed with standard laboratory feed and water ad libitum. Ethical permission was obtained from Atatürk University, Faculty of Veterinary Medicine.

Experimental Design

24 mice were assigned into four groups of six animals each. Group-1 served as control allowed for feed the normal diet. Group II, III, and IV mice applied an intraperitoneal injection (i.p) of 0.1 ml of saline containing 100 mg/kg DEN three times (11). To the groups III, and IV rats, AuNPs were given at $5 \mu g/g/day$ and $10 \mu g/g/day$ orally by gavage, respectively. The dosage of all rats was given for 15 days according to their designated experimental oral doses. All rats were tested for locomotor measurements and then used for biochemistry analysis.

Locomotor Activity

The locomotor activity was investigated in an open field cage. The apparatus was connected to a video system. The mice were initially placed into the center of the open field cage, and then the activity was monitored for 10 min. Total distance and resting time were determined (12).

Oxidative Stress Analysis

Biochemical analyze of Total Antioxidant Capacity (TAC) and Total Oxidant Status (TOS) were performed accordingly to the manufacturers' instructions (Rel Assay Diagnostics, Gaziantep, Turkey) (13-14).

GSH and LDH Analysis

GSH and LDH activity were performed accordingly to the manufacturers' instructions (Elabscience, İstanbul, Turkey).

Statistical Analysis

Statistical calculations were carried out using SPSS 22.0 software. To determine the statistical significance of the results, the one-way ANOVA test was applied. The differences between the groups were considered significant at $P < 0.05$.

Results

All results are shown in Figure 1. According to the results we obtained, the resting time was 38% and the total distance was 4895,708 cm in the control group. In the + control group exposed to DEN, these values were found to be 65% and 2093,25%, respectively. In the Au-NP's groups, these values approached the control group depending on the dose. While 5 $\mu\text{g/g/day}$ was 56% and 3431,234, these values were found to be 43% and 4021,778 at 10 $\mu\text{g/g/day}$ doses. Similarly, the oxidation level was highest in the DEN group (19,24), while the antioxidant level was found to be significantly higher in the other groups. GSH and LDH results showed correlation the other results. All results were compared with the positive control group and were found to be statistically significant ($P < 0.05$, $P < 0.01$)

Figure 1. a) Resting time results obtained as a result of locomotor activity test, b) Total distance results obtained as a result of locomotor activity test, c) Total antioxidant capacity results, d) Total oxidant status results, e) LDH results, f) GR results (*; $P < 0.05$ and ** $P < 0.01$)

Discussion

Today, Au-NPs have been widely used in nonmedicine. It is widely used in the targeting of many therapeutic agents, especially because they are both antioxidants and well transported (15). In our study, DEN-induced toxicity in mice was tried to be eliminated by utilizing the antioxidant properties of these nanoparticles. For this purpose, TAC, TOS, LDH and GR activities were examined after the application and the findings proved that the toxicity was reduced.

Most of the behavioral parameters exhibited by a living organism indicate a circadian rhythm. The daily rhythm can continue under stable environmental conditions. The study of locomotor activity in rodents is one of the most common methods used to monitor this endogenous timing system. Recent research has shown that locomotor activity and arousal affect both spontaneous activity and sensory evoked responses throughout mouse sensory cortices (16).

In our study, toxicity was tried to be eliminated by treatment with Au-NPs after DEN application and locomotor activity was tested. Although locomotor activity was observed to decrease after DEN application, it was shown in Figure 1.a and b that it increased in a dose-dependent manner with Au-NPs. Movement speed (Figure 1a) and movement time (Figure 1b) were observed to be faster in the Au-NPs

10 µg/ml group. Based on these results, we believe that the use of Au-NPs should become widespread against many toxic agents that we are exposed to in our daily lives. We think that AU encapsulated formulations of therapeutic agents, especially in the treatment of many diseases, will play an important role in the fight against that disease.

References

1. Al-Radadi, N. S., & Adam, S. I. (2020). Green biosynthesis of Pt-nanoparticles from Anbara fruits: Toxic and protective effects on CCl₄ induced hepatotoxicity in Wister rats. *Arabian Journal of Chemistry*, 13(2), 4386-4403.
2. Mieszawska, A. J., Mulder, W. J., Fayad, Z. A., & Cormode, D. P. (2013). Multifunctional gold nanoparticles for diagnosis and therapy of disease. *Molecular pharmaceutics*, 10(3), 831-847.
3. Muller, A. P., Ferreira, G. K., Pires, A. J., de Bem Silveira, G., de Souza, D. L., de Abreu Brandolfi, J., ... & Silveira, P. C. L. (2017). Gold nanoparticles prevent cognitive deficits, oxidative stress and inflammation in a rat model of sporadic dementia of Alzheimer's type. *Materials Science and Engineering: C*, 77, 476-483.
4. Ma, J. S., Kim, W. J., Kim, J. J., Kim, T. J., Ye, S. K., Song, M. D., ... & Lee, K. H. (2010). Gold nanoparticles attenuate LPS-induced NO production through the inhibition of NF-κB and IFN-β/STAT1 pathways in RAW264. 7 cells. *Nitric Oxide*, 23(3), 214-219.
5. Rizwan, H., Mohanta, J., Si, S., & Pal, A. (2017). Gold nanoparticles reduce high glucose-induced oxidative-nitrosative stress regulated inflammation and apoptosis via tuberin-mTOR/NF-κB pathways in macrophages. *International journal of nanomedicine*, 12, 5841.
6. Di Bella, D., Ferreira, J. P., Renee de Nazare, O. S., Echem, C., Milan, A., Akamine, E. H., ... & Rodrigues, S. F. (2021). Gold nanoparticles reduce inflammation in cerebral microvessels of mice with sepsis. *Journal of nanobiotechnology*, 19(1), 1-15.
7. de la Monte, S. M., & Tong, M. (2009). Mechanisms of nitrosamine-mediated neurodegeneration: potential relevance to sporadic Alzheimer's disease. *Journal of Alzheimer's Disease*, 17(4), 817-825.
8. Tolba, R., Kraus, T., Liedtke, C., Schwarz, M., & Weiskirchen, R. (2015). Diethylnitrosamine (DEN)-induced carcinogenic liver injury in mice. *Laboratory animals*, 49(1_suppl), 59-69.
9. Cheon, S. Y., & Song, J. (2021). The Association between Hepatic Encephalopathy and Diabetic Encephalopathy: The Brain-Liver Axis. *International Journal of Molecular Sciences*, 22(1), 463.
10. Hassan, S. A., Ali, A. A., Yassine, M., Sohn, D., Pfeffer, M., Jänicke, R. U., ... & von Gall, C. (2021). Relationship between locomotor activity rhythm and corticosterone levels during HCC development, progression, and treatment in a mouse model. *Journal of Pineal Research*, 70(3), e12724.
11. Lee, J., & Lim, K. T. (2012). SJSZ glycoprotein (38 kDa) prevents thymus atrophy and enhances expression of IL-2 and IL-12 in diethylnitrosamine-induced hepatocarcinogenesis. *International immunopharmacology*, 13(3), 362-369.
12. York, J. M., Blevins, N. A., McNeil, L. K., & Freund, G. G. (2013). Mouse short-and long-term locomotor activity analyzed by video tracking software. *Journal of visualized experiments: JoVE*, (76).
13. Erel, O. (2004). A novel automated direct measurement method for total antioxidant capacity using a new generation, more stable ABTS radical cation. *Clinical biochemistry*, 37(4), 277-285.
14. Erel, O. (2005). A new automated colorimetric method for measuring total oxidant status. *Clinical biochemistry*, 38(12), 1103-1111.
15. Zheng Y, Wu Y, Liu Y, Guo Z, Bai T, Zhou P, Wu J, Yang Q, Liu Z, Lu Z (2019). Intrinsic Effects of Gold Nanoparticles on Oxygen–Glucose Deprivation/Reperfusion Injury in Rat Cortical Neurons. *Neurochemical Research*, 44, 1549–1566.

Formulation and Cytotoxicity Evaluation of Ternary Complexes as Non-Viral Gene Delivery System

Büşra Cesur^{1,2}, Devrim Demir-Dora^{1,2,3}

¹ Akdeniz University, Faculty of Medicine, Department of Medical Pharmacology, Antalya, Turkey

² Akdeniz University, Faculty of Medicine, Department of Gene and Cell Therapy, Antalya, Turkey

³ Akdeniz University, Healty Sciences Institute, Department of Medical Biotechnology, Antalya, Turkey

ABSTRACT

Niosomes are non-ionic surfactant vesicles that become important non-viral gene delivery systems. They have advantages of low toxicity and easy production on a large scale. In this study it was aimed to develop ternary complexes of BPEI, pDNA and modified niosomes prepared by using linear polyethylenimine, low molecular weight chitosan and β -cyclodextrin polymers. Cytotoxic effects of these gene delivery systems were evaluated on HEK-293T cell line and β -cyclodextrin niosomes and niopolyplexes were found as the most safest gene delivery systems.

Keywords: gene delivery, nonviral vectors, niosomes, niopolyplexes, cytotoxicity.

INTRODUCTION

The human embryonic kidney HEK-293T cell line are typically used for gene therapy cell culture assays. Developing safe gene delivery vectors are important for gene therapy purposes. Although the drawbacks of using viral vectors are its immunogenicity and cytotoxicity, nonviral vectors have less cytotoxicity, Niosomes known as bilayer structure have many applications in nanomedicine, including cosmetics, drug delivery and gene therapy. Niosomes are non-ionic surfactant vesicles which are more stable and less toxic than liposomes. Hydrophilic, hydrophobic or amphiphilic compounds can be loaded into niosomes [1, 2]. In this study, we have developed and evaluated the cytotoxicity of ternary complexes of branched polyethylenimine (BPEI), pDNA and modified niosome prepared by using linear polyethylenimine (LPEI), low molecular weight chitosan (LMWC) and β -cyclodextrin (β -CD).

MATERIALS AND METHODS

Materials

Span 40, cholesterol, low molecular weight chitosan (LMWC) and β -Cyclodextrin (β -CD) were purchased from Sigma & Aldrich. Linear polyethylenimine (LPEI) was purchased from Polysciences. LV-RFP pDNA was purchased from Addgene. DNA molecular weight marker 1 kb DNA ladder was purchased from Thermo. DMEM cell culture medium, MTT, fetal bovine serum (FBS) and trypsin were purchased from Sigma & Aldrich. LB broth media was obtained from Sigma & Aldrich. HEK 293T cell line were supplied by American Type

Culture Collection (ATCC). All other chemicals used were of analytical grade and were obtained from Sigma & Aldrich.

Plasmid DNA Isolation

pLV-RFP pDNA was amplified using *E. coli* DH5 α strain and purified by using QIAGEN Plasmid Maxi Kit. pDNA was checked by 1% agarose gel electrophoresis and concentration of DNA was determined by measuring UV absorbance at 260 and 280 nm.

Preparation of Niosomes

Niosomes were prepared by thin film hydration technique and niosome formulation was modified by using non ionic surfactant, cholesterol and different polymers (LPEI, LMWC, β -CD) at molar ratios of 20Mm: 20Mm: 10Mm, respectively. Span 40 was used as non ionic surfactant which have HLB value of 6,7. LPEI, LMWC and β -CD were used as polymers respectively. Cholesterol, surfactant and polymers were dissolved in chloroform. The organic solvent was then removed above the lipid transition temperature by using a rotary evaporator at 60°C, low pressure, leaving a thin layer of solid mixture deposited on the flask. The dried surfactant film was hydrated with 1 mL deionized water at 60°C. Vesicle size was reduced by sonication for 15 minutes and by using ultrasonic homogenizator for 30 minutes. Niosome formulations modified by using LPEI, LMWC and β -CD were coded as N₁, N₂ and N₃ respectively and characterized with respect to vesicle size, zeta potential and polydispersity index.

Preparation of Niopolyplexes

Ternary complex of modified niosome, polycation and pDNA, has been developed as a second generation non-viral gene delivery vector [3]. First generation gene delivery vector polyplexes were prepared by mixing the cationic branched polyethyleneimine (BPEI) with the anionic pLV-RFP plasmid DNA at 1:1w/w ratio. And then modified niosomes and polyplexes at a ratio of 1:1 (w/w) were incubated for 30 minutes at room temperature for electrostatic interaction and DNA binding was checked by 1% (w/v) agarose gel electrophoresis.

Zeta Potential and Vesicle Size Analysis of Niosomes

The hydrodynamic diameter of the niosomes were determined by Dynamic Light Scattering (DLS) using a Zetasizer (Malvern Zetasizer ZEN3600). All modified niosomes (N₁, N₂, N₃) were measured at room temperature in triplicate for vesicle size and zeta potential analysis.

In vitro cytotoxicity assay

Cytotoxicity of modified niosomes (N₁, N₂, N₃) were determined by MTT [(3-(4, 5-dimethylthiazol-2-yl)-2, 5-diphenyl-tetrazolium bromide blue-indicator dye]-based assay. HEK-293T cells were seeded in 96 well plates at a density of 7,000 cells per well. After 24 h incubation at 37 °C in 5% CO₂ atmosphere, the culture medium was replaced with fresh medium alone (negative control) or containing various amounts of each formulation and incubated for 48 h. Following each incubation time, MTT solution was added to each well and the cells were further incubated at 37 °C for another 4 h. After that, the culture medium was replaced with isopropanol to dissolve formazan crystals. The optical density of each well was read at 570 and 630 nm using a microplate reader.

RESULTS AND DISCUSSION

Gel Retardation Assay of Niosome Formulations

DNA binding ability of modified niosome and niopolyplex formulations were checked by 1 % (w/v) agarose gel electrophoresis. Although pDNA was not complexed by N₁, N₂, N₃ niosomes (Figure 1), it was retarded by niopolyplexes (Figure 2).

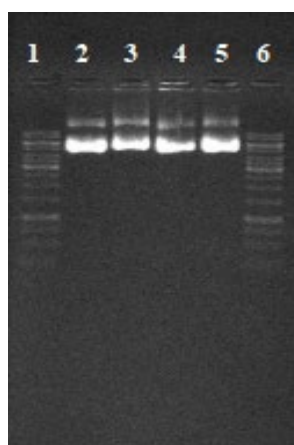


Figure 1. Gel retardation assay photograph of niosomes.

1. 1 kb DNA molecular weight standard
2. Naked pDNA (7539 bp)
3. N₁: pDNA
4. N₂: pDNA
5. N₃: pDNA
6. 1 kb DNA molecular weight standard, respectively.

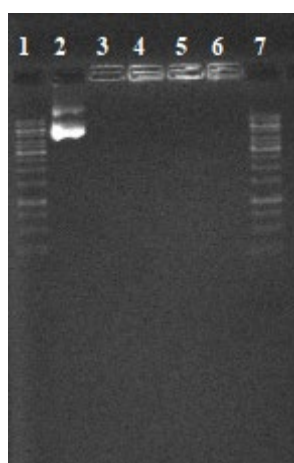


Figure 2. Gel retardation assay photograph of niopolyplexes.

1. 1 kb DNA molecular weight standard
2. Naked pDNA (7539 bp)
3. BPEI: pDNA
4. N₁ niopolyplex
5. N₂ niopolyplex
6. N₃ niopolyplex
7. 1 kb DNA molecular weight standard, respectively.

Zeta Potential and Vesicle Size Analysis of Niosomes

Vesicle size, zeta potential and PDI values of N₁, N₂ and N₃ niosomes are seen in Table 1. Zeta potential and vesicle size of the niosomes were effected by type of polymers. While the smallest vesicle sized niosomes were obtained by using LPEI, the biggest vesicle sized niosomes were obtained by using β -CD. According to PDI results the most favorable niosome was N₁ prepared by LPEI.

Table 1. Vesicle size, zeta potential and PDI values of niosomes.

Sample Code	Zeta Potential (mV)	Vesicle Size (nm)	PDI
N ₁	-15 ± 3,8	185,1 ± 3,4	0,346
N ₂	-11,9 ± 2,4	203,4 ± 4,3	1
N ₃	-15,2 ± 2,8	232,2 ± 4,2	0,61

In vitro cytotoxicity assay

Niosomes formulations and only polymers were examined on HEK-293T cells for evaluation of their cytotoxic effects (Figure 3 and Figure 4). Although LMWC and β -CD were found

toxic on HEK-293T cells, preparation of modified niosomes by these polymers have increased the cell viability. However β -CD was found the most cytotoxic polymer, modified niosome N₃ was the less cytotoxic niosome as seen from Figure 3.

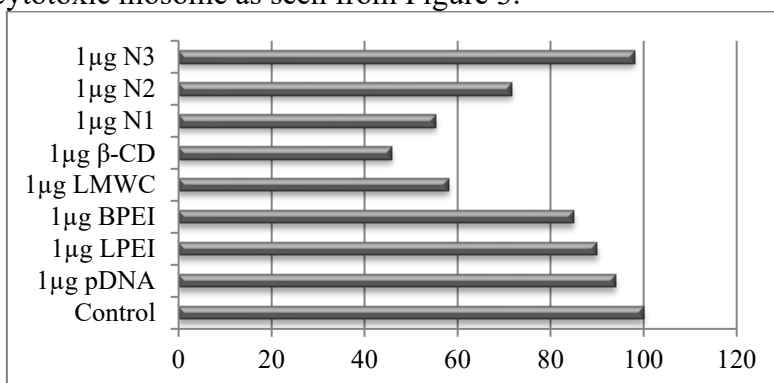


Figure 3. HEK 293T % cells proliferation (polymers and N₁, N₂, N₃ niosomes).

As seen from the Figure 4, formation of niopolyplexes affected the cytotoxicity of niosomes and only polymers. Although modified niosome prepared by using LPEI (N₁) was the most cytotoxic delivery system, formulation of N₁ niopolyplexes decreased the cytotoxicity on HEK-293T cell line. Ternary complex formation of β -CD niopolyplexes (N₃) has no effect on cytotoxicity of N₃ niosomes and N₃ niopolyplexes was found the most safe gene delivery system. LMWC niopolyplexes were found the most cytotoxic gene delivery system (Figure 4).

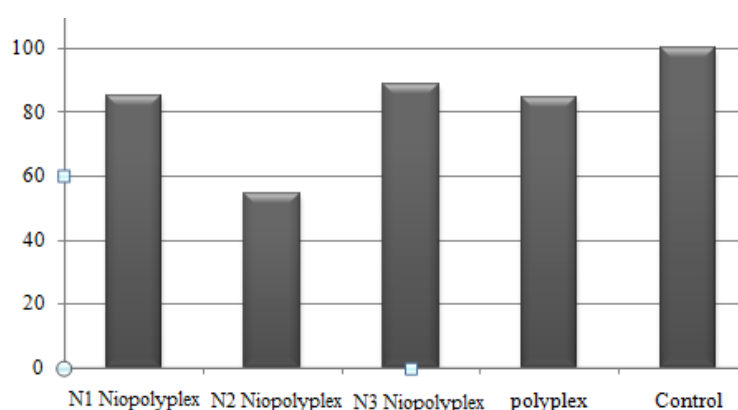


Figure 4. HEK-293T % cells proliferation (polyplex and N₁, N₂, N₃ niopolyplexes).

CONCLUSION

In this study, we aimed on development of new niosome formulations for gene delivery. Formulations developed in this study have favorable vesicle size for plasmid DNA delivery. Considering all the data as obtained, it was observed that different polymers have different effects on the vesicle sizes, zeta potentials, and toxic effects of the modified niosomes prepared with the non-ionic surfactant Span 40. Niopolyplexes combining the advantages of polyplex and niosomes have reduced cytotoxicity of LPEI niosomes N₁ by the time has no effect on cytotoxicity of β -CD niosomes N₃ but increased cytotoxicity of LMWC niosomes N₂. β -CD niosomes and niopolyplexes N₃ were observed as the most safest gene delivery systems.

REFERENCES:

1. Zu, H. and Gao, D.. Non-viral Vectors in Gene Therapy: Recent Development, Challenges, and Prospects. *The AAPS Journal*, 2021; 23(4), 1-12.

2. Cesur, B., and Demir-Dora, D. Non-biological complex drugs. *Türk Hijyen ve Deneysel Biyoloji Dergisi*, 2019;76(2), 221-228.
3. Chen, W., Li, H., et al. Lipopolyplex for therapeutic gene delivery and its application for the treatment of Parkinson's disease. *Frontiers in aging neuroscience*, 2016; 8, 68.

OP-12

Evaluation of Linear Polyplexes as Non-viral Gene Delivery Systems for Triple-negative Breast Cancer Cells

Devrim Demir-Dora^{1,2,3}, Feride Öner^{1,2}

¹ Akdeniz University, Faculty of Medicine, Department of Medical Pharmacology, 07070, Antalya, Turkey

² Akdeniz University, Faculty of Medicine, Department of Gene and Cell Therapy, 07070, Antalya, Turkey

³ Akdeniz University, Health Sciences Institute, Department of Medical Biotechnology, 07070, Antalya, Turkey

ABSTRACT

Gene therapy is one of the treatment options for triple-negative breast cancer. Non-viral polymeric delivery systems can be used for efficient delivery of genes into the nucleus. In our study 4T1 cell line was used as triple-negative breast cancer model and linear polyethylenimine polyplexes were prepared and evaluated in terms of transfection efficiency and cytotoxicity as non-viral gene delivery system. L2 polyplexes with a ratio of LPEI:pDNA 2:1 (w:w) were found the most optimal ratio for LV-RFP plasmid DNA and triple-negative mouse breast cancer cell line 4T1, in terms of high transfection efficiency and low cytotoxicity.

INTRODUCTION

Triple-negative breast cancer is an invasive type of breast cancer that lacks of receptors estrogen (ER), progesterone (PR), or HER2 (1). It has limited treatment options one of which is gene therapy. Gene therapy success depends on the efficient delivery of therapeutic genes into the target cells. Genetic materials such as pDNA and RNA can be delivered by viral or non-viral vectors and viral or non-viral vectors can be used to deliver genes efficiently into the cell nucleus or cytoplasm (2,3). Polyethyleneimine (PEI) is an efficient polycationic non-viral gene delivery vector which has good DNA binding capacity (4,5). 4T1 cell line is widely used as triple-negative breast cancer model.

The aim of this study was the development of a polymeric DNA delivery system with high transfection efficiency and low cytotoxicity into triple-negative mouse breast cancer cell line 4T1 .

MATERIALS AND METHODS

Materials

Linear polyethyleneimine (LPEI) (Polysciences, Inc Cat. No. 23966 ~25.000 mw) was used as cationic polymer. LV-RFP plasmid DNA was purchased from Addgene, 26001. Triple-negative mouse breast cancer cell line 4T1 was from ATCC. All other chemicals were of analytical grade.

Methods

Plasmid DNA Isolation

Plasmid DNA (Plasmid 26001:LV-RFP) was amplified by using *E. coli* DH5 α strain and purified by using QIAGEN maxi kit. The purity and concentration of DNA was determined by measuring UV absorbance at 260 and 280 nm. Electrophoretic mobility of plasmid DNA was checked by 1% (w/v) agarose gel electrophoresis.

Preparation of Linear Polyethyleneimine: pDNA Polyplexes

1 mg/ml linear polyethyleneimine (LPEI) solution was prepared in distilled water and adjust to pH 7.0. LV RFP pDNA was used at 1 μ g/ μ l concentration. LPEI/pDNA complexes were freshly prepared at different w/w ratios. Linear polyethylenimine (LPEI) and pDNA were mixed at increasing weight:weight (w:w) ratios of polyethylenimine as 1:1, 2:1, 3:1, 4:1, 5:1 and 6:1, and coded as L1, L2, L3, L4, L5 and L6 respectively. pDNA is added on LPEI solution and after mixing, incubated at 37°C for 30 minutes to form complexes. pDNA binding ability of linear polyethylenimine solution were checked by 1% (w/v) agarose gel electrophoresis.

In Vitro Transfection Studies

Triple-negative mouse breast cancer cell line 4T1 was used for transfection studies. 4T1 cells were seeded into the 96 well plate at a density of 5x10³ cells/well, cultured for 18h before transfection. LPEI:pDNA polyplexes were freshly prepared at different weight ratio of 1:1, 2:1, 3:1, 4:1, 5:1 and 6:1, respectively. Polyplexes were incubated for 4h at 37°C and then DMEM was replaced with fresh DMEM. After 24., 48. and 72. hours, fluorescence signal was observed by the fluorescence microscope.

Cell Proliferation Assay (MTT Assay)

The MTT test is one of the methods used to test cell viability and proliferation. The basis of the method is based on the measurement of metabolic activities of living cells. Viable cells convert MTT in the medium into colored formazan crystals. For the MTT test, MTT solution in the presence of medium was added to the cells cultured in 96-well culture dishes and incubated at 37°C for 4 hours. At the end of the time, the medium was removed and DMSO (Sigma D8418) was added, after 5 minutes of shaking, the absorbance was measured on the spectrophotometer at 570-640 nm.

RESULTS AND DISCUSSION

Preparation of Linear Polyethyleneimine: pDNA Polyplexes

pDNA binding ability of LPEI were checked by 1% (w/v) agarose gel electrophoresis. Positively charged LPEI have provided electrostatic interaction with negatively charged pDNA.

As seen from the Figure 1, pDNA was complexed at all LPEI:pDNA (w/w) ratios.

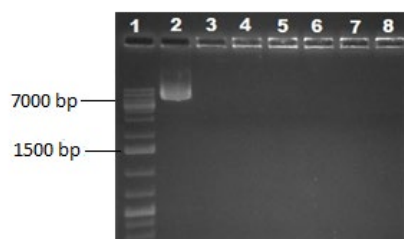


Figure 1: Agarose gel electrophoresis photograph of LPEI:pDNA polyplexes

Sample 1: DNA molecular weight standard (1 kb plus DNA ladder Thermo)

Sample 2: Naked plasmid DNA (LV-RFP)

Sample 3: LPEI:pDNA 1:1 (w:w)

Sample 4: LPEI:pDNA 2:1 (w:w)

Sample 5: LPEI:pDNA 3:1 (w:w)

Sample 6: LPEI:pDNA 4:1 (w:w)

Sample 7: LPEI:pDNA 5:1 (w:w)

Sample 8: LPEI:pDNA 6:1 (w:w)

In Vitro Transfection Studies

Transfection was achieved by all ratios of LPEI:pDNA polyplexes on triple-negative mouse breast cancer cell line 4T1, moreover the most efficient transfection were observed by L2 and L3 polyplexes.

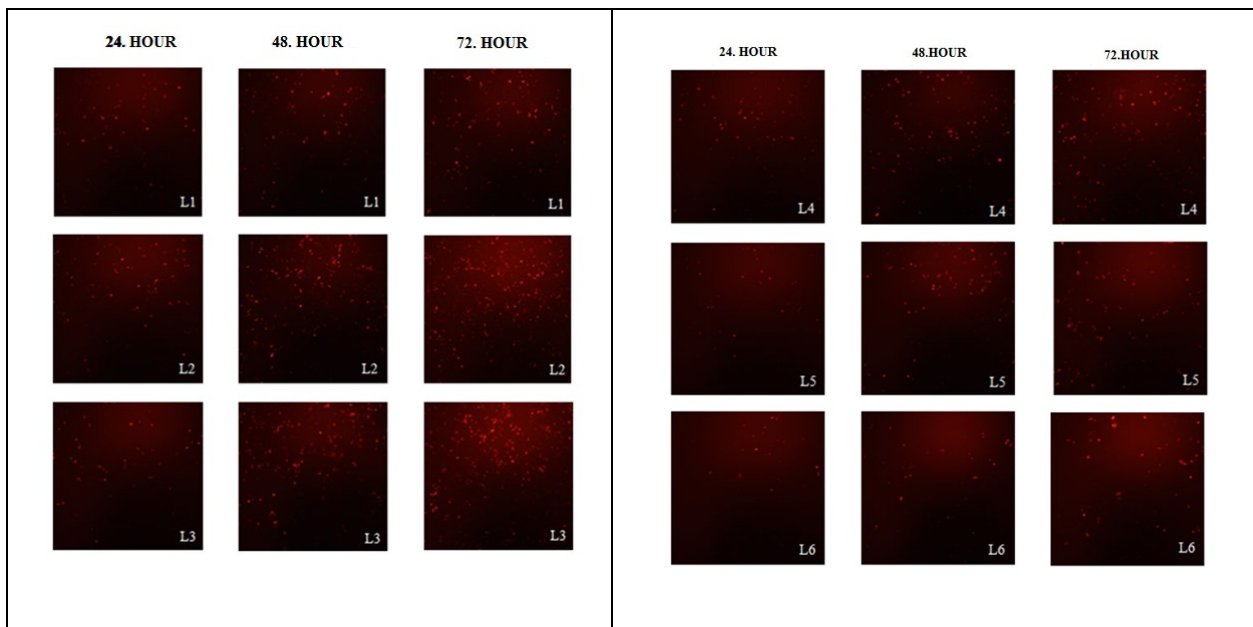


Figure 2: Fluorescence microscopy photographs of 4T1 cells transfected with polyplexes

Cell Proliferation Assay of LPEI:pDNA Polyplexes

Cytotoxicity of LPEI:pDNA polyplexes on triple-negative mouse breast cancer cell line 4T1 were evaluated and the less cytotoxic polyplex were found L1 and L2. On the other hand the most cytotoxic polyplex was found L6 because of increasing polymer ratio.

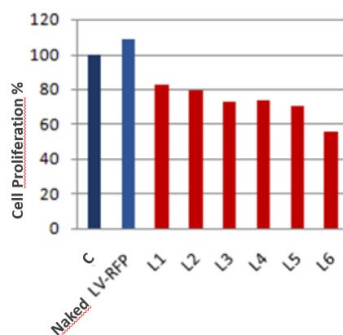


Figure 3: Cytotoxicity of LPEI:pDNA polyplexes on 4T1 cell line

Conclusion

Extracellular and intracellular barriers such as serum proteins, nuclease enzymes are responsible for the degradation or aggregation of the DNA in the circulatory system. Cationic polyplexes can keep the integrity of the genetic material which is to be transported to the cell nucleus and therefore can be used as gene delivery systems. Positively charged polyethyleneimine can interact electrostaticly with negatively charged pDNA. Determination of cytotoxicity is important for nucleic acid delivery systems. Linear polyethyleneimine is toxic at increasing concentrations, affecting cell viability. In our study, L2 polyplexes with a ratio of LPEI:pDNA 2:1 (w:w) were found a more optimal gene delivery system than the other polyplexes for LV-RFP plasmid DNA and triple-negative mouse breast cancer cell line 4T1, in terms of high transfection efficiency and low cytotoxicity.

REFERENCES

1. Chavez KJ, Garimella SV ,Lipkowitz S. “Triple negative breast cancer cell lines: one tool in the search for better treatment of triple negative breast cancer” *Breast disease*, 2010, 32, 1-2, 35
2. Demir-Dora D. Non-viral delivery systems for gene therapy. In: Bağcı G, ed., *Recent Developments in Gene and Cell Therapy*, 1st Edition, Ankara: Türkiye Klinikleri; 2021. p.20-6.
3. Durymanov M., Reineke j., “Non Viral Delivery Nucleic Acids: Insight Into Mechanisms of Overcoming Intracellular Barriers”, *Frontiers in Pharmacology*, August 2018, Volume 9, Article 971
4. Devrim Demir Dora, Feride Öner, ‘PEI-Polyplex Mediated Delivery of STAT3-shRNA pDNA into Triple-Negative Breast Cancer Cells’ 19th International Pharmaceutical Technology Symposium, IPTS Proceedings, pp98-99, 17-19 September 2018, Antalya 2018.
5. Sadeghpour H., Khalvati B., Entezar-Almahdi E., Savadi N., Alhashemi S.H., Raoufi M., Dehshahri A. “Double domain polyethylenimine based nanoparticles for integrin receptor mediated delivery of plasmid DNA” *Scientific Reports*, 2018, 8:6842

OP-13

COVID-19: Endogenous Retinoic Acid Theory and Retinoic Acid Depletion Syndrome.

Sarohan AR¹

Author information

Medical Hypotheses, 10 Sep 2020, 144:110250

DOI: [10.1016/j.mehy.2020.110250](https://doi.org/10.1016/j.mehy.2020.110250) PMID: 33254555 PMCID: PMC7481114

Free to read & use [Share with email](#) [Share with twitter](#) [Share with linkedin](#) [Share with facebook](#)

Abstract

This study presents two new concepts and definitions to the medical literature. One of those is "endogenous retinoic acid theory" and the other "retinoic acid depletion syndrome". A new classification will be provided for the immune system: "retinoic acid-dependent component" and "retinoic acid non-dependent component". If this theory is verified, all the diseases where the retinoic acid metabolism is defective and retinoic acid levels are low will be identified and new approaches will be developed for treating such diseases. When the need for retinoic acids increases, such as acute infection, high fever, severe catabolic process, or chronic antigenic stimulation, cytochrome oxidase enzymes are inhibited by drugs or internal mechanisms. Metabolism and excretion of retinoic acids stored in the liver are prevented. In this way, retinoic acid levels in the blood are raised to therapeutic levels. This is called "Endogenous Retinoic Acid Theory". Retinoic acids also manage their metabolism through feedback mechanisms. Despite compensatory mechanisms, causes such as high fever, serious catabolic process and excessively large viral genome (SARS-CoV-2), excessive use of RIG-I and Type I interferon synthesis pathway using retinoic acid causes emptying of retinoic acid stores. As a result, the RIG-I pathway becomes ineffective, Type I IFN synthesis stops, and the congenital immune system collapses. Then the immune mechanism passes to TLR3, TLR7, TLR8, TLR9, MDA5 and UPS pathways in the monocyte, macrophage, neutrophil and dendritic cells of the adaptive immune defense system that do not require retinoic acid. This leads to excessive TNF α and cytokine discharge from the pathway. With the depletion of retinoic acid stores as a result of this overuse, the immune defense mechanism switches from the congenital immune system to the adaptive immune system, where retinoic acids cannot be used. As a result of this depletion of retinoic acids, the shift of the immune system to the NF κ B arm, which causes excessive cytokine release, is called "retinoic acid depletion syndrome". COVID-19 and previously defined sepsis, SIRS and ARDS are each retinoic acid depletion syndrome. We claim that retinoic acid metabolism is defective in most inflammatory diseases, particularly COVID-19 (cytokine storm) sepsis, SIRS and ARDS. Finding a solution to this mechanism will bring a new perspective and treatment approach to such diseases.

Free full text

Med Hypotheses. 2020 Nov; 144: 110250.

Published online 2020 Sep 10. doi: [10.1016/j.mehy.2020.110250](https://doi.org/10.1016/j.mehy.2020.110250)

PMCID: PMC7481114

PMID: [33254555](https://pubmed.ncbi.nlm.nih.gov/33254555/)

COVID-19: Endogenous Retinoic Acid Theory and Retinoic Acid Depletion Syndrome

[Aziz Rodan Sarohan](#)

[Author information](#) [Article notes](#) [Copyright and License information](#)

This article has been [cited by](#) other articles in PMC.

Associated Data

[Supplementary Materials](#)

Introduction

In this study, the pathophysiological processes involved in COVID-19 and retinoic acid metabolism were examined. The indispensable role of retinol (vitamin A-retinoic acid) in the immune system is clearly demonstrated here. Based on the literature findings and observations, it is understood that retinoic acids have a central regulatory function in the immune system. This study reveals the central and indispensable regulatory role of retinoic acids on key molecules such as Type-I IFN synthesis, transcription factors, DNA and proteasomes. Everything that happens in the periphery depends on whether the retinoic acid regulation in the center is working properly. Considering in terms of structure and function, retinol (vitamin A) is not only a vitamin but also a hormone. In fact, retinol is a major hormone and regulator of the immune system. Zinc plays a role as a cofactor in the functioning of retinol in the immune system.

Retinol is converted into active RA derivatives such as all-trans RA, 9-Cis trans RA and 13-Cis trans RA by taking it into the cell in cases where the need for host increases such as acute infection. These active derivatives of retinol mediate the synthesis of Type-I IFN, the most powerful antiviral mediator of host defense, through nuclear retinoic acid receptors (RAR and RXR). Synthesized Type-I IFN (α and β) cleans the virus from the body by strengthening the cellular and humoral immune system. It also allows the development of a permanent immune response against the virus. Once the hypothesis asserted here is supported with clinical studies, the scientific community will agree that vitamin A deserves the definition of growth factor or hormone A, which was its designation when it was first discovered. Most importantly, we will have a new and simple option for the treatment of COVID-19.

The reason that this mechanism was not noticed until now was the assumption that retinoic acid, which is an endogenous ligand, can always be found in the medium. However, the amount of retinoic

acid in the human body is limited and is approximately at levels that can last for three months for a person [1]. Retinoic acid can be consumed rapidly due to reasons such as extreme viral load, high fever and extreme catabolic degradation, particularly continuous and long RIG-I stimulation. Retinoic acids can also limit biological effects very rapidly due being metabolized prevalently and rapidly [1] [2]. Retinoic acid metabolism is performed by the cytochrome P450 (CYP26) enzymes [2] [3] [4]. High fever observed in acute infections, extreme catabolic process, the extremely large genome as in SARS-CoV-2 and heavy viral load lead to fast depletion of the retinoic acids stored in the liver. Retinoic acid levels have previously been found to be severely reduced and depleted during viral infections such as measles and RVS [5] [6] [7].

The Hypothesis: Endogenous retinoic acid theory and retinoic acid depletion syndrome

This study presents two new concepts and definitions of medical literature. One is “*endogenous retinoic acid theory*” and the other is “*retinoic acid depletion syndrome*”. With this study; the immune system will obtain a new classification as “retinoic acid-dependent component” and “retinoic acid non-dependent component”. Moreover, it will provide a new perspective for other viral infections, particularly in the treatment of COVID-19, and certain bacterial infectious diseases, immune system and autoimmune diseases, vaccine and adjuvant molecules, sepsis and cytokine storm, allograft reactions degenerative neurological diseases and cancer physiopathology.

When the need for retinoic acids such as acute infection increases. With drugs or internal mechanisms, liver cytochrome oxidase enzymes are inhibited and excretion of retinoic acids stored in the liver is prevented. In this way, raising retinoic acids to therapeutic levels is called “*Endogenous Retinoic Acid Theory*” (TERA). Retinoic acids also manage their own metabolisms with feedback mechanisms. Despite such compensatory mechanisms, the retinol stores of the body quickly get depleted as a result of overuse of the RIG-I pathway, which includes retinoic acid receptors, due to reasons such as high fever, severe catabolic process and oversized viral genome (SARS-CoV-2). As a result, the RIG-I pathway is passivized and the immune defense mechanism shifts to the TLR3, TLR7, TLR8, TLR9, MDA5 and UPS pathways found in neutrophil, macrophage and dendritic cells belonging to the adaptive immune component elements, and causes over-discharge of cytokine (cytokine storm) through the NFκB arm. Such over immune response results in severe clinical presentations. Retinoic acid stores get quickly depleted as a result of overuse of retinoic acids in the RIG-I pathway and the Type-I Interferon synthesis pathway. Then the immune defense mechanism shifts to the NFκB pathway, where retinoic acid cannot be used and which results in cytokine release, is called “*Retinoic Acid Depletion Syndrome*” (RADS).

Such over-release of cytokine causes severe clinical presentations that may further lead to endothelial damage, hypoxia, necrosis and multiorgan damage (cytokine storm, SIRS, ARDS). COVID-19 and the previously described sepsis, SIRS and ARDS and many inflammatory events are each a retinoic acid depletion syndrome.

We claim that retinoic acid metabolism is defective in COVID-19 (cytokine storm) and most inflammatory diseases such as sepsis, SIRS and ARDS. It is asserted that the RIG-I pathway does not function healthily and retinoic acid metabolism is defective in certain diseases such as severe viral and bacterial infection diseases, including COVID-19, chronic autoimmune diseases, sepsis, cytokine

storm, SIRS and ARDS and chronic degenerative neurological diseases. Finding a solution to this mechanism will require a new perspective and treatment approach to such diseases.

It is very easy to prove or disprove the thesis put forward here. It will be sufficient to examine the retinol levels in the serum of severe COVID-19 patients. Serum retinol levels of COVID-19 patients have not yet been studied anywhere in the world. Our clinical trial is still ongoing to determine serum retinol levels in COVID-19 patients. The symptoms and findings observed in COVID-19 patients that support this thesis will be listed below. COVID-19 patients have many entities, symptoms and findings regarding the regulation of endogenous retinoic acids. Most of these are currently based on observations. The findings observed particularly in COVID-19 patients with severe clinical presentation, dramatically resemble the symptoms and findings of vitamin A (retinol) deficiency.

COVID-19 pathogenesis and retinoic acid depletion syndrome

Caused by SARS-CoV-2, this disease was named as COVID-19 by the World Health Organization (WHO) and quickly spreads all over the world [8]. The COVID-19 outbreak was declared an epidemic by the World Health Organization after causing the death of tens of thousands of people [9]. Millions of people infected and more than 600,000 died in the outbreak [9][10]. Currently, there is no approved specific treatment for this virus yet. A vaccine is also not yet developed against the coronavirus. The COVID-19 epidemic is continuing to be a major problem for the whole world [8][11].

As COVID-19, the largest epidemic of modern times turned into a pandemic, an urgent search was started throughout the world for a therapeutic drug against COVID-19 to control the epidemic and decrease the high mortality rates. Due to the time-consuming processes of developing new medications, the fastest solution to this pandemic was the idea to reposition existing medications. This search put focus once again on vitamin A (retinol) and its active derivatives retinoic acids, which were used in the past during the measles epidemics but then got forgotten in time [5].

The congenital immune response of the host is important in controlling the infection. It achieves this through Type I interferon by increasing the immune response [14]. SARS-CoV-2 is an enveloped single-strand RNA virus with its largest genome. The genome size of RNA viruses is generally less than 10 kB, but the genome length of SARS-CoV-2 is 30 kB [12]. As the SARS-CoV-2 genome has a single-stranded RNA structure, the immune response developed against it essentially functions through RIG-I, which is the congenital immune system component [15]. RIG-I is the major receptor of the immune system that identifies viral, single-stranded RNA ligands [15][16]. RIG-I is activated after the viral RNA ligand binds [17][18]. The RIG-I pathway, which is the most studied and most well-known component of the congenital immune system, functions as dependent on retinoic acid [17][18].

Some viruses are recognized by the host as RIG-I dependent. These viruses include the West Nile virus, the Japanese Encephalitis virus, Influenza A virus, the Sendai virus, Flavivirus and Coronaviruses [15][16]. The extremely large size of the SARS-CoV-2 genome (30 kB) and high virulence, causes a lot more RNA fragments to be scattered from the virus when it is degraded during the defense of the host. Over-stimulation of RIG-I due to the high viral load also causes the retinoic acid stores of the body to rapidly deplete due to high fever and severe catabolic process. The RIG-I pathway, where viral ssRNA ligands are first recognized, retinoic acid and retinoic acid receptors are used are very important in viral infections and are perhaps the most active pathway in the body until retinoic acids are depleted.

The RIG-I pathway is deactivated after retinoic acids are depleted. In the following process, the immune mechanism shifts to the NF κ B pathway that causes over-release of TNF α and cytokine through neutrophil where retinoic acid is not used and the TLR3,TLR7,TLR8,TLR9, MDA5 receptors and UPS (ubiquitin/proteasome system) pathways in the macrophage and dendritic cells. Over-discharge of TNF α and cytokine (cytokine storm) takes place with the activation of this mechanism. The UPS degradation mechanism gains activity in the absence of retinoic acids. UPS degradation covers are opened.

During SARS-CoV-2 infection, IL-1 α is transported and released on the cell surface due to apoptosis and inflammation. It initiates sterile inflammation in adjacent cells. Other chemokines released from macrophages due to viral replication or inflammation is required for IL-1 β release. After binding to IL-1 α and IL-1 β receptors, they stimulate the release of inflammatory cytokines and TNF- α via the NF- κ B pathway. IL-1 release; It causes fever, hyperferritinemia, vasodilation, hematopoiesis inhibition, as well as the release of chemokines, acute phase proteins, adhesion molecules and cytokines, especially IL-6. IL-6 plays a central role in cytokine storm [21].

Chemokines are chemotactic cytokines generated by leukocytes and other cell types. Chemokines are a large molecule family that direct leucocytes to the infection area and play a role in lymphocyte migration. IL5, IL-8, IL-10 and granulocyte–macrophage-colony stimulating factor (GM-CSF) also continuously increase during the cytokine storm and play a role in the emergence of the pathological response [20] [21].

In COVID-19, the reason why the disease was very mild in some people and very severe in others is thought to be related to the amount of retinol previously stored in the patient's liver. Whether there is enough retinol in the patient's liver seems to be an effective factor in the patient's response to the disease. In COVID-19, the falling levels of retinoic acids, which are rapidly depleted in the body, and the resulting excessive cytokine release syndrome, are responsible for most of the disease, severe clinical and symptoms. Two separate clinical studies from Egypt reported to the US NIH clinical trials are underway to determine the effectiveness of Isotretinoin, a retinoic acid derivative, in COVID-19 [22].

COVID-19, retinoic acids, ocular and nervous system

The clinical picture, which is common in severe COVID-19 patients and is referred to as “pink eye” [23] [24], is nothing more than conjunctivitis seen in severe vitamin A deficiency. Most likely, retinitis and other vision problems in these patients also develop due to atrophy and necrosis caused by a lack of retinoic acid in nerve cells in the retina.

Although attempts are made to explain the taste and olfactory disorders in COVID-19 patients with ACE2 receptors it is clear that it takes place through retinoic acid receptors [25]. It is interesting that vitamin A deficiency also leads to taste and olfactory disorders. This also suggest that vitamin A deficiency also develops in COVID-19. The findings and symptoms that arise in the nervous system and eyes of COVID-19 patients are nothing but the results of retinoic acid deficiency manifested through retinoid acid receptors.

Dizziness, headache, impaired consciousness, acute cerebrovascular disorder, ataxia and epilepsy are observed in COVID-19 patients as central nervous system involvement and hypogeusia, hyposmia, hypopsia and neuralgia are observed as peripheral nervous system involvement. Muscle involvement was also observed in patients [26] [54]. Acute hemorrhagic necrotizing encephalopathy cases related to COVID-19 were also reported. Hypodensity in bilateral medial thalamuses was observed in the unenhanced cranial BT taken in the patients [35]. Likewise, this area is one where

retinoic acid receptors are densely located [27]. The first Guillain-Barré syndrome that could be related to COVID-19 was reported by Zhao et al [28].

Retinoic acids play a central role in increasing neuroplasticity and neurogenesis. Retinoic acids are vital for hippocampus and the hypothalamus that control memory and alertness. All-trans retinoic acid (atRA) can be created from the retinoic acid in the brain. This is important for long-term potentiation (LTP). Vitamin A deficiency also causes circadian dysfunction. Cognitive dysfunction is also frequently observed [27] [29].

Components of the metabolic pathways for retinoids have been clearly defined for the adult brain [29]. All-trans-retinoic acid was shown to be synthesizable in certain areas of the brain. Certain neuronal-specific genes contain recognition sequences for retinoid receptors and can be arranged directly by retinoids. Retinoid receptors have a prevalent distribution in the adult nervous system. This distribution is different from that observed during embryonic development and suggests that retinoid signaling could play a physiological role in the adult cortex, amygdala, hypothalamus hippocampus, striatum and related areas of the brain [29] [34].

Disruption of retinoid signal pathways in rodent models resulted in disruption in synaptic plasticity, learning and memory behaviors. Retinoid signal pathways also play a role in the pathophysiology of Alzheimer's disease, schizophrenia and depression [29].

COVID-19, retinoic acids and ARDS

SARS-CoV-2 binds to the receptors on the alveolar and gastrointestinal epithelium cells and activates these cells in the natural and acquired immune system to cause the release of high amounts of cytokines, particularly IL-6 [20] [21]. The inflammatory response generated by the over cytokine release observed with T-cell and monocyte/macrophage activation causes an increase in vascular permeability and exudative liquid accumulation in the alveoli and thereby cause release (ARDS). Multiorgan damages and cardiovascular complications are added to the clinical presentation as the situation gets more severe (SIRS) [20] [21] [36].

In COVID-19, development of ARDS is essentially associated with inflammatory cytokine release and the exudative liquid accumulation that is caused as a result. The effect should also not be ignored on ARDS pathogenesis of the lack of retinol derivatives lecithin, colin and inositol in the medium and the potential disruption of surfactant synthesis, subject to depletion of retinoic acids in the body due to severe catabolic status and severe infection. These retinol derivatives that have a significant place in the structure of surfactant are important topics that need to be investigated regarding the development and severity of the ARDS presentation.

Surfactant deficiency has a very significant ratio in Respiratory Distress Syndrome (RDS) observed in newborns. Respiratory distress syndrome observed in newborns due to surfactant insufficiency constitutes one-fourth of the infant mortalities in developed countries [38]. Death due to pneumonia in newborn measles was shown to be reduced by 50% with vitamin A fortification, for the first time in 1952 [5]. The function of lecithin, colin and inositol synthesized from vitamin A and added to the structure of surfactant in reducing deaths caused by pneumonia should be taken into consideration. Retinoids play key roles in the formation and continued functioning of lung alveoli. Retinoids must play a role in the functioning of the mature lung because they are proving to be pharmacologically useful in treating certain lung diseases. The lung is a major tissue for the storage of retinol as retinyl esters. Exogenous RA can stimulate retinol uptake and storage in the lung; for example, when neonatal rats were treated with retinol combined with retinoic acid (RA; 9-*cis*-RA; Am580, an analog of RA) lung

retinyl esters increased approximately 5–7 times more than after an equal amount of retinol alone. Thus, retinoids are stored in the lung and active retinoids regulate the level of precursor storage [39].

COVID-19, retinoic acids and autoimmunity

Toll Like receptors recognize molecules bound to the pathogen and cause pathogen-specific innate and adaptive immune responses in the host. These receptors can also be stimulated by host DNA and RNA fragments released as a result of apoptosis or due to lysis of infected cells or mitochondria degradation [40] [41]. Of the 11 TLRs identified in humans, TLR3, TLR7, TLR8 and TLR9 are expressed in endolysosomes. These recognize viral DNA, RNA and synthetic nucleic acids [20] [41]. Tol-like receptors constitute the TIR (Toll-IL-1) receptor area with the interleukin-1 receptors. RA (atRA), plays a role in immune homeostasis in a steady state. However, atRA activates pathogenic T cells under inflammation conditions. Thus, atRA induces effector T cell responses also during infections or autoimmune diseases [42].

The adaptive immune system cells case TNF α and inflammatory cytokine discharge through NF κ B over the TLR3, TLR7, TLR8, TLR9 MDA5 and UPS pathways found in monocyte, macrophage and dendritic cells [20] [41]. The TLR7, TLR8, TLR9 and MDA5 receptors located in the neutrophil, macrophage and dendritic cells of the adaptive immune system, were determined to recognize the self-DNA fragments of the host in autoimmune diseases such as lupus, psoriasis, arthritis and multiple sclerosis [43]. This mechanism triggers the release of pro-inflammatory cytokines that contribute to the autoimmune disease pathogenesis [43].

It could be considered that the reason for observing autoimmune diseases such as Kawasaki in COVID-19 is related to this mechanism. Clarification of the pathophysiological mechanism here will be instructive for us in the treatment of tens of autoimmune diseases, particularly Type-I diabetes. The first Guillain-Barré syndrome that could be related to COVID-19 was reported by Zhao et al [28]. It is suspected that the fibrinogen and heat shock proteins (HSP) of the host bind to the toll-like receptors [44]. This may increase the tendency to thrombosis in addition to hypoxia and endothelial damage in COVID-19.

Toll-like receptors (TLR3, TLR7 and TLR8) play an important role in the activation of the immune system and their agonists can thus function as promising vaccine adjuvants. However, TLR over-stimulation causes chronic immune activation [45]. The presentation of SSPE after the measles vaccine may be a dramatic clinical picture that develops through the retinoic acid receptors in the brain as a result of the depletion of retinoic acids as a result of continuous stimulation of the RIG-I or TLR pathway with vaccine antigens. The reason for this thought is that the antigen is able to constantly stimulate receptors, and the measles virus lowers vitamin A (retinoic acid) levels during infection.

It is predicted that if retinoic acid levels are at normal limits and the RIG-I pathway functions healthily, endogenous antigens of the host can be prevented from being presented to the TLR7, TLR8, TLR9, MDA5 receptors and UPS pathway of the adaptive immune system. It can be that failure of the RIG-I pathway to function healthily or defective retinoic acid metabolism may play a role in the pathophysiological process in autoimmune diseases.

Retinoic acids and inhibitors of retinoic acid metabolism are used in dermatological diseases such as ichthyosis and psoriasis and good results are obtained. Similarly, these observations and evaluations suggest that retinoic acid metabolism may be defective in such dermatological diseases [2] [31].

COVID-19, RIG-I and retinoic acid depletion syndrome mechanism

RIG-I (retinoic acid-inducible gene-1) and MDA-5 (melanoma differentiation-associated gene-5) are cytoplasmic RNA helicases. RIG-I, as the name implies, is a cytosolic receptor synthesized due to retinoic acids. Critical for antiviral responses in the host. RIG-I is an important molecule in the innate immune system for identifying the viruses inside the cell.

Coronaviruses are recognized by the host as dependent on RIG-I [15] [16] [18]. The RIG-I pathway, which is the most studied and most well-known component of the congenital immune system, functions as dependent on retinoic acid [18]. RIG-I is the major receptor of the immune system that identifies viral, single-stranded RNA ligands. RIG-I is activated after the viral RNA ligand binds [17] [18]. This activation also activates retinoic acid receptors and initiates its own (RIG-I) synthesis from the DNA DDX58 promoter gene area. At the same time as the activation of RIG-I, the immune defense cascade that leads up to Type-I IFN release also starts to operate [18].

The RAR and RXR receptors, which mediate the nuclear transcription of RIG-I, the most important pathway in the immune response developed against single-stranded RNA viruses, get activated with retinoic acid. Retinoic acid receptors (RXR/RAR) are not active before retinoic acid binds [17] [22]. Retinoic acid increases RIG-I synthesis and activity by binding to the DNA through the nuclear receptors [18] [22].

Apart from the RIG-I synthesis step, another mechanism that consumes retinoic acid in the cell is the stages in which Type-I interferon is synthesized by CREB (cyclicAMP-response element binding protein) and kinase activation. In the CREB stage, retinoic acid participates in interferon synthesis through retinoic acid receptors in the structure of transcription factors. In the kinase activation phase, retinoic acids can provide interferon synthesis by kinase activation without the need for a transcription complex [13]. Apart from the RIG-I synthesis step, excessive use of these two pathways also consumes retinoic acids. Another way in which retinoic acids are used and consumed is UPS suppression. Retinoic acids inhibit NFκB activation by preventing degradation [33].

RIG-I and MDA-5 also detect double-stranded RNA (dsRNA) which is a replication intermediate substance for RNA viruses [17] [18]. SsRNA viruses (such as SARS-CoV-2) are typically not detected as ssRNA but are detected through intermittent replication products in the form of dsRNA [17] [15]. The dsRNA ligand may come from single-stranded RNA (ssRNA) or double-stranded RNA (dsRNA) viruses [18] [15]. RIG-I can also detect a dsRNA copied from dsDNA by a DNA-dependent RNA polymerase III (Pol III) [46] [47]. Some DNA viruses are identified by RIG-I through this mechanism. The identification of certain DNA viruses including HSV-1, EBV, VACV and Adenovirus by the host also depends on RIG-I through this mechanism [46] [47].

The viral 5' dsRNA terminal acts as a RIG-I stimulant [48]. 5'-diphosphateRNA (5' ppRNA) fragments found in viruses increase the expression of RIG-I by binding to RIG-I in in-vitro environments [18]. 5' ppp RNA sequences (RIG-I agonists) synthesized through transcription or chemical synthesis were shown to provide better RIG-I activation [18] [49]. These agonists have broad-spectrum antiviral potential. They can also be optimized as vaccine adjuvants [50] [51]. 5'-triphosphate RNA is a strong ligand for RIG-I [49].

Viral RNA ligand starts an inflammatory response through RIG-I. Upon binding of the RNA ligand to RIG-I, RIG-I undergoes a series of conformational and posttranslational changes to ensure full activation. Double helix RNA viruses are identified through RIG-I and IPS-1(interferon promotor stimulator-1) [18]. The short double helix triphosphate RNA pattern (5' pppRNA/dsRNA) located in the

Viral RNA 5'-terminal, binds to the RIG-I to activate the mitochondrial adapter protein, the mitochondrial antiviral signaling protein and IPS-1 (interferon promotor stimulator / RIG-I adapter trigger). These activated mediators activate the primary immune defense by initiating Type-I IFN and proinflammatory cytokine release. With the interaction between RIG-I, and ASC and Caspase-1 from another path and the stimulation of IL β 1 release, adapter proteins ensure that the activation of CARD-9, Bcl10, Mitochondrial antiviral signal protein (MAVS) and nuclear factor kappaB (NF- κ B) [18]. This arm, which increases inflammation, works when retinoic acid is exhausted.

When retinoic acid is depleted due to the extremely large RNA genome, high fever and severe catabolic process, the RIG-I and IPS-1 pathway, which are components of the congenital immune defense system, cease to function and the mechanism shifts to adaptive immune system cells to continue with the NF κ B pathway through neutrophil, macrophage and dendritic cells. This results in release of TNF α and inflammatory cytokine.

However, if retinoic acid is present, the mechanism will continue to produce Type-I IFN *via* RIG-I / IRF3-7. And these changes result in an increase in the release of Type-I IFN. After Type-I Interferons (IFN-I; IFN α and IFN β) leave the cell, they bind to the IFN-I receptors on the surface of the cell they came from or other proximal cell receptors [52]. This increases antiviral activity and ensures that more IFN-I is produced. IFN-I also activates the JAK-STAT pathways and increases the expression of the genes stimulated with IFN (ISGs) [52].

Type-I IFNs have three main functions. They prevent the virus from multiplying and limit its spread to host cells. It induces the natural immune response, the especially cytotoxic effect on the virus through inflammatory responses. In particular, it activates secondary immune responses that result in a permanent immune response [52] [53]. In some COVID-19 patients, the cause of inadequate antibody response may be due to retinol depletion. Adequate antibody response does not occur as a result of both cellular and humoral immune system collapse as a result of the discontinuation of Type-I IFN synthesis.

The RIG-I pathway, where viral ssRNA ligands are first recognized and retinoic acid and retinoic acid receptors used is very important in viral infections and is perhaps the most active pathway in the body until retinoic acids are depleted. Overstimulation of RIG-I due to the high viral load also causes the retinoic acid stores of the body to rapidly deplete due to high fever and severe catabolic process.

The RIG-I pathway is deactivated after retinoic acids are depleted. In the following process, the immune mechanism shifts to the NF κ B arm, which causes TNF α and excessive cytokine release *via* TLR3, TLR7, TLR8, TLR9, MDA5 and UPS pathways of the neutrophil, macrophage and dendritic cells of the adaptive immune system without retinoic acid. Over-discharge of TNF α and cytokine (cytokine storm) takes place with the activation of this mechanism.

Another mechanism that aggravates the picture is that host DNA and RNA fragments from apoptosis and mitochondria lysis cause excessive cytokine discharge from the NF κ B arm through adaptive immune system cells with MDA5 and TLR3, TLR7, TLR8, TLR8, TLR9 receptors. This is due to toll receptors and MDA5 can also be stimulated by DNA fragments released as a result of apoptosis or due to lysis of infected cells or mitochondria degradation [17] [41]. This vicious cycle aggravates the situation even further.

Vitamin A deficiency and viral infections

Vitamin A (Retinol) is required for the healthy functioning of the immune system. Decreased vitamin A during infection weakens the host defense. The level of vitamin A drops even further particularly during viral infections [37].

Infectious diseases depress circulating retinol and contribute to vitamin A depletion. Enteric infections may alter the absorptive surface area, compete for absorption-binding sites, and increase urinary loss. Febrile systemic infections also increase urinary loss and metabolic utilization rates and may reduce apparent retinol stores if fever occurs frequently. A great deal of evidence supports an association of Vitamin A Deficiency (VAD) with the severity of infection once acquired, except for respiratory diseases, which are non-responsive to treatment. The severity of pneumonia associated with measles, however, is an exception because it decreases with the treatment of vitamin A supplementation. Measles virus infection is especially devastating to vitamin A metabolism, adversely interfering with both efficiencies of utilization and conservation [55].

Vitamin A deficiency significantly increases mortality in measles. Vitamin A deficiency is an important problem that impacts millions of children in developing countries. Vitamin A deficiency can be considered to be reported only in third-world countries, however, in a study conducted in California, vitamin A deficiency was found in 50% of the children with measles. The mortality rate in newborns was shown to be reducible by 50% with vitamin A fortification, for the first time in 1932 [5] [37].

Respiratory Syncytial Virus (RSV) is today the most frequently encountered virus that causes infection in the respiratory tract. It is a very frequent cause of respiratory diseases in small children. Vitamin A level is low in children infected with RSV. In addition, low vitamin A has a relation with the disease similar to that mentioned for measles [7]. Vitamin A treatment is an effective option in newborn RSV infections. This is because it is a low-cost, prevalent, applicable and readily available treatment [7]. Vitamin A deficiency increases mortality in AIDS. Vitamin A replacement also provides benefit for other infections in AIDS. Vitamin A deficiency is encountered frequently in HIV infection. This deficiency is related to the adjuvant T lymphocyte decrease in circulation, which is distinctive for HIV. Vitamin A deficiency increases mortality in AIDS [56].

The World Health Organization (WHO) gives high-dose (200,000 I.U.) vitamin A supplements as prophylactic to children once every six months to prevent vitamin A deficiency in underdeveloped countries [57]. The risk of measles is reduced due to the effective vaccination program. However, vitamin A treatment is an important requirement in the treatment of other viral infections during childhood [5].

The level of vitamin A decreases significantly in infections caused by the respiratory syncytial virus and the measles virus. These two viruses use the RIG-I pathway in the immune response mechanism of the host [17]. In addition, it should be noted that both of these viruses have single-stranded RNA like SARS-CoV-2.

Retinoic acid is obtained from tissues depending on the specific need of the cell. Retinol, which is one of the most active metabolites of retinoids, is found at a low concentration in the blood. The normal vitamin A (retinol) range is 28–86 $\mu\text{g} / \text{dL}$. Vitamin A deficiency is defined as serum retinol levels below 28 $\mu\text{g} / \text{dL}$ [55].

Retinoic acids, immun system and IgA

Malabsorption, protein-energy malnutrition, liver diseases, zinc deficiency, viral infections, high fever, severe catabolic process, hyperthyroidism and abetalipoproteinemia caused by bile acid or pancreatic disorders lead to vitamin A deficiency [19] [34] [57].

Infectious diseases that induce the acute-phase response also impair the assessment of vitamin A status by transiently depressing serum retinol concentrations. Vitamin A deficiency impairs innate immunity by impeding normal regeneration of mucosal barriers damaged by infection, and by diminishing the function of neutrophils, macrophages, and natural killer cells. Vitamin A is also required for adaptive immunity and plays a role in the development of T both-helper (Th) cells and B-cells. In particular, vitamin A deficiency diminishes antibody-mediated responses directed by Th2 cells, although some aspects of Th1-mediated immunity are also diminished [37]-[39].

Vitamin A deficiency is related to immune system failure. Its deficiency causes deterioration in effective antibody response, a decrease in the number of T-helper cells and a disruption in the mucous barrier of the gastrointestinal tract, genitourinary system and respiratory system [57].

Persons with vitamin A deficiency are more prone to infections and have higher mortality rates.

Furthermore, "vitamin A stores get depleted during the course of the infection" [55]-[57]. This causes a negative vicious cycle. The frequency of Measles, Chicken Pox, RSV, AIDS and pneumonia increase in vitamin A deficiency [57].

Vitamin A (retinol) is essential in ensuring the continuity of the functioning and integrity of skin and mucosal cells and defends the body against infections through the mucosal mechanical barrier and humoral IgA. Retinoic acids (RA), which are the active metabolite of vitamin A, are today considered as a significant factor in the normal development and regulation of the immune system [39]-[55].

Retinoic acid develops its role in the immune system through specific receptors. Carotenoids usually modulate T-cell proliferation. Increasing normal cell activity is another important objective of carotenoids. "Vitamin A deficiency increases sensitivity against diseases including measles, diarrhea and lung infections" [37].

RA stimulates the differentiation of adjuvant T-cells (Th2) and regulatory T-cells (Treg) and inhibits the differentiation of Th1 and Th17 [42]. RA also stimulates the differentiation of B-cells and ensures antibody production [58]. When retinoic acid is absent in the body, antibodies, especially Ig A, cannot be produced. One study showed that RA had an effect through RAR α , which directly affects IgA synthesis and secretion on B-cells [37]-[58]. The vitamin A metabolite atRA, plays a key role in mucosal immune responses. atRA also regulates the differentiation of the Foxp3 (+) regulating T-Cell (T-reg) and the Th17 effector T-Cell. Therefore, although atRA can be used as an effective "mucosal adjuvant" in vaccines, it is also considered as necessary for creating the gut immune tolerance [42]-[50]. All-trans RA (atRA), is produced in macrophage and dendritic cells that can express retinal dehydrogenase from vitamin A. atRA binds to nuclear retinoic acid receptors that are expressed in lymphoid cells and function as transcription factors to regulate cell homing and differentiation. atRA, which is produced by CD103 (+) dendritic cells and alveolar macrophages, induce the transformation of pure T-Cells into Foxp3 (+) regulating T-Cells and thereby, work with TGF γ to protect the mucosal tolerance [59]. atRA plays a role in immune homeostasis in a steady state. However, it activates pathogenic T cells under conditions of inflammation. Therefore, atRA induces effector T-Cell responses during infections or autoimmune diseases [42]. The possible reason for this is that atRa activates only the RAR receptor, whereas 9-Cis-RA can activate both RXR and RAR receptors. The role of retinoic acid in the production of immunoglobulin A could be presented as a result of a broad review consisting of 151 articles. Immunoglobulin A is inhibited in the lack of retinoic acid [60].

The current treatment of COVID-19 and the cytochrome P450 system

The cytochrome oxidase enzyme system (CYP450) is a system that is responsible for the metabolism and detoxification of the toxins and drugs particularly found in the endoplasmic reticulum of liver cells. Only three of these (CYP1, CYP2, CYP3) are responsible for drug metabolism [30]. CYP3A4 accounts for 40% of the cytochrome oxidase system and is the main mono-oxidase enzyme responsible for drug metabolism [30].

The P450 mono-oxidase system shows heterogeneity among humans. The activity of this enzymatic system varies between individuals and societies. This heterogeneity is the reason that the biotransformation of drugs and compounds differs among individuals and societies [30] [61]. The P450 system is an important area of drug-drug, drug-diet and drug-disease-condition interactions. The functional change in this system has significant consequences regarding an insufficient therapeutic response or increased toxicity. Selecting specific P450 enzymes when starting drug therapy will provide rational drug development, more effective clinical trial evaluation and better therapeutic approaches in patients requiring special attention [30] [61].

Enzyme synthesis increases when induction occurs in the P450 system. The biotransformation of the drug that metabolizes with this enzyme increases accordingly. The serum level thus decreases. As for inhibition, in contrast with induction, the enzyme synthesis decreases and the serum level of the concerned compound increases. Enzyme inhibition occurs very rapidly and the blood level of the metabolized drug quickly increases. In such a case, the pharmacological effects of the drug or endogenous compound increase [30] [61].

With the inhibition of the cytochrome oxidase system, the serum retinoic acid levels are increased by preventing the excretion of retinol esters previously stored in the liver and the retinoids taken with food. Retinoid acids increasing in the serum modulate the RIG-I pathway through nuclear receptors to operate the primary immune system [18] [22].

The mechanism of action of these drugs, particularly Hydroxychloroquine, used in the treatment of COVID-19, on SARS-CoV-2 is not clearly known. Therefore, although recovery is observed in patients, it is not certain that such recovery is directly related to these drugs. It is likely that such therapeutic efficacy is achieved by retinoic acid derivatives whose metabolism is halted and serum levels are increased as a result of inhibition of the cytochrome P450 oxidase system by the drugs used in the treatment. The real reason for success in cases with early treatment is also probably due to the prevention of the depletion of retinoic acid stores in the liver by early treatment.

All the drugs bound to a certain protocol by the COVID-19 Science and Advisory Board in our country, as in many countries throughout the world, and used in COVID-19 treatment, inhibit the cytochrome P450 system ([Table 1](#)). The table below shows the drugs included in the COVID-19 treatment protocol and their stimulation / inhibition status on the CYP P450 system.

Table 1

Drugs included in the COVID-19 treatment protocol and their stimulation / inhibition status on the CYP P450 system.

Drug	Cytochrome Enzyme-CYP			Sti. / Inh
Hydroxychloroquine	CYP2A4	CYP2C8		Inhibition SPS:refid::bib30 [30]
	CYPA5	CYP2D6	CYP3A4	
Lopinavir/Ritonavir	C CYP2D6	CYPC2-18	CYP3A4	Inhibition [30]
	CYP2A4	CYPC2-19	CYP2C9	
Favipiravir	OAT1/OAT3	CYP2C8	P-GP	Inhibition [32]

Drug	Cytochrome Enzyme-CYP	Sti. / Inh
	CYP2E1	
Oseltamivir		CYP3A4 Inhibition [30]
Clarithromycin	CYP2D6	CYP3A4 Inhibition [30]

The results of the studies conducted on Remdesivir in the USA were disclosed recently. A success ratio of 30% is mentioned there for Remdesivir in -American society [36]. The study conducted in China found this drug to be unsuccessful against COVID-19 [36]. The likely reason for this is the cytochrome P450 system that varies in terms of activity among individuals and societies.

Alcohol (Ethanol), decreases serum levels by increasing the metabolism of retinoic acids by stimulating cytochrome oxidase enzymes. In this respect, the use of alcohol has a negative impact on COVID-19 prognosis. Ethanol activates the P450 system while red wine inhibits it [30]. French people were consuming high amounts of red wine on the first days of the COVID-19 pandemic. It was stated that red wine (not white wine) consumption protected people from COVID-19 and that it was even good for the patients. This has some truth to it due to two reasons. Red wine inhibits the cytochrome P450 system through CYP3A4 and also the flavonoids in red wine have a similar structure to retinoic acids and can show a regulatory effect on the immune system [30] [61].

The reason why COVID-19 progresses more in males than females (ignoring smoking) is that the cytochrome oxidase system is less inhibited in males than females. This is because estradiol inhibits the P450 system much more effectively and prevalently with respect to testosterone. Estradiol inhibits CYP1A2, CYP2A6, CYP3A4 whereas testosterone only inhibits CYP2D6 [30] [62].

Conclusion

An effective immune response against RNA viruses proceeds based on the innate primary immune system and the adaptive immune system. The first path here is the innate immune system mediated by RIG-I, which functions as dependent on retinoic acids and proceeds through retinoic acid receptors (RXR-RAR). Retinoic acids are used in the regulation of this mechanism. The second path is the adaptive immune system which does not include retinoic acids but includes TLR3, TLR7, TLR8, TLR9 and MDA5 receptors in the neutrophil, monocyte, macrophage and dendritic cells in the lungs and guts and continues through NFκB to result in TNFα and over cytokine release.

Another way is UPS-NFκB shunt. Here, retinoic acids inhibit proteasomal degradation *via* the UPS system. In case retinoic acids are depleted, this inhibition mechanism disappears and proteasomal degradation takes place. Proteasomal degradation causes NFκB activation and causes TNFα and excessive cytokine secretion.

According to the hypothesis, in acute situations such as severe infection, retinoic acids are depleted and the defense system of the host shifts into the adaptive immune system, which gives an acute and extremely inflammatory response. On the one side, the RIG-I / IRF3-7 pathway of the congenital immune system and the production of Type-I interferon, on the other side, the UPS-NFκB pathway of the adaptive regulatory immune system that secretes TNFα and cytokine, these two systems must be in balance. Production of Type-I interferon through the RIG-I and IRF3-7 pathway enhances strong immune defense and a permanent immune response in the host. If the balance shifts to the side of the UPS / NFκB and cytokine discharge, inflammatory pathogenetic mechanisms are triggered in the disease-causing host.

If a sufficient amount of retinoic acid is available in the body, the immune response developed against viruses will take place through the RIG-I pathway that belongs to the innate immune system. The healthy functioning of this pathway will clear the infectious agent from the body and improve the immune response through Type I IFN. Healthy functioning of this pathway is particularly dependent on the availability of a sufficient amount of retinoic acid derivatives. Having enough retinoic acid will provide permanent immunity. However, rapid depletion of retinoic acids in the body during the acute infection process leads to the response of the adaptive immune system. This leads to the development of severe and serious clinical presentations and complications that may result in death. Therefore, having enough retinol in the body is vital and necessary.

What provides the balance between these two systems? Does the metabolic defect of retinoic acids and depletion of endogenous retinoic acids disrupt this balance? Can replacing retinoic acids restore this impaired balance? The answer to these questions will provide an understanding of the pathogenesis of all acute and chronic, benign and malignant, inflammatory and granulomatous, autoimmune and degenerative diseases listed above, and perhaps offer us new and simpler treatment options.

In this case, all drugs and compounds that inhibit the liver cytochrome P450 oxidase system may be effective against COVID-19 by preventing retinoic acid metabolism. In fact, it is not difficult to predict that even Ketoconazole, which is used as an antifungal, can have significant efficacy in COVID-19 treatment as a strong cytochrome oxidase P450 inhibitor (if sufficient retinoic acid is available in the body) [30]. Retinoic acid metabolism inhibitors (RAMBA) that block endogenous retinoic acid metabolism and provide therapeutic efficacy by increasing endogenous retinoic acid levels in order to avoid the teratogen side effect of retinoic acids have started being used in dermatological indications in recent years [31]. Retinoic acids, zinc and RAMBAs may work against COVID-19, which continues with full intensity.

The evaluations and observations regarding the above mentioned retinoic acid metabolism also support our hypothesis about endogenous retinoic acids. Considering the fact that COVID-19 turned into a pandemic and the socio-economic consequences of the disease, the endogenous retinoic acid theory, the retinoic acid depletion syndrome that we assert and the information, findings and observations they are based on should not be ignored. An important conclusion to be drawn from this is the presence of much information, documents and observations that retinoic acid derivatives and zinc could be effective in the treatment of COVID-19. The success achieved with vitamin A in measles and other viral infections should be kept in mind. Therefore, it is necessary to focus on these drugs for COVID-19 treatment and urgently start clinical studies with these drugs. The inclusion of these drugs into the COVID-19 treatment protocol as a result of clinical studies will provide significant benefits both in terms of public health and socio-economic perspective.

The endogenous retinoic acid theory and retinoic acid depletion syndrome we obtained as a result of this study will be widely discussed in the medical community. There are almost no organ systems in the human body, without retinoic acids. For now, immune system-dependent retinoic acid mechanisms are highlighted. Studies on the retinoic acid mechanism of action will continue to increase in the coming years.

Declaration of Competing Interest

The authors declare that they have no known competing financial interests or personal relationships that could have appeared to influence the work reported in this paper.

Acknowledgments

I would like to thank Prof. Dr. Murat Kızıl, Assoc. Prof. Dr. Ahmet Çağan İnkaya and Dr. Muhittin Çelik who encouraged me for this work and they did not withhold his support during the writing phase.

Footnotes

Appendix A Supplementary data to this article can be found online at <https://doi.org/10.1016/j.mehy.2020.110250>.

Supplementary data Appendix A.

The following are the Supplementary data to this article:

Supplementary data 1:

[Click here to view](#) (1.0K, xml)

References

1. Blomhoff R., Blomhoff H.K. Overview of retinoid metabolism and function. *J Neurobiol.* 2006;66(7):606–630. [\[Abstract\]](#) [\[Google Scholar\]](#)
2. Catharine Ross A., Zolfaghari Reza. Cytochrome P450s in the regulation of cellular retinoic acid metabolism. *Annu Rev Nutr.* 2011 Aug;21(31):65–87. [\[Europe PMC free article\]](#) [\[Abstract\]](#) [\[Google Scholar\]](#)
3. Nelson C.H., Buttrick B.R., Isoherranen N. Therapeutic potential of the inhibition of the retinoic acid hydroxylases CYP26A1 and CYP26B1 by xenobiotics. *Curr Top Med Chem.* 2013;13(12):1402–1428. [\[Europe PMC free article\]](#) [\[Abstract\]](#) [\[Google Scholar\]](#)
4. Pelkonen O, Rautio A, Rauino H et.al. CYP2A6: a human coumarin 7-hydroxylase. *Toxicology.* 2000; 144(1-3): 139-147. [\[Abstract\]](#)
5. Huiming Y., Chaomin W., Meng M. Vitamin A for treating measles in children. *Cochrane Database Syst Rev.* 2005;2005(4):CD001479. [\[Europe PMC free article\]](#) [\[Abstract\]](#) [\[Google Scholar\]](#)
6. Ziad Al Tanoury, Aleksandr Piskunov and Cécile Rochette-Egly. Vitamin A and retinoid signaling: genomic and nongenomic effects. *J Lipid Res.*2013; 54: 1761–1775. [\[Europe PMC free article\]](#) [\[Abstract\]](#)
7. Dowell S.F., Papic Z., Bresee J.S., Larrañaga C., Mendez M., Sowell A.L., Gary H.E., Jr, Anderson L.J., Avendaño L.F. Treatment of respiratory syncytial virus infection with vitamin A: a randomized, placebo-controlled trial in Santiago. Chile. *Pediatr Infect Dis J.* 1996;15(9):782–786. [\[Abstract\]](#) [\[Google Scholar\]](#)
8. World Health Organization. Novel coronavirus situation report-2. <https://www.who>. January 22, 2020.

9. Park S.E. Epidemiology, virology, and clinical features of severe acute respiratory syndrome coronavirus-2 (SARS-CoV-2; Coronavirus Disease-19) Clin Exp Pediatr. 2020;63(4):119–124. [[Europe PMC free article](#)] [[Abstract](#)] [[Google Scholar](#)]
10. Lai C.C., Wang C.Y., Wang Y.H. Global epidemiology of coronavirus disease 2019 (COVID19): disease incidence, daily cumulative index, mortality, and their association with country healthcare resources and economic status. Int J Antimicrob Agents. 2020;19 [[Europe PMC free article](#)] [[Abstract](#)] [[Google Scholar](#)]
11. Canrong Wu, Yang Liu, Yueying Yang, Peng Zhang, Wu Zhong, Yali Wang, Qiqi Wang, Yang Xu, Mingxue Li. Analysis of therapeutic targets for SARS-CoV-2 and discovery of potential drugs by computational methods. Acta Pharm Sin B. 2020 Feb 27. [[Europe PMC free article](#)] [[Abstract](#)]
12. Chen Y, Liu Q, Guo D. Emerging coronaviruses: genome structure, replication and pathogenesis. J Med Virol. 2020 Apr; 92(4): 418-423. [[Europe PMC free article](#)] [[Abstract](#)]
13. Weaver B.K., Kumar K.P., Reich N.C. Affiliation Interferon Regulatory Factor 3 and CREB-binding protein/p300 Are Subunits of Double-Stranded RNA-activated Transcription Factor DRAF1. Mol Cell Biol. 1998;18(3):1359–1368. [[Europe PMC free article](#)] [[Abstract](#)] [[Google Scholar](#)]
14. Kaitlin J. Soye, Claire Trottier and Wilson H. Miller, Jr. RIG-I Is Required for the Inhibition of Measles Virus by Retinoids. PLoS One. 2011; 6(7): e22323. [[Europe PMC free article](#)] [[Abstract](#)]
15. Kell A.M., Gale M. RIG-I in RNA virus recognition. Virology. 2015;2015(479–480):110–121. [[Europe PMC free article](#)] [[Abstract](#)] [[Google Scholar](#)]
16. Solis M, Nakhaei P, Jalalirad M, Lacoste J, Douville R, Arguello M, et al. “RIG-I-mediated antiviral signaling is inhibited in HIV-1 infection by a protease-mediated sequestration of RIG-I”. Journal of Virology. February 2011; 85 (3): 1224–36. [[Europe PMC free article](#)] [[Abstract](#)]
17. Yoneyama M., Kikuchi M., Natsukawa T., Shinobu N., Imaizumi T. The RNA helicase RIG-I has an essential function in double-stranded RNA-induced innate antiviral responses. Nat Immunol. 2004;5:730–737. [[Abstract](#)] [[Google Scholar](#)]
18. Liu Yiliu, Olagnier David, Lin Rongtuan. Host and viral modulation of RIG-I-mediated antiviral immunity. Front Immunol Virol. January 2017;03(479–480):110–121. [[Google Scholar](#)]
19. Irwin J.J., Sterling T., Mysinger M.M., Bolstad E.S., Coleman R.G. ZINC: a free tool to discover chemistry for biology. J Chem Inf Model. 2012;52:1757–1768. [[Europe PMC free article](#)] [[Abstract](#)] [[Google Scholar](#)]
20. Doyle and O'Neill. Toll-like receptors: From the discovery of NFκB to new insights into transcriptional regulations in innate immunity. Biochemical Pharmacology. Volume 72, Issue 9, 2006; Pages: 1102-1113. [[Abstract](#)]
21. Zhang C, Wu Z, Li JW, Zhao H, et al. (2020). The cytokine release syndrome (CRS) of severe COVID19 and Interleukin-6 receptor (IL6R) antagonist Tocilizumab may be the key to reduce the mortality. Int J Antimicrob Agents. 2020 May; 55(5): 105954. [[Europe PMC free article](#)] [[Abstract](#)]
22. Allenby G., Bocquel M.T., Saunders M., Kazmer S., Speck J., Rosenberger M., Lovey A., Kastner P., Grippo J.F., Chambon P., Levin A.A. Retinoic acid receptors and retinoid X receptors: interactions

with endogenous retinoic acids. *Proc Natl Acad Sci USA*. 1993;90(1):30–34. [[Europe PMC free article](#)] [[Abstract](#)] [[Google Scholar](#)]

23. Francesca Colavita, Daniele Lapa, Fabrizio Carletti, Eleonora Lalle, Licia Bordi, Patrizia Marsella, Emanuele Nicastrì, Nazario Bevilacqua, Maria Letizia Giancola et al. SARS-CoV-2 Isolation From Ocular Secretions of a Patient With COVID-19 in Italy With Prolonged Viral RNA Detection. *Annals of Internal Medicine*. 2020. [[Europe PMC free article](#)] [[Abstract](#)]

24. Kiser Philip D., Golczak Marcin, Palczewski Krzysztof. Chemistry of the Retinoid (Visual) Cycle. *Chem Rev*. 2014;114(1):194–232. [[Europe PMC free article](#)] [[Abstract](#)] [[Google Scholar](#)]

25. Baig A.M., Khaleeq A., Ali U. Evidence of the COVID-19 virus targeting the CNS: tissue distribution, host-virus interaction, and proposed neurotropic mechanisms. *ACS Chem Neurosci*. 2020;11:995–998. [[Europe PMC free article](#)] [[Abstract](#)] [[Google Scholar](#)]

26. Guan W.J., Ni Z.Y., Liang W.H. Clinical characteristics of coronavirus disease 2019 in China. *N Engl J Med*. 2020;382:1708–1720. [[Europe PMC free article](#)] [[Abstract](#)] [[Google Scholar](#)]

27. Lorena S. Navigatore-Fonzo, RebecaL. Golini, IvanaT. Ponce, SilviaM. Delgado, Gabriela Plateo, María Sofia Gimenez and Ana Cecilia Anzulovich. Retinoic acid receptors move in time to the clock in the hippocampus. Effect of a vitamin A-deficient diet. *J NutrBiochem*. 2013 May; 24(5): 859–867. [[Europe PMC free article](#)] [[Abstract](#)]

28. Zhao H., Shen D., Zhou H. Guillain-Barré syndrome associated with SARS-CoV-2 infection: causality or coincidence? *Lancet Neurol*. 2020 May;19(5):383–384. [[Europe PMC free article](#)] [[Abstract](#)] [[Google Scholar](#)]

29. Lane MA, Bailey SJ. Role of retinoid signalling in the adult brain. *Prog Neurobiol*. 2005 Mar; 75(4): 275-93. [[Abstract](#)]

30. Yüksel Nevzat. Sitokrom P450 Sistemi ve İlaç Etkileşimleri. *J Clin Psy*. 2001;4(1):5–16. [[Google Scholar](#)]

31. Vahlquist, A, Blockhuys, S, Steijlen, P, Van Rossem, K, Didona, B, Blanco, D, Traupe, H. Oral liarozole in the treatment of patients with moderate/severe lamellar ichthyosis: results of a randomized, double-blind, multinational, placebo-controlled phase II/III trial. *Br J Dermatol*. 2013; 170 (1): 173–81. [[Europe PMC free article](#)] [[Abstract](#)]

32. <https://www.drugbank.ca/drugs/DB12466>.

33. Fang Yanfen, Zhou Xinglu, Lin Meihua, Ying Meidan, Luo Peihua. Inhibition of all-trans-retinoic acid-induced proteasome activation potentiates the differentiating effect of retinoid in acute myeloid leukemia cells. *Mol Carcinog*. 2011;50(1):24–35. [[Abstract](#)] [[Google Scholar](#)]

34. Morris Deborah R., Levenson Cathy W. Zinc regulation of transcriptional activity during retinoic acid-induced neuronal differentiation. *J NutrBiochem*. 2013;24(11):10.1016. [[Europe PMC free article](#)] [[Abstract](#)] [[Google Scholar](#)]

35. Poyiadji N., Shahin G., Noujaim D. COVID-19 associated Acute Hemorrhagic Necrotizing Encephalopathy: CT and MRI Features. *Radiology*. 2020;31 [[Google Scholar](#)]

36. Gilead Announces Results From Phase 3 Trial of Investigational Antiviral Remdesivir in Patients With Severe COVID-19 Study Demonstrates Similar Efficacy with 5. and 10. Day Dosing Durations of Remdesivir. Gilead Sciences, Inc. Apr. 29, 2020.
37. Zhiyi Huang, Yu Liu, Guangying Qi, David Brand, and Song Guo Zheng. Role of Vitamin A in the Immune System. *J Clin Med*. 2018 Sep 6;7(9):258. [[Europe PMC free article](#)] [[Abstract](#)]
38. Wirbelauer J., Speer C.P. The role of surfactant treatment in preterm infants and term newborns with acute respiratory distress syndrome. *J Perinatol*. 2009;29:S18–S22. [[Abstract](#)] [[Google Scholar](#)]
39. Gudas Lorraine J. Emerging Roles for Retinoids in Regeneration and Differentiation in Normal and Disease States. *Biochim Biophys Acta*. Author manuscript; available in PMC 2013 Jan 1. Published in final edited form as. *Biochim Biophys Acta*. 2012;1821(1):213–221. [[Europe PMC free article](#)] [[Abstract](#)] [[Google Scholar](#)]
40. Gebhardt A, Laudénbach BT, Pichlmair A. Discrimination of Self and Non-Self Ribonucleic Acids. *J Interferon Cytokine Res*. 2017 May; 37(5): 184-197. [[Europe PMC free article](#)] [[Abstract](#)]
41. Choe J., Kelker M, Wilson I. Crystal structure of human toll-like receptor 3 (TLR3) ectodomain. *Science*. 2005;309(5734):581–585. [[Abstract](#)] [[Google Scholar](#)]
42. Raverdeau Mathilde. Modulation of T cell and innate immune responses by retinoic acid. *J Immunol*. 2014;192(7):2953–2958. [[Abstract](#)] [[Google Scholar](#)]
43. Ling Kong, Lei Sun, Hongxin Zhang, Qin Liu, Ye Liu, Linhua Qin, Guojun Shi, Jun-Hao Hu, et al. An Essential Role for RIG-I in Toll-like Receptor-Stimulated Phagocytosis. *Cell Host & Microbe*. Volume 6, Issue 2, 20 August 2009; Pages: 150-161. [[Abstract](#)]
44. Chang Hong, Yu Dong-Sheng, Liu Xiu-Qin, Zhang Qiu-Ye, Cheng Na, Zhang Shou-Qing, Qu Zheng-Hai. Clinical significance of TLR3 and TLR4 in peripheral blood mononuclear cells from children with Henoch-Schönlein purpura nephritis. *Exp Ther Med*. 2014;7(6):1703–1707. [[Europe PMC free article](#)] [[Abstract](#)] [[Google Scholar](#)]
45. Nour Bou Karroum, Georges Moarbess, Jean-François Guichou, Pierre-Antoine Bonnet, Cindy Patinote. Novel and Selective TLR7 Antagonists Among the Imidazo[1,2-a]pyrazines, Imidazo[1,5-a]quinoxalines, and Pyrazolo[1,5-a]quinoxalines Series. *J Med Chem*. 2019 Aug 8; 62(15):7015-7031. [[Abstract](#)]
46. Melchjorsen J., Rintahaka J., Soby S., Horan K.A., Poltajainen A., Ostergaard L. Early innate recognition of herpes simplex virus in human primary macrophages is mediated via the MDA5/MAVS-dependent and MDA5/MAVS/RNA polymerase III-independent pathways. *J Virol*. 2010;84:11350–11358. [[Europe PMC free article](#)] [[Abstract](#)] [[Google Scholar](#)]
47. Chiu Y.H., Macmillan J.B., Chen Z.J. RNA polymerase III detects cytosolic DNA and induces type I interferons through the RIG-I pathway. *Cell*. 2009;138:576–591. [[Europe PMC free article](#)] [[Abstract](#)] [[Google Scholar](#)]
48. Weber M., Gawanbacht A., Habjan M., Rang A., Borner C., Schmidt A.M. Incoming RNA virus nucleocapsids containing a 5'-triphosphorylated genome activate RIG-I and antiviral signaling. *Cell Host Microbe*. 2013;13:336–346. [[Europe PMC free article](#)] [[Abstract](#)] [[Google Scholar](#)]
49. <https://www.invivogen.com/Products/3p-hprna>.

50. Hochheiser K., Klein M., Gottschalk C., Hoss F., Scheu S., Coch C. Cutting edge: The RIG-I ligand 3pRNA potently improves CTL cross-priming and facilitates antiviral vaccination. *J Immunol.* 2016;196:2439–2443. [[Abstract](#)] [[Google Scholar](#)]
51. Goubau D., Schlee M., Deddouche S., Puijssers A.J., Zillinger T., Goldeck M. Antiviral immunity via RIG-I-mediated recognition of RNA bearing 5'-diphosphates. *Nature.* 2014;514:372–375. [[Europe PMC free article](#)] [[Abstract](#)] [[Google Scholar](#)]
52. Ivashkiv LB, Donlin LT. Regulation of type I interferon responses. *Nature Rev Immunol.* January 2014; 14 (1): 36-49. [[Europe PMC free article](#)] [[Abstract](#)]
53. Platanius L.C. Mechanisms of type-I- and type-II-interferon-mediated signalling. *Nat Rev Immunol.* 2005;5:375–386. [[Abstract](#)] [[Google Scholar](#)]
54. Mao L., Wang M., Chen S. Neurological manifestations of hospitalized patients with COVID-19 in Wuhan, China: a retrospective case series study. *JAMA Neurol.* 2020;10 [[Google Scholar](#)]
55. FAO, WHO. Vitamin and mineral requirements in human nutrition, 2nd ed. Geneva, World Health Organization, 2004.
56. Mehta S., Fawzi W. Effects of vitamins, including vitamin A, on HIV/AIDS patients. *Vitam Horm.* 2007;75:355–383. [[Abstract](#)] [[Google Scholar](#)]
57. Martha Stipanuk Marie Caudill. Vitamin A, Biochemical, Physiological, & Molecular Aspects of Human Nutrition, Biochemical, Physiological, and Molecular Aspects of Human Nutrition. 3rd edition. March 2012. Page Count: 968.
58. Pantazi E, Marks E, Stolarczyk E, Lycke N, Noelle RJ, Elgueta R. Cutting edge: retinoic acid signaling in b cells is essential for oral immunization and microflora composition. *J Immunol.* 2015; 195: 1368–1371. [[Europe PMC free article](#)] [[Abstract](#)]
59. Cassani Barbara. Vitamin A and immune regulation: role of retinoic acid in gut-associated dendritic cell education, immune protection and tolerance. *Mol Aspects Med.* 2012;33(1):63–76. [[Europe PMC free article](#)] [[Abstract](#)] [[Google Scholar](#)]
60. Rodrigo Mora J., von Andrian Ulrich H. Role of retinoic acid in the imprinting of gut-homing IgA-secreting cells. *Semin Immunol.* 2009 Feb;21(1):28–35. [[Europe PMC free article](#)] [[Abstract](#)] [[Google Scholar](#)]
61. Danielson PB. The Cytochrome P450 Superfamily: Biochemistry, Evolution and Drug Metabolism in Humans. *Current Drug Metabolism.* Volume 3, Issue 6, 2002. [[Abstract](#)]
62. Khawja A Usmani, Jun Tang. Human Cytochrome P450: Metabolism of Testosterone by CYP3A4 and Inhibition by Ketoconazole. *CurrProtocToxicol.* 2004 Jun;Chapter 4:Unit4.13. [[Abstract](#)]

Single Guide RNA (sgRNA) Design and Off-target Determination for the Multidrug Resistance Gene-PDR1 from *Saccharomyces cerevisiae* with crispRdesignR Bioinformatic Application

Elif Çisem Çöldür¹, Devrim Demir-Dora^{1,2,3}

¹Department of Gene and Cell Therapy, Faculty of Medicine, Akdeniz University, 07070, Antalya, Turkey

²Department of Medical Pharmacology, Faculty of Medicine, Akdeniz University, 07070, Antalya, Turkey

³Department of Medical Biotechnology, Health Sciences Institute, Akdeniz University, 07070, Antalya, Turkey

INTRODUCTION

Clustered Regularly Interspaced Palindromic Repeats (CRISPR) and CRISPR-associated protein nuclease (Cas) constitute the CRISPR-Cas system which is commonly used in gene editing. Naturally, the CRISPR-Cas system is found in about 50% of bacteria and 90% of archaea as a prokaryotic adaptive immune system for invasive bacteriophages or plasmids [1]. CRISPR-Cas system has two main components which are namely Cas9 endonuclease and single-guide RNA (sgRNA). CRISPR-Cas system acts with the teamwork of these two component and sgRNA bind to Cas9 to form CRISPR-Cas9/sgRNA complex. Firstly, the target region of the DNA to be modified is found with help of target-specific sgRNA. After that, Cas9 endonuclease cut the target DNA region like a scissor. Then, double-strand breaks (DSB) are formed and they can be repaired by nonhomologous end-joining (NHEJ) pathway or homology-directed repair (HDR) pathway [2, 3]. However, Cas9 cleavage can occur at undesired locations in the genome which is defined as an off-target effect. When a different location in the DNA sequence contains some homology and few mismatches with sgRNA, off-target cleavage can occur. This off-target effect can lead to abnormal gene functions and lethal mutations [4]. The off-target effect can be reduced by choosing the best sgRNA targeting sequence with a lower off-target score [5, 6]. Therefore, using software to design sgRNA with minimum off-target effects is critical for the success of the CRISPR-Cas systems.

Various therapeutic applications like cancer immunotherapy, genetic diseases, or viral infections caused by different viruses such as Hepatitis B viruses (HBV) and Human immunodeficiency virus (HIV) are done by the CRISPR-Cas systems [1,7]. *Saccharomyces cerevisiae* can cause severe infections in patients with cancer, chronic disease and immunosuppression such as transplant recipients [8]. Moreover, severe clinical cases including pneumonia, endocarditis, fungemia, and infections of the skin and urinary tract that were caused by *Saccharomyces cerevisiae* were reported [9]. Therefore, the gene PDR1 that is known as pleiotropic drug resistance protein 1 from *Saccharomyces cerevisiae* was selected as the target sequence. Because this gene is responsible for multidrug resistance, gene editing of the gene PDR1 was considered for inhibit drug resistance [10]. Several tools exist for sgRNA design such as Synthego Design Tool, Broad Institute GPP sgRNA Designer, CHOPCHOP and CRISPR-Era Benchling CRISPR Guide RNA Design tool. However, some of these tools are available as online websites.

In this study it was aimed to design sgRNA and determine possible off-targets for the gene PDR1 from *Saccharomyces cerevisiae* by `crispRdesignR` tool in R. RGui and RStudio were used for this study to show that researchers can design their sgRNAs by using their simple codes with help of `crispRdesignR` apart from the patterns offered online.

MATERIALS AND METHODS

Materials

RGui and RStudio, the gene PDR1 sequence as FASTA format, the whole genome of *Saccharomyces cerevisiae* from BSgenome/Bioconductor, genome annotation file of *Saccharomyces cerevisiae* as gtf file from Ensembl.

Installation of RGui and RStudio

`crispRdesignR` tool works in the RGui and Rstudio programs. These programs have been downloaded to the computer from the link below:

<https://www.r-project.org/>

Installation of the gene PDR1 sequence (FASTA)

The gene PDR1 sequence was found on the National Center for Biotechnology Information website. PDR1 is written on the search button. Genomic regions, transcripts, and products tab was selected inside the full report of PDR1 drug-responsive transcription factor PDR1 [*Saccharomyces cerevisiae* S288C]. Then clicked send to and FASTA format was selected.

Installation whole genome of *Saccharomyces cerevisiae* (BSgenome/Bioconductor)

To install whole genome of *Saccharomyces cerevisiae*, the code was run in the R below:

```
#if (!requireNamespace("BiocManager", quietly = TRUE))
#install.packages("BiocManager")
#BiocManager::install("BSgenome.Scerevisiae.UCSC.sacCer2")
```

Installation of the genome annotation file of *Saccharomyces cerevisiae* as gtf file from Ensembl

The genome annotation file of *Saccharomyces cerevisiae* as gtf was loaded from Ensembl that was linked as: <https://www.ensembl.org/info/data/ftp/index.html>

`crispRdesignR`

The `crispRdesignR` was run in the RStudio program according to codes that were listed below:

```
#install.packages("seqinr")
#install.packages("crispRdesignR")
library(seqinr)
library(crispRdesignR)
data <- sgRNA_design("C:\\Users\\HP\\Downloads\\pdr1.fasta" ,
BSgenome.Scerevisiae.UCSC.sacCer2::BSgenome.Scerevisiae.UCSC.sacCer2,"C:/Users/HP/
Desktop/crispRdesignR-master/crispRdesignR-
```

master/example_data/Saccharomyces_cerevisiae.R64-1-1.92.gtf.gz", "NAG", calloffs = TRUE, annotateoffs = FALSE)

Then #data was written and all possible sgRNAs with off-target effects were listed in the console of R.

The crispRdesignR was run in the RGui program according to codes that were listed below:

```
#install.packages("seqinr")
#install.packages("crispRdesignR")
library(crispRdesignR)
crispRdesignRUI()
```

Then upload the fasta format file (PDR1) and your gtf file to the relevant field on the opening page. And clicked to find sgRNA and all possible sgRNAs with off-target effects were listed.

RESULTS

67 of sgRNA sequences were designed by using crispRdesignR and results were given in Table 1.

Table 1. Some sgRNA sequences that were designed by crispRdesignR

	sgRNA sequence	PAM	Direction	Start	End	GC content
1	CTAAGAACGGGTGACATATT	GAG	+	17	39	0.35
2	TATTGAGACGGGTCCGGATA	CAG	+	33	55	0.50
3	ACAGAATCGTCCGGGACTC	CAG	+	52	74	0.60
4	GGACTCCAGCAACTTTTCTA	CAG	+	66	88	0.45
5	AGCAACTTTTCTACAGGTTT	CAG	+	73	95	0.35
6	TTTCTACAGGTTTCAGCGGC	AAG	+	80	102	0.50
7	GTTTCAGCGGCAAGATTCGT	AAG	+	89	111	0.50
8	AGCGGCAAGATTCGTAAGCC	AAG	+	94	116	0.55
9	GATTCGTAAGCCAAGGTCGA	AAG	+	102	124	0.50
10	CGTAAGCCAAGGTCGAAAGT	AAG	+	106	128	0.50
11	GCCAAGGTCGAAAGTAAGTA	AAG	+	111	133	0.45
12	AGTAAAGCGTGCGATAACTG	TAG	+	127	149	0.45
13	GCGTGCGATAACTGTAGAAA	AAG	+	133	155	0.45
14	GCGATAACTGTAGAAAAAGA	AAG	+	137	159	0.35
15	GAAAGATAAAATGTAATGGG	AAG	+	155	177	0.30
16	AATGGGAAGTTCCCTGCGC	AAG	+	169	191	0.55
17	AGTTTCCCTGCGCAAGCTGT	GAG	+	176	198	0.55
18	GCTGTGAGATATATTCATGT	GAG	+	191	213	0.35

DISCUSSION

This study aimed to design sgRNAs and determine their off-target effects to choose the best sgRNA for CRISPR experiments of the gene PDR1 with help of one of the bioinformatics applications R. To design sgRNAs, crispRdesignR software was used and results were given in Table 1. According to the literature, the GC content of sgRNA is one of the important factors for selecting sgRNA sequences. Generally, the GC content of the sequence should be between 40-80%. Higher GC content like more than 50% enhances the stability of sgRNA and DNA hybridization and causes off-target effects [11]. Therefore, sgRNAs that have 40% or 45% GC content can be considered as possible sgRNAs for CRISPR experiments like

sequences numbered as 4, 11, 12 and 13 in Table 1. Length of sgRNA is also an important factor that can be caused off-target effect or lowered off-target effect. Approximately 17-24 nucleotide length can be considered as optimal length for sgRNA. Potential sgRNA sequences according to GC content which were 4, 11, 12 and 13 formed by 22 nucleotides that is also an optimal range parameter for length.

CONCLUSION

sgRNA sequences that are numbered as 4,11,12 and 13 were found good candidates for CRISPR experiment of the multidrug resistance gene PDR1 from *Saccharomyces cerevisiae* according to parameters like the GC content and length of sequences. Gene editing of multidrug resistance gene PDR1 via CRISPR/Cas9 system could be an alternative therapeutic option for *S. Cerevisiae* infection. According to findings, researchers can design their sgRNAs for various genes and many genomes that can be found in the BSgenome with simple codes by using `crispRdesignR` tool in RGui and Rstudio. In this way, more comprehensive studies can be conducted than provided by online resources.

REFERENCES

1. Bayat, Hadi, Fatemeh Naderi, Amjad Hayat Khan, Arash Memarnejadian, and Azam Rahimpour. 2018. "The Impact of CRISPR-Cas System on Antiviral Therapy." *Advanced Pharmaceutical Bulletin* 8 (4): 591–97. <https://doi.org/10.15171/apb.2018.067>.
2. Chen, Fengqian, Martin Alphonse, and Qi Liu. 2020. "Strategies for Nonviral Nanoparticle-Based Delivery of CRISPR/Cas9 Therapeutics." *Wiley Interdisciplinary Reviews: Nanomedicine and Nanobiotechnology* 12 (3): 1–14. <https://doi.org/10.1002/wnan.1609>.
3. Wang, Hong Xia, Ziyuan Song, Yeh Hsing Lao, Xin Xu, Jing Gong, Du Cheng, Syandan Chakraborty, et al. 2018. "Nonviral Gene Editing via CRISPR/Cas9 Delivery by Membrane-Disruptive and Endosomolytic Helical Polypeptide." *Proceedings of the National Academy of Sciences of the United States of America* 115 (19): 4903–8. <https://doi.org/10.1073/pnas.1712963115>.
4. Naeem, Muhammad, Saman Majeed, Mubasher Zahir Hoque, and Irshad Ahmad. 2020. "Latest Developed Strategies to Minimize the Off-Target Effects in CRISPR-Cas-Mediated Genome Editing." *Cells* 9 (7): 1–23. <https://doi.org/10.3390/cells9071608>.
5. Yip, Bon Ham. 2020. "Recent Advances in CRISPR/Cas9 Delivery Strategies." *Biomolecules* 10 (6). <https://doi.org/10.3390/biom10060839>.
6. Addgene. 2016. "CRISPR 101 : A Desktop Resource Created and Compiled by Addgene." *Addgene* 2016 (January 2016): 1–125.
7. Nidhi, Sweta, Utpal Anand, Patrik Oleksak, Pooja Tripathi, Jonathan A. Lal, George Thomas, Kamil Kuca, and Vijay Tripathi. 2021. "Novel Crispr–Cas Systems: An Updated Review of the Current Achievements, Applications, and Future Research Perspectives." *International Journal of Molecular Sciences* 22 (7): 1–42. <https://doi.org/10.3390/ijms22073327>.
8. Algazaq, Jumanah N., Kevan Akrami, Fernando Martinez, Allen McCutchan, and Ajay R. Bharti. 2017. "Saccharomyces Cerevisiae Laryngitis and Oral Lesions in a Patient with Laryngeal Carcinoma ." *Case Reports in Infectious Diseases* 2017: 1–4. <https://doi.org/10.1155/2017/2941527>.
9. Terme, Salsomaggiore. 1999. "Molecular and Epidemiological Characterization of Vaginal." *Society* 37 (7): 2230–35.
10. Balzi, E., W. Chen, S. Ulaszewski, E. Capieaux, and A. Goffeau. 1987. "The Multidrug Resistance Gene PDR1 from *Saccharomyces Cerevisiae*." *Journal of Biological Chemistry* 262 (35): 16871–79. [https://doi.org/10.1016/s0021-9258\(18\)45464-6](https://doi.org/10.1016/s0021-9258(18)45464-6).
11. Modrzejewski, Dominik, Frank Hartung, Heike Lehnert, Thorben Sprink, Christian Kohl, Jens Keilwagen, and Ralf Wilhelm. 2020. "Which Factors Affect the Occurrence of Off-Target Effects Caused by the Use of CRISPR/Cas: A Systematic Review in Plants." *Frontiers in Plant Science* 11 (November). <https://doi.org/10.3389/fpls.2020.574959>.

OP-15

Mechanisms of ovarian cancer-released exosome uptake for elucidating the effects in the recipient cells

Gizem Yılmaz¹, Zehra Tavşan², Hülya Ayar Kayalı^{1,2,3,*}

¹ Izmir International Biomedicine and Genome Institute, Dokuz Eylul University, Izmir, Turkey

² Izmir Biomedicine and Genome Center, Dokuz Eylul University, Izmir, Turkey

³ Department of Chemistry, Division of Biochemistry, Faculty of Science, Dokuz Eylul University, Izmir, Turkey

* Corresponding Author

Introduction

Exosomes referred as nanoparticles, serve as 30-100 nm of vehicles carrying a unique composition of proteins, soluble factors, mRNAs, and microRNAs, especially resulting oncogenic differentiation [1]. In addition to the transfer of oncogenic signals, the intercommunication by exosomes between tumor cells and diverse cell types in their surrounding tumor microenvironment is essential for overcoming several obstacles including evasion of growth and apoptotic control, to survive in an inhospitable microenvironment. As a result of exosome-mediated communications, cells orchestrate reprogramming which cells evolve and shape their signaling mechanisms. The communications start with attaching or entering exosomes into the recipient cells either one or multiple uptake mechanisms, including clathrin-mediated endocytosis, caveolae-mediated endocytosis, and clathrin- and caveolae independent endocytosis, phagocytosis, and micropinocytosis. Exosomal cargo delivered into cytosolic compartments and target different locations while simultaneously triggering specific intracellular signal cascades.

Ovarian cancer is the fifth most common cause of cancer death in women. It has a low incidence among gynecological diseases. But difficulties in diagnosis at early stages, especially prognosis at the late stages of disease, low survival rate after surgery and chemotherapy and drug resistance with recurrence of disease require the explanation of the carcinogenesis mechanism in detail. Understanding how drug-resistant ovarian cancer cells communicate with primary ovarian tumor cells, ovarian epithelial and mesothelial cells in the primary and secondary metastasis microenvironment is crucial for the development of new targets for the prevention and treatment of ovarian cancer. The aim of this study was to demonstrate the uptake routes of drug-resistant ovarian cancer released exosomes in primary cancer cells (A2780), epithelial cells (OSE) and mesothelial (MeT-5A) cells.

Materials and Methods

Cell culture

A2780cis, A2780, ovarian surface epithelial and mesothelial cells were cultured in RPMI medium supplemented with 10% FBS, 2 mM L-glutamine, 100 units/ml penicillin and 100 µg/ml streptomycin. All cells were cultured in a humidified incubator with 5% CO₂ at 37 °C.

Exosome isolation

FBS was depleted bovine exosomes by ultracentrifugation at 100,000xg for 70 min and filtrated before use. Subconfluent cultures was maintained for 48 h in the complete growth medium containing of 10% exosome depleted FBS. The culture mediums were collected and centrifuged to discard the cells. The supernatants were filtrated by 0.2 µm sterile filter and then

100 kDa cut-off filtration system. At the last step of isolation, exosomes were pelleted by ultracentrifugation at 100,000 x g. The exosome pellets were stored at -20 °C.

Cell viability

Cells were seeded in a dark 96-well microplate and the inhibitors of exosome uptake pathways were treated for 24 h. Cell viability was calculated using Calcein AM Cell Viability Assay Kit (abcam) according to the manufacturer's protocol.

Exosome labelling

The exosome pellets were resuspended in sterile, filtrated PBS and labelled by PKH26 Red Fluorescent Cell Linker Kit for General Cell Membrane Labeling Kit (Sigma) according to the manufacturer's protocol.

Exosome uptake mechanism

Subconfluent cells were treated with the inhibitors of uptake pathways at the concentrations which were determined by cell viability experiments. After the incubation period (Table 1), cells were incubated with PKH26-labelled exosomes for 6 h. Cells were washed, detached, and supplemented with 1% BSA (w/v). Exosome uptake was analyzed by flow cytometry on a FACS-Calibur instrument integrated with Cell-Quest software (BD Biosciences).

Results

The uptake mechanism of exosomes has been contentious due to several controversial studies which assume different exosome uptake pathway including energy-dependent endocytosis [2, 3], micropinocytosis [4, 5], direct fusion with the plasma membrane [6, 7] and phagocytosis [8]. Before understanding the effects of exosomes on the recipient cells, the uptake routes of exosomes had to be clarified.

Cell viability was calculated after the treatments of drugs which inhibit the different exosome uptake routes. Optimal drug concentrations were selected according to the decreases in the cell viability less than 30%. The selected concentrations and incubation times was showed in Table 1.

Table 1: The optimum concentrations and incubation time of inhibitors.

<u>Inhibitor</u>	<u>Uptake Mechanism</u>	<u>Optimum Concentration</u>	<u>Incubation Time</u>
Chlorpromazine (CPZ)	Clathrin-Mediated Endocytosis	5 µM	30 min at 37° C and during analysis
Cytochalasin D (CYT)	Phagocytosis by Actin Depolymerization	5 µg/ml	30 min at 37° C and during analysis
Dynasore (DYN)	Clathrin-mediated and Caveole-dependent Endocytosis	10 µM	30 min at 37° C and during analysis
5-(nethyl-n-isopropyl)-amiloride (EIPA)	Macropinocytosis	50 µM	30 min at 37° C and during analysis
Filipin III (FLP)	Caveole-dependent and Lipid Raft-mediated Endocytosis	2.5 µM	48 hours at 37° C and during analysis
Genistein (GEN)	Caveole-dependent Endocytosis	10 µM	30 min at 37° C and during analysis
Nocadazole (NOCA)	Microtubule Depolymerization	40 ng/ml (A2780) 75 ng/ml (OSE, MeT-5A)	Overnight at 37° C and during analysis

Flow cytometry results showed that each cell demonstrates different exosome uptake mechanisms for internalization and main route of internalization was energy-dependent active endocytosis. The internalization of exosomes was inhibited 23.3, 12.1 and 10.6% by DYN, CYT and GEN treatments, respectively. The results indicated that these cells chose clathrin-mediated and caveole-dependent endocytosis as well as phagocytosis by actin depolymerization. OSE cells also preferred similar routes and especially, treatment of CYT

almost blocked exosome uptake by 89% in OSE cells. In MeT-5A cells, internalization of exosomes was reduced to 83.8 and 93% after treatments with DYN and CYT. Nevertheless, exosomes contain many different molecules on the cell surface. It gives chance to use different uptake mechanisms as seen in our studies. Therefore, chemical inhibition of any pathway alone rarely abrogated the exosome uptake. Still, combination of inhibitors may provide an opportunity for the further studies.

Discussion

The reprogramming recipient cells depend on the exosome uptake pathway [9, 10]. Similar our results, ovarian cancer, prostate cancer and glioblastoma cells internalized the exosomes by endocytic pathway [2, 5, 11]. In addition to macropinocytosis, HeLa cells used clathrin-independent endocytosis [12]. In general, several cells chose at least two different uptake pathways to ensure phenotypic responses.

References

- [1] L. Cheng, S. Wu, K. Zhang, Y. Qing and T. Xu, "A comprehensive overview of exosomes in ovarian cancer: Emerging biomarkers and therapeutic strategies", *Journal of Ovarian Research*, vol. 10, no. 73, 2017.
- [2] K. J. Svensson, H. C. Christianson, A. Wittrup, E. Bourseau-Guilmain, E. Lindqvist, L. M. Svensson, M. Mörgelin and M. Belting, "Exosome uptake depends on ERK1/2-heat shock protein 27 signaling and lipid raft-mediated endocytosis negatively regulated by caveolin-1", *Journal of Biological Chemistry*, vol. 288, no. 24, pp. 17713-17724, 2013.
- [3] T. Tian, Y.-L. Zhu, F.-H. Hu, Y.-Y. Wang, N.-P. Huang and Z.-D. Xiao, "Dynamics of exosome internalization and trafficking", *Journal of Cellular Physiology*, vol. 228, no. 7, pp. 1487-1495, 2013.
- [4] D. Fitzner, M. Schnaars, D. v. Rossum, G. Krishnamoorthy, P. Dibaj, M. Bakhti, T. Regen, U.-K. Hanisch and M. Simons, "Selective transfer of exosomes from oligodendrocytes to microglia by macropinocytosis", *Journal of Cell Science*, vol. 124, pp. 447-458, 2011.
- [5] T. Tian, Y.-L. Zhu, Y.-Y. Zhou, G.-F. Liang, Y.-Y. Wang, F.-H. Hu and Z.-D. Xiao, "Exosome uptake through clathrin-mediated endocytosis and macropinocytosis and mediating miR-21 delivery", *Journal of Biological Chemistry*, vol. 289, no. 32, pp. 22258-22267, 2014.
- [6] I. D. Conde, C. N. Shrimpton, P. Thiagarajan and J. A. López, "Tissue-factor-bearing microvesicles arise from lipid rafts and fuse with activated platelets to initiate coagulation", *Blood*, vol. 106, no. 5, pp. 1604-1611, 2005.
- [7] I. Parolini, C. Federici, C. Raggi, L. Lugini, S. Palleschi, A. D. Milito, C. Coscia, E. Iessi, M. Logozzi, A. Molinari, M. Colone, M. Tatti, M. Sargiacomo and S. Fais, "Microenvironmental pH is a key factor for exosome traffic in tumor cells", *Journal of Biological Chemistry*, vol. 284, no. 49, pp. 34211-34222, 2009.
- [8] D. Feng, W.-L. Zhao, Y.-Y. Ye, X.-C. Bai, R.-Q. Liu, L.-F. Chang, Q. Zhou and S.-F. Sui, "Cellular internalization of exosomes occurs through phagocytosis," *Traffic*, vol. 11, no. 5, pp. 675-687, 2010.
- [9] K.M. Hussain, K.L.J. Leong, M.M.L. Ng, J.J.H. Chu, "The essential role of clathrin-mediated endocytosis in the infectious entry of human enterovirus 71", *Journal of Biological Chemistry*, vol. 286, pp. 309–321, 2011.
- [10] X.X. Zhang, P.G. Allen, M. Grinstaff, "Macropinocytosis is the major pathway responsible for DNA transfection in CHO cells by a charge-reversal amphiphile", *Molecular Pharmacology*, vol. 8, pp. 758–766, 2011.
- [11] C. Escrevente, S. Keller, P. Altevogt, J. Costa, "Interaction and uptake of exosomes by ovarian cancer cells", *BMC Cancer*, vol. 11, pp.108, 2011.

[12] H. Costa Verdera, J.J. Gitz-Francois, R.M. Schiffelers, P. Vader, "Cellular uptake of extracellular vesicles is mediated by clathrin-independent endocytosis and macropinocytosis", *The Journal of Controlled Release*, vol. 266, pp. 100-108, 2017.

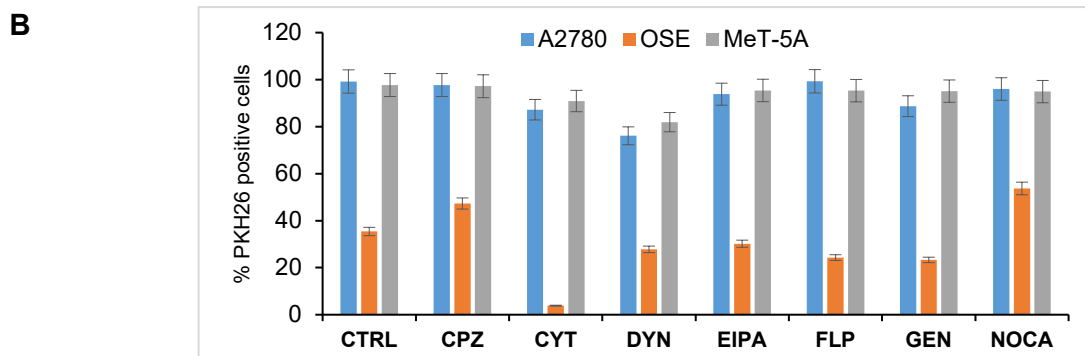
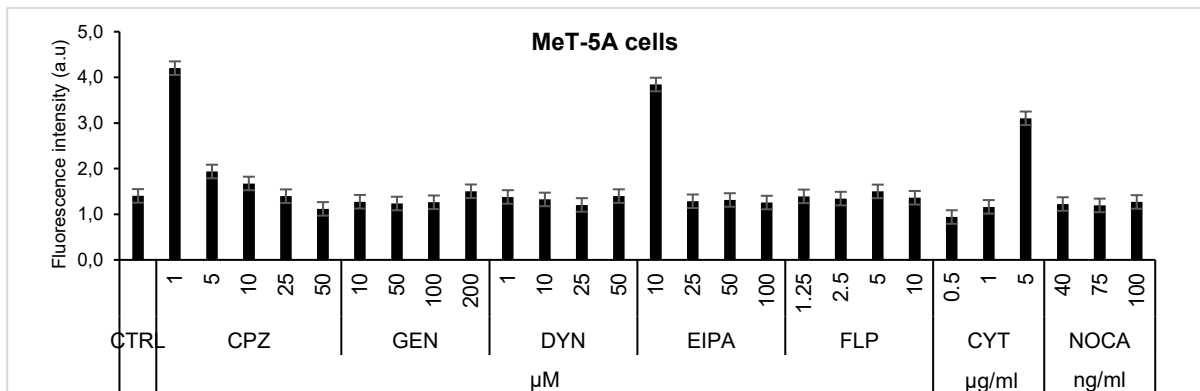
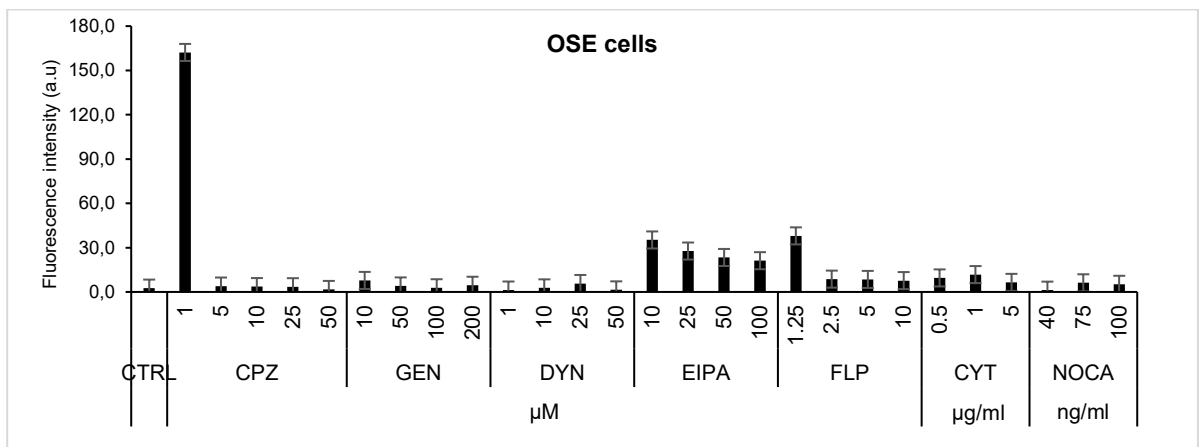
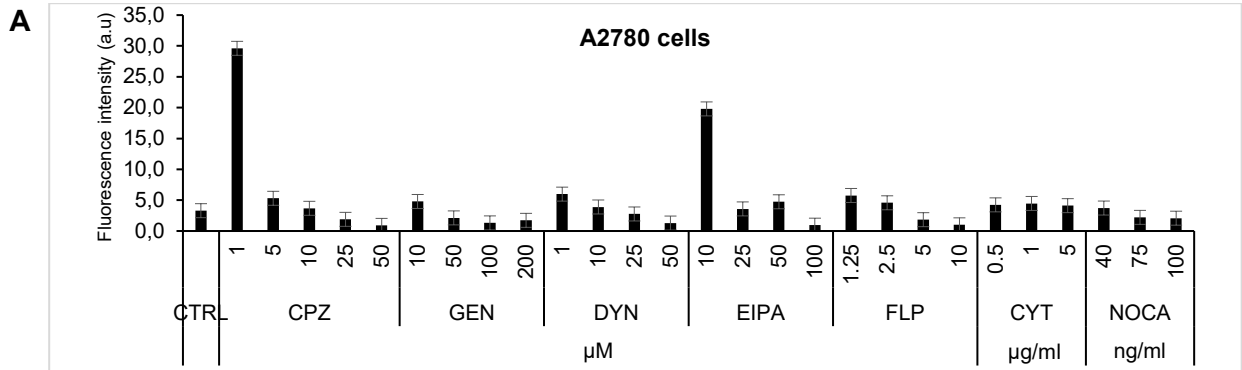


Figure 1. (A) Viability of A2780, OSE and MeT-5A cells (B) The percent of PKH26 positive cells. Mean \pm SD of three independent experiments was shown.

OP-16

Investigation of the Effects of 5-Fluorouracil Combination of Fe₃O₄ in Glioblastoma (U373)

Cancer: an in vitro experiment

Aysegul Yilmaz¹, Ali Taghizadehghalehjoughi², Sidika Genc¹, Yesim Yeni¹, Ahmet Hacimuftuoglu¹, Abbas Jafarizad³, Mehdi Jaymand⁴

¹ *Department of Medical Pharmacology, Faculty of Medicine, Ataturk University, Erzurum, Turkey*

² *Department of Toxicology and Pharmacology, Faculty of Veterinary, Ataturk University, Erzurum, Turkey*

³ *Faculty of Chemical Engineering, Sahand University of Technology, Tabriz, Iran*

⁴ *Pharmaceutical Nanotechnology Research Center, Tabriz University of Medical Sciences, Tabriz, Iran*

Abstract

Glioblastoma is one of the most difficult types of brain tumors to treat. Growth is facilitated further through cell migration and disruption of the cell outer matrix. 5-fluorouracil, an analogue of uracil, is an important chemotherapeutic drug that is used effectively. Since it cannot pass to the brain, high doses should be used in glioblastoma diseases. It seems that the nanoparticle method can be used to increase the effect of 5-fluorouracil and reduce its side effects. We aim at this with our study and we analyze MTT, TAS and TOS for this purpose. U373 cell line was obtained from Atatürk University, Department of Medical Pharmacology. Combined doses of 5-fluorouracil 4, 8 and 16µg/mL, Fe₃O₄ 6µg/mL, 5-fluorouracil + Fe₃O₄ 6µg/mL were used. The formed groups were applied to the U373 cell line. At the end of 24 and 72 hours, MTT, TAS and TOS analyzes were measured. Methylthiazole diphenyl tetrazolium (MTT), TAS and TOS results were analyzed using SPSS, IBM 21.00 program with one way ANOVA method. Viability was most affected by 5-fluorouracil 16µg/mL dose (74%). It was observed that the antioxidant effect decreased significantly when 5-fluorouracil 16µg/mL dose and Fe₃O₄ were used in combination, while the oxidant effect increased. Based on our results, Fe₃O₄ can be used to increase the effectiveness of drugs. Thus, while the dose of the drug taken is reduced, its effect and targeting can be increased.

INTRODUCTION

Glioblastoma multiforme is one of the most common types of brain tumors and one of the most difficult to treat [1]. Despite technological advances in surgery, radiation therapy and

chemotherapy, GBM is largely resistant to treatment. Its growth is facilitated by cell migration and disruption of the extracellular matrix structure [2]. One of the main barriers to GBM treatment is its location in the brain and the presence of the blood brain barrier (BBB), which limits drugs entering the central nervous system (CNS) [3]. BBB prevents many essential drugs as well as toxins from reaching the brain tissue. Since an estimated 99% of the drugs developed do not exceed the BBB, the number of neurological treatments is severely limited [4]. 5-fluorouracil (5-FU) is also a compound that cannot effectively cross the blood-brain barrier. 5-FU, a fluorinated analogue of uracil, is an important chemotherapeutic component used in therapy [5]. Since high doses are required for it to be effective in the brain, its toxic properties increase. In order to solve all these limitations, the most promising method in GBM treatment is seen as nano-technology. Low toxicity, biocompatibility and high accessibility to the target tissue or organ are among the positive effects of nanoparticles [6].

Systemic administration of 5-FU using a biodegradable carrier such as nanoparticles is widely investigated as a way to increase the efficacy of 5-FU and reduce the side effects of chemotherapy.

In our study, we used Fe₃O₄ nanoparticle to increase the efficiency of 5-fluorouracil and decrease cell viability on the U373 glioblastoma line. We presented the results of our study together with MTT, TAS, TOS and SPSS analyses.

Materials and Methods

U373 cell line was obtained from Atatürk University, Department of Medical Pharmacology. Combined doses of 5-fluorouracil 4, 8 and 16 µg/mL, Fe₃O₄ 6 µg/mL, 5-fluorouracil + Fe₃O₄ 6 µg/mL were used. The formed groups were applied to the U373 cell line. At the end of 24 and 72 hours, MTT, TAS and TOS analyzes were measured. Methylthiazole diphenyl tetrazolium (MTT), TAS and TOS results were analyzed using SPSS, IBM 21.00 program with one way ANOVA method.

Results

When we looked at the viability rates (figure 1), we observed that 5-fluorouracil decreased the viability of U373 depending on the increasing dose and time. The highest rate was found at the dose of 5-fluorouracil 16 µg/mL (74% viability rate). When the same 5-fluorouracil dose was applied in combination with Fe₃O₄ 6 µg/mL, it was observed that the viability decreased to 66%. When we look at the antioxidant and oxidant results, it was observed that 5-fluorouracil decreased

the antioxidant level and increased the oxidant level depending on the increasing dose and time. The most effective group was 5-fluorouracil 16 μ g/mL (it decreased the antioxidant level 1.2 times, increased the oxidant level 1.25 times). It was determined that the effect on U373 increased when 5-fluorouracil was applied in combination with Fe₃O₄ 6 μ g/mL. While the effect increased depending on the dose and time, it was found that the maximum dose of 5-fluorouracil 16 μ g/mL affected the antioxidant-oxidant level on the cell.

Discussion

Based on our results, we observed that the Fe₃O₄ component increased the effect of temozolomide in the U373 cell line at vitality, oxidant and antioxidant levels. Zhang [7] and his team showed that Fe₃O₄ increased the efficacy on glioblastoma. Buteică [6] et al. also observed that Fe₃O₄ (0.25 - 1 μ g/ml) they used in glioblastoma cell line decreased the viability. Lu [8] et al. observed the antiproliferative effects of Fe₃O₄ in the U251 cell line.

According to the results we obtained, Fe₃O₄ was found to be effective in the glioblastoma cell line.

References

1. Nieland, L., et al., *Extracellular Vesicle-Mediated Bilateral Communication between Glioblastoma and Astrocytes*. Trends Neurosci, 2021. 44(3): p. 215-226.
2. Ozdemir-Kaynak, E., A.A. Qutub, and O. Yesil-Celiktas, *Advances in Glioblastoma Multiforme Treatment: New Models for Nanoparticle Therapy*. Front Physiol, 2018. 9: p. 170.
3. Jnaidi, R., A.J. Almeida, and L.M. Goncalves, *Solid Lipid Nanoparticles and Nanostructured Lipid Carriers as Smart Drug Delivery Systems in the Treatment of Glioblastoma Multiforme*. Pharmaceutics, 2020. 12(9).
4. Timbie, K.F., B.P. Mead, and R.J. Price, *Drug and gene delivery across the blood-brain barrier with focused ultrasound*. J Control Release, 2015. 219: p. 61-75.
5. Cho, Y.H., et al., *5-FU promotes stemness of colorectal cancer via p53-mediated WNT/beta-catenin pathway activation*. Nat Commun, 2020. 11(1): p. 5321.
6. Buteica, S.A., et al., *IN VITRO AND IN VIVO EFFECTS OF Fe₃O₄/SALICYLIC ACID MAGNETIC NANOPARTICLES ON THE HUMAN GLIOBLASTOMA CELLS*. Digest Journal of Nanomaterials and Biostructures, 2014. 9(3): p. 959-965.
7. Zhang, X., et al., *Radiosensitivity enhancement of Fe₃O₄@Ag nanoparticles on human glioblastoma cells*. Artif Cells Nanomed Biotechnol, 2018. 46(sup1): p. 975-984.

8. Lu, Q., et al., *Fe₃O₄@Au composite magnetic nanoparticles modified with cetuximab for targeted magneto-photothermal therapy of glioma cells*. *Int J Nanomedicine*, 2018. 13: p. 2491-2505.

Figures;

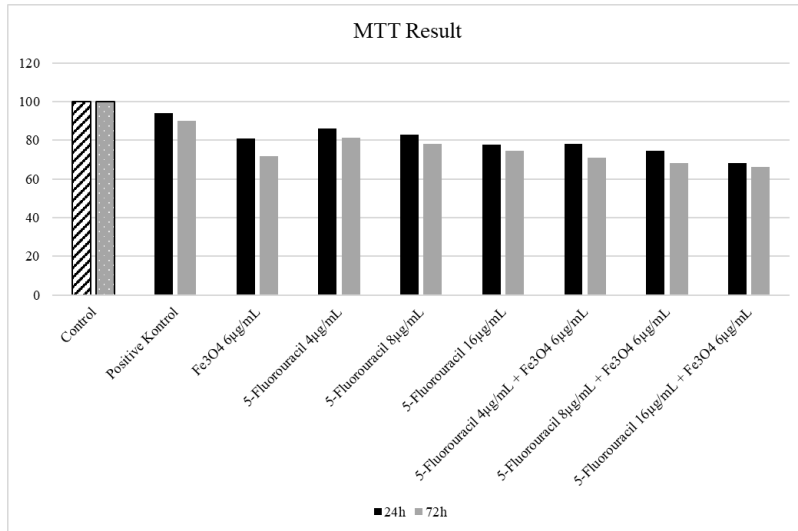


Figure 1

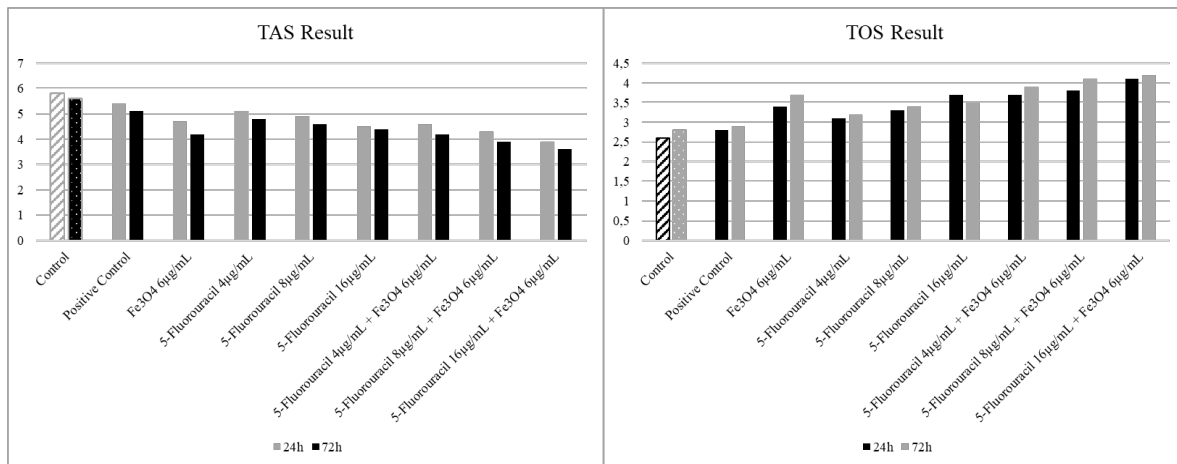


Figure 2

OP-17

Effects of Fe₃O₄ on Cell Viability and Oxidative Stress in Combination with Temozolomide in Glioblastoma (U373) Cancer Line

Aysegul Yilmaz¹, Ali Taghizadehghalehjoughi², Sidika Genc¹, Yesim Yeni¹, Ahmet
Hacimuftuoglu¹, Abbas Jafarizad³, Mehdi Jaymand⁴

¹ *Department of Medical Pharmacology, Faculty of Medicine, Ataturk University, Erzurum,
Turkey*

² *Department of Toxicology and Pharmacology, Faculty of Veterinary, Ataturk University,
Erzurum, Turkey*

³ *Faculty of Chemical Engineering, Sahand University of Technology, Tabriz, Iran*

⁴ *Pharmaceutical Nanotechnology Research Center, Tabriz University of Medical Sciences,
Tabriz, Iran*

Abstract

Glioblastoma multiforme is the most common primary brain tumor. Despite the developing technology, glioblastoma is still a treatment-resistant disease. Temozolomide is an alkylating agent that inhibits the cell cycle and causes cell death, and is widely used in glioblastoma patients. The U373 cell line was obtained from the department of medical pharmacology. Combined doses of 4, 8 and 16 µg/mL, Fe₃O₄ 6 µg/mL, temozolomide + Fe₃O₄ 6 µg/mL were used. The created groups were applied to the U373 cell line. At the end of 24 and 72 hours, MTT, TAS and TOS analyzes were measured. Methylthiazole diphenyl tetrazolium (MTT), TAS and TOS results were analyzed using SPSS, IBM 21.00 program with one way ANOVA method. According to our. MTT results, the most effective group for viability was Temazolamide 16 µg/mL + Fe₃O₄ 6 µg/mL. According to the oxidant and antioxidant results, Temazolamide 16 µg/mL + Fe₃O₄ 6 µg/mL was the group that decreased the antioxidant level by 2 times and increased the oxidant level by 2.1 times. According to our results, Fe₃O₄ can be used to increase the effectiveness of drugs. Thus, while the dose of the drug taken is reduced, its effect and targeting can be increased.

INTRODUCTION

Glioblastoma multiforme (GBM) is the most common primary brain tumor, accounting for 45.2% of malignant primary brain and central nervous system tumors in adults [1]. Despite technological advances in surgery, radiotherapy and chemotherapy, GBM is largely resistant to treatment. In addition, GBM has the property of rapid growth, which is facilitated by cell migration and degradation of the extracellular matrix [2]. Unlike other tumors, the main barrier to the treatment of GBM is its location in the brain and the presence of the blood-brain barrier (BBB), which limits drugs entering the central nervous system (CNS) [3]. BBB prevents many essential drugs as well as toxins from reaching the brain tissue. Since an estimated

99% of the drugs developed do not exceed the BBB, the number of neurological treatments is severely limited [4]. Temozolomide (TMZ), on the other hand, is an alkylating agent that breaks the DNA double chain structure, thus causing cell cycle arrest and cell death. Due to its short half-life, high doses of TMZ can cause a number of side effects. High doses are required to reach effective concentrations in the brain, resulting in toxicity. In order to solve all these limitations, nano-technology has been seen as the most promising method in GBM treatment. Non-toxicity, biocompatibility and high accessibility to the target tissue or organ are among the positive effects of nanoparticles [5].

Systemic administration of TMZ using a biodegradable carrier such as nanoparticles is widely explored as a way to increase the efficacy of TMZ and reduce the side effects of chemotherapy.

In our study, we used Fe₃O₄ nanoparticle to increase the efficiency of temozolomide and decrease cell viability on the U373 glioblastoma line. We presented the results of our study together with MTT, TAS, TOS and SPSS analyses.

Material And Method

U373 cell line was obtained from Atatürk University, Department of Medical Pharmacology. Combined doses of temazolamide 4, 8 and 16 µg/mL, Fe₃O₄ 6 µg/mL, temazolamide + Fe₃O₄ 6 µg/mL were used. The created groups were applied to the U373 cell line. At the end of 24 and 72 hours, MTT, TAS and TOS analyzes were measured. Methylthiazole diphenyl tetrazolium (MTT), TAS and TOS results were analyzed using SPSS, IBM 21.00 program with one way ANOVA method.

Results

According to our MTT results in Figure 1, it was determined that pure temozolomide decreased viability with increasing dose and time. The most significant decrease was seen in temozolomide 16 µg/mL dose (30% reduction in viability). It was observed that the viability decreased up to 54% in the Temazolamide + Fe₃O₄ 6 µg/mL combined groups (Temazolamide 16 µg/mL + Fe₃O₄ 6 µg/mL, 72nd hour). In the antioxidant results in Figure 2, it was observed that the antioxidant level decreased depending on time and dose in pure temozolomide and combined groups. The most significant decrease was seen in temozolomide 16 µg/mL dose (1.4 fold decrease). In combination with Fe₃O₄, it was observed that 16 µg/mL of temozolomide caused a 2-fold reduction in antioxidant levels. Similar results were seen at the oxidant level (figure 3). According to these results, it was determined that temozolomide increased the oxidant level depending on the increasing dose and time. In combination with Fe₃O₄, the oxidant level increased depending on the increasing dose and time. The most important group was the combination of 16 µg/mL + Fe₃O₄ in temozolomide, which increased the oxidant level by 2.1 times.

Discussion

Based on our results, we observed that the Fe₃O₄ component increased the effect of temozolomide in the U373 cell line at vitality, oxidant and antioxidant levels. Gabriel [6] et al also showed that the Fe₃O₄ component is effective on glioblastoma. Zhang [7] et al also showed that Fe₃O₄ increased the efficiency in the U251 cell line. When we look at its effects on vitality, we observed in our results that Fe₃O₄ increased the effect of temozolomide. Buteică [5] et al. also observed that Fe₃O₄ (0.25-1 µg/ml) they used in glioblastoma cell line decreased the viability.

According to the results we have obtained, we have demonstrated that Fe₃O₄ increases the effect of temozolomide in the glioblastoma cell line with our vitality, oxidant and antioxidant studies. Increasing the effectiveness by using auxiliary agents in treatment methods can both eliminate the possibility of toxic dose and target-oriented treatment can be done by developing the nanoparticle method. The use of nanoparticles as an auxiliary minimizes the side effects.

References

- Nieland, L., et al., *Extracellular Vesicle-Mediated Bilateral Communication between Glioblastoma and Astrocytes*. Trends Neurosci, 2021. **44**(3): p. 215-226.
- Ozdemir-Kaynak, E., A.A. Qutub, and O. Yesil-Celiktas, *Advances in Glioblastoma Multiforme Treatment: New Models for Nanoparticle Therapy*. Front Physiol, 2018. **9**: p. 170.
- Jnaidi, R., A.J. Almeida, and L.M. Goncalves, *Solid Lipid Nanoparticles and Nanostructured Lipid Carriers as Smart Drug Delivery Systems in the Treatment of Glioblastoma Multiforme*. Pharmaceutics, 2020. **12**(9).
- Timbie, K.F., B.P. Mead, and R.J. Price, *Drug and gene delivery across the blood-brain barrier with focused ultrasound*. J Control Release, 2015. **219**: p. 61-75.
- Buteica, S.A., et al., *IN VITRO AND IN VIVO EFFECTS OF Fe₃O₄/SALICYLIC ACID MAGNETIC NANOPARTICLES ON THE HUMAN GLIOBLASTOMA CELLS*. Digest Journal of Nanomaterials and Biostructures, 2014. **9**(3): p. 959-965.
- Rego, G.N.A., et al., *Therapeutic evaluation of magnetic hyperthermia using Fe₃O₄-aminosilane-coated iron oxide nanoparticles in glioblastoma animal model*. Einstein (Sao Paulo), 2019. **17**(4): p. eAO4786.
- Zhang, X., et al., *Radiosensitivity enhancement of Fe₃O₄@Ag nanoparticles on human glioblastoma cells*. Artif Cells Nanomed Biotechnol, 2018. **46**(sup1): p. 975-984.

Figures;

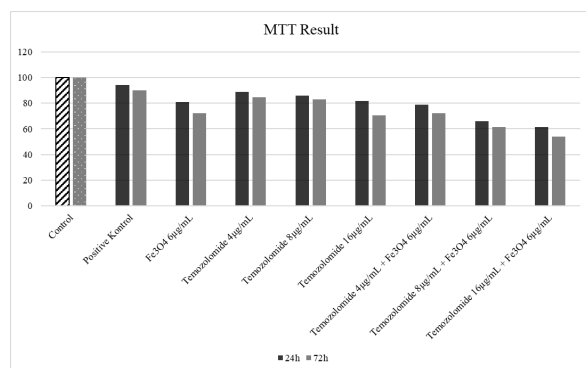


Figure 1

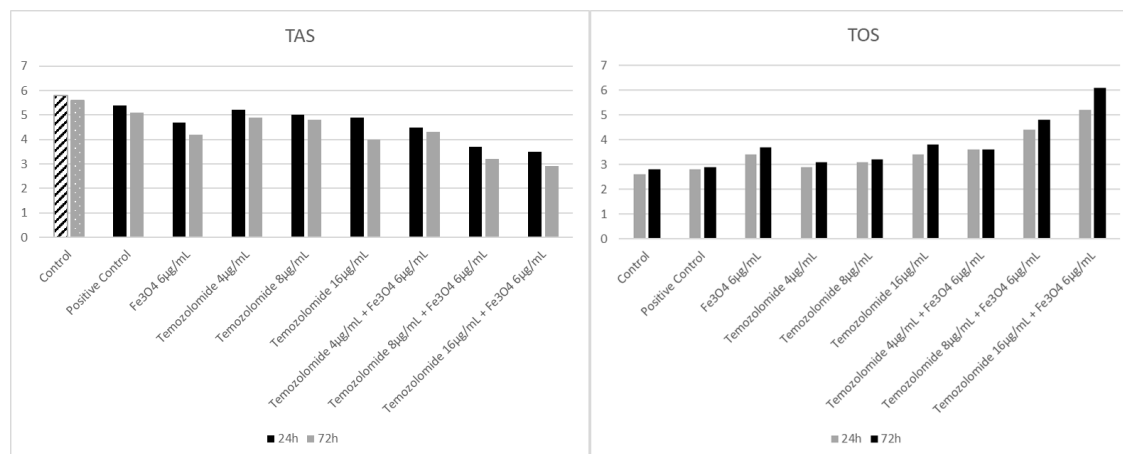


Figure 2

The Role of CRISPR/Cas9 Applications in the Treatment of Duchenne Muscular Dystrophy

1) Burçak KURT

1) Uşak University, Department of Molecular Biology And Genetics, Uşak, Turkey

burcakkurttt@gmail.com

Abstract:

Gene therapy is one promising approach for treatment of Duchenne muscular dystrophy (DMD) using the CRISPR/Cas9 gene editing system.

The two forms of dystrophin-associated muscular dystrophies, known as Duchenne and Becker muscular dystrophy are caused by genetic defects in the huge DMD gene (79 exons), located at Xp21 and coding for the 427- kDa protein known as dystrophin (1,2) The central portion of the dystrophin gene locus is a preferential site of deletions causing DMD. More than 25% of all DMD deletions occur in Intron 44 which is 248 kb in length.

Using CRISPR to bypass DMD mutations, dystrophin expression has been efficiently restored in human cells and mouse models of DMD. CRISPR was first identified as a system for bacterial immunity. CRISPR/Cas-mediated genome editing has been shown to permanently correct DMD mutations and restore dystrophin function in mouse models. Germline editing by injecting zygotes with CRISPR/Cas9 editing components was first accomplished in mdx mice by correcting the mutated exon 23 using either HDR or NHEJ .Other CRISPR systems, including CRISPR/Cpf1, have been used to correct DMD mutations in both mdx mice and human-derived iPSCs by exon skipping or HDR

CRISPR/Cas9 can also be used to correct duplication mutations of the DMD gene. Wojtal et al. (2016) used a single gRNA against intron 27 to correct the DMD gene in primary patient fibroblasts with a duplication in exons 18–30. Because of the nature of the mutation, a single gRNA can be used in a multiplex approach, allowing for the deletion of multiple duplicated exons. Treated transdifferentiated myotubes exhibited 4.42% dystrophin protein of normal levels by Western blot, and restored expression of the dystrophin-associated glycoprotein complex (DAGC) protein α -dystroglycan. Using a similar concept, exon 2 and exon 55–59 duplication mutations have also been corrected in immortalized DMD patient muscle cells and DMD hiPSCs, respectively.

Since the guide RNA sequences to be used can be arranged according to the mutation carried by the patient, personalized treatment protocols will be possible. Use of patient-derived cells will increase the treatment efficiency as graft rejection or need for immunosuppressive drugs is not expected.

Keywords: SpCas9 and dual guide RNAs, CRISPR/Cas9, Duchenne Muscular Dystrophy

1.Introduction:

Duchenne Muscular Dystrophy; It can be described as a disease that has made its voice heard in the world in recent years, accepted in the class of rare diseases, studies on treatment methods,

and caused by disorders related to a single gene. In this study, which I will present as a review article, I have brought together the treatment methods developed using the CRISPR/Cas9 gene editing system. I would like to draw attention to the fact that it leads to pioneering studies and focuses on treatments.

1.1 Overview of Duchenne Muscular Dystrophy

More than 800 single gene mutation diseases result in loss of form or dysfunction of skeletal muscle. Among the most severe is Duchenne muscular dystrophy (DMD), which is caused by mutations in the X-linked dystrophin gene, a massive gene spanning ~2.3 megabases (1). DMD affects 1 in 3500–5000 males born worldwide, making it the most common inherited neuromuscular disorder (2,3). The disease progresses rapidly, with muscle weakness and wasting observed initially in the proximal muscles, spreading distally. Patients experience multiple organ system dysfunction, and often lose their mobility by the age of 12 years (4,5). Death usually occurs in the second or third decade of life due to respiratory and/or cardiac complications(6).

1.2 Dystrophin

DMD is caused by loss-of-function mutations in the dystrophin (DMD) gene which codes for a cytoskeletal protein called dystrophin (1,7). Dystrophin functions via the dystrophin glycoprotein complex (DGC) to link the actin cytoskeleton of muscle cells to the extracellular matrix, providing mechanical support to myofibers during cycles of contraction and relaxation (8,9,10)

2.1 CRISPR Mediated Strategies for DMD

2.1.1 Exon Skipping

Antisense oligomer (AO) induced exon skipping is being investigated to restore functional dystrophin expression in models of muscular dystrophy and DMD patients (11). AO intervention during dystrophin pre-mRNA processing aims to exclude one or more exons associated with the primary DMD-causing mutation, while maintaining or restoring the dystrophin mRNA reading frame. A clinical trial of AO-induced exon skipping in DMD patients has demonstrated proof of principle that this antisense strategy can restore some dystrophin expression in DMD muscle (12). Within a nucleus, introns are removed an estimated 40 times faster than in vitro processing of synthetic pre-mRNA transcripts (13). The most effective AOs appear to preferentially target predicted SF2/ASF (IgM-BRCA1) (25%) or SC35 (28%) motifs, compared to 22, 17, and 8% targeting SF2/ASF, SRp40, and SRp55, respectively.

These percentages are calculated from the number of ESE motifs, either completely or partially occurring within the oligomer annealing site, divided by the total number of ESE motifs within the target exons (11).

2.1.2 Exon Deletion

Exon deletion strategies may also be used to correct exon duplication mutations, which occur in ~5% of DMD patients. Approximately 65–72% of all DMD patients carry a deletion of one or more exons. Deletions tend to cluster in a hotspot region between exons 45 and 55 of the dystrophin gene (15,16). A common strategy for correcting single or multiple exon deletions is to delete the out-of-frame exon and restore the ORF. This can be achieved by deleting one exon or the entire hotspot region. Specifically, two sgRNAs flanking the targeted exon(s) can be delivered with Cas9 to excise the single or multiple mutated exons, resulting in restoration of the ORF by splicing adjacent in-frame exons (17,18,19). A single sgRNA can be designed to target the intron region adjacent to the duplicated exon, and in the presence of Cas9, the single sgRNA will generate two cuts and delete one of the duplicated exons. Removal of one of the duplicated exons can renew the dystrophin gene ORF and produce full-length dystrophin protein, indistinguishable from normal dystrophin (20).

2.1.3 Base Editing

It is estimated that 25–35% of DMD patients have point mutations (15,16). These RNA-guided nucleotide-specific base editors, which consist of a cytidine deaminase or an engineered adenine deaminase fused with a Cas9 nickase (nCas9) or catalytically deficient Cas9 (dCas9), do not produce DNA DSBs like Cas9 and do not rely on the NHEJ repair pathway. A donor DNA template for HDR is not required, and small indels through error-prone NHEJ at the target site are not produced. Most recently, CRISPR/Cas9 adenine base editors were used to substitute a single adenine to guanine in a DMD mouse model that harbors an exon 20 nonsense mutation (21). This strategy has been used to disrupt splicing acceptor sites (22) and can be used to disrupt premature stop codons for inducing exon skipping. This opens new therapeutic opportunities for DMD.

3. Results

Among the DMD treatment methods produced with CRISPR/Cas 9, methods such as exon skipping, exon deletion, genome editing, DMD with in vivo studies are available and open to development. The most popular results are currently being applied to mice, rabbits and dogs in animal models. We recommend that you review our references.

4. References

- 1) Hoffman EP, Brown RH Jr, Kunkel LM *Cell*. 1987 Dec 24; 51(6):919-28.
- 2) Evidence-based path to newborn screening for Duchenne muscular dystrophy. Mendell JR, Shilling C, Leslie ND, Flanigan KM, al-Dahhak R, Gastier-Foster J, Kneile K, Dunn DM, Duval B, Aoyagi A, Hamil C, Mahmoud M, Roush K, Bird L, Rankin C, Lilly H, Street N, Chandrasekar R, Weiss RB *Ann Neurol*. 2012 Mar; 71(3):304-13.
- 3) Population frequencies of inherited neuromuscular diseases--a world survey. Emery AE *Neuromuscul Disord*. 1991; 1(1):19-29.
- 4) Update on the management of Duchenne muscular dystrophy. Manzur AY, Kinali M, Muntoni F *Arch Dis Child*. 2008 Nov; 93(11):986-90.
- 5) Current and emerging treatment strategies for Duchenne muscular dystrophy. Mah JK *Neuropsychiatr Dis Treat*. 2016; 12():1795-807.
- 6) Antisense oligonucleotides for the treatment of cardiomyopathy in Duchenne muscular dystrophy. Nguyen Q, Yokota T *Am J Transl Res*. 2019; 11(3):1202-1218.
- 7) Dystrophin: the protein product of the Duchenne muscular dystrophy locus. Hoffman EP, Brown RH Jr, Kunkel LM *Cell*. 1987 Dec 24; 51(6):919-28.
- 8) A role for the dystrophin-glycoprotein complex as a transmembrane linker between laminin and actin. Ervasti JM, Campbell KP *J Cell Biol*. 1993 Aug; 122(4):809-23.
- 9) Membrane organization of the dystrophin-glycoprotein complex. Ervasti JM, Campbell KP *Cell*. 1991 Sep 20; 66(6):1121-31.
- 10) Dystrophin, its interactions with other proteins, and implications for muscular dystrophy. Ervasti JM *Biochim Biophys Acta*. 2007 Feb; 1772(2):108-17.
- 11) Mitrpant C, Adams AM, Meloni PL, Muntoni F, Fletcher S, Wilton SD. Rational design of antisense oligomers to induce dystrophin exon skipping. *Mol Ther*. 2009 Aug; 17(8):1418-26.
- 12) van Deutekom JC, Janson AA, Ginjaar IB, Frankhuizen WS, Aartsma-Rus A, Bremmer-Bout M, et al. Local dystrophin restoration with antisense oligonucleotide PRO051. *N Engl J Med*. 2007; 357:2677-2686.
- 13) Wetterberg I, Zhao J, Masich S, Wieslander L., and , Skoglund U. In situ transcription and splicing in the Balbiani ring 3 gene. *EMBO J*. 2001; 20:2564-2574.
- 14) Long C., McAnally J.R., Shelton J.M., Mireault A.A., Bassel-Duby R., Olson E.N. Prevention of muscular dystrophy in mice by CRISPR/Cas9-mediated editing of germline DNA. *Science*. 2014; 345:1184-1188. doi: 10.1126/science.1254445.
- 15) The TREAT-NMD DMD Global Database: analysis of more than 7,000 Duchenne muscular dystrophy mutations. Bladen CL, Salgado D, Monges S, Foncuberta ME, Kekou K, Kosma K, Dawkins H, Lamont L, Roy AJ, Chamova T, Guerguelcheva V, Chan S, Korngut L, Campbell C, Dai Y, Wang J, Barišić N, Brabec P, Lahdetie J, Walter MC, Schreiber-Katz O, Karcagi V, Garami M, Viswanathan V, Bayat F, Buccella F, Kimura E, Koeks Z, van den Bergen JC, Rodrigues M, Roxburgh R, Lusakowska A, Kostera-Pruszyk A, Zimowski J, Santos R, Neagu E, Artemieva S, Rasic VM, Vojinovic D, Posada M, Bloetzer C, Jeannet PY, Joncourt F, Díaz-Manera J, Gallardo E, Karaduman AA, Topaloğlu H, El Sherif R, Stringer A, Shatillo AV, Martin AS, Peay HL, Bellgard MI, Kirschner J, Flanigan KM, Straub V, Bushby K, Verschuuren J, Aartsma-Rus A, Bérout C, Lochmüller H *Hum Mutat*. 2015 Apr; 36(4):395-402.
- 16) Entries in the Leiden Duchenne muscular dystrophy mutation database: an overview of mutation types and paradoxical cases that confirm the reading-frame rule. Aartsma-Rus A, Van Deutekom JC, Fokkema IF, Van Ommen GJ, Den Dunnen JT *Muscle Nerve*. 2006 Aug; 34(2):135-44.
- 17) A Single CRISPR-Cas9 Deletion Strategy that Targets the Majority of DMD Patients Restores Dystrophin Function in hiPSC-Derived Muscle Cells. Young CS, Hicks MR, Ermolova NV, Nakano H, Jan M, Younesi S, Karumbayaram S, Kumagai-Cresse C, Wang D, Zack JA, Kohn DB, Nakano A, Nelson SF, Miceli MC, Spencer MJ, Pyle AD *Cell Stem Cell*. 2016 Apr 7; 18(4):533-40.
- 18) Multiplex CRISPR/Cas9-based genome editing for correction of dystrophin mutations that cause Duchenne muscular dystrophy. Ousterout DG, Kabadi AM, Thakore PI, Majoros WH, Reddy TE, Gersbach CA *Nat Commun*. 2015 Feb 18; 6():6244.
- 19) Adenoviral vectors encoding CRISPR/Cas9 multiplexes rescue dystrophin synthesis in unselected populations of DMD muscle cells. Maggio I, Liu J, Janssen JM, Chen X, Gonçalves MA *Sci Rep*. 2016 Nov 15; 6():37051.
- 20) Correction of diverse muscular dystrophy mutations in human engineered heart muscle by single-site genome editing. Long C, Li H, Tiburecy M, Rodriguez-Caycedo C, Kyrychenko V, Zhou H, Zhang Y, Min YL, Shelton JM, Mammen PPA, Liaw NY, Zimmermann WH, Bassel-Duby R, Schneider JW, Olson EN *Sci Adv*. 2018 Jan; 4(1):eaap9004.

- 21) Adenine base editing in mouse embryos and an adult mouse model of Duchenne muscular dystrophy. Ryu SM, Koo T, Kim K, Lim K, Baek G, Kim ST, Kim HS, Kim DE, Lee H, Chung E, Kim JS *Nat Biotechnol.* 2018 Jul; 36(6):536-539
- 22) Lim KRQ, Yoon C, Yokota T. Applications of CRISPR/Cas9 for the Treatment of Duchenne Muscular Dystrophy. *J Pers Med.* 2018 Nov 24;8(4):38. doi: 10.3390/jpm8040038. PMID: 30477208; PMCID: PMC6313657.

OP-20

PRESENTATION TYPE PREFERENCE*

ORAL PRESENTATION

POSTER PRESENTATION

PREPARATION AND CHARACTERIZATION OF MEIS PROTEIN INHIBITOR LOADED ALBUMIN NANOPARTICLES

Gizem Değer and Gülay Büyükköroğlu

Department of Pharmaceutical Biotechnology, Faculty of Pharmacy, Eskisehir, Turkey
ggizemdegerr@gmail.com

INTRODUCTION

The most common pancreatic neoplasm is pancreatic ductal adenocarcinoma (PDAC), with a 5-year median survival rate of 8% of patients. The tumor microenvironment of PDAC is characterized by an abundant stroma surrounding pancreatic cancer cells and often occupying most of the tumor mass. Overcoming this stromal barrier in PDAC has a decisive role in the success of treatment [1-3].

Human serum albumin binds a wide variety of drug molecules[4]. Anticancer agents combined with albumin have been found to accumulate in tumoral cells through receptor-mediated albumin uptake pathways. Active substances entrapped in albumin nanoparticles are retained until the nanoparticles reach to the therapeutic area where they can be continuously released slowly. Albumin can contribute to improved tumor specificity, reduced drug-induced cytotoxicity and maintain the concentration of therapeutically active agents such as drugs, peptides, proteins and genes over a long period of time [5-6].

SPARC protein released into the extracellular environment during neoplastic progression is expressed in the stromal region or in various types of malignant cells to influence tumor development, invasion, metastasis, angiogenesis, and inflammation. SPARC-induced changes in the tumor microenvironment can suppress or promote the progression of different types of cancer, depending on the tissue and cell type. SPARC expression in PDAC is carried out by stromal barrier cells. Albumin has attracted attention in drug targeting studies with its efficient binding to SPARC [7-8].

The MCAM molecule, which also plays an

active role in ductal adenocarcinoma of the pancreas, is activated by MEIS and the metastasis process is initiated. The MEIS inhibitor-2, developed by Fatih Kocabaş and colleagues, binds to the MEIS protein and suppresses tumoral activity, and therefore it is promising for PDAC drug targeting studies [9].

In this study, MEIS inhibitor-2 (Meis2i) loaded albumin nanoparticles were prepared and various characterization studies were carried out. Finally, the effectiveness of the prepared formulation on pancreatic cancer cells was investigated.

MATERIALS AND METHODS

Materials

Human Serum Albumin was purchased from Sigma Aldrich, Germany. MEIS inhibitor-2 was a kind gift from Meinox Technologies, Turkey.

Methods

Preparation of Meis2i Loaded Albumin Nanoparticles (HSAM4)

20 mg of human serum albumin was placed in a beaker with a volume of 10 ml and 2 ml distilled water was added. A clear albumin solution was obtained by keeping this beaker set at 400 rpm in an environment at 28°C with a magnetic stirrer for 10 minutes. Then, 1 ml of ethanol was added dropwise to this solution to denature the albumin. On the other hand, 4 mg of Meis2i was weighed in a cryotube and dissolved in 3 ml of ethanol by sonication for 30 seconds. This phase containing the active substance was dropped into the aqueous phase containing the albumin. Finally, nanoprecipitation was completed by adding 2 ml of ethanol dropwise. The beaker was kept under the same conditions for 24 hours to completely remove the ethanol.

Some of the formulations prepared by repeating these processes were lyophilized and some of the nanoparticles were stored in powder form.

Particle Size, PDI and Zeta Potential Measurement

The particle size and zeta potential of the HSAM4 were detected using a zeta sizer (Malvern ZS-90, UK).

Entrapment Efficiency

A new method has been developed in Ultra Performance Liquid Chromatography (UPLC) to quantify a new active substance, MEIS inhibitor-2. This method was validated in the guidance of ICH, 2005.

Entrapment Efficiency of HSAM4 was calculated with the equation shown below.

Entrapment efficiency (%) = Amount of drug in the nanoparticle / Amount of drug initially added * 100

Dissolution Study

To study the release of Meis2i from HSAM4 nanoparticles, 1200 µg of lyophilized HSAM4 was weighed and dispersed in 2 ml pH 7.4 distilled water. This mixture was then transferred to 4 ml cryotubes, each containing 500 µL. Next, the volume of the cryotubes was made up to 3 ml with pH 7.4 PBS solution adjusted to 37°C. The prepared release media were placed horizontally on a magnetic stirrer with heater placed on a shaker to keep the temperature constant at 37°C and left to shake at 130 rpm. The shaking process was stopped at the specified times and 500 µL of sample was taken from the tubes. Samples were centrifuged at 16000 rpm for 5 minutes to isolate Meis2i from the particles into the release medium. After centrifugation, the supernatant fractions were separated for analysis. The release study with nanoparticles was continued for 21 days. N=3 studied.

MTT Assay

In this study, human pancreatic duct-derived pancreatic cancer cell line (PANC-1) and human endothelial cell line (HUVEC) were used to evaluate the effects of formulations at the cellular level. Cell culture was done for processes such as cell growth and application of formulations. For all cell lines, DMEM containing 10% Fetal Bovine Serum, 1% penicillin-streptomycin, 1% glutamine was

preferred. During the processes such as cell reproduction and MTT studies, the cells were kept at 37°C in atmospheric conditions containing 5% CO₂ and 95% air.

RESULTS AND DISCUSSION

Particle Size and Zeta Potential

The table given below shows the measurement results.

Table 1. Measurement results of HSAM4 and HSAM4L.

Formulation	Size	PDI	Zeta Potential
HSAM4	215,567	0,277	-32,133
HSAM4L	328,867	0,341	-26,6

Entrapment Efficiency

It was determined that 93% of Meis2i was loaded into HSAM4 nanoparticles. This ratio suggested that the chosen polymer and nanoparticle preparation method is ideal for the active substance.

Dissolution Study

The *in vitro* release profile of Meis2i is shown in Figure 1. below.

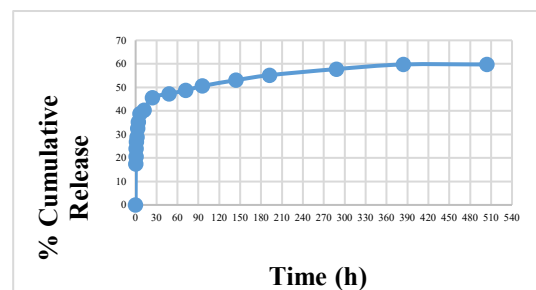


Figure 1. *In vitro* release profile of Meis2i

MTT Assay

The 24th and 48th hour MTT results of HSAM4, and active substance (Meis2i) applied to healthy and pancreatic cancer cells at different concentrations are given below.

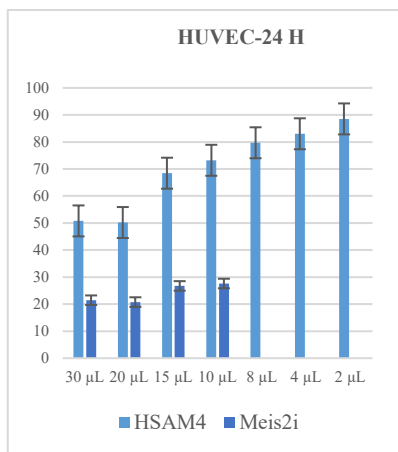


Figure 2. 24 h MTT results/HUVEC

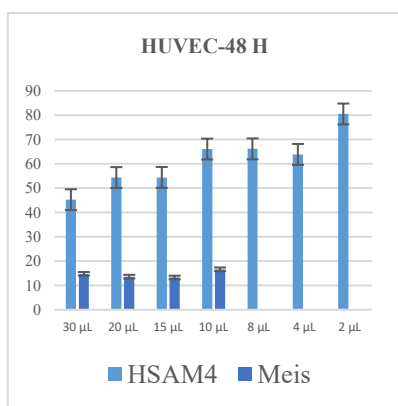


Figure 3. 48 h MTT assay results/HUVEC

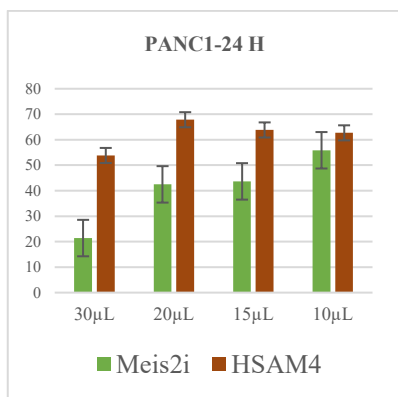


Figure 4. 24 h MTT assay results/PANC1

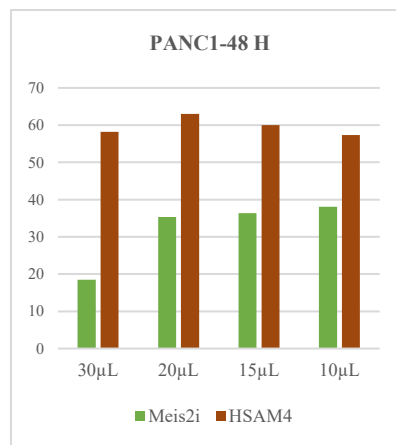


Figure 4. 24 h MTT assay results/PANC1

CONCLUSION

The small particle size of the prepared nanoparticles is an advantage for the accumulation of the applied drug in the tumoral area. In addition, when the zeta potential results are examined, it is seen that the zeta potential of the colloidal system is in desired range for its stability.

The results of the release study prove that albumin nanoparticles are capable of releasing the anti-cancer agent into the body in a controlled manner for a long time.

In addition, it is seen that the active substance alone exhibits high cytotoxic activity in healthy cells. Healthy cells showed high viability with the HSAM4 formulation in which the active substance was encapsulated. Conversely, the formulation appears to be toxic to pancreatic cancer cells.

REFERENCES

1. Winer, L. K., Dhar, V. K., Wima, K., Morris, M. C., Lee, T. C., Shah, S. A., Ahmad, S.A., Patel, S. H. (2019). The Impact of Tumor Location on Resection and Survival for Pancreatic Ductal Adenocarcinoma. *Journal of Surgical Research*, 239, 60-66.
2. Lunardi, S., Muschel, R. J. and Brunner, T. B. (2014). The stromal compartments in pancreatic cancer: are there any therapeutic targets? *Cancer Letters*, 343(2), 147-155.
3. Kota, J., Hancock, J., Kwon, J., Korc, M. (2017). Pancreatic cancer: Stroma and its current and emerging targeted therapies. *Cancer Letters*, 391, 38-49.

4. Yamasaki, K., Chuang, V. T. G., Maruyama, T., & Otagiri, M. (2013). Albumin–drug interaction and its clinical implication. *Biochimica et Biophysica Acta (BBA)-General Subjects*, 1830(12), 5435-5443.
5. Sozer, S. C., Egesoy, T. O., Basol, M., Cakan-Akdogan, G., Akdogan, Y. (2020). A simple desolvation method for production of cationic albumin nanoparticles with improved drug loading and cell uptake. *Journal of Drug Delivery Science and Technology*, 60, 101931.
6. Zeeshan, F., Madheswaran, T., Panneerselvam, J., Taliyan, R., Kesharwani, P. (2021). Human serum albumin as multifunctional nanocarrier for cancer therapy. *Journal of Pharmaceutical Sciences*, In press.
7. Chlenski, A. and Cohn, S. L. (2010). Modulation of matrix remodeling by SPARC in neoplastic progression. *In Seminars in Cell & Developmental Biology*, 21(1), 55-65.
8. Yu, X. Z., Guo, Z. Y., Di, Y., Yang, F., Ouyang Q., Fu, D. L., Jin, C. (2017). The relationship between SPARC expression in primary tumor and metastatic lymph node of resected pancreatic cancer patients and patients' survival. *Hepatobiliary & Pancreatic Diseases International*, 16(1), 104-109.
9. Von Burstin, J., Bachhuber, F., Paul, M., Schmid, R. M., Rustgi, A. K. (2017). The TALE homeodomain transcription factor MEIS1 activates the pro-metastatic melanoma cell adhesion molecule Mcam to promote migration of pancreatic cancer cells. *Molecular Carcinogenesis*, 56(3), 936-944.

ACKNOWLEDGMENT

This study was supported by Anadolu University Scientific Research Foundation (Project No: 1909S104). We would also like to thank Assoc.Pr. Fatih Kocabaş for supplying the Meis inhibitor-2.

OP-21

Differentiating of Benign and Malignant Thyroid Nodules with ANFIS by Using GA Algorithm and Proposing a Novel Computer Aided Diagnosis (CAD) Based Risk Stratification System of Thyroid Nodules

Ahmet Cankat ÖZTÜRK¹, Bülent HAZNEDAR², Hilal HAZNEDAR³, Osman EROĞUL¹, Seyfettin ILGAN⁴, Adem KALINLI⁵

¹ Department of Biomedical Engineering TOBB ETU University, Ankara, Turkey

² Department of Computer Engineering Gaziantep University, Gaziantep, Turkey

³ Institute of Science and Technology, Department of Computer Engineering Erciyes University, Kayseri, Turkey

⁴ Department of Nuclear Medicine Guven Hospital, Ankara, Turkey

⁵ Presidency Office, Rectorate, Middle East Technical University, Ankara, Turkey

Abstract

The purpose of this article is to differentiate malignant from benign thyroid nodules using Adaptive-Network Based Fuzzy Inference Systems (ANFIS) with Genetic Algorithm (GA) and ANFIS trained with derivative-based classical algorithms and to evaluate their diagnostic performances. In addition we propose a novel computer aided diagnosis (CAD) based risk stratification system for the thyroid nodule's US classification that is not in the literature.

1. Introduction

Although ultrasonography is the most commonly used and most effective imaging technique in the evaluation of thyroid nodules, the gold standard in the differential diagnosis of thyroid nodules is fine needle aspiration biopsy (FNAB). Even though it is an effective method, applying FNAB to all nodules is not a practical solution. Unnecessary FNAB application both creates a burden on the health system and causes anxiety in the patient as it is an invasive procedure. It is current practice to classify the nodules into risk classes according to their ultrasonographic features and to make the FNAB recommendation according to these features. Though the guidelines used show significant similarities, they suggest different risk classification categories and dimension criteria [1-2].

However ultrasonography is considered to be the most important imaging technique in the evaluation of thyroid nodules, its most important disadvantage is that it is a subjective method. Therefore, the need for an objective and effective method that can reduce the rate of misdiagnosis is becoming increasingly critical in the evaluation of ultrasound images for thyroid nodules. Since it is an important technique used in a common health problem, differential diagnosis of thyroid nodules is one of the subjects of studies on machine learning and deep learning methods.

In this study, thyroid nodules of patients with histopathologically confirmed diagnoses were evaluated. Sonographic images of thyroid nodules were evaluated retrospectively by a specialist sonographer (S.I.) with more than 20 years of experience in thyroid sonography and the sonographic features of the nodules were determined specifically. By using these features determined by the sonographer, classification studies were carried out using an innovative approach such as training the ANFIS model with the GA algorithm in the differential diagnosis of malignant/benign nodules, which are considered to be real world problems. In addition, the performance of the innovative approach used is also compared to the performance of ANFIS trained with derivative-based classical algorithms. In addition, the Decision Tree algorithm was

used to determine the most effective features in the differential diagnosis of malignant/benign. Thus, a guide that does not exist in the literature has been proposed, showing the effect of sonographic finding on the differential diagnosis of malignant/benign.

2. Materials and Methods

In order to successfully classify malignant/benign differential diagnoses using sonographic features of thyroid nodules, the outcome and antecedent parameters of the ANFIS model are optimized with the GA algorithm. Therefore, the proposed hybrid approach can be considered as a combination of ANFIS and GA methods.

2.1. Dataset description

In this study, a data set covering 398 thyroid nodules with histopathologically confirmed results of 224 patients with thyroid cancer who were operated at Güven Hospital between September 2012 and September 2016 and whose records were kept prospectively was used. Ultrasonographic images of patients with known surgical pathologies were evaluated retrospectively and nodules whose all sonographic features could be evaluated were included in the study. This retrospective study was approved by the Güven Hospital Scientific Committee and the informed consent requirement was waived.

Sonographic examinations were performed with a Siemens Acuson ultrasound system and a 12 MHz transducer. The nodules were examined retrospectively and 27 sonographic features of the nodules and their sub-features were specifically determined.

The largest diameter was taken as the nodule size. The mean age of 224 patients was 40.98 (range, 16-77 years) and 49 (21,875%) of these patients were male and 175 (78,125%) were female. Of the 398 nodules of 224 patients examined, 284 were malignant and 114 were benign.

2.2. Adaptive neuro-fuzzy inference system (ANFIS)

ANFIS is an artificial system developed considering Takagi Sugeno fuzzy model [3]. The created model has both learning ability of neural networks and the ability to inference feature of fuzzy logic. It calculates the output by distributing the input data blurred with membership functions over the network with fuzzy rules. Since this process provides inference capability to the ANFIS model, its performance in estimation problems is quite high. Thus, a hybrid artificial intelligence model with combining two methods is created.

2.3. Genetic Algorithm

Genetic Algorithm (GA), the basic principles of which were introduced by John Holland in the 1970s, has been successfully applied in many types of problems [4]. GA is a heuristic algorithm used to find exact or approximate results in an optimization or search problem. This algorithm is inspired by techniques in evolutionary biology such as inheritance, mutation, selection and crossover.

2.4. Training ANFIS using the GA algorithm

ANFIS has two different types of parameters that need to be optimized, premise and consequent. Derivative-based algorithms are generally used to optimize these parameters of

ANFIS. However, optimizing the ANFIS parameters has been one of the main problems due to the slow convergence of derivative-based algorithms, their local minima, and their dependence on initial values. In this context, a population-based genetic algorithm, which is a powerful algorithm that will eliminate the aforementioned disadvantages of derivative-based algorithms, has been used to optimize the parameters of a difficult model such as ANFIS.

3. Results and Discussion

The training and test datasets of 398 thyroid nodules, including 27 sonographic features, were created by randomly determining the nodules, using the random sampling method. In this context, it is divided into two different groups as 70-30% and 80-20%. In addition, the K-part method, one of the cross validation methods, was also used in order to accurately evaluate the generalization ability of the methods. The purpose of the K-part cross-validation method is to test the validity of the results by repeating an experiment under independent conditions. In this study, 5-fold and 10-fold cross validation methods were used for data splitting. In order to measure the performance of the proposed method, three most commonly used measurements, namely accuracy, sensitivity and specificity, were used.

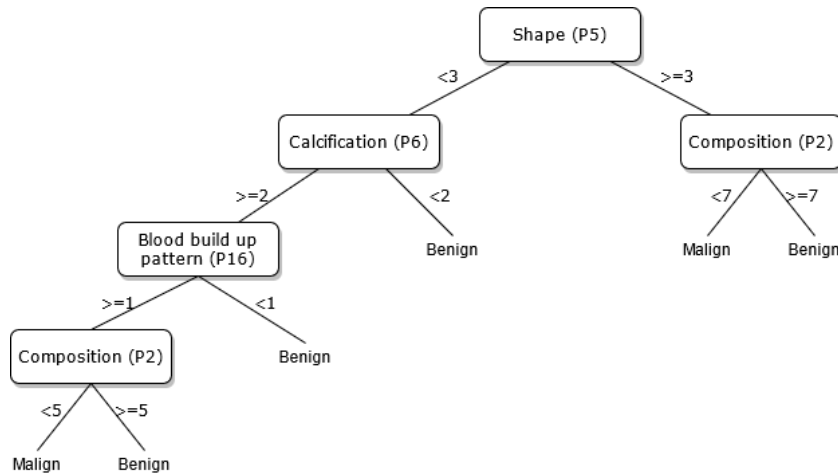
First, classification results were obtained for the histopathological malignant/benign differential diagnosis of nodules within the scope of 27 uniquely determined sonographic findings. The results obtained for each method are given in Table 1, and it was seen that the proposed ANFIS-GA method was more successful than the ANFIS trained with derivative-based classical algorithms method.

Tablo 1. Percentage accuracy (AC), sensitivity (SN) and specificity (SP) of different methods for 27 feature

Classifier	Data Splitting Methods											
	%70-30 splitting			%80-20 splitting			10-fold validation			5-fold validation		
	AC	SN	SP	AC	SN	SP	AC	SN	SP	AC	SN	SP
ANFIS-HB	74.79	65.63	78.16	81.25	72.22	83.87	81.38	69.82	86.06	78.86	65.80	84.28
ANFIS-BP	84.87	71.79	91.25	85,00	66.67	90.32	82.68	64.74	90.60	82.92	65.83	89.76
ANFIS-GA	89.08	89.29	89.01	88.75	83.33	90.32	85.68	74.99	89.93	86.42	79.96	89.58

As can be seen in the results given in Table 1, the overall performance of the proposed method for almost all measurements was found to be more successful than the derivative-based algorithms.

In this study, in addition to the classification processes, an original and new guide, which is not in the literature, has been proposed to assist sonographers in the differential diagnosis of malignant/benign nodules. In this context, decision tree algorithm, one of the data mining methods, was used.



Şekil 1. Trimmed decision tree of 27 sonographic findings

4. Conclusions

It has been seen once again that the GA algorithm is more successful than derivative-based algorithms in the training of ANFIS parameters. In addition, the decision tree algorithm was applied to determine the most effective features in the differential diagnosis of malignant/benign. Thus, a guide that does not exist in the literature has been proposed, showing the effect of sonographic finding on the differential diagnosis of malignant/benign. It has been understood that the proposed method is robust and reliable with the results obtained from the different measurements used in the comparison process. Thus, in the future, it is planned to apply the proposed method to real-world problems in different fields.

5. References

1. Edward G. Grant, Franklin N. Tessler, Jenny K. Hoang, Jill E. Langer, Michael D. Beland, Lincoln L. Berland, John J. Cronan, Terry S. Desser, Mary C. Frates, Ulrike M. Hamper, William D. Middleton, Carl C. Reading, Leslie M. Scutt, A. Thomas Stavros, Sharlene A. Teehey, "Thyroid Ultrasound Reporting Lexicon: White Paper of the ACR Thyroid Imaging, Reporting and Data System (TIRADS) Committee", *Journal of the American College of Radiology*, <https://doi.org/10.1016/j.jacr.2015.07.011>, 2015
2. Yan Zhuang, Cheng Li, Zhan Hua, Ke Chen and Jiang Li Lin, "A novel TIRADS of US classification", *BioMedical Engineering OnLine*, <https://doi.org/10.1186/s12938-018-0507-3>, 2018.
3. J. S. R. Jang, "ANFIS: Adaptive-Network-Based Fuzzy Inference System," *IEEE Trans Syst Man Cybern*, vol. 23, no. 3, pp. 665–685, 1993.
4. M. Mitchell, *An introduction to genetic algorithms*. MIT press, 1998.

Automatic Classification of fMRI Signals with Deep Learning Method

Cemre Candemir^{1,*}, Osman Tayfun Bişkin², Özgül Uslu³, Ali Saffet Gönül⁴ and Mustafa Alper Selver⁵

¹International Computer Institute, Ege University, Izmir, TURKEY

² Department of Electrical-Electronics Engineering, Mehmet Akif Ersoy University, Burdur, TURKEY

³ Department of Neuroscience, Institute of Health Sciences, Ege University, Izmir, TURKEY

⁴ Department of Psychiatry, SoCAT LAB, Faculty of Medicine, Ege University, Izmir, TURKEY

⁵ Department of Electrical-Electronics Engineering, Dokuz Eylul University, Izmir, TURKEY

* Correspondence: cemre.candemir@ege.edu.tr

Abstract:

The main motivation of the study is to accurately predict the type of stimulus from the activation patterns of functional Magnetic Resonance Imaging (fMRI) signals in cases where the type of stimulus not given, or the design of the task is unknown. However, it is a very challenging goal in several aspects. In this context, we propose using long-short term memory (LSTM) for the fMRI signal classification system. The proposed LSTM model categorizes a given signal into sub-categories by using some inherent features of the dataset. The results show that LSTM model has over ~90% accuracy values in terms of precision, recall, and F_1 score for 3 different fMRI tasks.

Keywords: fMRI; classification; deep learning; LSTM

1. Introduction

Functional Magnetic Resonance Imaging (fMRI) is a mode of magnetic resonance imaging (MRI) where the focus is not on the structure of tissues but

on the change of blood oxygen levels in the brain while a task has been performing [1]. fMRI provides a non-invasive method that aims to locate the brain regions responsible for the sought functions. It has several advantages such as providing high spatial resolution and not using radiation, among the other neuroimaging methods. Therefore, it has been using safely both for clinical applications, such as detecting damages caused by neurological diseases, and research for many years [2].

Activation detection in fMRI studies is an important field that has been studied extensively. However, it can be observed that fMRI applications have been developing quite rapidly in the last 20 years [3]. Moreover, it gained further acceleration with deep learning applications. With the deep learning methodologies, not only the detection of the activation areas, but also many groundbreaking studies are carried out, such as the mapping of the whole brain, the establishment of networks between brain areas, the prediction of the seen objects and dreams [4]–[6].

In this study, we aim to predict and classify the fMRI signals, which are acquired by a set of different triggered stimuli sets with deep learning methods. It is a very tough question to accurately predict the type of stimulus from the activation patterns of fMRI signals in cases where the type of stimulus given, or the design of the task is unknown. The challenging points can be summarized in several topics. The most distinctive point is individual differences which bring the multi-subject variability and makes the classification stage much more sophisticated. The other aspect is the structure of the fMRI data which is high dimensional data with low signal-to-noise (SNR) ratio. Finally, the critical point is representing the neuronal activity accurately with machine learning classifiers. In this context, we propose using long-short term memory (LSTM) for the fMRI signal classification system (Fig 1). The proposed LSTM model categorizes a given signal into sub-categories by using some inherent features of the dataset. The results show that LSTM model has over ~90% accuracy values in terms of precision, recall, and F_1 score.

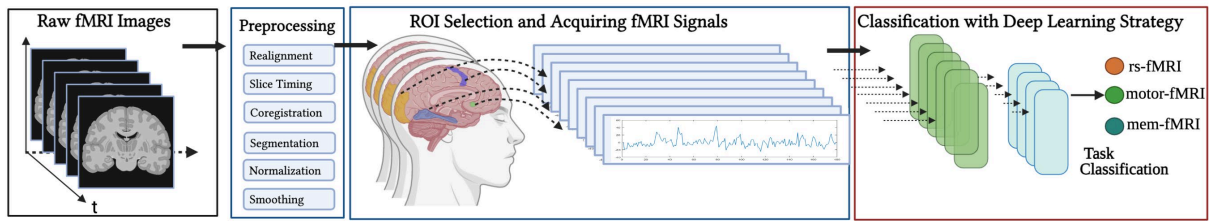


Fig 1. Flowchart of the proposed task classification system with deep learning strategy. Proposed LSTM categorizes a given random signal into three categories, which are resting fMRI, motor fMRI and memory fMRI tasks according to the inherent features of the signals.

2. Materials and Methods

2.1. Datasets and fMRI Signal Acquisition

In this study, a collection of fMRI dataset was constructed with multi-task and multi-subject ($n=44$, mean age $22,12 \pm 1.8$). fMRI images were acquired by using a 3T whole body MRI scanner in Ege University, Turkey. All task designs and fMRI acquisitions were conducted by SoCAT lab, and all procedures approved by the ethics committee of the university.

The fMRI signals collection consists of three different structured fMRI data set conducted with the following tasks: 1) resting-state (rs-fMRI), 2) motor (motor-fMRI), and 3) memory (mem-fMRI). In these tasks, rs-fMRI represents the intrinsic neuronal activity while the participants stay still during the fMRI scan. Motor-fMRI presents the motor activity that emerged while the participants performing finger tapping activity during the fMRI scan. Finally, mem-fMRI signifies the working visual memory activity while the participants have been triggering by visual stimuli.

Parameters of the functional imaging are as follows: echo time (TE) = 30 ms, repetition time (TR) = 3 for the rs-fMRI and mem-fMRI, TR = 2 for the motor-fMRI, voxel size = $3 \times 3 \times 3$, field of view (FOV) = 200×200 mm, slice thickness = 3.5 mm.

After the raw fMRI images are gathered, it requires a preliminary procedure that contains several preprocessing steps. By this way, artifacts can be eliminated or minimized, and functional images can be aligned to a single subject template. The followed preprocessing procedure is realignment, slice timing,

coregistration, segmentation, normalization, and smoothing, respectively. All procedure was done in Matlab with using Statistical Parametric Maps (SPM) toolbox. After the preprocessing, fMRI time series (i.e., signals) are gathered from related areas and detrended before feeding to the deep learning classification model.

2.2. Proposed LSTM Model

Recurrent Neural Networks (RNNs) are intensively used in time series application having temporal dependencies. However, vanishing gradient problem may limit the capability of RNNs. Therefore, long-short term memory (LSTM) was proposed in [7] to overcome with this problem. Fig. 2 shows the internal architecture of an LSTM.

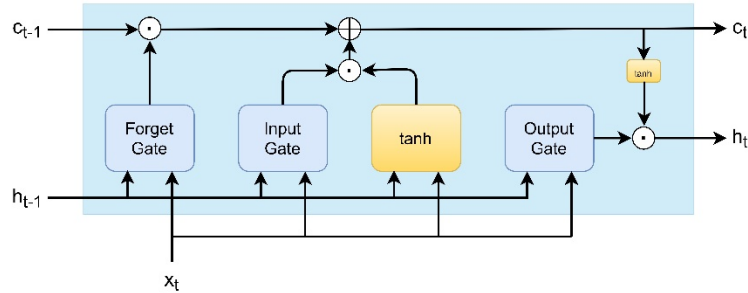


Fig 2. The internal architecture of an LSTM unit.

LSTM network has three gates, named input, output, and forget, and these gates control the data stream inside the layers. Input and output activation information is conducted by means of input and output gates of the unit. Forget gate is responsible to reset the memory of the unit. Then, input (i_t), output (o_t), and forget gates (f_t) of an LSTM layer can be formulated as $i_t = \sigma(W_i[h_{t-1}, x_t] + b_i)$, $o_t = \sigma(W_o[h_{t-1}, x_t] + b_o)$, and $f_t = \sigma(W_f[h_{t-1}, x_t] + b_f)$, respectively. Here x_t represents a time series data at a given time t . W_i , W_o , and W_f represent input, output, and forget weight parameters, respectively. b_i , b_o , and b_f are bias parameters and h_t is the hidden state vector. The hidden state vector is written as $h_t = o_t \odot \tanh(c_t)$, where $c_t = i_t \odot \tilde{c}_t + f_t \odot c_{t-1}$ and c_t denote the cell state. Here \odot represents the Hadamard product and $\tilde{c}_t = \tanh(W_c[h_{t-1}, x_t] + b_c)$, where b_c and W_c are bias and weights parameters.

3. Results

First, fMRI signals are padded before feeding the deep neural. In this way, all fMRI signals become 1×600 vectors. Thus, each signal can be represented by $\mathbf{x} = [x_1, x_2, \dots, x_T]$ where $T = 600$. In the experiments performed, a two-layer network is used to classify fMRI signal into rs-fMRI, motor fMRI, and Mem-fMRI tasks. We employed LSTM deep learning model having two layers with 100 and 75 hidden units, respectively. The first and second hidden units are followed by dropout layers with 0.2 and 0.1 dropout ratios. Adam[8] optimizer is utilized for minimizing the loss function during the training and the learning rate of the optimizer is taken as $lr = 0.001$. Batch size is chosen as 128 and model is trained with 300. Numerical results for the task classification experiment are given in Table 1. Classification performances of models are computed in terms of precision, recall, and F_1 score.

Table 1. Classification performances of models for the task-classification experiment

Task	Precision	Recall	F1-score
Memory-fMRI	93.09	88.74	90.87
Motor-fMRI	95.92	94.99	94.95
rs-fMRI	95.41	97.26	96.33

4. Conclusions

In this study, a LSTM model is developed to classify the fMRI signals. fMRI signals are acquired from three different structured tasks, which are resting state, motor, and memory tasks. Classifying fMRI signals requires machine learning strategies, due to the challenging nature of these kind of signals. It is very difficult to accurately classifying these signals visually or manually, as the signals comes from differently stimulated tasks and contains individual differences among the subjects. On the other hand, machine learning classifiers can provide a powerful identification and classification using some inherent features of the signals. Our computational results show that LSTM model is a powerful strategy with its $\sim 90\%$ accuracy values in terms of precision, recall, and F_1 score on this problem.

References

- [1] S. Ogawa, T. M. Lee, A. R. Kay, and D. W. Tank, "Brain magnetic resonance imaging with contrast dependent on blood oxygenation.," *Proc. Natl. Acad. Sci. U. S. A.*, vol. 87, no. 24, pp. 9868–9872, Dec. 1990.
- [2] C. J. Price, "A review and synthesis of the first 20 years of PET and fMRI studies of heard speech, spoken language and reading," *NeuroImage*, vol. 62, no. 2, pp. 816–847, Aug. 2012, doi: 10.1016/j.neuroimage.2012.04.062.
- [3] P. A. Bandettini, "Twenty years of functional MRI: The science and the stories," *NeuroImage*, vol. 62, no. 2, pp. 575–588, Aug. 2012, doi: 10.1016/j.neuroimage.2012.04.026.
- [4] S. Yu, N. Zheng, Y. Ma, H. Wu, and B. Chen, "A Novel Brain Decoding Method: A Correlation Network Framework for Revealing Brain Connections," *IEEE Trans. Cogn. Dev. Syst.*, vol. 11, no. 1, pp. 95–106, Mar. 2019, doi: 10.1109/TCDS.2018.2854274.
- [5] Y. Gao, Y. Zhang, H. Wang, X. Guo, and J. Zhang, "Decoding Behavior Tasks From Brain Activity Using Deep Transfer Learning," *IEEE Access*, vol. 7, pp. 43222–43232, 2019, doi: 10.1109/ACCESS.2019.2907040.
- [6] T. Horikawa, Y. Kamitani, and Y. Kamitani, "Generic decoding of seen and imagined objects using hierarchical visual features," *Nat. Commun.*, vol. 8, no. 1, Art. no. 1, May 2017, doi: 10.1038/ncomms15037.
- [7] S. Hochreiter and J. Schmidhuber, "Long Short-Term Memory," *Neural Comput.*, vol. 9, no. 8, pp. 1735–1780, Nov. 1997, doi: 10.1162/neco.1997.9.8.1735.
- [8] D. P. Kingma and J. Ba, "Adam: A Method for Stochastic Optimization," *ArXiv14126980 Cs*, Jan. 2017, Accessed: Aug. 26, 2021. [Online]. Available: <http://arxiv.org/abs/1412.6980>

Generation of cell models using CRISPR/Cas9-based gene therapy to study molecular functions of IDH in colorectal cancer

Esra Bulut Atalay^{1,2}, Ece Çakıroğlu^{1,2}, Şerif Şentürk^{1,2}, and Hülya Ayar Kayalı^{1,2,3*}

¹ *Izmir International Biomedicine and Genome Institute, Dokuz Eylül University, Izmir, Turkey*

² *Izmir Biomedicine and Genome Center, Izmir, Turkey*

³ *Department of Chemistry, Division of Biochemistry, Faculty of Science, Dokuz Eylul University, Izmir, Turkey*

*Corresponding Author

Abstract

CRISPR/Cas9 method is based on Cas9-sgRNA mediated cleavage of a target DNA sequence, creating double-strand DNA breaks which are subsequently repaired via the NHEJ or HDR pathways. CRISPR/Cas9-based genome editing has been used for various purposes such as engineering genetic models with specific point mutations or simply knocking out a target gene. Isocitrate dehydrogenase (IDH) enzymes catalyze the decarboxylation of isocitrate to α -Ketoglutarate (α -KG) in the TCA cycle. When tumor-based point mutations occur in arginine residues (such as R140, R170, etc.) in the active site, mutant IDH enzymes catalyze 2 Hydroxyglutarate (2HG) conversion from α -KG. While 2HG is found in very small amounts in healthy cells, its excessive synthesis and accumulation in cancer cells direct the cell to metastasis. In the present study, two different cell models have been developed to understand the role of 2HG in colorectal cancer metastasis. In the first model, the IDH1 gene was silenced by CRISPR/Cas9 method in SW620 cells. The gRNAs were cloned into the px458 vector and plasmid isolation was performed from the clones obtained after transformation of this vector into E.coli. The plasmids were then transfected into SW620 and cells with GFP expression were enriched by FACS sorting. IDH1 protein level was analyzed by the Western blotting method. Sanger sequencing confirmed the generation of a cell model carrying the IDH1^(wt/KO) genetic profile. In the second model, R132H mutation was generated. First, cells were treated with 200 ng/ml nocodazole to block them in the M phase and the Cas9 enzyme was used to generate site-specific double-strand DNA breaks. Synchronized cells were given RNP complex to repair the generated DNA breaks by the HDR mechanism. Nucleofection was performed with the SF cell line 4D nucleofection kit and the nucleofection rate was determined as 44%. After nucleofection, 5 single-cell clones were selected and Sanger sequencing revealed that the IDH1^(wt/R132H) mutation was successfully generated in one clone. The CRISPR/Cas9 method allows site-specific and high-efficiency point mutation generation and can also be used to knock out the target gene.

Keyword: CRISPR/Cas9 method, gene therapy, colorectal cancer

Introduction

CRISPR/Cas9-based gene therapy is one of the encouraging methods used to treat human genetic diseases such as cancer. To date, it has been used in vivo (in patient) or in vitro (in various cell types). This method is based on the fact that the Cas9 enzyme cuts only the target region by recognizing the complementary sequences of the sgRNAs selected for the target gene region in the genomic DNA (Senturk vd., 2017). CRISPR/Cas9-based genome editing has also been used to create genetic models specifically to study and treat human genetic diseases associated with point mutations (Wu et al., 2020).

The TCA cycle, which forms a large part of aerobic respiration, is the energy production step. Decarboxylation of isocitrate to α -Ketoglutarate (α -KG) occurs by isocitrate dehydrogenase (IDH) enzymes in the TCA cycle (Sajani et al., 2017). When tumor-based point mutations occur in arginine residues (such as R140, R132, R170, etc.) in the active sites of IDH1 and IDH2 enzymes, this mutation affects the catalytic activity of the enzyme. Mutant IDH enzymes gain neomorphic enzymatic activity and catalyze 2-HG conversion from α -KG instead of isocitrate to α -KG conversion (Dang et al., 2009). Healthy cells have low levels of 2HG. High level of expression and accumulation of 2HG in cells affects many metabolic pathways and it is known that it plays an active role in the pathogenesis of some cancer types. However, the role of mutant and wild-type IDH enzymes in malignant transformation and development in colorectal cancer remains unclear (Grassian et al., 2012). In the present study, wild-type IDH1 enzyme will be transformed into a mutant in colorectal cancer (SW620) cell line by CRISPR/Cas9 method. In addition, a different cell model will be developed by silencing the IDH1 enzyme with the CRISPR/Cas9 method.

Method

Cell Culture: The SW620 cell line was grown in RPMI medium containing 10% FBS and 1% Penicillin-streptomycin in incubation with 5% CO₂.

Design and transfection of sgRNAs: 2 different sgRNAs for the IDH1 enzyme were selected from the Brunello library and cloned into a pX458 vector that expresses Cas9 protein and contains GFP-tag. After the transformation of the sgRNA cloned pX458 vector into E.coli, 5 clones were selected and plasmid isolation was performed with the Nucleospin plasmid kit. After checking the absence of mutations in the isolated plasmids by Sanger sequencing, the sgRNA cloned plasmid was transfected into SW620 cells with the polyethylenimine (PEI) agent. The sgRNA cloned to plasmid targeting the Renilla gene was used as a control.

Selection of colonies after FACS analysis: After transfection, cells containing GFP-tag were differentiated by FACS analysis, and they were seeded as single-cell in 96 well plate. Proliferating cells were seeded in 12 well, 6 well plates, and then T25 flask, respectively (Giuliano et al., 2019).

Western Blot Method: The cell pellet was fragmented by sonication in RIPA buffer and then centrifuged at 13,300 rpm for 15 minutes. Cell lysates were mixed with SDS-PAGE loading buffer at a ratio of 3:1 and incubated at 95 °C for 15 minutes. Samples containing 30 micrograms of protein were loaded onto 12% SDS-PAGE gels and run at 100 V. The nitrocellulose membrane transferred from the gel was washed 3 times with TBST (TBS solution containing 0.1% Tween-20) after blotting in 5% milk powder. It was incubated with primary antibody solutions for 2 hours. Washed membranes were incubated with HRP-conjugated secondary antibody solution for 1 hour and visualized by the ECL western blotting analysis system. GAPDH was used as the control antibody (Subaşı et al., 2020).

In vitro transcription of sgRNA: Two sgRNAs selected for the IDH1 gene will be amplified by PCR as the in vitro transcript product of target donor DNA. The DNA sequence will be generated by overlapping PCR with 4 primer pairs. Afterward, IVT (in vitro transcription) reaction was performed with the T7 polymerase enzyme with PCR product. The synthesized RNA sequences were purified with the QIAmp RNeasy Mini Kit (Li et al., 2017).

Preparation of RNP (Ribonucleoprotein) complex and selection of colonies after nucleofection: RNP complexes were prepared with 100 pmol Cas9 protein, 130 pmol sgRNA, and 100 pmol of Cas9 protein. Later ssDNA addition, the RNP complex was formed at 37 °C for 10 minutes. After nocodazole (100,

200, and 400 ng/ml) treatment, nucleofection was performed with the SF cell line 4D nucleofector kit. After 3 days, the nucleofection rate was determined by FACS analysis. Cells were seeded in a 96 well plate, one cell per well and single-cells were a cell display device (solentim cell metric). When single-cells proliferated, they were grown in 12 well and 6 well plate and T25 flask, respectively. DNA isolation was carried out with QIAGEN DNA isolation kit from 5 selected colonies and the target region amplified by PCR was sent to Sanger sequencing (Li et al., 2017).

Result: Single-cell colonies in which the IDH1 gene was silenced were obtained successfully. The protein level of the IDH1 gene was determined by the Western Blot method and it was observed that the level of IDH1 decreased significantly in 1 colony out of 8 colonies (Figure 1A). Since IDH1 protein synthesis is not completely finished, it was checked by the Sanger sequencing method and gene silencing was found to be heterogeneous (IDH1^{wt/KO}) (Figure 1B).

To create the R132H mutation firstly cells treated with 100, 200, and 400 ng/ml nocodazole to determine the optimum concentration. Cells were stained with propidium iodide (PI) dye and the phase in which the cell was retained was determined by flow cytometry. It is shown that the best concentration was 200 ng/ml and the cells were kept in the G2/M phase (Figure 1C). The nucleofection rate was determined by FACS analysis as %34,5 and %44 for control and second gRNA, respectively (Figure 1D). Cells were tested with a cell imaging device after seeding in 96 well plates, one cell per well (Figure 1E). 5 colonies were selected from single-cells. Sanger sequencing results show that 1 colony contains heterogeneous R132H mutation (IDH1^{wt/R132H}) (Figure 1F).

Discussion: Typically, the Cas9 enzyme cuts only the target region by recognizing the complementary sequences of the sgRNAs in the genomic DNA. It leads to a double-strand break (DSB) in the target DNA. There are two different cellular DNA repair machinery to repair DSB is homology-directed repair (HDR) or non-homologous end joining (NHEJ) (Wu et al., 2020). To generate point mutation, Cas9-mediated DSB is repaired via the HDR method. The treatment of Nocodazole, an antineoplastic agent, kept the cell in the M phase and as a result of giving RNP complex and template DNA to the synchronized cells, the target point mutation was successfully created. According to the Sanger sequencing results, it was observed that the mutation occurred heterogeneously (IDH1^{wt/R132H}). The wild-type allele will continue to carry out the reaction of oxidative decarboxylation of α -KG. However, the mutant allele will gain neomorphic enzymatic activity and carry out the reduction of α -KG to 2HG. Some metabolites must be present in the steady-state phase for the cell to survive. Considering that the TCA cycle is in the important stage of energy production, one allele of the IDH1 gene is expected to remain wild-type.

Selected gRNAs in the silencing of the IDH1 gene successfully recognized the target gene and DSB breaks were created with the Cas9 protein. Similarly, the IDH1 gene was not completely silenced (IDH1^{wt/KO}). The fact that an allele remains wild type is thought to be because it is necessary for the TCA cycle to continue.

Conclusion: CRISPR/Cas method has already shown great potential in generating disease models because of its advantages. In the current project, R132H mutation was successfully generated and the IDH1 gene was knocked out to investigate the effects of 2HG in colorectal cancer metastasis. The used method allows site-specific and high-efficiency point mutation generation and can be used for the creation of new models in the future.

References: Dang, L., White, D.W., Gross, S., Bennett, B.D., Bittinger, M.A., Driggers, E.M., Fantin, V.R., Jang, H.G., Jin, S., Keenan, M.C., Marks, K.M., Prins, R.M., Ward, P.S., Yen, K.E., Liaw, L.M., Rabinowitz, J.D., Cantley, L.C., Thompson, C.B., Vander Heiden, M.G., Su, S.M. 2009. Cancer-associated IDH1 mutations produce 2-hydroxyglutarate, *Nature*, 462(7274), 739-44.

Giuliano, C. J., Lin, A., Sheltzer, J. 2019. Generating single cell-derived knockout clones in mammalian cells with CRISPR/Cas9, *Current protocols in molecular biology*, 128(1).

Grassian, A. R., Lin, F., Barrett, R., Liu, Y., Jiang, W., Korpai, M., Astley, H., Gitterman, D., Henley, T., Howes, R., Levell, J., Korn, J.M., Pagliarini, R. 2012. Isocitrate dehydrogenase (IDH) mutations promote a reversible ZEB1/mir-200-dependent epithelial-mesenchymal (EMT) transition, *Journal of Biological Chemistry*, 287(50), 42180-42194.

Li, H., Beckman, K. A., Pessino, V., Huang, B., Weissman, J. S., Leonetti, M. D. 2017. Design and specificity of long ssDNA donors for CRISPR-based knock-in, *BioRxiv*, 178905.

Sajnani, K., Islam, F., Smith, R.A., Gopalan, V., Lam, A.K.Y. 2017. Genetic alterations in Krebs cycle and its impact on cancer pathogenesis, *Biochimie*, 135, 164-172.

Senturk, S., Shirole, N. H., Nowak, D. G., Corbo, V., Pal, D., Vaughan, A., Tuveson D. A., Trotman L. C., Kinney J. B., Sordella, R. 2017. Rapid and tunable method to temporally control gene editing based on conditional Cas9 stabilization, *Nature communications*, 8, 14370.

Subaşı, E., Atalay, E.B., Erdoğan, D., Sen, B., Pakyapan, B., Kayalı, H.A. 2020. Synthesis and characterization of thiosemicarbazone-functionalized organoruthenium (II)-arene complexes: Investigation of antitumor characteristics in colorectal cancer cell lines, *Materials Science and Engineering: C*, 106, 110152.

Wu, S. S., Li, Q. C., Yin, C. Q., Xue, W., Song, C. Q. 2020. Advances in CRISPR/Cas-based gene therapy in human genetic diseases, *Theranostics*, 10(10), 4374.

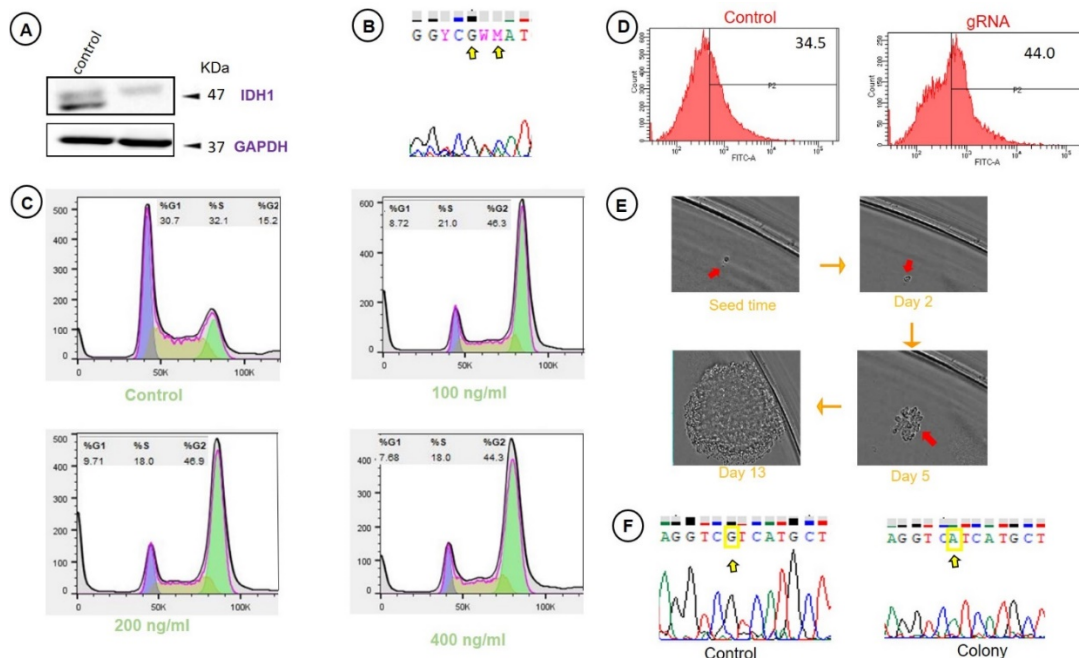


Figure 1: Western blot was used to analyze the protein level in the single-cell colony and control after IDH1 knockout by the CRISPR/Cas9 method (A). Sanger sequencing results show that the IDH1 gene silenced heterogenous in 1.colony (B). The cells were PI stained after nocodazole treatment with 100, 200, and 400 ng/ml. The control cells were treated with DMSO(C). FACS analysis for GFP protein expression after nucleofection for both control and second gRNA (D). Clonality report for single-cell during 13 days (E). Sanger sequencing results of both control and fifth colony which carry R132H mutation (F).

Radiomics-Machine Learning Analysis for Discrimination of Malign and Benign Breast Lesions on Mammography Images

Erkan AKKUR¹, Oğuz LAFCI², Galip ÖZDEMİR¹, Pelin Seher ÖZTEKİN², Osman EROĞUL¹,
Pınar CELEPLİ³, Pınar Nercis KOSAR²

¹ Department of Biomedical Engineering TOBB ETU University, Ankara, Turkey

² Department of Radiology, Ankara Training and Research Hospital, Ankara, Turkey

³ Department of Pathology, Ankara Training and Research Hospital, Ankara, Turkey

Abstract

In this study, it is aimed to investigate the analysis radiomics-machine learning on diagnostic performance in differential malign and benign breast lesions using mammography images. In this retrospective study included 101 patients (40 benign and 61 malign). 195 of region of interests (ROIs) were drawn manually by two expert radiologists. Then, using gray level thresholding and morphological operations techniques, each of ROI were segmented on "MATLAB 2020a" program. 126 radiomic features were extracted for each ROI. For eliminating redundant radiomics features, Kruskal Wallis and Relief feature selection methods were used respectively. A total 44 radiomics features were selected after feature selection process. Logistic regression, naive bayes, support vector machine and k-nearest neighbors machine learning algorithms (ML) were used to as classifiers. 10-fold cross validation was applied to measure and evaluate machine learning models. Accuracy, sensitivity and specificity were used as the primary measures of performance of radiomics-machine learning model. Among the machine learning algorithms, support vector machine had the best performance (93.3%, 95.6%, 91.1%). In addition, we found that the feature selection method improved the performance for all ML models. By building the radiomics-ML based analysis with the optimal feature subset, the performance of discrimination of benign and malign lesions showed excellent results which we believe would be useful for clinical practice.

Keywords: Radiomics, Machine Learning, Feature Selection, Breast Cancer

1. Introduction

Digital mammography is the first choice of imaging method for early detection of breast cancer [1]. It may be difficult to discriminate the benign and malign lesions while using mammography due to the overlaps breast tissue and individual differences in the breast density [2]. Furthermore, mammography images have massive hidden features which may not be seen by visually. However, radiomics is a new image-analysis approach which is useful for defining hidden information on radiological images as it extracts the high number of quantitative features from such images. When combined with machine learning techniques, the radiomics analysis seeks to improve the diagnostic performance to distinguish benign and malignant lesions in recent years [3]. The aim of this study was to investigate optimal machine learning for discrimination of breast malign and benign lesion using radiomics features. In addition, we investigated whether feature selection method can improve the performance radiomics-machine learning analysis.

2. Materials and Methods

This retrospective study was approved by the Ankara Training and Research Committee and the informed consent requirement was waived. All patients who underwent digital mammography were retrieved from the Picture Archiving and Communication System (PACS) between April 2015 and April 2020. All patients underwent mammography using IMS Giotto (Bologna-Italy). The inclusion criteria were as follows: (1) patients who had suspected breast lesions and accepted digital mammography; and (2) patients were confirmed with benign and

malign breast lesions by histopathologic examinations or the ones who were confirmed with benign lesions as a result of two years radiological periodic follow-up. A total 101 female patients (age range, 34-89 years, mean age, 57,5 years) with breast tumors were enrolled in this study. There were 40 patients in benign group, and 61 patients in malign group.

2.1. Selection of Region of Interest

All digital mammography images were saved as digital imaging and communications in medicine (DICOM) data. Firstly, mediolateral oblique (MLO)/craniocaudal (CC) position on DICOM images, 195 of region of interests (ROIs) were defined manually by two expert radiologists (figure 1-b). Disagreements between the expert radiologists were resolved by consensus. Then, using gray level thresholding and morphological operations techniques, each of ROI were segmented on “MATLAB 2020a” program (figure 1-c).

2.2. Radiomics Workflow

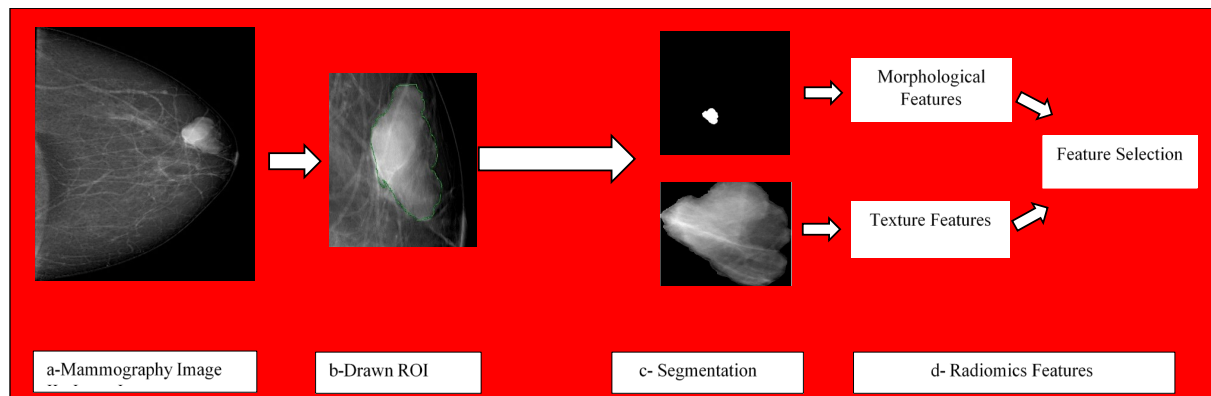


Figure 1:Radiomics Workflow

Figure 1 shows an outline of the radiomics analysis in this study. The typical radiomic analysis includes morphological and textural features (figure 1-d). Morphological features reflect that shape and physical characteristics of the ROI [4]. Texture features can be divided as: (i) first order statistics, (ii) second order statistics, and (iii) higher order statistics. Histogram is recognized as the first-order statistics method that global textural features can be extracted from the intensity histogram of the ROI [5]. Gray-level co-occurrence matrix (GLCM) is of the second-order statistical method that measures textural features based on relationship between two pixels [5-6]. High-order statistical methods are gray level run length matrix (GLRM) that are based on relation between a pixel and the neighbor pixels [5,7]. For GLRM and GLCM matrices can be defined different matrices for different angles as 0° , 45° , 90° and 135° [5-7].

Table 1:Radiomics Features

Methods	Radiomics Features	Feature Numbers
Morphological	Area, Perimeter, Convex Area, Solidity, Eccentricity, Dispersion, Compactness etc.	15
Histogram	Mean, Standard Deviation, Variance, Kurtosis, Skewness, Interquartile Range etc.	15
GLCM	Contrast, Correlation, Energy, Entropy, Homogeneity, Sum Average, Sum Variance etc.	52
GLRM	Short Run Emphasis, Long Run Emphasis, Gray Level Nonuniformity, Run Percentage etc.	44

Total	126
-------	-----

In this study, 126 radiomics were calculated as follows 15 morphological, 15 histogram-based, 52(13x4) GLCM and 44 (11x4) GLRM features. GLCM and GLRM features were calculated separately for four directions as 0°, 45°, 90° and 135. Table 1 shows the radiomics features derived from the images. All radiomics features were calculated using “MATLAB 2020a” program.

2.3. Feature Selection

Feature selection is a process that eliminates unnecessary features to improve the performance results of classification. Firstly, 126 radiomics features were subjected to Kruskal Wallis feature selection method commonly known as one-way ANOVA test to find out benign and malign discriminating features for 5% significance level. Then, we applied Relief feature selection method to the non-redundant feature set generated and choose top-ranked features [8].

2.4. Machine Learning Techniques

In the literature, machine learning techniques are generally used for classification. For the breast lesion classification, the four machine learning methods were used, namely logistic regression (LR), naive bayes (NB), support vector machine (SVM) and k-nearest neighbors (K-NN) [3]. Ten folds cross validation was used to measure and evaluate machine learning models. Accuracy, sensitivity and specificity performance metrics were used to assess the performance of machine learning methods which are formulated as:

$$\text{Accuracy} = \frac{TP+TN}{TP+TN+FP+FN} * 100, \text{ Sensitivity} = \frac{TP}{TP+FN} * 100, \text{ Specificity} = \frac{TN}{TN+FP} * 100$$

3. Results

A total 44 radiomics features remained after Kruskal Wallis-Relief (KWR) feature selection process, including 10 morphological parameters, 3 histogram parameters, 15 GLCM and 16 GLRM parameters. The 44 radiomics features were imported to the machine learning models for discrimination analysis.

Table 2: Overall Classification Performance of Machine Learning Methods

Methods	Accuracy		Sensitivity		Specificity	
	WFS	KWR	WFS	KWR	WFS	KWR
LR	84,6	92,8	85,3	93,1	83,5	86,1
NB	90,3	92,8	91,3	94	89,9	91,1
SVM	91,3	93,3	95,5	95,6	84,8	91,1
K-NN	86,7	91,8	89,7	95,6	81,1	86,1

Table 2 shows the difference in classification results by the classifier when classification was performed on without any filter selection (WFS), combining Kruskal-Wallis-Relief (KWR) feature selection. The accuracy, sensitivity and specificity of each classifier; using without any feature selection (WFS) was LR: 84.6, 85.3, 83.5; NB:90.3, 91.3, 89.9; SVM:91.3, 95.5, 84.8; K-NN:86.7, 89.7, 81.1 and the classification performance was the highest SVM adopted as a classifier. The accuracy, sensitivity and specificity of each classifier; using by combining

Kruskal Wallis and Relief feature selection (KWR) was LR:92.8, 93.1, 86.1; NB:92.8, 94, 91.1; SVM:93.3, 95.6, 91.1; K-NN:91.8, 95.6, 86.1 and the classification performance was the highest SVM adopted as a classifier. As can be seen in the results given in Table 2, combining Kruskal Wallis and Relief feature selection (KWR) method improved the accuracy, sensitivity, specificity values for all machine learning methods.

4. Discussion and Conclusion

In this study, we conducted a radiomics-machine learning model to investigate the discrimination malign and benign breast lesions. Morphological and texture features namely histogram, GLCM and GLRM were extracted as radiomics features. Kruskal Wallis-Relief feature selections were used to eliminate redundant radiomics features. Logistic regression, naive bayes, support vector machine and k-nearest neighbors machine algorithms were calculated to differentiate benign and malign breast lesions on digital mammography images. To verify the reliability and repeatability, 10-fold cross validation was adopted. Applying feature selection methods enhanced the classification performance all machine learning models. In the accuracy, sensitivity and specificity, the best performance of proposed model is using support vector machine learning model with values of 93.3 %, 95.6%, and 91.1% respectively. In view of the foregoing, the model using in this study achieved an excellent result in discrimination benign and malign breast lesions which can be evaluated in clinical practice.

5. References

1. Iranmakani S., Mortezaazadeh T., Sajadian F., Ghazaini M.F., Ghafari A., Khazerloo D., Musa A.E. A review of various modalities in breast imaging: technical aspects and clinical outcomes. *Egyptian Journal of Radiology and Nuclear Medicine* 2020:51-57.
2. Sakai A., Onishi Y., Matsui M., Adachi H., Teramoto A., Saito K, Fujita H., A method for the automated classification of benign and malignant masses on digital breast tomosynthesis images using machine learning and radiomic features. *Radiological Physics and Technology* 2020 Mar;13(1):27-36.
3. Koçak B., Durmaz E.B., Ateş E., Kılıçkesmez Ö., Radiomics with artificial intelligence: a practical guide for beginners. *Diagn. Interv. Radiol.* 2019; 25:485-495.
4. Vadivel A. Surendiran B., A fuzzy rule-based approach for characterization of mammogram masses into BI-RADS shape categories, 2013 *Computers in Biology and Medicine*, 43, 259-267.
5. Stelzer P.D., Steding O., Raudner M.W., Euller G., Clauser P., Baltzer P.A.T., Combined texture analysis and machine learning in suspicious calcifications detected by mammography: Potential to avoid unnecessary stereotactical biopsies. *European Journal of Radiology* 132 (2020) 109309.
6. Kleczek P., (2021). `GLCM_Features(glc)` (<https://www.mathworks.com/matlabcentral/fileexchange/56661-glcm-features-glc>) MATLAB Central File Exchange. Retrieved:23.04.2021.
7. Wei X., *Gray Level Run Length Matrix Toolbox v1.0*, Software, Beijing Aeronautical Technology Research Center, 2007.
8. Shakir H., Deng Y., Rasheed H., Khan T.M.R., Radiomics based likelihood functions for cancer diagnosis, *Scientific Reports* 9501 (2019).

Syllabus Design of a Single Application Based Medical Imaging Computer Laboratory

Mazlum Unay ^{1,*}, M. Alper Selver ¹

¹ The Institute of Natural and Applied Sciences, Dokuz Eylul University, 35390, Buca, Izmir, Turkey

* Correspondence: unaymazlum@gmail.com

Abstract: Medical imaging systems (MIS) lecture, which is an important part of the biomedical engineering (BME) curriculum, encompasses a wide range of approaches, including physics, instrumentation, data gathering, image production, modeling, and quality evaluation. Although many BME curricula include a well-structured MIS course that introduces students to all contemporary diagnostic imaging systems, MIS laboratory work is usually confined to image processing. A laboratory has been designed with new design criteria to improve the applicability and understanding of MIS-related studies and to improve the points where traditional laboratories are not sufficiently resourceful. In this study, the functioning of conventional X-ray, Computed Tomography (CT), and Magnetic Resonance Imaging (MRI) modalities are simulated utilizing the Shepp-Logan phantom. Traditional biomedical image acquisition techniques have been analyzed using the same phantom to facilitate an understanding of their differences and similarities. A practical learning method for imaging systems is established by utilizing simulations for each modality. All possible circumstances in each imaging method, such as executing in various sizes, will be able to be observed through controllable parameters in all simulations. Accordingly, it became possible to simulate and compare various scenarios and discuss their effects on image formation and quality. Particularly, projection and back-projection methods are used for X-ray based imaging and, the use of under-sampled k-space is analyzed for MRI. Modern reconstruction methods are discussed. Thanks to the fact that all applications of the designed concept are carried out on the same phantom, the working principles of the imaging systems can be discussed comparatively.

Keywords: Computer laboratory, engineering curriculum, Shepp-Logan phantom, X-ray imaging, magnetic resonance imaging

1. Introduction

Medical Imaging Systems (MIS) are quite complicated machines that include components from almost every branch of EEE. MIS courses encompass a variety of modalities, including conventional X-ray imaging, Computed Tomography (CT), and Magnetic Resonance Imaging (MRI) and others [1]. Beginning with the fundamental physical concepts underlying these imaging systems, data collection, image formation, equipment, and quality aspects are analyzed [2, 3].

The conventional lecture format prevents students from developing practical abilities in relation to operational and emerging challenges in MIS, which need considerable background knowledge. Thus, more laboratory experiments are required to provide a complete understanding [4, 5]. Unfortunately, these modalities are only available in hospitals and research institutions. Computer studies are used to solve this limitation, however, they are mostly focused on image processing [6] and evaluation [7]. In this thesis, a two-dimensional (2D) and three-dimensional (3D) experiment-based course were built, with the same example used in certain

modalities to enhance learning efficiency. Students are asked to evaluate the findings obtained by generating a sample of varying parameters [8–10].

While the proposed schedule has been proven to be instructional and motivating, it has been shown to have limitations in reality [11]. Each experiment has a distinct and specific purpose, which the student should understand before beginning the lab study. This technique has been observed to have two downsides. The first drawback is that comparisons across modalities are restricted since each experiment has a distinct objective. Second, it may be quite difficult for students to comprehend the essence of the experiments, particularly at the semester's conclusion. The students conclude that the precise aims of each experiment make obtaining extra resources for study very challenging. Taking these drawbacks of the existing lab schedule into account, new design criteria are established to improve MIS understanding. As a result, three new design criteria (NDC) have been established to accomplish these objectives:

NDC-1) All imaging experiments should be performed on the same subject such that the students can learn the properties of the object to be imaged just once at the beginning of the semester. There should be both 2D and 3D models together with analytical representations of the same object in Cartesian (i.e. image) and frequency (i.e. Fourier) domains (if possible).

NDC-2) The subject should have varying properties that would cause alterations on the acquired images such that students have the possibility to compare the results of different experiments and can make direct observations on the advantages and disadvantages of a selected modality.

NDC-3) The content of the experiment should allow students to directly search for the material so that students can access detailed information on the subject before and after laboratory hours.

2. Materials and Method

In this section, the Shepp-Logan phantom used to simulate each imaging system will be described. Following an overview of the emergence of X-ray and CT imaging systems, fundamental information regarding both imaging systems is discussed.

2.1. The Shepp-Logan Phantom

In 1974, the Shepp-Logan phantom was created as a tool to simulate image reconstruction [12]. To simulate the head, the model utilized ten ellipses of various sizes and densities. An optional 11th ellipse can be used to depict brain hemorrhage inside the skull to test image reconstruction. In general, phantoms with a size of 256x256 can be used in both 2D and 3D. A 2D Shepp-Logan phantom with a size of 256x256 is Figure 1 a.

Due to its versatility, the Shepp-Logan phantom has been used in a broad range of imaging modalities. The phantom's adaptability placed it in a very beneficial area since it can be adjusted and modified as needed. The phantom's usefulness has improved due to the flexibility of changing the number of ellipses, densities, and ellipse locations[13].

2.2. X-ray

The electromagnetic spectrum is a description and classification of electromagnetic waves based on their varying wavelengths. X-rays including visible light, ultraviolet light, infrared light, gamma rays, and microwaves, are forms of electromagnetic radiation. Medical imaging is amongst the most popular and useful applications of X-rays. X-rays are used to diagnose and treat cancer, as well as to explore the environment.

The theory of X-ray imaging is that radiation is scattered and absorbed when it propagates through an object. Radiation passes in varying levels through an object with differences in thickness or intensity, affecting the image exposure. In X-ray imaging, it is the result of a 2D projection of X-rays due to the attenuating properties of all tissues along their path [14].

2.3. Computed Tomography

CT is a non-invasive method for visualizing internal characteristics of solid structures and collecting digital data on their 3D geometries and properties. It provides specialists with a more precise view of the human body and enables the secure, simple, and quantitative localization

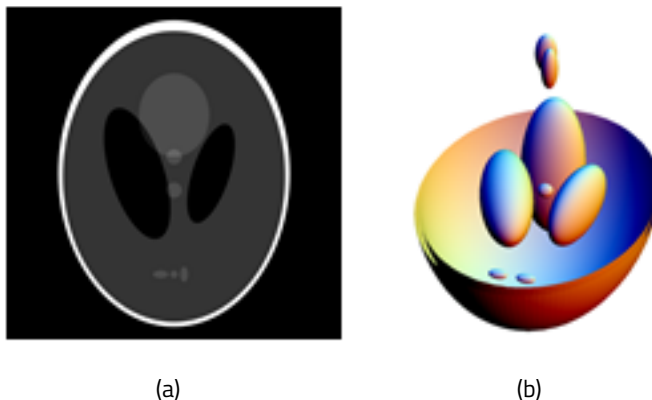


Figure 1 a) The 2D Shepp-Logan phantom, b) The 3D Shepp-Logan phantom of lesions, and other conditions that would be painful, hazardous, or perhaps even impossible to detect using other techniques [15].

Tomographic reconstruction is a multidimensional inverse [16] problem in which the aim is to estimate a complex structure from limited projections. The back-projection technique has commonly been the most frequently used method for reconstructing images from projections [17]. Projections are obtained with angles between 0 and 180 degrees. Each projection reveals a different feature of the entity. Additionally, the more projections performed, the higher the quality of the final image produced [16].

2.4. Magnetic Resonance Imaging

MRI is a relatively recent method and has been in existence since the early 1980s. MRI is a safe and effective medical test used by physicians to detect medical problems. It produces accurate images of muscles, soft tissues, bone, and almost all other body's internal structures using a strong magnetic force radio frequency signals, and a computer[18].

K-space is a matrix of numbers that represents the spatial frequencies with in MRI. The prevalent portrayal of k-space as a "galaxy" sustains the mystery. Each k-space "star" is simply a data point extracted directly via the MR signal. The brightness within each star demonstrates the star's specific spatial frequency's relative contribution to the final image.[19].

Imaging speed and total duration of data acquiring in MRI are considered as the most momentous topics especially in clinical experiments of MRI [20]. Parallel imaging was developed to expand the abilities of MRI beyond its technological and physiological limitations. Although a traditional MRI system obtains information by quickly swapping magnetic field gradients open and close, this imposes a limit on the scanning rate. Parallel imaging is an advantageous option in this

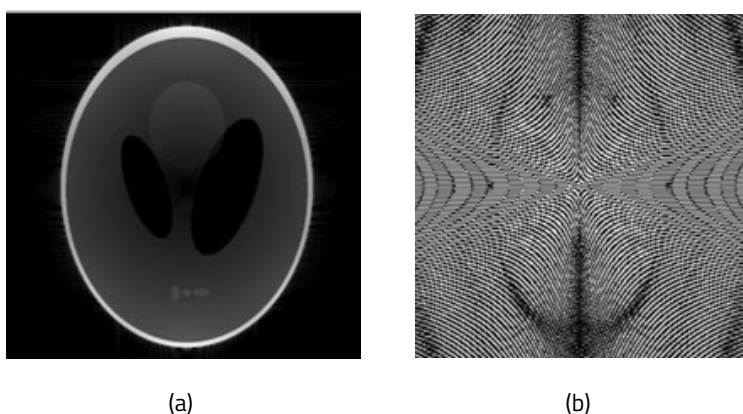


Figure 2 (a) The presence of raw information in k-space. (b) The related image information obtained with 2D inverse FT

situation since it enables the processing phase to be accelerated by using a variety of image restoration approaches.

The assumption underlying Parallel Imaging with Localized Sensitivities (PILS) is that each single-coil in the array has a localized sensitivity map, indicating that their sensitivity is limited to a narrow area [21]. PILS is one of the MRI methods that relies on the image domain to reconstruct a composite image obtained with the k-space from each receiver coil.

Sensitivity Encoding (SENSE) is the other parallel MRI method that works on the image domain to create a composite image from aliased receiver coil images. It is referred to as an "unfolding" mechanism, related to the processes of unfolding the images that have been folded over one another [20]. Folded images, often referred to as aliased images, are the products of rapid k-space data acquisition. It causes reduced field-of-view images generated by the receiver coil when the number of information-filled lines in the K-space decreases. Depending on how many pixels are overlapped, the unfolding process for pixels in images can be performed using a reduced field-of-view.

3. Results

In this section, the method for X-ray, CT and MRI systems and the results from the same phantom will be shown. For each imaging system. Since the Shepp-Logan phantom is common

to each process, we begin by obtaining the phantom on Matlab. First, 3D Shepp-Logan phantom is created on MATLAB. The size of the 3D phantom is 256x256x256. The axial section of

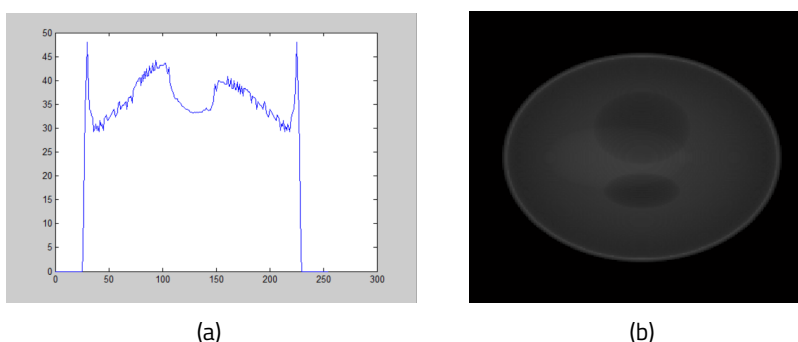


Figure 3 (a) Projection of 2D phantom. (b) Projection of 3D Shepp-Logan phantom

the phantom is used 2D phantoms. The size of the 2D phantom is 256x256. X-ray imaging results are obtained by taking projections of phantoms in both dimensions.

A significant amount of data is lost as a consequence of the projection. Due to the overlapping information, all data in one dimension is merged with data in the other. As a consequ-

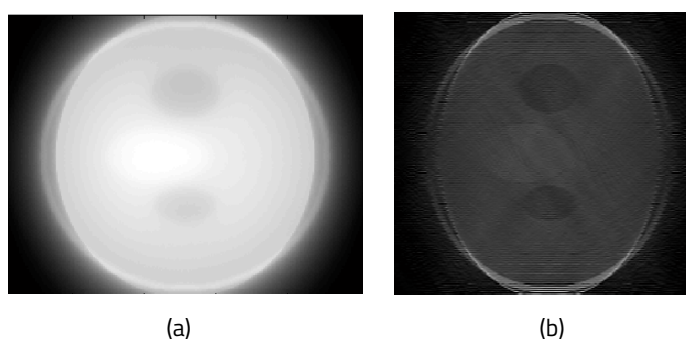


Figure 4 (a) Final image of back-projection method for 2D phantom. (b) Final image of filtered back-projection method for 2D phantom

ence, projecting a 3D phantom yields a 2D output. In X-ray imaging, the outcome of a single projection angle is analyzed. By varying the projection angle, different information about the phantom may be acquired. This fundamental information serves as the foundation for CT.

After a total of 180 projections procedures are complete, the outputs are compiled into a matrix known as a sinogram. Once the sinogram is produced, the reconstruction step can begin,

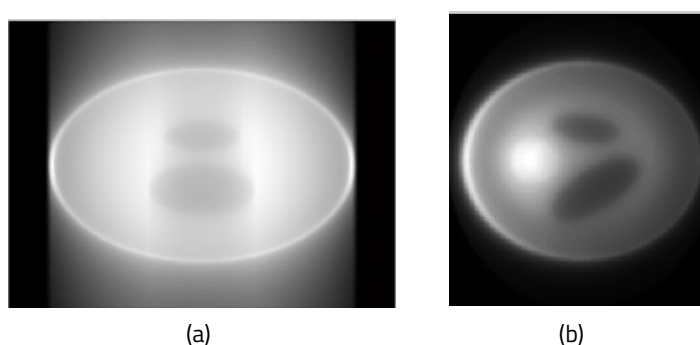


Figure 5 (a) 150th axial section of back-projection method results for 3D phantom. (b) 150th axial section of filtered back-projection method results for 3D phantom

which may be done using a variety of methods. Both the back-projection method and the filtered back-projection techniques have been applied. First, each row of the sinogram representing the projections is extracted independently and put in a distinct matrix, such that each repeats itself. Each matrix is rotated by the projection angle associated with each projection. The sum

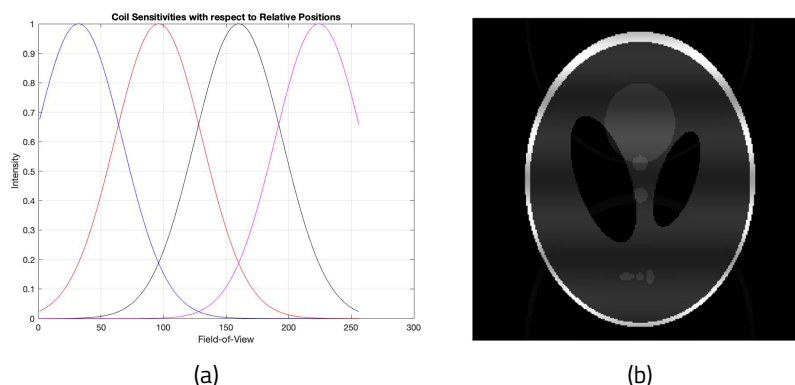


Figure 6 (a) Gaussian sensitivity maps corresponding each receiver coil. (b) The final composite image acquired with PILS algorithm

of the rotated matrices is computed.

The only difference between the two methods is that each projection is filtered before it is used. 2D phantom results are shown in Figure 4 and 3D phantom results are shown in Figure 5 for both methods. Using the appropriately sized filter for projections minimizes the problem of low-frequency component overlap. Because of the filtering procedure, there seems to be no brightness issue.

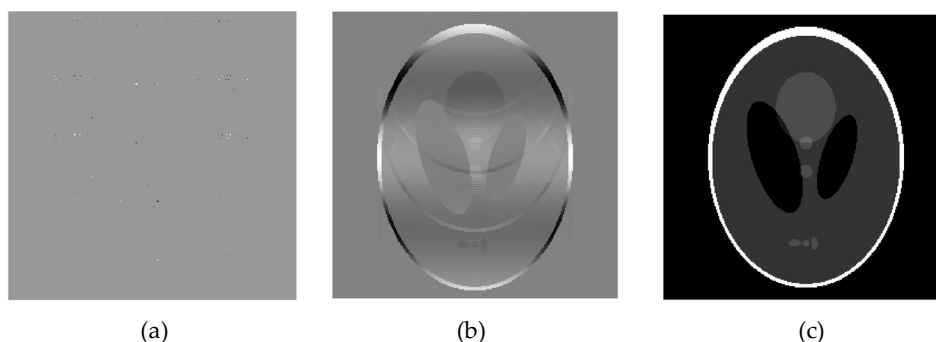


Figure 7 (a) The image reconstructed by SENSE had an unfolding problem when the number of coils is four and the acceleration factor is five (b) The image reconstructed by SENSE had a contrast problem when the number of coils is eight and the acceleration factor is five (c) The image reconstructed by SENSE had no problem when the number of coils is sixteen and the acceleration factor is four

The total coil numbers are set to four, eight or sixteen respectively and the acceleration value is incrementally increased from two to six for each coil number scenario for the SENSE method. While observing the outcomes of each example, it was noted that some outcomes failed to unfold, some had contrast issues, and some were accurate. Table 1 represents the conclusions of each condition.

Acceleration factor	Coil number	Four Coils	Eight Coils	Sixteen Coils
	2		A	A
3		CP	CP	CP
4		F	A	A
5		F	CP	CP
6		F	F	CP

Table 1. The SENSE algorithm's reconstruction outcomes; "A" stands for "accomplished," "CP" stands for "contrast problem," and "F" stands for "failed in the unfolding process in reconstruction."

4. Discussion

In the first x-ray experiment, the results show considerable loss of information and loss of quality especially in terms of contrast. Due to the superposition in one dimension, all information is overlapped. Despite the fact that it is just a single projection, it may give useful information about the phantom if a precise projection angle is used to distinguish components from one another. However, determining this particular projection angle is very challenging. On the other hand, acquiring results with a single projection has the advantage of becoming quick and practical.

The second experiment covers CT and provides great opportunity to compare single projection radiographic images to multi-projection tomographic images. The students can change several parameters such as the number of projections to understand the important acquisition factors. The target object is available both in 2D and 3D, which improves the algorithmic capabilities of the students.

MRI reconstruction is performed under various under-sampling masks. Under-sampled k-space generation is also covered as a separate topic. Understanding different pulse-sequ-

ence types and their effect on reconstructed image quality is discussed extensively. For instance, compared to the PILS reconstruction technique, the SENSE technique gave more accurate results while reconstructing the composite image from under sampled k-space at the same time. The PILS technique is sensitive to slight changes in the sensitivity map and some effects in the form of strip-like forms or aliased regions can be seen on the reconstructed image. The SENSE technique is more commonly used in clinics for the reasons stated.

5. Conclusions

This paper aims to design a laboratory where students can learn the topics covered in the MIS course practically by using the knowledge they have acquired in the BME curriculum. In this context, while the projection applications for X-ray are carried out, the back-projection method for CT has been examined. By controlling the occupancy of the k-space for MRI, investigations were made to reduce the scan time as much as possible in order to obtain satisfactory results. Various reconstruction techniques have been performed within the scope of parallel imaging. Moreover, all of these experiments are applied to the same target object, which enables comparisons among different modalities.

References

- [1] M. A. Haidekker, *Medical Imaging Technology*. Springer Briefs in Physics, 2013.
- [2] J. Prince and J. Links, *Medical Imaging Signals and Systems*. Pearson Prentice Hall, 2006.
- [3] Z. H. Zho, J. Jones, and M. Singh, *Foundations of Medical Imaging*. John Wiley and Sons Inc., 1993.
- [4] S. Kaçar and C. Bayilmis, "A web-based educational interface for an analog communication course based on MATLAB" *IEEE Trans. Educ.*, vol. 56, no. 3, pp. 346–354, 2013.
- [5] R. J. Stanley, S. E. Watkins, A. Gopal, and R. H. Moss, "A web-shareable real-world imaging problem for enhancing an image-processing curriculum," *IEEE Trans. Educ.*, vol. 47, no. 2, pp. 211–219, 2004.
- [6] A. Dikshit, D. Wu, C. Wu, and W. Zhao, "An online interactive simulation system for medical imaging education," *Comput. Med. Imaging Graph.*, vol. 29, no. 6, pp. 395–404, 2005.
- [7] M. Sonka, E. L. Dove, and S. M. Collins, "Image systems engineering education in an electronic classroom," *IEEE Trans. Educ.*, vol. 41, no. 4, pp. 263–272, 1998.
- [8] D. S. Alexiadis and N. Mitianoudis, "MASTERS: A virtual lab on multimedia systems for telecommunications, medical, and remote sensing applications," *IEEE Trans. Educ.*, vol. 56, no. 2, pp. 227–234, 2013.
- [9] T. Glatard et al., "A virtual imaging platform for multi-modality medical image simulation," *IEEE Trans. Med. Imaging*, vol. 32, no. 1, pp. 110–118, 2013.
- [10] J. E. Wilhjelm, M. J. Pihl, M. N. Lonsdale, and M. Jensen, "An active learning approach to the physics of medical imaging," *Med. Eng. Phys.*, vol. 30, no. 5, pp. 607–614, 2008.
- [11] C. B. Paschal, K. R. Nightingale, and K. M. Ropella, "Undergraduate biomedical imaging education," *Ann. Biomed. Eng.*, vol. 34, no. 2, pp. 232–238, 2006.
- [12] L. A. Shepp, B. F. Logan, and M. Hill, "THE FOURIER RECONSTRUCTION OF A HEAD SECTION" *IEEE Trans. Nucl. Sci.*, vol. 21, no. 4, pp. 21–43, 1974.
- [13] M. Guerquin-Kern, "Matlab code for MRI simulation and reconstruction," p. 8, 2012, [Online]. Available: <http://bigwww.epfl.ch/algorithms>.
- [14] M. Sandborg, "Radiography and Fluoroscopy : Physical principles and biohazards," 1995.
- [15] L. A. Shepp and J. B. Kruskal, "Computerized Tomography: The New Medical X-Ray Technology," *Am. Math. Mon.*, vol. 85, no. 6, pp. 420–439, 1978.
- [16] F. Kharfi, "Mathematics and Physics of Computed Tomography (CT): Demonstrations and Practical Examples," *Imaging Radioanal. Tech. Interdiscip. Res. - Fundam. Cut. Edge Appl.*, 2013.

- [17] S. Suzuki and S. Yamaguchi, "Comparison between an image reconstruction method of filtering backprojection and the filtered backprojection method," *Appl. Opt.*, vol. 27, no. 14, p. 2867, 1988.
- [18] R. W. Chan, J. Y. C. Lau, W. W. Lam, and A. Lau, *Magnetic resonance imaging*, vol. 1–3. Elsevier, 2018.
- [19] S. Sykora, E. Byte, V. R. Sanzio, and C. Primo, "K-space formulation of MRI," *Science (80-.)*, no. 2, pp. 1–14, 2010.
- [20] M. Blaimer, F. Breuer, M. Mueller, R. M. Heidemann, M. A. Griswold, and P. M. Jakob, "SMASH, SENSE, PILS, GRAPPA. How to Choose the Optimal Method," *Top. Magn. Reson. Imaging*, vol. 15, no. 4, pp. 223–236, 2004.
- [21] M. A. Griswold, P. M. Jakob, M. Nittka, J. W. Goldfarb, and A. Haase, "Partially Parallel Imaging with Localized Sensitivities (PILS)," *Magn. Reson. Med.*, vol. 44, no. 4, pp. 602–609, 2000.

Detection of colistin resistant *Klebsiella pneumoniae* bacteria using surface-enhanced Raman spectroscopy combined with machine learning

Fatma Uysal Ciloglu¹, Mehmet Hora², Aycan Gundogdu², Mahmut Tokmakci¹, Omer Aydin^{1*}

¹Department of Biomedical Engineering, Erciyes University, Kayseri, Turkey

²Genome and Stem Cell Center (GenKok), Erciyes University, Kayseri, Turkey

Abstract: Although antibiotics are among the most successful therapeutic agents developed so far, the widespread use of these compounds leads to the emergence of resistant microorganisms. The most important way to slow down the development of antibiotic resistance in bacteria is to prevent the use of wrong and unnecessary antibiotics. To achieve this, rapid and reliable identification of bacteria is needed. However, bacterial identification techniques currently in use in clinics have some challenging processes. To address this challenge, label-free surface-enhanced Raman spectroscopy (SERS) combined with some machine learning techniques were used for discrimination of colistin resistant and susceptible *Klebsiella pneumoniae*. A total of 9 colistin resistant and 7 colistin susceptible *K. pneumoniae* isolates were utilized. To discriminate similar SERS spectra collected from colistin resistant and susceptible isolates, principal component analysis and support vector machine classifier were performed. The classification accuracy was found more than 90%. Furthermore, the classification model discriminates colistin resistant and susceptible *K. pneumoniae* with an area under curve (AUC) of 0.95. Our results demonstrate that SERS coupled with machine learning can be used for the detection of antibiotic-resistant and susceptible bacteria. The proposed method is a label-free, easy implemented, and reliable technique with high sensitivity for clinical use.

Keywords: colistin resistance, *Klebsiella pneumoniae*, surface-enhanced Raman spectroscopy, principal component analysis, support vector machine

1. Introduction

Antimicrobial resistance has become a growing global threat around the world. It is expected to threaten the lives of 10 million people annually by 2050 [1]. This is more than twice the number of deaths caused by Covid-19 disease. The next pandemic crisis is already here and if adequate precautions are not taken, it will threaten the lives of millions of people.

The increase in gram-negative bacteria, especially resistant to more than one drug, poses a great threat to our country and the world. *Klebsiella pneumoniae*, which is included in this bacterial group, causes many infections that threaten human health such as pneumonia, urinary tract infections, meningitis, and sepsis [2]. These bacteria first gained resistance to β -lactam group antibiotics and then became resistant to carbapenems. In this situation, the use of colistin antibiotic has become the last option in treatment. However, overuse of colistin has led to the emergence of colistin-resistant *K. pneumoniae* (colR-Kp) within a short period [3].

Prescribing the right antibiotics is the key step to combat antimicrobial resistance. Rapid and reliable detection of bacteria is a main need to correct prescription. However, antimicrobial susceptibility test (AST) that is used to determine bacteria's antibiotic resistance suffers from its major drawbacks. For example, phenotypic AST contains long incubation periods or genotypic AST is required highly trained personnel. Therefore, there is an urgent need for alternative diagnostic tools that performs rapid and correct diagnosis. The surface-enhanced

Raman spectroscopy (SERS) is a vibrational technique based on the inelastic scattering of laser light. This technique provides both molecular fingerprint information about the sample and high signal to noise ratio. To provide high signal enhancement, SERS active substrates are brought to the close vicinity of samples. Colloidal silver nanoparticles (AgNPs) are mostly preferred as SERS substrate. SERS is used detection of bacteria's antibiotic resistance in the literature [4,5].

In this study, we aim to discriminate colR-Kp and colistin-susceptible *K. pneumoniae* (colS-Kp) using label-free SERS coupled with machine learning algorithms. We hypothesize that the cell wall structure of colR-Kp and colS-Kp might represent some subtle differences due to the drug resistance mechanism. These differences can be uncovered by using SERS. Thanks to the principal component analysis (PCA) and support vector machine (SVM), SERS spectral data collected from antibiotic resistant and susceptible *K. pneumoniae* isolates can be discriminated.

2. Materials and Methods

2.1 AgNPs Synthesis

AgNPs were synthesized according to the classical method reported by Lee and Meisel [6]. Briefly, 90 mg silver nitrate (AgNO₃, Merck, Darmstadt, Germany) was added in 500 mL ultrapure water. This solution was heated until boiling. Then, 10 mL aliquot of 1% sodium citrate (Merck, Darmstadt, Germany) was added drop by drop into the solution. The solution was kept boiling for about 1 hour. Synthesized AgNPs were centrifuged at 5500 rpm for 1 hour. A portion of the supernatant was discarded to form 4x concentrated AgNPs.

2.2 Bacterial Sample Preparation

9 colistin resistant, 7 colistin susceptible *K. pneumoniae* isolates were used in this study. *K. pneumoniae* isolates were obtained from our microorganism collection (Genome and Stem Cell Center, GenKok). The bacteria were cultivated on blood agar at 37 °C for 24 hours. The samples were collected with sterile plastic inoculating loops and washed 3 times. A 5 µl of each washed bacterium was added to a 100 µL of 4X concentrated Ag colloidal suspension. A 5 µL of each mixture was dropped on a CaF₂ slide and dried at room temperature about 30 minutes for SERS measurements.

2.3 SERS Measurements

SERS measurements were performed using a confocal Raman microscope (WITec Alpha 300M+, WITec) equipped with a near infrared 785 nm laser at 5 mW laser power. 50x objective lens was used and the integration time was 1s in all measurements.

2.4 Data Analysis

Pre-processing techniques that are cosmic ray removal, background subtraction (5th degree polynomial) and Savitzky Golay smoothing (5th order, width 11 points) were applied to remove noise components. Then all spectral vectors were standardized using standard normal variate. PCA were utilized for feature extraction purpose. SVM classifier were used to perform classification of extracted features from spectral data.

3. Results and Discussion

A total of 315 spectra were collected from colistin resistant and susceptible *K. pneumoniae*. The mean SERS spectra of *K. pneumoniae* strains are illustrated in Figure 1. SERS

spectra of colR-Kp and colS-Kp demonstrate a lot of similar peak positions except for some differences in relative band intensities. The band intensities of colR-Kp are more prominent than colS-Kp. There are some major differences in the intensity of 660, 735, 1060 and 1327 peak positions. These peaks are more intense in colR-Kp as seen in difference spectrum. This situation can be sourced from resistance mechanism of *K. pneumoniae* bacteria to colistin. Since the negative charge of the outer membrane decreases in colR-Kp [3]. Therefore, AgNPs may show easily binding to resistant bacteria and this provides higher signal enhancement.

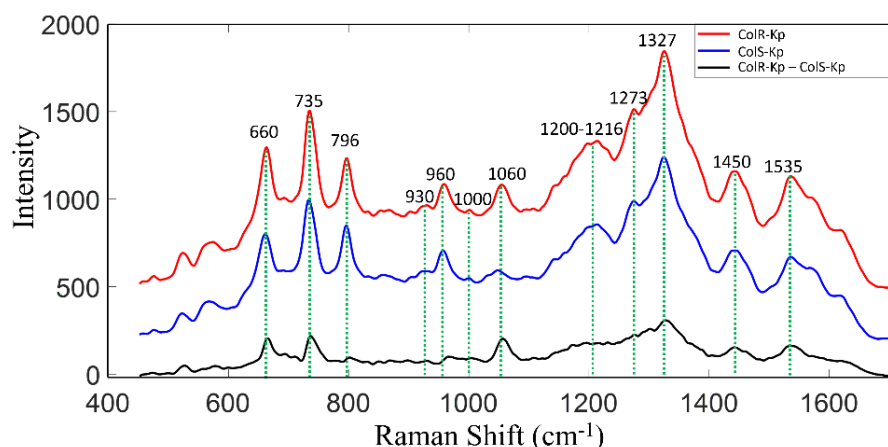


Figure 1. The mean SERS spectra of colR-Kp, colS-Kp, and the difference between colR-Kp-colS-Kp

Discrimination of colR-Kp and colS-Kp SERS spectra is extremely difficult with the naked eye due to the high spectral similarity. This situation necessitates using machine learning algorithms. First, PCA was utilized to extract features. Then, extracted features were given to the SVM classifier to classify two groups. 10- fold cross validation was used to determine the model performance and this repeated for 20 runs. The accuracy for each run and area under curve (AUC) value are shown in Figure 2a and b, respectively. As seen in these figures, SVM classified two groups with a mean accuracy of 90.4% and AUC of 0.95.

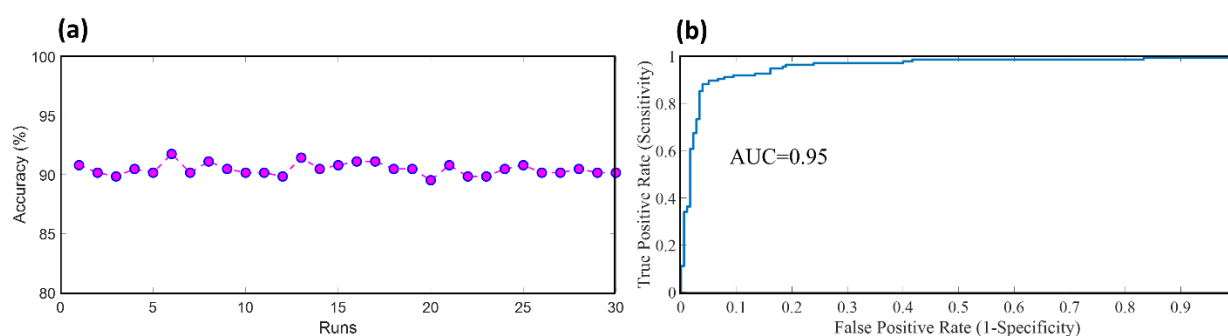


Figure 2. (a) Accuracy values of SVM classifier for 20 runs. (b) AUC value obtained from ROC curve of SVM classifier

Our results demonstrate that SERS coupled with machine learning have a great potential to detect antibiotic-resistant and susceptible bacteria.

4. Conclusion

In conclusion, label-free SERS and machine learning provide promising tool for discrimination of antibiotic-resistant and susceptible bacteria. Therefore, proposed method is highly useful for bacterial identification studies.

Acknowledgement

This work was financially supported by the Erciyes University Scientific Research Projects Coordination Unit under grant number FDK-2020-9741.

References

- [1] O'Neill, J. Tackling Drug-Resistant Infections Globally: Final Report And Recommendations, https://www.biomerieuxconnection.com/wp-content/uploads/2018/04/Tackling-Drug-Resistant-Infections-Globally_-Final-Report-and-Recommendations.pdf (2016).
- [2] Podschun, R., & Ullmann, U. Klebsiella spp. as nosocomial pathogens: epidemiology, taxonomy, typing methods, and pathogenicity factors. *Clinical microbiology reviews*, 11(4), 589-603 (1998)
- [3] Ah, Y. M., Kim, A. J., & Lee, J. Y. Colistin resistance in Klebsiella pneumoniae. *International journal of antimicrobial agents*, 44(1), 8-15 (2014).
- [4] Ciloglu, F. U., Saridag, A. M., Kilic, I. H., Tokmakci, M., Kahraman, M., & Aydin, O. Identification of methicillin-resistant Staphylococcus aureus bacteria using surface-enhanced Raman spectroscopy and machine learning techniques. *Analyst*, 145(23), 7559-7570 (2020).
- [5] Ciloglu, F. U., Caliskan, A., Saridag, A. M., Kilic, I. H., Tokmakci, M., Kahraman, M., & Aydin, O. Drug-resistant Staphylococcus Aureus Bacteria Detection with the Combination of Surface-enhanced Raman Spectroscopy and Deep Learning Techniques. Preprint (2021).
- [6] Lee, P. C. & Meisel, D. Adsorption and surface-enhanced Raman of dyes on silver and gold sols. *The Journal of Physical Chemistry* 86(17), 3391-3395 (1982).

Investigation of Mammalian Cells Expressing SARS-CoV-2 Proteins by Surface-Enhanced Raman Scattering

Munevver Akdeniz¹, Omer Aydın²

¹ERNAM-Nanotechnology Research and Application Center, Erciyes University, Kayseri 38039, Turkey

²Department of Biomedical Engineering, Erciyes University, Kayseri 38039, Turkey

Abstract: Coronavirus Disease 2019 (COVID-19) is infectious disease that caused by SARS-CoV-2 virus. Since the first day of its emergence, virus has spread rapidly around the world by transmission from person to person, causing a pandemic. COVID-19 is currently detected using nucleic acid tests and serological tests. However, these tests are expensive, time consuming and give false negative results. These disadvantages can be eliminated with Surface-enhanced Raman Scattering (SERS), which enhanced Raman signals as a result of interaction of plasmonic nanostructures with analyte. In this study, it was aimed to demonstrate applicability of virus detection by using structural proteins of SARS-CoV-2 virus with this method. For this purpose, plasmids carrying M, N and E protein codes of virus were transfected into mammalian cell line (HEK293) and a virus-infected cell model was created. Proteins of the plasmid transfected cells were isolated. SERS spectra of proteins were collected by using gold substrate. Collected spectra were classified Principal Component Analysis (PCA). The results obtained revealed that SERS is a rapid, low-cost, reliable and promising method for the detection of COVID-19.

Keywords: COVID-19 Detection, SARS-CoV-2, SERS, Transfection, Plasmid, PCA

1. Introduction

Coronavirus Disease 2019 (COVID-19) is a viral respiratory disease caused by SARS-CoV-2 virus and firstly appeared in Wuhan, China at the end of 2019. COVID-19 spread rapidly from Wuhan to other regions of China and from there to world. On January 30, 2020, World Health Organization (WHO) is declared COVID-19 as an epidemic due to uncontrolled, rapid spread. Rapid detection of infected human is important because disease is highly contagious. With the emergence of COVID-19, the need to develop rapid, sensitive, and specific diagnostic methods is increased to control and prevent the pandemic[1]. COVID-19 is confirmed by nucleic acid-based polymerase chain reaction (PCR) and serological tests. Reverse transcriptase-polymerase chain reaction (RT-PCR) is the most common used method for the diagnosis of SARS-CoV-2. RT-PCR is a multi-step method that includes nucleic acid amplification, purification and extraction. Serological tests are tests that detected antibody response to SARS-CoV-2. Serological tests cannot be used for diagnosis in early stages of disease because development of antibody response requires time. At the same time, these tests are time-consuming, give false negative results, require trained person, require costly reagent such as primers, antibodies [2]. Because of reasons, there is a need for rapid, sensitive and reliable diagnostic methods to detect cases of COVID-19 disease and to prevent spread of epidemic.

Raman spectroscopy gives information about vibrational property of the analyte and is not affected by water. However, it has some major drawbacks like, low-intensity signals and longtime accumulation time. Therefore, Raman spectroscopy has limited use. To overcome this problem, power signals are obtained by using metal nanoparticles. This method is called SERS. SERS is a method that enhances Raman signals based on interaction of molecules and metallic

nanoparticles such as gold and silver. This enhancement is due to surface plasmons formed around metallic nanoparticles and charge transfer between molecule and nanoparticle [3].

In this study, by creating virus infected cell model, we aim to detect COVID-19 with SERS using structural proteins of SARS-CoV-2. We believe that membrane(M), Nucleocapsid (N) and Envelope (E) structural proteins will show differences on the spectrum after they enter the cell. These differences can be demonstrated using SERS and PCA.

2. Materials and Methods

2.1. AuNP Synthesis and Preparation SERS Substrate

AuNP were synthesized using the Turkevich method [4]. Briefly, 10 mg of HAuCl₄ (Sigma, Germany) was dissolved in 100 mL of dH₂O and heated on a magnetic stirrer until boiling. Then, 700 μ L of 1% sodium citrate (Sigma, Germany) solution was added rapidly to boiling solution. The solution was boiled for 15 minutes.

The SERS substrate was prepared using the procedure described in the literature [5]. Briefly, 50 μ L of AuNP mixed with 1 μ L of 10 mM CuSO₄ (Sigma, Germany) solution (50:1). The mixed solution was dropped onto CaF₂ and left to dry at room temperature. The mixed solution was dropped on CaF₂ and was left air-drying at room temperature.

2.2. Cell Culture and Plasmid Transfection

HEK-293 human embryonic kidney cell line cultured in Dulbecco's modified essential medium (DMEM)(Lonza, Switzerland). The cell culture medium contained 10% fetal bovine serum (FBS) (Biological Industries, Israel), penicillin (100 U/mL) and streptomycin (100 U/mL)(Gibco, Scotland) and cells were maintained with 5% CO₂ at 37°C.

For plasmid transfection, plasmids with gene sequence of structural proteins of SARS-CoV-2 virus were transfected human embryonic kidney (HEK293) cells with PEI (Polyethyleneimine)(Sigma, Germany) that is a cationic polymer. The complexation ratio of PEI/plasmid was determined according to gel electrophoresis assay following our published protocol. PEI/plasmid of complex were given to HEK293 cells in opti-MEM (Gibco, Scotland). 72 hours were incubated.

2.3. Western Blotting

Proteins of the transfected cells were isolated using RIPA (Thermo Scientific) lysis buffer. Concentrations of proteins were determined using the Bradford assay. 35 μ g total protein was loaded into wells of SDS-PAGE gels. Proteins separated by electrophoresis were transferred to PVDF membranes and incubated with primary antibodies of target proteins at +4°C overnight with shaking. Proteins incubated with secondary antibodies for 2 hours at room temperature were visualized with Chemi-Doc device using ECL substrate.

2.4. Cellular Uptake

Cellular uptake of plasmid, morphology of transfected cells and stability of transfection were examined with GFP (green fluorescent protein) using fluorescence microscope and flow cytometry.

2.5. SERS Measurement

To obtain the SERS spectra of the proteins isolated from the cells, 2 μ g of protein was dropped onto the SERS substrate and dried at room temperature before the spectra were collected. All SERS spectra were collected using the WiTech alpha M+ Raman Microscopy System (Germany). Proteins were excited using a 785 nm diode laser with a laser power of 30 mW and a 50X objective. Integration time was 2 sn in all measurements.

2.6. Data Analysis

Pre-processing techniques that are cosmic ray removal, background subtraction (5th degree polynomial) and Savitzky Golay smoothing (5th order, width 11 points) were applied by using WiTec Project Plus 5. Spectra were normalized and PCA was performed with the 'pca' function using MATLAB (Mathworks, USA) software.

3. Results and Discussion

Cellular uptake was optimized with the GFP plasmids and evaluated fluorescence microscopy and Flow cytometry. The transfection efficiency of GFP plasmid was around 52% at 24/1 (PEI/plasmid) ratio. It was observed that transfection efficiency of GFP was decreased at 32/1 ratio (Figure 2). According to obtained optimization results, M, N and E plasmids were transfected into cells using 1/24 plasmid/PEI ratio. Non-plasmid transfected HEK293 cells were used as a control group.

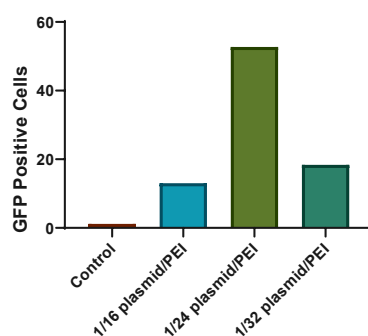


Figure 1. Cellular uptake results obtained by flow cytometry

After plasmids are transfected into cell, it was aimed to produce M, N and E proteins. Protein expression levels M, N and E plasmids was evaluated by Western Blotting. To get SERS spectra, initially proteins of the plasmid transfected cells were isolated. SERS spectra of proteins were collected with gold SERS substrate. For prepared gold SERS substrate, 50 nm AuNP and CuSO₄ were used. As seen in Figure 2, CuSO₄ was used for aggregation of AuNPs. Then, same concentration of protein was dropped onto substrate. Spectra were collected after drying at room temperature.

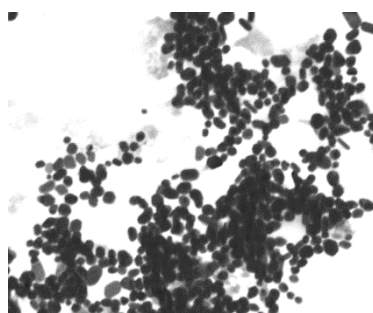


Figure 2. STEM image of SERS substrate prepared with AuNP and CuSO₄

At least 15 spectra were collected from each group. Generally, peaks around 670, 710, 800, 950, 1040, 2120 cm⁻¹ were observed on the spectra (Figure 3 A). Peak around 670 cm⁻¹ is assigned tyrosine. Peaks around 710-800 cm⁻¹ is assigned tryptophan and tyrosine. Peak around 1040 cm⁻¹ is assigned phenylalanine. Intensities of the peaks were different between each transfected cell. These intensities of peaks are thought to be due to the proteins in which transfected plasmids are expressed.

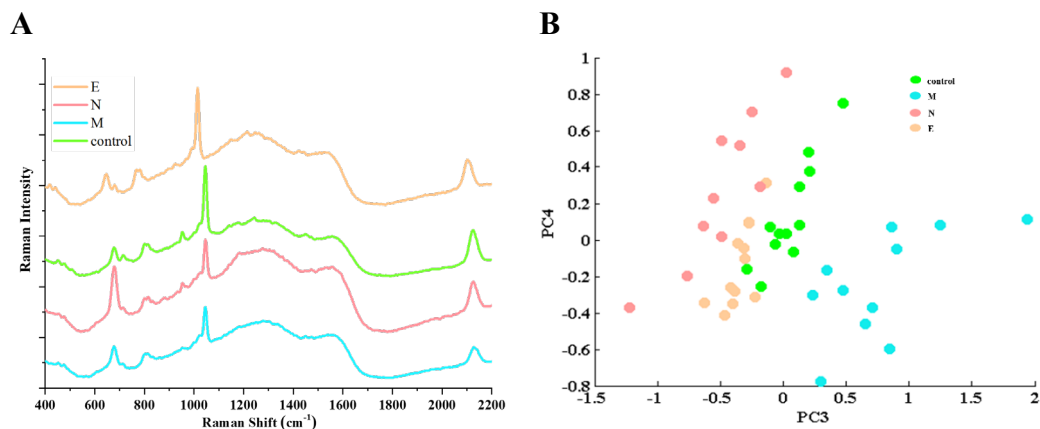


Figure 3. A) Mean SERS spectra of proteins isolated from plasmid transfected cells, B) PCA scores of SERS spectra

PCA was applied obtained spectra to distinguish groups. PCA makes classification by reducing size of multidimensional data without loss of data. PCA scatter plots have shown clear differentiation between control, M, N and E groups (Figure 3 B). With results obtained from this study, it has been shown that SERS is a method that can be applied for detection of COVID-19.

4. Conclusion

In conclusion, COVID-19 can be detected with SERS using other structural proteins besides virus and spike protein. SERS is rapid, sensitive and low cost and therefore promising for further study.

Acknowledgement

“This work has been supported by Erciyes University Scientific Research Projects Coordination Unit under grant number #10780”

References

- [1] M. A. Shereen, S. Khan, A. Kazmi, N. Bashir, and R. Siddique, “COVID-19 infection: Origin, transmission, and characteristics of human coronaviruses,” *J. Adv. Res.*, vol. 24, pp. 91–98, 2020, doi: 10.1016/j.jare.2020.03.005.
- [2] B. D. Kevadiya *et al.*, “Diagnostics for SARS-CoV-2 infections,” *Nat. Mater.*, vol. 20, no. 5, pp. 593–605, 2021, doi: 10.1038/s41563-020-00906-z.
- [3] K. Kneipp, “Surface Enhanced Raman Scattering,” *Phys. Today*, vol. 60, no. November, pp. 40–46, 2007, [Online]. Available: www.physicstoday.org.
- [4] J. Turkevich, P. C. Stevenson, and J. Hillier, “A study of the nucleation and growth processes in the synthesis of colloidal gold,” *Discuss. Faraday Soc.*, vol. 11, no. c, pp. 55–75, 1951, doi: 10.1039/DF9511100055.
- [5] J. Lim *et al.*, “Identification of Newly Emerging Influenza Viruses by Surface-Enhanced Raman Spectroscopy,” *Anal. Chem.*, vol. 87, no. 23, pp. 11652–11659, Dec. 2015, doi: 10.1021/acs.analchem.5b02661.

OP-28

Models of Spike, Envelope and Membrane Proteins of SARS-CoV-2 Variants and Possible Drug Therapeutics

Ahmet Ozan Özgen*¹, Gizem Tutkun*¹, Uğur Bilge*¹

*¹Department of Medical Biotechnology, Akdeniz University, Antalya, Turkey

*Corresponding author. E-mail: gizemtutkun17@gmail.com, Tel: +905389568606

ABSTRACT

The new Severe Acute Respiratory Syndrome linked to the novel coronavirus (SARS-CoV-2) is a widespread, rapidly growing infectious disease with a high morbidity and mortality. Treatment protocols and new studies regarding therapeutics vary due to the complexity of the pathogenesis of this virus. Monitoring the genetic diversity of the virus and emerging mutations during this ongoing pandemic is critical to understand its evolution and its potential impact. The four main structural proteins of SARS-CoV-2 are spike surface glycoprotein (S), small envelope (E), membrane (M) and core proteins (N). Many mutations have been reported in all these four regions since the emergence of the virus. We focus on the development of three structural proteins (S, E and M) involved in the immunopathological functions of SARS-CoV-2. Mutations in the sequence of these proteins may lead to changes in the structure and in the interactions of the proteins, and then further affect the physiological features of the virus, and in turn these could have a significant effect on the progression of the pandemic. In this study, mutation frequencies in the five well-known SARS-CoV-2 variants have been modelled and analysed. The results present the mutation frequencies in these structural proteins, the mutations on envelope and membrane proteins are far less frequent than spike protein. Focusing on the less mutated proteins can be beneficial for the future drug and vaccine research.

INTRODUCTION

The new Severe Acute Respiratory Syndrome linked to the novel coronavirus which caused by Severe acute respiratory syndrome coronavirus 2 (SARS-CoV-2) is a β -coronavirus belonging to the Coronaviridae family, which is a RNA virus detected for the first time, in Wuhan, China, in December 2019 (Shamsi et al., 2021; Troyano-Hernández et al., 2021). Since then, the newly identified virus is referred as SARS-CoV-2 has spread throughout the world in this ongoing pandemic because it is far more contagious as compared to other earlier recognized human SARS-CoV (2002) and MERS-CoV (2013). Just like SARS-CoV and MERS-CoV, SARS-CoV-2 started by zoonotic transmission and is transmitted from person to person by respiratory tract and contact (Alsulami et al., 2021).

Spreading around the world so quickly, SARS-CoV-2 has mutated in the regions where it spread, and some of these mutations included changes that caused the virus to peak again. These variants have been identified as “Variants of Concern” because of their more efficient binding to human cells, increased ability to evade the immune system, and rapid transmission (Scudellari, 2021). The four worrisome variants in the foreground, Alpha, Beta, Delta and Gamma, emerged in the UK, South Africa, India and Brazil, respectively and identified as Variants of Concern by WHO (*Tracking SARS-CoV-2 Variants*, n.d.).

The Coronavirus (CoV) virion, which has an RNA genome, contains 4 major structural proteins: the nucleocapsid (N) protein, the transmembrane (M) protein, the envelope (E) protein, and the spike (S) protein (Hasöksüz et al., 2020).

The SARS-CoV-2 N protein, an abundant RNA-binding protein critical for viral genome packaging, contains three dynamically disordered regions that house putative temporally helical binding motifs. The two folded domains interact minimally, making the full-length N protein a flexible and multivalent RNA-binding protein (Cubuk et al., 2021).

Although the SARS-CoV-2 E protein is a small structural protein, deletion of this protein weakens or even eliminates virulence. This is because the E protein is involved in many aspects of the viral life cycle, such as promoting packaging and reproduction of the virus (Cao et al., 2021).

The most abundant structural protein of SARS-CoV-2 is the M glycoprotein (Buxbaum, 2015). The M protein can bind to all other structural proteins. Bindi Binding with the M protein helps stabilize N proteins and promotes the completion of viral assembly by stabilizing the N protein-RNA complex within the internal virion (Mousavizadeh & Ghasemi, 2021). Since the M protein cooperates with the S protein, mutations can affect host cell attachment and entry of viruses (Buxbaum, 2015).

The SARS-CoV-2 S protein has a total length of 1273 aa and consists of a signal peptide (amino acids 1–13) located at the N-terminus, the S1 (14–685 residues) subunit and the S2 (686–1273 residues) subunit. The regions as called S1 and S2 are responsible for receptor binding and membrane fusion, respectively. S protein trimers visually form a characteristic bulbous, crown-like halo surrounding the viral particle (Y. Huang et al., 2020).

The 3D representation of mutations in S, M, and E, which play an important role of these four main proteins on the cell surface and in the entry of viral RNA into the host cell, further facilitates the understanding of the structural changes that occur in SARS-CoV-2 (Alsulami et al., 2021).

MATERIALS and METHODS

The RNA sequences were gathered National Center for Biotechnology Information, regarding Variants of Concern which are determined by WHO (*Severe Acute Respiratory Syndrome Coronavirus 2 Isolates of VoCs 2020; Tracking SARS-CoV-2 Variants*, n.d.).

Translation process of the RNA to Amino Acid sequence, multiple sequence alignment and presentation of sequence comparison between variants were carried out in RStudio, Version 1.4.1717 by using the method from the study of Toparslan et al., 2020.

The Wuhan variant's structural proteins used as reference for visual comparison, and program database (PDB) files were downloaded from the studies applied with I-TASSER server (X. Huang, Pearce, et al., 2020; X. Huang, Zhang, et al., 2020; Zhang et al., 2020; Zheng et al., 2021). 3D representations of the structural proteins were carried out in PyMOL Molecular Graphics System, Version 1.2r3pre, Schrödinger, LLC.

RESULTS

Amino acid sequences of three major structural proteins (S, E, and M) prominent in host cell entry of the four variants of concern and sequences of the same proteins belonging to the Wuhan lineage were obtained from NCBI. Amino acid sequences and the mutations of the three proteins belonging to these four variants and the Wuhan lineage were shown.

Mutation counts, including deleted regions in the spike protein, were 10, 8, 10, and 12 for Alpha, Beta, Delta, and Gamma, respectively (Figure – 1). The same mutations between variants are shown with the same colours. The envelope protein also had a single mutation (P71L) only in the Beta variant. There was also a single mutation in the membrane protein only in the Delta variant (I82T).

The results obtained are consistent with the mutations previously reported in the literature, and these structural proteins considered important for possible drug targets (Pachetti et al., 2020; Portelli et al., 2020; Shen et al., 22021; Vilar & Isom, 2021). To show these mutations on 3D models, spike proteins (Figure – 2), envelope proteins (Figure – 3) and membrane proteins (Figure – 4) models of the Wuhan lineage.

Figure – 1: AA Comparisons of VoCs and Wuhan Strain

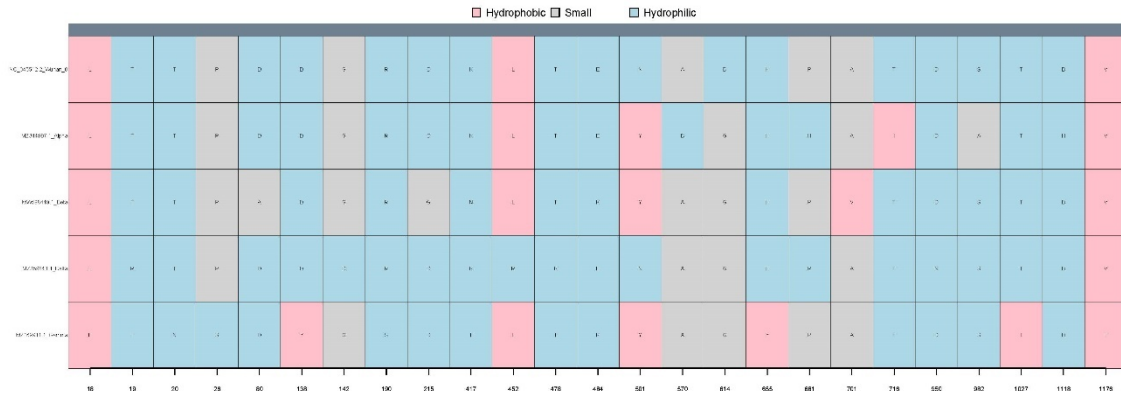


Figure – 2: S Proteins of the VoCs and Wuhan Strain

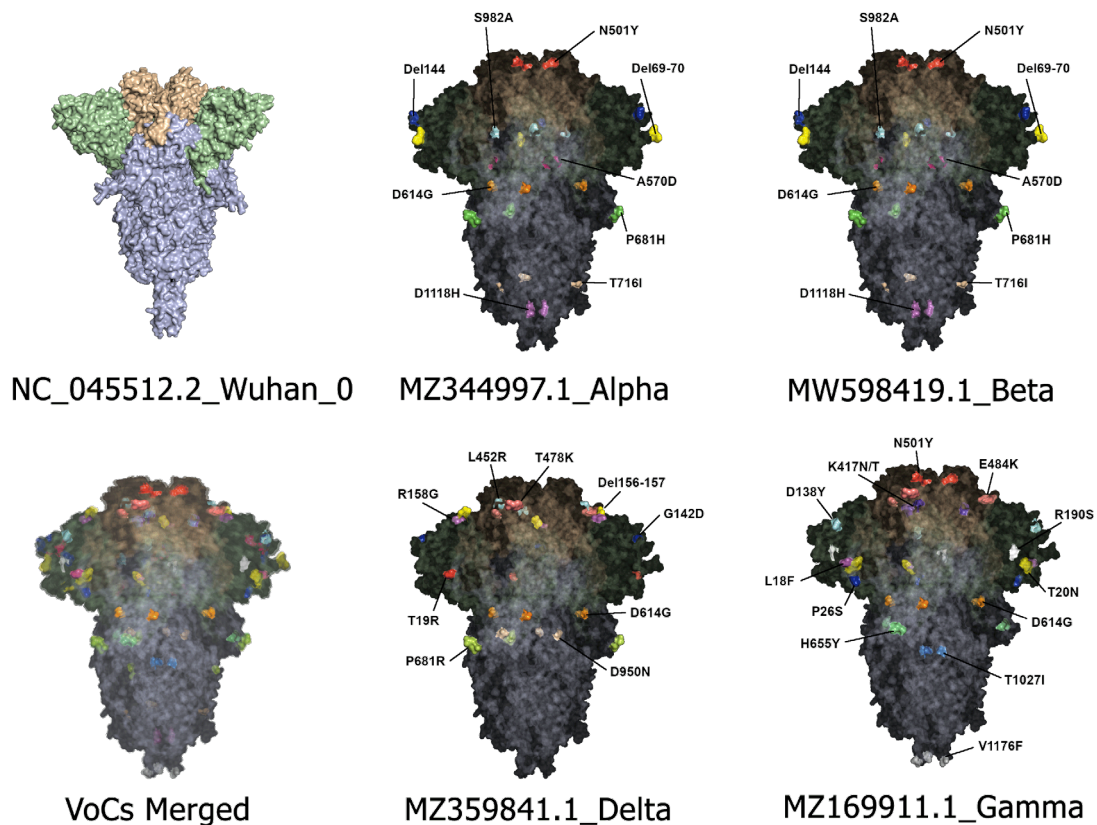


Figure – 2: E Proteins of Wuhan & Beta Strains

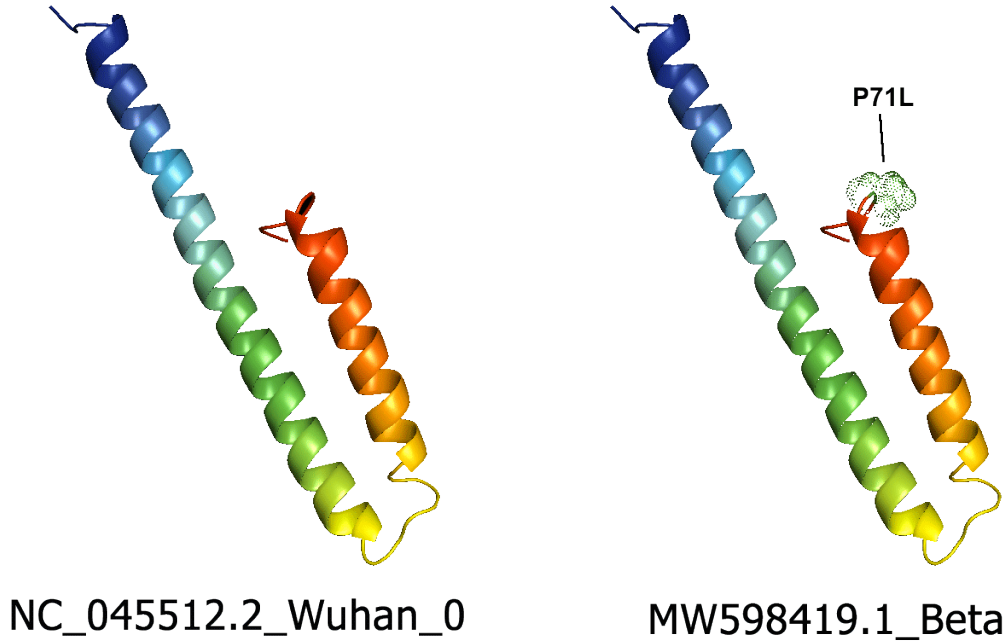
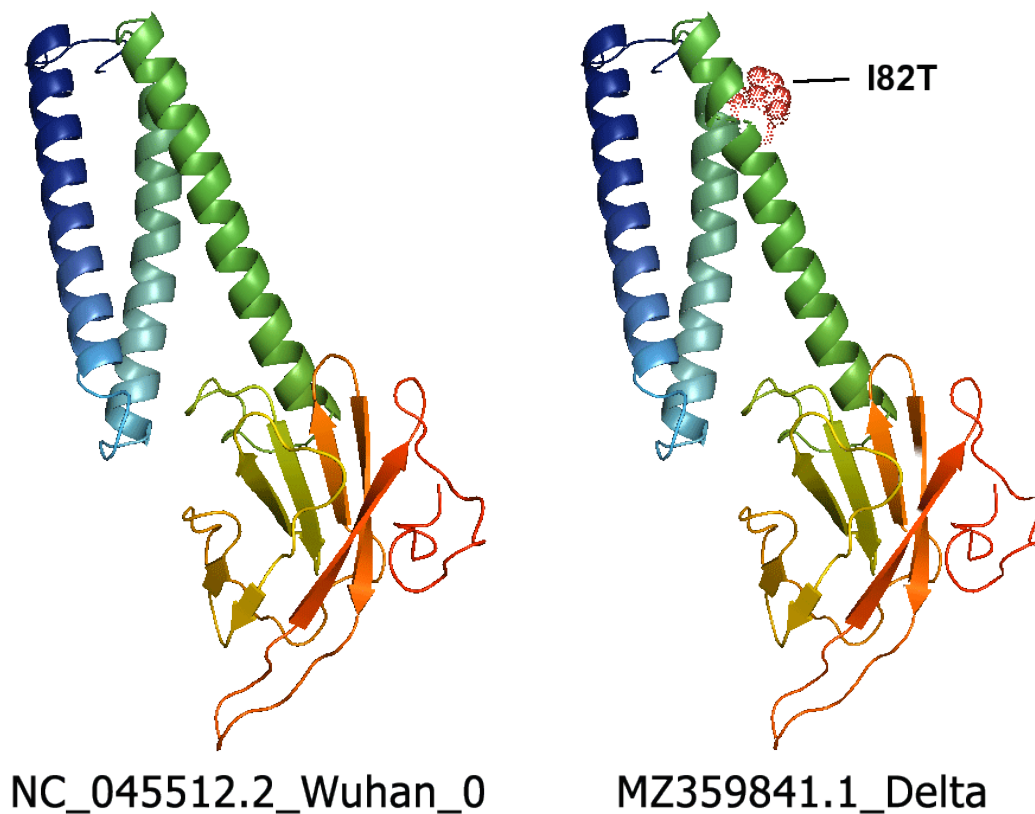


Figure – 3: M Proteins of Wuhan & Delta Strains



DISCUSSION and CONCLUSION

In silico studies can be advantageous in terms of reducing financial burden and the total time spent. In addition, the 3D representation of SARS-CoV-2 and mutations facilitates the understanding of the structural changes that occur. In addition, the locations of mutations reveal the most frequently mutated and non-mutated regions. Therefore, these models can help identify target regions in the development of therapeutics such as drugs and vaccines.

The results indicate that several mutations occurred in the spike proteins of SARS-CoV-2 the variants, particularly in the S1 subunit, Receptor Binding Domain and Antibody Binding Domain. Only a small number of mutations are observed in the envelope and membrane proteins. For the future studies regarding vaccine and drug development, it could be beneficial to focus on less mutated structural proteins.

CONFLICT of INTEREST

The authors declare that there is no conflict of interest.

REFERENCES

- Alsulami, A. F., Thomas, S. E., Jamasb, A. R., Beaudoin, C. A., Moghul, I., Bannerman, B., Copoiu, L., Vedithi, S. C., Torres, P., & Blundell, T. L. (2021). SARS-CoV-2 3D database: Understanding the coronavirus proteome and evaluating possible drug targets. *Briefings in Bioinformatics*, 22(2), 769–780. <https://doi.org/10.1093/bib/bbaa404>

- Buxbaum, E. (2015). Protein Structure. In E. Buxbaum, *Fundamentals of Protein Structure and Function* (pp. 15–64). Springer International Publishing. https://doi.org/10.1007/978-3-319-19920-7_2
- Cao, Y., Yang, R., Lee, I., Zhang, W., Sun, J., Wang, W., & Meng, X. (2021). Characterization of the SARS-CoV-2 E Protein: Sequence, Structure, Viroporin, and Inhibitors. *Protein Science*, *30*(6), 1114–1130. <https://doi.org/10.1002/pro.4075>
- Cubuk, J., Alston, J. J., Incicco, J. J., Singh, S., Stuchell-Brereton, M. D., Ward, M. D., Zimmerman, M. I., Vithani, N., Griffith, D., Wagoner, J. A., Bowman, G. R., Hall, K. B., Soranno, A., & Holehouse, A. S. (2021). The SARS-CoV-2 nucleocapsid protein is dynamic, disordered, and phase separates with RNA. *Nature Communications*, *12*(1), 1936. <https://doi.org/10.1038/s41467-021-21953-3>
- Hasöksüz, M., Kiliç, S., & Saraç, F. (2020). Coronaviruses and SARS-COV-2. *Turkish Journal of Medical Sciences*, *50*(SI-1), 549–556. <https://doi.org/10.3906/sag-2004-127>
- Huang, X., Pearce, R., & Zhang, Y. (2020). De novo design of protein peptides to block association of the SARS-CoV-2 spike protein with human ACE2. *Aging*, *12*(12), 11263–11276. <https://doi.org/10.18632/aging.103416>
- Huang, X., Zhang, C., Pearce, R., Omenn, G. S., & Zhang, Y. (2020). Identifying the Zoonotic Origin of SARS-CoV-2 by Modeling the Binding Affinity between the Spike Receptor-Binding Domain and Host ACE2. *Journal of Proteome Research*, *19*(12), 4844–4856. <https://doi.org/10.1021/acs.jproteome.0c00717>
- Huang, Y., Yang, C., Xu, X., Xu, W., & Liu, S. (2020). Structural and functional properties of SARS-CoV-2 spike protein: Potential antivirus drug development for COVID-19. *Acta Pharmacologica Sinica*, *41*(9), 1141–1149. <https://doi.org/10.1038/s41401-020-0485-4>
- Mousavizadeh, L., & Ghasemi, S. (2021). Genotype and phenotype of COVID-19: Their roles in pathogenesis. *Journal of Microbiology, Immunology and Infection*, *54*(2), 159–163. <https://doi.org/10.1016/j.jmii.2020.03.022>

Pachetti, M., Marini, B., Benedetti, F., Giudici, F., Mauro, E., Storici, P., Masciovecchio, C., Angeletti, S., Ciccozzi, M., Gallo, R. C., Zella, D., & Ippodrino, R. (2020). Emerging SARS-CoV-2 mutation hot spots include a novel RNA-dependent-RNA polymerase variant. *Journal of Translational Medicine*, 18(1), 179. <https://doi.org/10.1186/s12967-020-02344-6>

Portelli, S., Olshansky, M., Rodrigues, C. H. M., D'Souza, E. N., Myung, Y., Silk, M., Alavi, A., Pires, D. E. V., & Ascher, D. B. (2020). Exploring the structural distribution of genetic variation in SARS-CoV-2 with the COVID-3D online resource. *Nature Genetics*, 52(10), 999–1001. <https://doi.org/10.1038/s41588-020-0693-3>

Scudellari, M. (2021). How the coronavirus infects cells—And why Delta is so dangerous. *Nature*, 595(7869), 640–644. <https://doi.org/10.1038/d41586-021-02039-y>

Severe acute respiratory syndrome coronavirus 2 isolate SARS-CoV-2/human/BRA/1236/2021, complete genome (2035912854). (2021). [Data set]. NCBI Nucleotide Database. <http://www.ncbi.nlm.nih.gov/nuccore/MZ169911.1>

Severe acute respiratory syndrome coronavirus 2 isolate SARS-CoV-2/human/England/204820464/2020 ORF1ab polyprotein (ORF1ab), ORF1a polyprotein (ORF1ab), surface glycoprotein (S), ORF3a protein (ORF3a), envelope protein (E), membrane glycoprotein (M), ORF6 protein (ORF6), ORF7a protein (ORF7a), ORF7b (ORF7b), truncated ORF8 protein (ORF8), nucleocapsid phosphoprotein (N), and ORF10 protein (ORF10) genes, complete cds (2048747240). (2021). [Data set]. NCBI Nucleotide Database. <http://www.ncbi.nlm.nih.gov/nuccore/MZ344997.1>

Severe acute respiratory syndrome coronavirus 2 isolate SARS-CoV-2/human/GHA/nmimr-SARS-CoV-2-TRA-201/2021, complete genome (1984072141). (2021). [Data set]. NCBI Nucleotide Database. <http://www.ncbi.nlm.nih.gov/nuccore/MW598419.1>

Severe acute respiratory syndrome coronavirus 2 isolate SARS-CoV-2/human/IND/GBRC711/2021 ORF1ab polyprotein (ORF1ab), ORF1a polyprotein (ORF1ab), surface glycoprotein (S), ORF3a protein (ORF3a), envelope protein (E), membrane glycoprotein (M), ORF6 protein (ORF6),

ORF7a protein (ORF7a), and ORF7b (ORF7b) genes, complete cds; ORF8 gene, complete sequence; and nucleocapsid phosphoprotein (N) and ORF10 protein (ORF10) genes, complete cds (2050056574). (2021). [Data set]. NCBI Nucleotide Database.

<http://www.ncbi.nlm.nih.gov/nuccore/MZ359841.1>

Severe acute respiratory syndrome coronavirus 2 isolate Wuhan-Hu-1, complete genome

(1798174254; Version 2). (2020). [Data set]. NCBI Nucleotide Database.

http://www.ncbi.nlm.nih.gov/nuccore/NC_045512.2

Shamsi, A., Mohammad, T., Anwar, S., Amani, S., Khan, M. S., Husain, F. M., Rehman, Md. T., Islam, A., & Hassan, M. I. (2021). Potential drug targets of SARS-CoV-2: From genomics to therapeutics. *International Journal of Biological Macromolecules*, *177*, 1–9.

<https://doi.org/10.1016/j.ijbiomac.2021.02.071>

Shen, L., Bard, J. D., Triche, T. J., Judkins, A. R., Biegel, J. A., & Gai, X. (2021). Emerging variants of concern in SARS-CoV-2 membrane protein: A highly conserved target with potential pathological and therapeutic implications. *Emerging Microbes & Infections*, *10*(1), 885–893.

<https://doi.org/10.1080/22221751.2021.1922097>

Tracking SARS-CoV-2 variants. (n.d.). Retrieved 21 August 2021, from

<https://www.who.int/emergencies/emergency-health-kits/trauma-emergency-surgery-kit-who-tesk-2019/tracking-SARS-CoV-2-variants>

Troyano-Hernández, P., Reinoso, R., & Holguín, Á. (2021). Evolution of SARS-CoV-2 Envelope, Membrane, Nucleocapsid, and Spike Structural Proteins from the Beginning of the Pandemic to September 2020: A Global and Regional Approach by Epidemiological Week. *Viruses*, *13*(2), 243. <https://doi.org/10.3390/v13020243>

Vilar, S., & Isom, D. G. (2021). One Year of SARS-CoV-2: How Much Has the Virus Changed? *Biology*, *10*(2), 91. <https://doi.org/10.3390/biology10020091>

Zhang, C., Zheng, W., Huang, X., Bell, E. W., Zhou, X., & Zhang, Y. (2020). Protein Structure and Sequence Reanalysis of 2019-nCoV Genome Refutes Snakes as Its Intermediate Host and the

Unique Similarity between Its Spike Protein Insertions and HIV-1. *Journal of Proteome Research*, 19(4), 1351–1360. <https://doi.org/10.1021/acs.jproteome.0c00129>

Zheng, W., Zhang, C., Li, Y., Pearce, R., Bell, E. W., & Zhang, Y. (2021). Folding non-homologous proteins by coupling deep-learning contact maps with I-TASSER assembly simulations. *Cell Reports Methods*, 1(3), 100014. <https://doi.org/10.1016/j.crmeth.2021.100014>

Algorithm-based approach to uncover potential microRNAs related to cancers of the gastrointestinal track

1. Background

MicroRNAs (miRNAs) are short (~22 nt long) endogenous non-coding RNAs which transcribed as short hairpin precursors (~70 nt) [1, 2,]. MiRNAs play important roles in biological processes like cell proliferation, development, immune reaction and tumor invasion by targeting specific messenger RNAs (mRNAs), and regulate gene expression either by mRNA degradation or translational inhibition [3,4]. Several studies also indicate that many miRNAs are implicated in human diseases [5], including cancer [6], immune related diseases [7], Parkinson's disease [8], etc. Identifying the miRNAs associated with diseases could contribute to better understanding the pathogenesis, diagnosis, treatment, and prognosis of diseases and help to develop new drugs [9]. With an estimated 4.8 million new cases and 3.4 million deaths worldwide in 2018, cancers of the gastrointestinal (GI) tract represent over one-quarter (26%) of the global cancer incidence and over one-third (35%) of all cancer-related deaths. The current standard method for identifying miRNAs involved in a disease is miRNA expression profiling, which is a time consuming, labor-intensive and expensive experimental approach [10]. In the recent years, a number of computational methods have been proposed to predict the associations between miRNAs and diseases. In this study, we propose a network integration approach using the 'maximal clique' algorithm to predict potential miRNA–disease associations.

2. Methods

2.1. Data pre-processing

- a) Collection of data from relevant sources
- b) Inference of functional similarity from MiRGOFS

2.2. Reconstruction of heterogeneous networks

- a) Disease–miRNA network
- b) miRNA-miRNA associations network:

c) Construction of the integrated network

2.3. Identification of new miRNAs-disease associations

The cytoHubba v.0.1 plug-in was used to select potential miRNAs-disease associations from the integrated network. CytoHubba is a Java plugin for ranking nodes in a network by their network features.

2.4. Running Maximal clique algorithm

After constructing the integrated miRNA-disease network by combining these two datasets, we employed the maximal clique algorithm.

3. Results

3.1 Ranking of miRNAs in the integrated network using MCC

We applied the algorithm MCC on our merged miRNA-disease network. First, the top 20 potential cancer-related miRNAs predicted by the algorithm were listed (Table 1).

To get more robust and accurate results, we decided to obtain the 10 highest ranking miRNAs based on the MCC algorithm (Table 2).

As shown in Figure 5, the miRNAs hsa-miR-107 and hsa-miR-1246 are related to cancers. It has been demonstrated that hsa-miR-107 is associated with colorectal, gastric and esophageal cancers [11]. In addition, in a study by Shi and colleagues, hsa-miR-1246 is suggested to be a potential biomarker for the early diagnosis of gastric and colorectal cancers [12].

3.2. Identification of potential diagnostic miRNAs based on their correlation scores

As shown in Table 3, each unknown miRNA was compared to hsa-miR-107 based on their pairwise functional similarity score.

In the next step we compared other novel miRNAs with the known hsa-miR-1246 and ordered them based on their scores. As shown in Table 4, the highest scoring miRNA is hsa-miR-1248 (score= 0.810089936).

4. Conclusion

MiRNAs represent an important class of regulators in carcinogenesis, as well as a new class of diagnostic and therapeutic targets. As we analyzed the miRNAs-disease associations network, we detected a few novel miRNAs. Based on our findings, the miRNA has-miR-1248 could possibly serve as a potential diagnostic marker for the early detection of GI cancers. It has been proved hsa-miR-1248 is related to lung cancer, and upregulation of miR-1248 was significantly inhibited the proliferation and invasion of NSCLC cells [13]. On the other hand, hsa-miR-1248 is predicted to regulate numerous cytokines, including IL-5 [14], facilitating in this way metastasis colonization via modulation of the immune-microenvironment [15].

However, further experimental validation on cancer patient samples is required to assess the biological significance of the signature miRNAs, detected in this study, in the diagnosis and clinical decision making of GI cancers. This will enable the generation of an enriched pool of miRNAs that would not only reveal yet undiagnosed cancers, but also, miRNAs exclusively associated with a certain type of GI cancer (e.g., stomach cancer) would allow the diagnosis of specific cancer types, as well. Overall, we expect that these findings may help in the identification of miRNA biomarkers so as to prevent cancer development by enabling its early detection.

5. References

1. Ambros V. The functions of animal microRNAs. *Nature*. 2004;431(7006):350–5.
2. Bartel DP. MicroRNAs: genomics, biogenesis, mechanism, and function. *Cell*. 2004;116(2):281–97.
3. Shi, H., Xu, J., Zhang, G., Xu, L., Li, C., Wang, L., Zhao, Z., Jiang, W., Guo, Z., and Li, X. (2013). Walking the interactome to identify human mirna-disease associations through the functional link between mirna targets and disease genes. *BMC systems biology*, 7(1), 101.
4. Jiang, Q. et al. Prioritization of disease microRNAs through a human phenome-microRNAome network. *BMC systems biology* 4, S2 (2010).

5. Jiang, Q., Wang, Y., Hao, Y., Juan, L., Teng, M., Zhang, X., Li, M., Wang, G., and Liu, Y. (2008). mir2disease: a manually curated database for microRNA deregulation.
6. Volinia, S., Galasso, M., Sana, M. E., Wise, T. F., Palatini, J., Huebner, K., and Croce, C. M. (2012). Breast cancer signatures for invasiveness and prognosis defined by deep sequencing of microRNA. *Proceedings of the National Academy of Sciences*, 109(8), 3024–3029.
7. Wei, L., Huang, Y., Qu, Y., Jiang, Y., and Zou, Q. (2012). Computational analysis of miRNA target identification. *Current Bioinformatics*, 7(4), 512–525.
8. Kim, J., Inoue, K., Ishii, J., Vanti, W. B., Voronov, S. V., Murchison, E., Hannon, G., and Abeliovich, A. (2007). A microRNA feedback circuit in midbrain dopamine neurons. *Science*, 317(5842), 1220–1224.
9. C. Bang, J. Fiedler, and T. Thum, “Cardiovascular importance of the microRNA 23/27/24 family,” *Microcirculation*, vol. 19, no. 3, pp. 208–214, 2012.
10. Chugh, P. & Dittmer, D. P. Potential pitfalls in microRNA profiling. *Wiley Interdiscip. Rev. RNA* 3, 601–616 (2012)
11. Sharma, P., Saini, N., & Sharma, R. (2017). miR-107 functions as a tumor suppressor in human esophageal squamous cell carcinoma and targets Cdc42. *Oncology Reports*, 37(5), 3116–3127. doi:10.3892/or.2017.5546.
12. Shi, Y., Wang, Z., Zhu, X., Chen, L., Ma, Y., Wang, J., ... Liu, Z. (2019). Exosomal miR-1246 in serum as a potential biomarker for early diagnosis of gastric cancer. *International Journal of Clinical Oncology*. doi:10.1007/s10147-019-01532-9.
13. Yang, T., Li, M., Li, H., Shi, P., Liu, J., & Chen, M. (2020). Downregulation of circEPST11 represses the proliferation and invasion of non-small cell lung cancer by inhibiting TRIM24 via miR-1248 upregulation. *Biochemical and Biophysical Research Communications*, 530(1), 348–354.
14. Panganiban R.P.L., Pinkerton M.H., Maru S.Y., Jefferson S.J., Roff A.N., Ishmael F.T. Differential MicroRNA Expression in Asthma and the Role of MiR-1248 in Regulation of IL-5. *Am. J. Clin. Exp. Immunol.* 2012;1:154–165.
15. Zaynagetdinov R., Sherrill T.P., Gleaves L.A., McLoed A.G., Saxon J.A., Habermann A.C., Connelly L., Dulek D., Peebles R.S., Fingleton B., et al. Interleukin-5 Facilitates Lung Metastasis by Modulating the Immune Microenvironment. *Cancer Res.* 2015; 75:1624–1634. doi: 10.1158/0008-5472.CAN-14-237.

Screening of Lactic Acid Bacteria From Turkish Microflora For Antihypertensive Potential**Zeynep AĞIRBAŞLI¹, Assoc. Prof. Dr. Efe Sezgin¹, Prof. Dr. Sebnem HARSA¹**¹ Department of Food Engineering, Izmir Institute of Technology, Gülbahce Campus, Urla, 35430 Izmir, Turkeyzevnepagirbasli@ivte.edu.tr ORCID: 0000-0002-4792-0694; efesezgin@ivte.edu.tr ORCID: 0000-0002-8000-7485, sebnemharsa@ivte.edu.tr

ORCID: 0000-0001-6794-299X

1. Introduction

Hypertension is generally described as “silent killer” since it rarely causes symptoms and leads to death. Alarmingly, reports on this global disease showed that approximately 1.13 billion people had hypertension in 2015 and its occurrence rate was higher in low- and middle-income countries compared to high-income countries (Risk, 2017). On the other hand, a recent meta-analysis interpreted data of 344716 participants from 48 randomised clinical trials and revealed a novel findings that the major cardiovascular events were lowered up to 10% regardless of the presence of cardiovascular diseases or status of blood pressure (normal or high-normal) when systolic blood pressure was lowered 5 mm Hg (Adler et al., 2021). In addition to pharmacological treatment, non-pharmacological changes are required for management of hypertension. Lifestyle conversions such as lowering sodium and alcohol consumption, increasing of potassium consumption and physical activities are recommended (Ozemek, Tiwari, Sabbahi, Carbone, & Lavie, 2020). In addition to dietary changes, beneficial effects of functional foods have been studied for their antihypertensive properties due to their bioactive compounds such as peptides from proteins, phenolic compounds, fiber and minerals. Most of the studies focus on the angiotensin I-converting enzyme (ACE) inhibitory activities (Huang, Davidge, & Wu, 2013). Proteolysis form ACE inhibitory peptides due to specific enzymatic activities; therefore fermentation and ACE-inhibitory activity are enhanced with high proteolytic activities of lactic acid bacteria (LAB) (Donkor, Henriksson, Vasiljevic, & Shah, 2007). On the other hand, LAB can form GABA from L-glutamic acid or its salts with the action of glutamate decarboxylase enzyme (GAD) (Diana, Rafecas, Arco, & Quilez, 2014). GABA show several activities such as antihypertensive, anti-oxidant and antidepressant functions. However, studies have mostly focused on GABA-producing microorganisms rather than GABA in isolation (Sarasa et al., 2020). The starter potential of LAB and yeast in fermented foods promotes the importance of their GABA production abilities (Diana et al., 2014). Presence of *gad* gene indicates the GABA synthesizing ability of LAB strain (Wu & Shah, 2017).

The aim of this study is to determine antihypertensive potential of LAB strains for their contribution in a functional food approach. In this purpose, high number of artisanal dairy LAB strains have been screened for their proteolytic and GABA producer potential and the presence of *gad* gene was screened by *in silico* tools for the LAB species.

2. Materials and Methods**2.1. LAB strains culture preparation**

Bacteria strains which had isolated from dairy product in previous thesis research was used (Erkuş, 2007). An aliquot of *Streptococcus thermophilus* species from stock culture collection maintained at -80 °C was inoculated into M17 broth (Merck, Germany) and incubated at 42°C for overnight under anaerobic conditions. Afterwards, LAB strains were propagated into M17 broth and incubated at 37 °C, for 24h, under anaerobic conditions.

2.2. Screening of LAB strains for GABA production

Thin-layer chromatography (TLC) method was selected to rapid screening of GABA producing LAB strains. Each activated strain was inoculated into 10 ml of M17 broth with 1% (w/v) monosodium glutamate (MSG) and incubated at 42°C for 48 h. Then, 1 µl of culture supernatant was spotted onto a TLC plate (Silica gel 60 F254; Merck Co., Germany). Separation was done with iso-butanol/acetic

acid/water (4:1:1; v/v). The plate was treated with ninhydrin solution to visualize the spots and heat treatment were used to colour development of spots (Sokovic Bajic et al., 2019).

2.3. Proteolytic Activity

For preliminary screening of proteolytic activity, cell cultures were vortexed and 10 µL LAB cultures were spotted on the surface of skim milk agar medium (prepared with 1% (w/v) skim milk powder (Oxoid)) and incubated at the optimal growth temperature for 48 h. Proteolytic activity was indicated as a clear zone around the colonies (El-Ghaish et al., 2010).

2.4. *In silico* screening of *gad* genes in *S. thermophilus*

GAD encoding *gad* gene and its transporter *gadC* gene of *S. thermophilus* genes were researched in National Center for Biotechnology Information (NCBI) (<https://www.ncbi.nlm.nih.gov/>) database ("Database resources of the national center for biotechnology information," 2018). Collected genes were aligned by Clustal Omega tool (<https://www.ebi.ac.uk/Tools/msa/clustalo/>) (Sievers et al., 2011).

3. Results

3.1. Qualitative GABA Producing Ability

Out of 72 *S. thermophilus* strains, no positive TLC results were obtained. Therefore, none of *S. thermophilus* strain produced GABA with 1% MSG as a substrate under standard medium pH conditions.

3.2. Proteolytic Activity

Modified method of El-Ghaish et al. (2010) were used to classify isolates based on colony size; colony size were determined by calculating the differences between colony size and colony plus zone size. Proteolytic activities were categorised as low (<3mm), medium (3-4.5 mm) and high (>4.5mm). Also zone clearance were classified based on transparency; lowest clarity (+), low clarity (+), medium (++), high clarity (+++). As a result, these clarities were numbered from 1 to 3; 3 explaining the highest zone clearance.

In general, isolates coded as cTY and c exhibited both strong and weak proteolytic activities in skim milk agar. Among 72 *S. thermophilus* strains, 34 of them showed medium proteolytic activity, whereas 5 of them possessed high activities.

3.3. *In silico* screening of *gad* genes in *S. thermophilus*

According to data in the NCBI database, *S. thermophilus* has *gadA* gene in some strains and *gadB* gene in other strains. In addition, some strains have been recorded with *gad* gene, they were not specified as *gadA* or *gadB*. Approximately, 29 of GAD encoding gene were detected in NCBI database as a result of screening of *gad* gene in *S. thermophilus* species.

S. thermophilus gadA and *gadB* genes were found highly conserved based on the sequence homology results of strains, it could be concluded that there is only one type of *gad* gene in *S. thermophilus*. Similarly, a recent research obtained same conclusion and named *gad* gene in *S. thermophilus* APC151 and ACA-DC2 as *gadB* gene (Cui et al., 2020). Furthermore, it was concluded that *gadR* gene was absent or not annotated in *S. thermophilus* species. Therefore, the *gad* gene of *S. thermophilus* was referred as *gadB* in this study. The alignment results showed high homology between *gadB* genes (98.2-100% similarity) Furthermore, similar results were obtained for *gadC* genes (97.77-100%).

4. Discussion

Qualitative proteolytic activity of *S. thermophilus* is detected as strain-dependent in skim milk agar method. Similarly, a study showed that strain-dependency of cell envelope-associated proteinase activity (PrtS⁺) in *S. thermophilus*. 12 of 30 strains possessed PrtS activity, 3 were classified with low activity and 7 of 30 strain did not contain *prtS* gene (Galia, Perrin, Genay, & Dary, 2009). The relation

between proteolytic activities and ACE inhibitory activity has been studied in several studies (Donkor et al., 2007), specifically for *S. thermophilus* (Gandhi & Shah, 2014). In addition, proteolytic system of several *S. thermophilus* strains were defined in a recent study (Hu, Cui, & Qu, 2021). These studies indicated the potential of ACE inhibitor activities were due to the proteolytic system of *S. thermophilus*.

On the other hand, screening of dairy based *S. thermophilus* studies are being increased (Somkuti, Renye Jr, & Steinberg, 2012). GABA containing cheese was produced by using GABA producer starter *S. thermophilus* 84C derived from cheese (Carafa et al., 2019). In another research, among 191 *S. thermophilus* strain, 20 of them possessed *gad* gene and only 5 of them synthesized GABA (Brasca et al., 2016). In another study only 3 out of 39 *S. thermophilus* isolates were found to be GABA producers (Valenzuela, Flórez, Vázquez, Vasek, & Mayo, 2019). These studies based on large isolate collections indicate that *S. thermophilus* strains can have low ability of GABA biosynthesis. On the other hand, GABA production level can be affected by coculture fermentation. For example, GABA yield by *S. thermophilus* in yogurt with coculture fermented with *L. delbrueckii subsp. bulgaricus* have been increased (Chen, Alcazar, Yang, Lu, & Lu, 2018).

5. Conclusions

Proteolytic strain can be useful candidate to produce ACE-inhibitory activity, GABA producer strain can show antihypertensive potential. Artisanal strains of our country have possessed antihypertensive properties; results obtained from this study revealed that at least five *S. thermophilus* strains have been identified as potential producer of ACE-inhibitory peptides. Although, they did not produced GABA under analysis conditions, these investigations will be carried out with other LAB strains that may possess GABA production. Therefore, the development of functional foods produced by selected LAB strains due to ACE inhibitor and GABA producing abilities may have antihypertensive potential.

REFERENCES

- Adler, A., Agodoa, L., Algra, A., Asselbergs, F. W., Beckett, N. S., Berge, E., . . . Bulpitt, C. J. (2021). Pharmacological blood pressure lowering for primary and secondary prevention of cardiovascular disease across different levels of blood pressure: an individual participant-level data meta-analysis. *The Lancet*, 397(10285), 1625-1636.
- Brasca, M., Hogenboom, J. A., Morandi, S., Rosi, V., D'Incecco, P., Silveti, T., & Pellegrino, L. (2016). Proteolytic activity and production of γ -aminobutyric acid by *Streptococcus thermophilus* cultivated in microfiltered pasteurized milk. *Journal of agricultural and food chemistry*, 64(45), 8604-8614.
- Carafa, I., Stocco, G., Nardin, T., Larcher, R., Bittante, G., Tuohy, K., & Franciosi, E. (2019). Production of naturally γ -aminobutyric acid-enriched cheese using the dairy strains *Streptococcus thermophilus* 84C and *Lactobacillus brevis* DSM 32386. *Frontiers in microbiology*, 10, 93.
- Chen, L., Alcazar, J., Yang, T., Lu, Z., & Lu, Y. (2018). Optimized cultural conditions of functional yogurt for γ -aminobutyric acid augmentation using response surface methodology. *Journal of dairy science*, 101(12), 10685-10693.
- Database resources of the national center for biotechnology information. (2018). *Nucleic acids research*, 46(D1), D8-D13.
- Diana, M., Rafecas, M., Arco, C., & Quílez, J. (2014). Free amino acid profile of Spanish artisanal cheeses: Importance of gamma-aminobutyric acid (GABA) and ornithine content. *Journal of Food Composition and Analysis*, 35(2), 94-100.
- Donkor, O. N., Henriksson, A., Vasiljevic, T., & Shah, N. P. (2007). Proteolytic activity of dairy lactic acid bacteria and probiotics as determinant of growth and in vitro angiotensin-converting enzyme inhibitory activity in fermented milk. *Le Lait*, 87(1), 21-38.
- El-Ghaish, S., Dalgalarondo, M., Choiset, Y., Sitohy, M., Ivanova, I., Haertlé, T., & Chobert, J.-M. (2010). Screening of strains of lactococci isolated from Egyptian dairy products for their proteolytic activity. *Food chemistry*, 120(3), 758-764.
- Erkuş, O. (2007). *Isolation, phenotypic and genotypic charecterization of yoghurt starter bacteris*. Izmir Institute of technology,
- Galia, W., Perrin, C., Genay, M., & Dary, A. (2009). Variability and molecular typing of *Streptococcus thermophilus* strains displaying different proteolytic and acidifying properties. *International Dairy Journal*, 19(2), 89-95.
- Gandhi, A., & Shah, N. P. (2014). Cell growth and proteolytic activity of *Lactobacillus acidophilus*, *Lactobacillus helveticus*, *Lactobacillus delbrueckii ssp. bulgaricus*, and *Streptococcus thermophilus* in milk as affected

- by supplementation with peptide fractions. *International journal of food sciences and nutrition*, 65(8), 937-941.
- Hu, T., Cui, Y., & Qu, X. (2021). Analysis of the proteolytic system of *Streptococcus thermophilus* strains CS5, CS9, CS18 and CS20. *International Dairy Journal*, 118, 105025.
- Huang, W.-Y., Davidge, S. T., & Wu, J. (2013). Bioactive natural constituents from food sources—potential use in hypertension prevention and treatment. *Critical reviews in food science and nutrition*, 53(6), 615-630.
- Ozemek, C., Tiwari, S., Sabbahi, A., Carbone, S., & Lavie, C. J. (2020). Impact of therapeutic lifestyle changes in resistant hypertension. *Progress in cardiovascular diseases*, 63(1), 4-9.
- Risk, F. N. (2017). Collaboration (NCD-RisC). Worldwide trends in blood pressure from 1975 to 2015: a pooled analysis of 1479 population-based measurement studies with 19.1 million participants. *Lancet*, 389(10064), 37.
- Sarasa, S. B., Mahendran, R., Muthusamy, G., Thankappan, B., Selta, D. R. F., & Angayarkanni, J. (2020). A brief review on the non-protein amino acid, gamma-amino butyric acid (GABA): its production and role in microbes. *Current microbiology*, 77(4), 534-544.
- Sievers, F., Wilm, A., Dineen, D., Gibson, T. J., Karplus, K., Li, W., . . . Söding, J. (2011). Fast, scalable generation of high-quality protein multiple sequence alignments using Clustal Omega. *Molecular systems biology*, 7(1), 539.
- Sokovic Bajic, S., Djokic, J., Dinic, M., Veljovic, K., Golic, N., Mihajlovic, S., & Tolinacki, M. (2019). GABA-producing natural dairy isolate from artisanal zlatar cheese attenuates gut inflammation and strengthens gut epithelial barrier in vitro. *Frontiers in microbiology*, 10, 527.
- Somkuti, G., Renye Jr, J., & Steinberg, D. (2012). Molecular analysis of the glutamate decarboxylase locus in *Streptococcus thermophilus* ST110. *Journal of Industrial Microbiology and Biotechnology*, 39(7), 957-963.
- Valenzuela, J. A., Flórez, A. B., Vázquez, L., Vasek, O. M., & Mayo, B. (2019). Production of γ -aminobutyric acid (GABA) by lactic acid bacteria strains isolated from traditional, starter-free dairy products made of raw milk. *Beneficial microbes*, 10(5), 579-587.
- Wu, Q., & Shah, N. P. (2017). High γ -aminobutyric acid production from lactic acid bacteria: emphasis on *Lactobacillus brevis* as a functional dairy starter. *Critical reviews in food science and nutrition*, 57(17), 3661-3672.

OP-31

Health-Promoting Role and Potential Applications of *Lactiplantibacillus pentosus*

Elvan, M. and Harsa, S.

1. Introduction

Lactic acid bacteria (LAB) are classified as generally recognized as safe (GRAS) and EFSA have granted qualified presumption of safety (QPS) status to several LAB species such as *Lactiplantibacillus pentosus*, depend on safety assessment criteria (EFSA, 2017). LAB are of great importance for food biotechnology and food industry. They are mainly used as starter culture in dairy and/or non-dairy products. Some of these bacteria show probiotic properties. They also play an important role in production of enzymes, vitamins, antimicrobial agents, and exopolysaccharides. The main uses of LAB in the food industry are fermented food production, food preservation, modification of the organoleptic characteristics of foods.

Lpb. pentosus is present naturally in plant and milk, and isolated from fermented olives, dairy, corn silage, dough, tea, humans, and sewage. *Lpb. pentosus* plays a crucial role during the cheese ripening and it is used commonly as a spontaneous starter culture in the vegetable, dairy, and meat fermentation. According to the previous studies, *Lpb. pentosus* was isolated from fermented olives (Blana et al., 2014) fermented gilaburu and shalgam beverages (Akman et al., 2021), pickled vegetables (Dallal et al., 2017), boza (Todorov & Dicks 2006), and was used as a starter culture in the fermentation of olives (Blana et al., 2014). *Lpb. pentosus* inhibited protein oxidation and degradation and reduced N-Nitrosamines, one of the most important carcinogens, in the dry fermented sausages (Xiao et al., 2018). Likewise, N-nitrosodimethylamine, classified as a Group 2A carcinogen, was lowered with inoculated *Lpb. pentosus* in fermented cooked sausages (Shao et al., 2021). *Lpb. pentosus* demonstrated remarkable cholesterol-lowering effects (Wongrattanapipat et al., 2021). Combination of probiotics, including *Lpb. pentosus*, showed beneficial activities in reducing postprandial distress syndrome (discomfort, distress, pain after eating) symptoms (Drago et al., 2021). Fermented food isolate *Lpb. pentosus* improved oral health through combating oral pathogens (Rahman et al., 2020). Fermented table olive isolate *Lpb. pentosus* showed antiproliferative effect on human colon cancer cells (Saxami et al., 2016).

The objective of this study is to determine the antimicrobial and antioxidative activity of *Lpb. pentosus* for their beneficial properties as health-promoting potential in order to alleviate various health problems such as infectious diseases e.g. oral infections, candidiasis; to relieve adverse effects of chemotherapy.

Material and methods

Lpb. pentosus NRRL B-227, *C. albicans* DSMZ 5817, and *S. mutans* ATCC 25175 was obtained from the ARS Culture Collection (USA), German Collection of Microorganisms and Cell Cultures GmbH (Germany), and American Type Culture Collection (USA), respectively.

1.1. Antimicrobial activity of *Lpb. pentosus*

1.1.1. Broth microdilution method

The supernatant of *Lpb. pentosus* was tested according to the standards of the CLSI (Clinical and Laboratory Standards Institute) using broth microdilution technique. 100 µL of *Lpb. pentosus* supernatant and 100 µL of pathogen suspension were transferred into well plate (Wayne, 2008) and plates incubated on the Varioskan (Varioskan™ LUX Multimode Microplate Reader, USA) at 37°C for 48 h, measurements were performed at 30-minute intervals at 600 nm.

1.1.2. Agar overlay test

The inhibitory effect of *Lpb. pentosus* cells were tested using the agar overlay test developed by Simark-Mattsson et al. (2007). MRS agar surface was inoculated with *Lpb. pentosus* and incubated in anaerobic conditions at 37°C for 24 h. Then, the top surface of the dishes was covered with 15 mL of Nutrient agar and BHI (Brain Heart Infusion) agar, containing *C. albicans* and *S. mutans* to be tested, respectively. After incubation, the circular clear region around *Lpb. pentosus* colonies showed positive inhibition.

1.2. Antioxidative activity of *Lpb. pentosus*

1.2.1. Scavenging of 2,2-Diphenyl-1-picrylhydrazyl (DPPH) free radical

The DPPH radical-scavenging activity of *Lpb. pentosus* was measured based on the method described by Li et al. (2012). Briefly, 0.5 mL of *Lpb. pentosus* cells, was added to 1 mL 0.05 mM ethanolic DPPH radical solution. The mixture was incubated for 30 min. Then, the absorbance of the solution was measured at 517 nm.

1.2.2. Scavenging of 2,2'-Azinobis-(3-ethylbenzothiazoline-6-sulfonate) (ABTS) radical

The ABTS radical-scavenging activity of *Lpb. pentosus* was determined according to Re et al. (1999) with slight modifications. Briefly, the radical solution was made by mixing 7 mM ABTS and 2.45 mM potassium peroxydisulfate and incubated in the dark. Then the solution was diluted to an absorbance of 0.70 ± 0.02 at 734 nm. Then, 100 μ L of the cells was added to 1 mL ABTS solution, the absorbance reading was measured at 734 nm.

2. Results and discussion

In this study, *Lpb. pentosus* was selected to perform antimicrobial and antioxidant activity experiments since it widely found in dairy and plants, commonly used in fermentation of the raw materials, safely showed beneficial health effects, and easily incorporated into food products. According to the findings, *Lpb. pentosus* demonstrated inhibitory activity against both *S. mutans*, the most cariogenic pathogen, and *C. albicans*, an opportunistic pathogen found in human mucosal tissues. Likewise, previous studies showed that *Lpb. pentosus* inhibited *Streptococcus uberis* and *Yersinia enterocolitica* (Eid et al., 2016), additionally, demonstrated bacteriostatic effect against *Staphylococcus aureus* (Ren et al., 2018).

A strong antibacterial activity of *Lpb. pentosus* supernatant on *S. mutans* was demonstrated via broth microdilution method. All tested concentrations of supernatant (dilution of 1:1, 1:2, 1:4, 1:8, 1:10) showed inhibitory effect. The difference between the control group (*S. mutans* + BHI) and test sample groups (*S. mutans* + supernatant) were demonstrated in **Figure 1.A**. *Lpb. pentosus* supernatant concentrations demonstrated the scattered absorbance curve in time scale as shown in **Figure 1.B**. Equal inoculation ratio of supernatant: *C. albicans* (1:1) showed antifungal activity. Immediate reduction was obtained in 6 h and this inhibition was maintained up to 36 h. Starting from 36 h of inhibition period a slight increase in density was seen. This may be caused by the metabolites interfere within the matrix. Agar overlay method showed clear inhibition zone of both pathogens using *Lpb. pentosus* cells, demonstrated in **Figure 2**. In this study, the broth microdilution test was performed using supernatant without free cells and the agar overlay method with living cells of *Lpb. pentosus*. Thus, it has been shown that not only *Lpb. pentosus* cells but also their metabolites in their supernatant have antimicrobial activity and play an important role in the inhibition of pathogens.

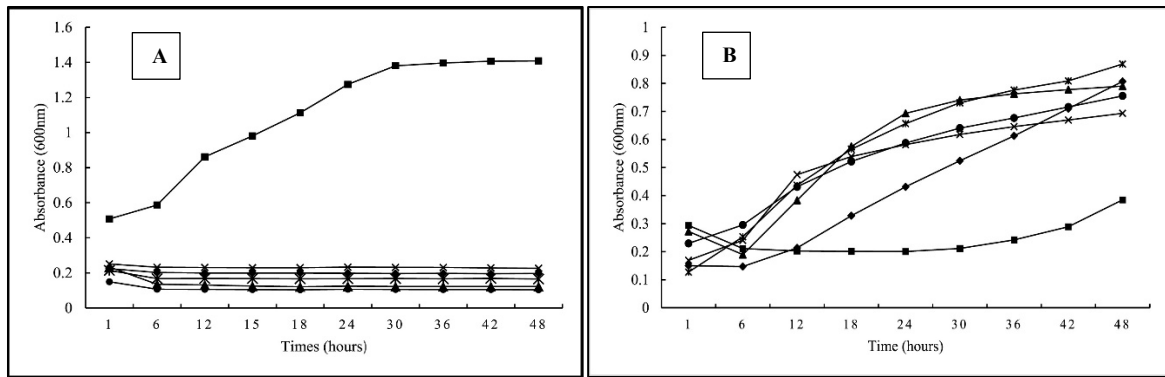


Figure 1. A) Antimicrobial effects of supernatant of *Lpb. pentosus* at different concentrations on *S. mutans*. ■ *S. mutans* growth, ◆ *S. mutans* growth with not diluted supernatant of *Lpb. pentosus*, ▲ *S. mutans* growth with 1/2 diluted supernatant of *Lpb. pentosus*, * *S. mutans* growth with 1/4 diluted supernatant of *Lpb. pentosus*, ● *S. mutans* growth with 1/8 diluted supernatant of *Lpb. pentosus*, × *S. mutans* growth with 1/10 diluted supernatant of *Lpb. pentosus*. **B)** Antimicrobial effects of supernatant of *Lpb. pentosus* at different concentrations on *C. albicans*. ◆ *C. albicans* growth, ■ *C. albicans* growth with not diluted supernatant of *Lpb. pentosus*, ▲ *C. albicans* growth with 1/2 diluted supernatant of *Lpb. pentosus*, × *C. albicans* growth with 1/4 diluted supernatant of *Lpb. pentosus*, * *C. albicans* growth with 1/8 diluted supernatant of *Lpb. pentosus*, ● *C. albicans* growth with 1/10 diluted supernatant of *Lpb. pentosus*.

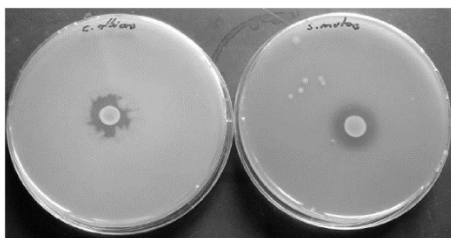


Figure 2. Inhibition zones of *S. mutans* and *C. albicans* caused by *Lpb. pentosus* with agar overlay test (n = 2).

Antioxidative activity of *Lpb. pentosus* was carried out applying DPPH and ABTS methods. The results demonstrated that *Lpb. pentosus* has the antioxidant capacity. Previous studies were confirmed that activity of this strain. According to the findings of a study, using the ABTS method, *Lpb. pentosus* ITA23, isolated from mulberry silage, demonstrated 166.34 and 39.11 μg trolox/mL antioxidative activity by its cells and cell-free extracts, respectively (Shokryazdan et al., 2017). In another study, dry sausage isolate *Lpb. pentosus* R3 cells and cell-free supernatant respectively showed 22% and 12% DPPH radical scavenging rate (Shao et al., 2021).

Considering the antimicrobial and antioxidative activity of *Lpb. pentosus*, this strain is suitable for use in many areas such as fermentation, biopreservation, and functional product development in the food industry. It is possible to produce many foods and beverages using cells, supernatant, microencapsulated or lyophilized form of *Lpb. pentosus*. This strain can be consumed and digested safely into our gastrointestinal system, since it can be attributed as a potential probiotic based on its beneficial effects, by incorporating it into lozenge formulations (Elvan et al., 2021), impregnating on the surface of table olives (Harsa et al., 2019; Rodríguez-Gómez et al., 2014), and fresh-cut fruit and vegetable slices, or incorporating during the formation of edible films and coatings (Sakman and Harsa, 2019).

References

Akman, P. K., Ozulku, G., Tornuk, F., & Yetim, H. (2021). Potential probiotic lactic acid bacteria isolated from fermented gilaburu and shalgam beverages. *LWT*, 149, 111705.

- Blana, V. A., Grounta, A., Tassou, C. C., Nychas, G. J. E., & Panagou, E. Z. (2014). Inoculated fermentation of green olives with potential probiotic *Lactobacillus pentosus* and *Lactobacillus plantarum* starter cultures isolated from industrially fermented olives. *Food microbiology*, 38, 208-218.
- Dallal, M. S., Zamaniahari, S., Davoodabadi, A., Hosseini, M., & Rajabi, Z. (2017). Identification and characterization of probiotic lactic acid bacteria isolated from traditional persian pickled vegetables. *GMS hygiene and infection control*, 12.
- Drago, L., Meroni, G., Pistone, D., Pasquale, L., Milazzo, G., Monica, F., ... & Gastrobiota Group. (2021). Evaluation of main functional dyspepsia symptoms after probiotic administration in patients receiving conventional pharmacological therapies. *Journal of International Medical Research*, 49(1), 0300060520982657.
- EFSA Panel on Biological Hazards (BIOHAZ), Ricci, A., Allende, A., Bolton, D., Chemaly, M., Davies, R., ... & Fernández Escámez, P. S. (2017). Update of the list of QPS-recommended biological agents intentionally added to food or feed as notified to EFSA 5: suitability of taxonomic units notified to EFSA until September 2016. *EFSA Journal*, 15(3), e04663.
- Eid, R., Jakee, J. E., Rashidy, A., Asfour, H., Omara, S., Kandil, M. M., ... & Seida, A. A. (2016). Potential antimicrobial activities of probiotic *Lactobacillus* strains isolated from raw milk. *J Probiotics Health*, 4(2), 138.
- Elvan, M., Baysal, A. H., & Harsa, S. T. (2021). Developing a functional lozenge with microencapsulated *Lactiplantibacillus pentosus* to improve oral and dental health. *Food Bioscience*, 40, 100883.
- Harsa, S., Baysal, A. H. & Elvan, M. (2019). Microencapsulation of *Lactobacillus pentosus* into whey protein-hemicellulose complex and empregnation on table olives”, (Project No: TUBİTAK-TOVAG 118O555), 01/10/2018- 01/10/2019.
- Li, S., Zhao, Y., Zhang, L., Zhang, X., Huang, L., Li, D., ... & Wang, Q. (2012). Antioxidant activity of *Lactobacillus plantarum* strains isolated from traditional Chinese fermented foods. *Food chemistry*, 135(3), 1914-1919.
- Rahman, N. Z. A., Hanafiah, R. M., Abd Ghafar, S. A., Abdullah, N., & Azman, N. N. (2020). Isolation and Antimicrobial Activity of Lactic Acid Bacteria against *Streptococcus mutans*. *Journal of International Dental and Medical Research*, 13(2), 417-421.
- Re, R., Pellegrini, N., Proteggente, A., Pannala, A., Yang, M., & Rice-Evans, C. (1999). Antioxidant activity applying an improved ABTS radical cation decolorization assay. *Free radical biology and medicine*, 26(9-10), 1231-1237.
- Ren, D., Zhu, J., Gong, S., Liu, H., & Yu, H. (2018). Antimicrobial characteristics of lactic acid bacteria isolated from homemade fermented foods. *BioMed research international*.
- Rodríguez-Gómez, F., Romero-Gil, V., García-García, P., Garrido-Fernández, A., & Arroyo-López, F. N. (2014). Fortification of table olive packing with the potential probiotic bacteria *Lactobacillus pentosus* TOMC-LAB2. *Frontiers in microbiology*, 5, 467.
- Sakman, Z.A. & Harsa, S. (2019). Empregnation of *Lactobacillus pentosus*, prominent to alleviate stress disorder, on apple slices for the development of functional Apple Snack, TUBITAK Project No: 21919B011803161209-A, 10/10/2018-10/08/2019.
- Saxami, G., Karapetsas, A., Lamprianidou, E., Kotsianidis, I., Chlichlia, A., Tassou, C., ... & Galanis, A. (2016). Two potential probiotic lactobacillus strains isolated from olive microbiota exhibit adhesion and anti-proliferative effects in cancer cell lines. *Journal of Functional Foods*, 24, 461-471.
- Shao, X., Xu, B., Zhou, H., Chen, C., & Li, P. (2021). Insight into the mechanism of decreasing N-nitrosodimethylamine by *Lactobacillus pentosus* R3 in a model system. *Food Control*, 121, 107534.
- Shokryazdan, P., Jahromi, M. F., Bashokouh, F., Idrus, Z., & Liang, J. B. (2017). Antiproliferation effects and antioxidant activity of two new *Lactobacillus* strains. *Brazilian Journal of Food Technology*, 21.
- Simark-Mattsson, C., Emilson, C. G., Håkansson, E. G., Jacobsson, C., Roos, K., & Holm, S. (2007). *Lactobacillus*-mediated interference of mutans streptococci in caries-free vs. caries-active subjects. *European journal of oral sciences*, 115(4), 308-314.
- Todorov, S. D., & Dicks, L. M. T. (2006). Screening for bacteriocin-producing lactic acid bacteria from boza, a traditional cereal beverage from Bulgaria: Comparison of the bacteriocins. *Process Biochemistry*, 41(1), 11-19.
- Wayne P.A. (2008) Reference method for broth dilution antifungal susceptibility testing of yeasts, approved standard M27–A3 (3), Clinical and Laboratory Standards Institute (CLSI), USA.
- Wongrattanapipat, S., Chirachoenchitta, A., Choowongwiththaya, B., Komsathorn, P., La-Ongkham, O., Nitisinprasert, S., ... & Nakphaichit, M. (2021). Selection of potential probiotics with cholesterol-

lowering properties for probiotic yoghurt production. Food Science and Technology International, 10820132211012252.

Xiao, Y., Li, P., Zhou, Y., Ma, F., & Chen, C. (2018). Effect of inoculating *Lactobacillus pentosus* R3 on N-nitrosamines and bacterial communities in dry fermented sausages. Food Control, 87, 126-134.

Investigation of Methylglyoxal Amount and Bioaccessibility with Using Different Herbal Teas

Büşra Yusufoglu^{1*}, Emine Karakuş¹, Mustafa Yaman²

^{1,1} Yildiz Technical University, Department of Chemistry, Davutpaşa/İstanbul*

² Istanbul Sabahattin Zaim University, Nutrition and Dietetics, Küçükçekmece/ Istanbul

Abstract

Recently, modern diets include processed foods such as biscuits, bakery products, ready-to-eat foods, some sauces. These products form different types of toxic compounds due to heat treatment, long-term storage and flavoring. When these toxic substances are consumed in daily life, some disease problems may occur in human metabolic health. Especially insulin resistance, cardiovascular disease, some neurodegenerative diseases. These components are known as α -dicarbonyl as methylglyoxal (MGO), glyoxal (GO) and 3-Deoxyglucosone (3-DG). One of these products MGO is highly reactive toxic metabolite both exogenous and endogenous. Dicarbonyls, also affect TNF- α and NF- κ B, and the end of this effect is endothelial dysfunction. α -dicarbonyl products can inhibit some natural source that contain polyphenol components, resveratrol, anthocyanin and proanthocyanidin. Herein, we developed novel functional snack foods and were determined both their amount of α -dicarbonyl products and bioaccessibility with using different herbal teas. As different herbal teas we used green tea and bergamout flavoured black tea. In this study, we have shown effect of natural components on glycation product on different samples. This research was supported by Yildiz Technical University-BAP Coordinator (Project No:FDK- 2020-4057; Project ID:4057, PhD Thesis Project), 100/2000 PhD Scholarships Program from Council of Higher Education and the Turkey Scientific and Technological Research Institution with 2211-C support programme, respectively.

Keywords: MGO, bioaccessibility, herbal teas, green tea, bergamout flavoured black tea

Introduction

Recent changes in dietary habits have brought about an enhanced consumption of exogenous and endogenous glycation products (Serin et al., 2021). During the thermal processing of various foods, one of these products, α -dicarbonyl compounds, plays a key role in color and flavor development. α -dicarbonyl compounds include methylglyoxal (MGO), glyoxal (GO) and 3-deoxyglucosone (3-DG) and are the most studied ones. In literature studies reported to be found in various food products, such as wine, carbonated soft drinks, fruit juices, coffee, high-fructose corn syrup, baked cookies, manuka honey and baby foods (Hamzalıoğlu and Gökmen, 2016).

Materials and Methods

In this paper, all chemicals and digestion enzymes were bought from Sigma-Aldrich (St. Louis, MO, USA). MGO was determined using the modified Mahar's method (Mahar, 2010). In order to determine the effectiveness of herbal tea for each sample, various herbal teas were added, such as green tea, bergamot flavoured and black tea according to Yaman's et al. method (Yaman and Mızrak, 2019).

Result and Discussion

The chromatogram obtained in the analysis of snack food sample 1 can be seen in Figure 1. MGO was separated using Inersil ODS-3 column, according to the reference method (Yusufoglu et al., 2020).

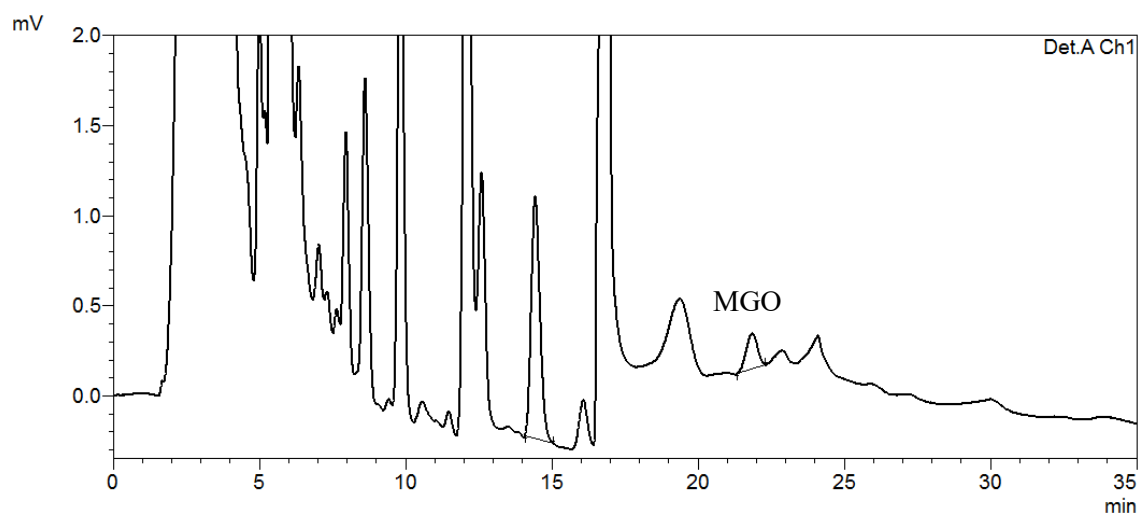


Figure 1. HPLC chromatogram of MGO in snack food sample 1.

Different types of snack foods contain oat meal and processed foods containing sugar. In this paper, we developed novel ready-to-eat products. One of the used materials is commercial oat meal, which contains

declared amount carbohydrate 53/100g, protein 14/100g, fat 7.5/100g, sugar 1.3/100g and fiber 13/100g. On the other hand, were used some heat treatment foods. These products are preparing simple and fastly for daily snacks, because of this they provide advantage. All results were given Table 1 and Table 2. MGO amounts of samples ranged from 0.53±0.02 to 13.05±0.59 in Table 1. Snack food sample 2 that apricot marmalade contains high amount MGO. In literature has shown apricot marmalade contains highly amount GO and MGO (Yusufoglu et al., 2020). When we are consuming SF 2 with green tea, amount of MGO is reducing %51.76±2.59 in Table 2.

As shown in Table 1, SF 4 had lower MGO levels. Owing to sample 4 consist of plum marmalade and oat meal. Plum marmalade is rich in phenolic and anthocyanin components as natural sources (Cevallos-Casals et al., 2006). According to studies, some natural sources prevent many diseases such as diabetes,

Table 1. Different sample types and their amount of α -DC (MGO)

Samples	Sample type	Initial value MGO ($\mu\text{g}/100\text{g}$)	After Digestion ($\mu\text{g}/100\text{g}$)	Increase Rate (%)
SF 1	Oat meal, rosehip marmalade	0.60±0.03	4.5±0.2	742.52±33.59
SF 2	Oat meal, apricot marmalade	13.05±0.59	6.0±0.3	45.46±2.06
SF 3	Oat meal, cranberry marmalade	0.60±0.03	3.0±0.1	498.33±22.55
SF 4	Oat meal, plum marmalade	0.53±0.02	9.8±0.4	1842.89±83.38
HT 1	Green Tea	0.28±0.01	0.5±0.0	192.21±8.70
HT 2	Bergamout flavoured black tea	0.23±0.01	0.9±0.0	390.00±17.64

SF: Snack Foods, HT: Herbal Tea

cardiovascular diseases, insulin resistance and other complications (Sharma et al., 2018).

In Table 2, snack food samples 1, 2, 3, and 4 were treated with herbal teas such as green tea (HT 1) and bergamout-flavored black tea (HT 2). HT1 was shown to have a lower level of hazardous glucose adduct that MGO 71.36±3.57, 51.76±2.59, 41.33±2.07 and 9.67±0.48, respectively. When HT 2 was compared to other

Table 2. Bioaccessibility of herbal teas all samples

Sample	After Digestion MGO		MGO increase rate compared rate to initial value %		MGO Reducing Rate %	
	HT 1	HT 2	HT1	HT2	HT1	HT2
SF 1	1.28±0.06	0.44±0.0	213.3±8.7	73.3±3.0	71.36±3.57	89.86±4.07
SF 2	2.87±0.13	3.55±0.2	22.0±0.9	27.1±1.1	51.76±2.59	40.40±1.83
SF 3	2.70±0.12	0.29±0.0	451.7±18.4	48.3±2.0	9.67±0.48	90.03±4.07
SF 4	5.73±0.26	0.18±0.0	1084.9±44.3	34.0±1.4	41.33±2.07	97.84±4.43

SF:Snack Foods, HT: Herbal Tea

treatments, it was shown to be reduced by 97.84±4.43, 90.03±4.07, 89.86±4.07 and 40.40±1.83 respectively.

References

1. Cevallos-Casals, B. A., Byrne, D., Okie, W. R., & Cisneros-Zevallos, L. (2006). Selecting new peach and plum genotypes rich in phenolic compounds and enhanced functional properties. *Food chemistry*, *96*(2), 273-280.
2. Hamzalıođlu, A., & Gökmen, V. (2016). Investigations on the reactions of α -dicarbonyl compounds with amino acids and proteins during in vitro digestion of biscuits. *Food & function*, *7*(6), 2544-2550.
3. Mahar, K. P., Khuhawar, M. Y., Kazi, T. G., Abbasi, K., & Channer, A. H. (2010). Quantitative analysis of glyoxal, methyl glyoxal and dimethyl glyoxal from foods, beverages and wines using HPLC and 4-nitro-1, 2-phenylenediamine as derivatizing reagent. *Asian Journal of Chemistry*, *22*, 6983-6990.
4. Serin, Y., Akbulut, G., Uđur, H., & Yaman, M. (2021). Recent developments in in-vitro assessment of advanced glycation end products. *Current Opinion in Food Science*.
5. Sharma, C., Kaur, A., Thind, S.S., Singh, B., & Raina, S. (2015). Advanced glycation End-products (AGEs): an emerging concern for processed food industries. *Journal of Food Science & Technology*, *52*(12), 7561-7576. doi:10.1007/s13197-015-1851-y
6. Yaman, M., & Mızrak, Ö. F. (2019). Determination and evaluation of in vitro bioaccessibility of the pyridoxal, pyridoxine, and pyridoxamine forms of vitamin B6 in cereal-based baby foods. *Food chemistry*, *298*, 125042.
7. Yusufoglu, B., Yaman, M., & Karakuş, E. (2020). Determination of the most potent precursors of advanced glycation end products in some high-sugar containing traditional foods using high-performance liquid chromatography. *Journal of Food Processing and Preservation*, *44*(9), e14708.

OP-33

Determination of total carbohydrate and total protein of Kastamonu Taşköprü garlic bulb

Authours; Ümmügülsüm POLAT KORKUNÇ, Emine KARAKUŞ

In this study, the nutrient content of the garlic bulb was analyzed, which is an important product in terms of Kastamonu. The goal of this work was to investigate changes in the different extraction volumes of Kastamonu Taşköprü garlic. The garlic was collected from the Taşköprü of Kastamonu extracted from the samples by solid-liquid extraction before the analysis. In addition, this study was studied with five different extraction volumes compared to other studies.

In the present work quantitative estimation of total carbohydrate and total protein in the different extraction volumes of Kastamonu Taşköprü garlic were observed using phenol sulphuric acid and Bradford method, respectively. Phenol sulphuric acid method is the most fast, easiest and reliable method among the quantitative assays for carbohydrate estimation. This method is widely used to determine the total amounts of carbohydrate in foods. The results are defined in the terms of a single carbohydrate, usually glucose. The Bradford assay has become the colorimetric method of choice, owing principally to its high sensitivity, perceived linearity, and the speed of analysis.

This presentation is supported by YTU-BAP with the project code TSA-2021-4114 and the project name 'Ülkemiz Kaynaklı Doğal Organosülfür Bileşiklerinin Kanseri İyileştirici Etkileri'.

**A Comparative Study on Anti-Cancer Properties of Dextran-Coated Nanoceria Against
Colon and Lung Cancer**

Elif Tarakcı^{1,2}, Feride Melisa Bilgin^{1,3}, Berrin Erdag⁴, Aylin Ozdemir Bahadir¹,
Saban Tekin¹, Hilal Yazici^{1*}

1. TUBITAK-Marmara Research Center, Genetic Engineering and Biotechnology Institute, Kocaeli 41470, Turkey.
2. Department of Biomedical Engineering, Yeditepe University, Istanbul 34755, Turkey.
3. Molecular and Translational Biomedicine Program, Acibadem Mehmet Ali Aydinlar University, Istanbul 34684, Turkey.
4. Department of Medical Sciences, Medical Faculty, Istanbul Aydin University, Istanbul 34295, Turkey.

*Corresponding author e-mail: hilal.yazici@tubitak.gov.tr

Nanoparticle-based cancer treatments have recently become an alternative field to conventional therapies. Nanoceria (cerium oxide), with tremendous pharmacological potential, have been drawing attention due to its redox catalyst behavior in cancer therapy unlike other metal, metal-oxide, and polymeric nanoparticles. This remarkable therapeutic feature of nanoceria is mainly derived from surface cerium atoms, which can cycle in between Ce^{+3} and Ce^{+4} . This feature allows nanoceria to behave as ion scavengers to modulate and associate with free radicals and make nanoceria as anti- or pro-oxidant therapeutics and radioprotective agents. There are various studies to define nanoceria's function through redox properties which were affected by particle size, shape, surface chemistry, and other factors such as coating agent, local pH, and ligands against various cancer types. However, there is very little experimental data on nanoceria's surface reactivity, redox reaction mechanism, ligand adsorption, and its role in signaling pathways. Therefore, there is a need to understand the detailed function of nanoceria to utilize and design it as a specific drug candidate for cancer. In this study, the pharmacological potential of nanoceria has been evaluated for different colon and lung cancer cell types with various EGFR-expression levels. Firstly, dextran-coated nanoceria was synthesized and detail characterized by UV-Vis, Dynamic Light Scattering (DLS). Following its cytotoxic behavior, reactive oxygen species scavenger features were examined against different lung and colon cancer cell lines with various EGFR-expression levels. This study is funded by the International Centre for Genetic Engineering and Biotechnology (ICGEB) under CRP/TUR 18-03 project number and TUBA-GEBIP Distinguished Young Scientist Award (Hilal Yazici, 2019).

Keywords: Nanoceria, Cancer treatment, Colon Cancer, Lung Cancer, Nanoparticle-based therapy

PP-02

Single Dose Mixed Species Malaria Vaccinations by Genetically Attenuated Blood Stage Malaria Parasites Induce Sterile Immunity Against Mixed Species Malaria Infection.

Gozde Deveci¹, Binnur Aydogan Temel², Ahmed S.I. Aly³

¹ Department of Microbiology, Beykoz Institute of Life Science and Biotechnology, Bezmialem Vakif University, Beykoz, 34820 Istanbul, Turkey, Department of Biotechnology, Institute of Health Sciences, Bezmialem Vakif University, 34093 Fatih, Istanbul, Turkey

ID: 0000-0001-7944-3469

² Department of Pharmaceutical Chemistry, Faculty of Pharmacy, Bezmialem Vakif University, Fatih, Istanbul 34093, Turkey, Department of Biotechnology, Institute of Health Sciences, Bezmialem Vakif University, Fatih, Istanbul 34093, Turkey

ID:0000-0001-5252-6619

³ Aly Lab., Beykoz Institute of Life Science and Biotechnology, Bezmialem Vakif University, Beykoz, 34820 Istanbul, Turkey

ID: 0000-0002-8607-307X

ABSTRACT

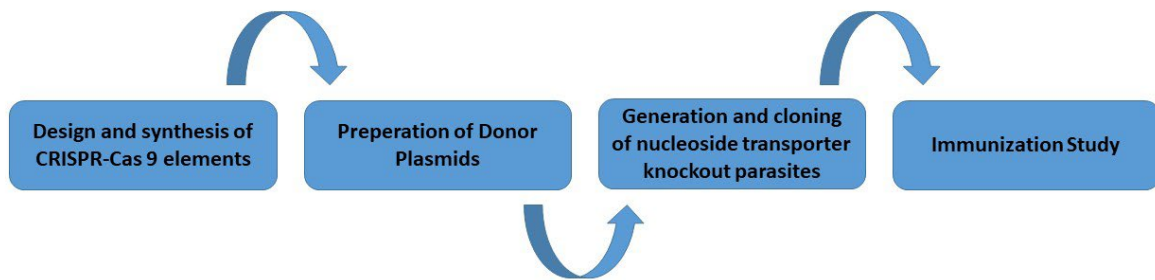
Malaria remains a major global health problem with a very long history of human mortality, mainly among pregnant women and children. One of the greatest challenges for Malaria treatment is the rapid development of drug resistance. Therefore, eradication of malaria can only be achieved with the application of very potent and safe vaccines. Nevertheless, there is no malaria vaccine currently available, and the most advanced candidate has recently reported a modest 0-30% efficacy against clinical malaria.

Interestingly, attenuated live whole parasite vaccines used in clinical trials induced complete sterile protection against malaria infection. The most potent and safe live attenuated malaria vaccines are the genetically attenuated parasites, generated by the deletion of essential genes. An excellent target pathway for genetic attenuation is the purine transport pathway. Malaria parasites cannot synthesize purines de novo and therefore, they need to salvage purines from the host through purine transporters.

Herein, we targeted the purine transporter gene (Nucleoside Transporter 1) gene for deletion in *Plasmodium berghei* and *Plasmodium yoelii* by homologous double crossover recombination facilitated by CRISPR/Cas9 technology. Nucleoside Transporter 1 deficient parasites in both species were enriched by drug selection treatment and FACS sorting. Single dose subcutaneous immunizations were done with *Pynt1(-)* and *Pbnt1(-)* as fresh ex-vivo or frozen-stock parasites of single species or mixed species conferred complete sterile protection challenge with wildtype *P. yoelii* and *P. berghei* parasites. This confirms the promise of using these attenuated parasites in mixed immunization doses to protect against the infections by two species of malaria parasites in humans.

Keywords: CRISPR-Cas9 Technology, Blood Stage Vaccine, Malaria, *Plasmodium berghei*, *Plasmodium yoelii*

MATERIALS & METHODS



RESULTS

Targeted deletion of PyNT1 and PbNT1 was achieved by double crossover homologous recombination with CRISPR-Cas9 Technology (Figure 1a). Knockout *Pynt1*(-) and *Pbnt1*(-) transgenic parasites were enriched by drug selection and FACS sorting until no wild-type genotype was detectable by genomic PCR. Integration of the gene replacement construct confirmed by deletion of nucleoside transporter gene 1 deletion by genomic PCR for *Pynt1*(-) and *Pbnt1*(-) parasites (Figure 1b.) GFP expressed *Pynt1*(-) and mCherry expressed *Pbnt1*(-) parasites were analyzed by confocal microscopy (Figure 1c.)

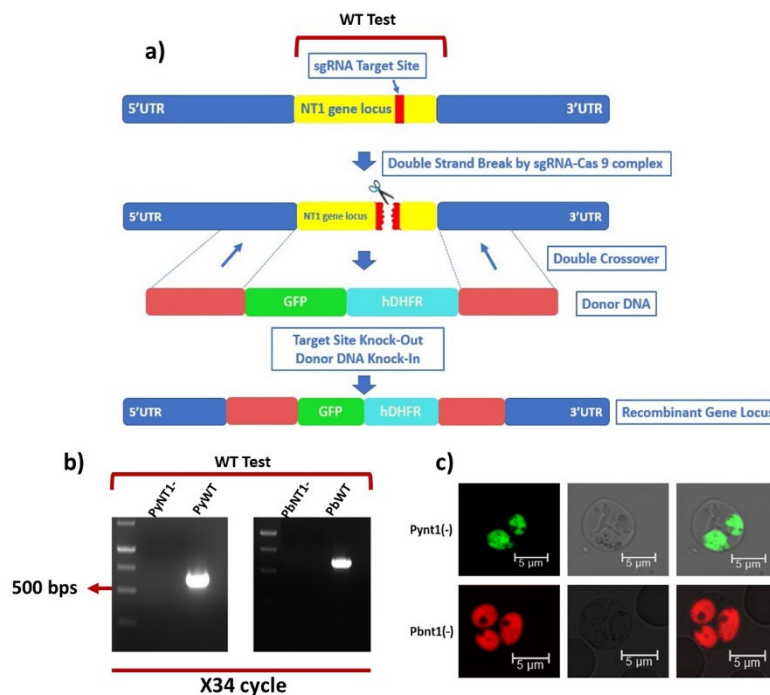


Figure 1. Targeted Deletion of Nucleoside transporter gene for *P. yoelii* and *P. berghei* species by CRISPR-Cas 9 Technology.

Mice immunizations were done subcutaneously and challenges with blood stages were done intravenously. Infections, immunizations and challenges with blood stage (BS) parasites BS of different genotypes were done subcutaneously. The number of asexual BS parasites per microliter of infected donor blood was determined by thin blood smears stained with Giemsa and the number of erythrocytes in the blood to prepare immunization and challenged doses. Challenged mice were analyzed daily for blood stage patency by thin blood till day 15 post challenge. (Table 1).

Blood Stage (BS) Immunization Dose	Immunization Route	Immunized Mice	Intravenous BS Challenge Dose	Challenge Period	Protected / Challenged
1000 Pynt1(-)	Subcutaneous	5 BALB/c	10.000 PyWT 17XNL Blood Stage	1 month	5/ 5
2000 Pynt1(-)	Subcutaneous	5 BALB/c	10.000 PyWT 17XNL 17 BS	1 month	5/ 5
10.000 Pynt1(-) FS	Subcutaneous	5 BALB/c	10.000 PyWT 17XNL 17 BS	1 month	5/ 5
1000 Pbnt1(-)	Subcutaneous	5 CD1	10.000 Pb ANKA WT BS	1 month	5/ 5
2000 Pbnt1(-)	Subcutaneous	5 CD1	10.000 Pb ANKA WT BS	1 month	5/ 5
10.000 Pbnt1(-) FS	Subcutaneous	5 CD1	10.000 Pb ANKA WT BS	1 month	5/ 5
20.000 Pbnt1(-) FS	Subcutaneous	5 CD1	10.000 Pb ANKA WT BS	1 month	5/ 5
10.000 Pbnt1(-)FS 10.000 Pynt1(-)FS	Subcutaneous	3 CD1 1 BALB/c	10.000 PyWT 17XNL BS	1 month	4/4
20.000 Pbnt1(-)FS 20.000 Pynt1(-)FS	Subcutaneous	4 CD1 1 BALB/c	10.000 PyWT 17XNL BS	1 month	5/5
10.000 Pbnt1(-)FS 10.000 Pynt1(-)FS	Subcutaneous	3 CD1 1 BALB/c	10.000 Pb ANKA WT BS	1 month	5/5
20.000 Pbnt1(-)FS 20.000 Pynt1(-)FS	Subcutaneous	4 CD1 1 BALB/c	10.000 Pb ANKA WT BS	1 month	5/5

Table 1. Immunizations with *Pynt1(-)* and *Pbnt1(-)* live attenuated blood stages confer sterile immunity against infection challenge by two different malaria parasite species.

CONCLUSION

According to results, subcutaneous immunization with *Pynt1(-)* and *Pbnt1(-)* conferred sterile protection against *P. yoelii* 17XNL and *P. berghei* ANKA. Herein, genetic live attenuated malaria parasites produced by CRISPR-Cas9 technology provides a platform for the malaria parasite blood stages vaccination platform especially for mixed species malaria parasite infections.

REFERANCES

1. Organization, W.H.O. Malaria. 2018; Available from: <https://www.who.int/malaria/en/>.
2. Hill, A.V., Vaccines against malaria. *Philos Trans R Soc Lond B Biol Sci*, 2011. 366(1579): p. 2806-14.
3. Keitany, G.J., M. Vignali, and R. Wang, Live attenuated pre-erythrocytic malaria vaccines. *Hum Vaccin Immunother*, 2014. 10(10): p. 2903-9.
4. Elbissati., et al., The plasma membrane permease PfNT1 is essential for purine salvage in the human malaria parasite *Plasmodium falciparum*. *PNAS*, 2006, 24(103):p.9286-9291
5. Aly, A.S., et al., Subpatent infection with nucleoside transporter 1-deficient *Plasmodium* blood stage parasites confers sterile protection against lethal malaria in mice. *Cell Microbiol*, 2010. 12(7): p. 930-8.
6. Riegelhaupt, P.M., et al., Transport of purines and purine salvage pathway inhibitors by the *Plasmodium falciparum* equilibrative nucleoside transporter PfENT1. *Mol Biochem Parasitol*, 2010. 169(1): p. 40-9.
7. Shinzawa, N., et al., Improvement of CRISPR/Cas9 system by transfecting Cas9-expressing *Plasmodium berghei* with linear donor template. *Commun Biol*, 2020. 3(1): p. 426.

PP-04

Process optimization for the development of a phage displayed human scFv library against SARS-CoV-2 virus

Aleyna AKDENİZ^{1,2}, Kübra BİLGİÇ^{2,3}, Oya ARI UYAR², Mustafa ÇÖRTÜK⁴, Şaban TEKİN^{2,5}, Aysin BAHADIR ÖZDEMİR², Bertan Koray BALCIOĞLU²

¹Canakkale 18 Mart University, Department of Molecular Biology and Genetics, Canakkale, Turkey

²TUBITAK Marmara Research Center (MAM), Genetic Engineering and Biotechnology Institute, Gebze, Kocaeli, Turkey

³Gebze Technical University, Department of Molecular Biology and Genetics, Gebze, Kocaeli, Turkey

⁴Yedikule Chest Diseases and Thoracic Surgery Training and Research Hospital, Department Chest Diseases, Istanbul, Turkey

⁵University of Health Sciences, Department of Basic Medical Sciences, Medical Biology, Istanbul, Turkey

SARS-CoV-2 causing severe acute respiratory syndrome appeared first, end of year 2019, in the city of Wuhan, Hubei province of China. Due to its spread to many countries in a short time, WHO declared, in January 2020, Covid-19 as pandemic threatening the global public health. The main targets of the studies carried out against the SARS-CoV-2 virus are reducing the death rate and the severe symptoms that may occur. Studies show that vaccines are essential to reduce the spread of the virus and the symptoms seen in infected patients. Despite these favorable results, mortality and hospitalization among infected patients are still continuing. Therefore, more effort are still necessary for the development of new vaccines and drugs to meet the needs. In this study, we aimed to construct a phage displayed anti-SARS-CoV-2 human single chain variable fragment (scFv) library. For this purpose, total RNA was isolated from white blood cells of convalescent Covid-19 patients. The extracted RNA was used as template for cDNA synthesis. To optimize the generation of light and heavy chain variable region library primers specific to the V_{H1} , V_{Lk1} alleles were selected for amplification. Once the V_{H1} , V_{Lk1} library was obtained, the Human scFv genes were generated. The scFv library was then cloned into a phagemid vector and transformed to *E.coli* TG1 strain. The presence of the scFvs in the transformation colonies was checked by the colony PCR method. PCR amplifications were then digested with BstNI enzyme for DNA fingerprinting analysis. The generated library showed diversity so a biopanning step against the S1 domain of the virus spike protein was initiated. After three rounds of biopanning the presence of scFvs and their diversity was checked again. Once the scFvs are characterized the binding of the selected scFv clones will be tested by phage ELISA.

This study will contribute to the development of a larger phage displayed scFv library by using a higher number of antibody heavy and light chain variable region allelic region. With the generation of these libraries we are intending to increase the chance of selecting a good SARS-CoV-2 neutralizing scFv for the treatment of COVID-19.

Key words: Anti-SARS-CoV-2, COVID-19, phage display, human scFv, human monoclonal antibody, bio-panning

"Bu alıřmalar "**COVID-19'a Karşı Nötralizan Antikor Geliřtirilmesi**" isimli TÜBİTAK 5203401 no'lu TARAL 1004 projesi tarafından desteklenmiřtir"

PP-05

The cellular uptake and endosomal escape mechanisms of chitosan-protamine-siRNA nanoplexes for efficient gene transfection and silencing

Emine Şalva¹, Ceyda Ekentok Atıcı², Birnur Cömez², Suna Özbaş², Jülide Akbuğa³

¹Inonu University, Faculty of Pharmacy, Department of Pharmaceutical Biotechnology, Malatya

²Marmara University, Faculty of Pharmacy, Department of Pharmaceutical Biotechnology, İstanbul

³Medipol University, Faculty of Pharmacy, Department of Pharmaceutical Technology, İstanbul

Aim: The use of antisense-based molecules in gene expression inhibition has allowed the design of a new pathway for therapeutics. In order to ensure that oligonucleotides with gene silencing potential can be used effectively in therapy, a suitable carrier system is required that can be transported to the target site. In this study, gene silencing activities of siRNA targeted to the LacZ gene were compared and the gene delivery capabilities, transfection efficiency, cellular uptake and endosomal escape mechanisms of nanoplexes prepared with siRNA and chitosan/protamine polymers were investigated.

Material and methods: Nanoplex formulations were prepared by simple complexation method of chitosan/protamine polymers and oligonucleotides. The particle size and zeta potential of the prepared nanoplexes were measured, and their serum and enzyme stability were investigated. In order to determine the transfection and gene silencing activities of the selected formulations, HEK293 cells stably expressing beta-gal were prepared, inhibition of beta-gal protein was measured by enzymatic assay and suppression by X-gal method was evaluated microscopically. Cellular uptake and endosomal escape mechanisms of nanoplexes were studied.

Results: Chitosan/Protamine/siLacZ nanoplexes have been observed to protect siRNA against enzymatic and serum degradation for up to 48 hours. It was observed that the transfection efficiency was the highest in the formulations prepared together with chitosan/protamine at a rate of 10/10/1. It was observed that the transfection increased significantly with the increase in the ratio of chitosan and protamine. Transfection efficiency was found to be 88.60% at a rate of 10/10/1. In the cellular uptake study, it was observed that the inhibitor that reduced cellular uptake the most was phenylarsine oxide, and the uptake of siRNA carried by nanoplexes was 56%. There was no decrease in cellular uptake when chlorpromazine hydrochloride inhibitor was administered. This indicated that the nanoplexes were not uptake by clathrin-mediated endocytosis. It was observed that cellular uptake was 75% with colchicine, this inhibitor decreases cellular uptake by inhibiting microtubules in cells.

Conclusion: It has been shown that cellular uptake and transfection studies with chitosan/protamine nanoplexes can be used as an effective carrier system for siRNA transport.

Keywords: siRNA, LacZ, cellular uptake, chitosan, protamine, nanoplexes

Acknowledgement: This study was supported by the Inonu University Scientific Research Project Centre with grant no:TDP-2019-1639.

**Expression, Purification and Characterization of Recombinant Human IL-2
(Aldesleukin)**

Buse Akgun¹, Gizem Dinler Doganay^{1,2}

¹Molecular Biology, Genetics-Biotechnology, Graduate School of Science, Engineering and Technology, Istanbul Technical University, 34469 Istanbul, Turkey

²Department of Molecular Biology and Genetics, Istanbul Technical University, 34469 Istanbul, Turkey

*Correspondence: gddoganay@itu.edu.tr

Abstract

Interleukin (IL) is an immunomodulatory protein class of cytokines that cause a wide range of cell and tissue response. Interleukins participate in the communication between leukocytes (white blood cells) and activate pathways by binding to high affinity receptors on the surface of cells. The first cytokine characterized to promote the development of T-cells is interleukin-2. IL-2 is essential in the regulation of immune cell proliferation and differentiation, including T cells, B cells, natural killer (NK) cells, lymphokine-activated killer cells, and macrophages. Aldesleukin is made in a genetically modified *E. coli* that contains an adapted form of the native human IL-2 gene. Aldesleukin differs from the natural IL-2 in that it is not glycosylated, lacks an N-terminal alanine residue, and the cysteine at amino acid position 125 is replaced by serine. Recombinant human IL-2 is pharmacologically indistinguishable from endogenous human IL-2. In addition, recombinant IL-2 is an FDA-approved therapy for metastatic renal cell carcinoma and melanoma. The aim of the study is to develop a functional recombinant form of the protein suitable for biopharmaceutical use.

To achieve high level of protein expression in *E. coli*, several parameters such as temperature, inducer concentration, and induction time were determined. *E. coli* cells were disrupted by sonication and the lysate was centrifuged. Then, pellet which contains inclusion bodies were solubilized at an alkaline pH in the presence of a 2 M urea solution. Dialysis was used to refold the solubilized proteins, which were further purified by chromatographic methods. To provide a better distinction, refolded proteins were collected and filtered by 0.45 µm sterile filter. Firstly, purification of recombinant IL-2 from total protein was performed by anion exchange chromatography (AEX). ÄKTA™ avant was used for chromatographic experiments. Additionally, protein's secondary structure was controlled by circular dichroism. Purification conditions were shown to be appropriate for protein structure using circular dichroism analysis.

Moreover, several characterization techniques are used to examine the active recombinant IL-2, including, peptide mapping, intact mass, and capillary electrophoresis.

To sum up, the drug substance of recombinant IL-2 was obtained in our lab and will be further developed for industrial applications.

Key words: IL-2, Aldesleukin, ion exchange chromatography

Expression of Soluble Tumor Necrosis Factor Receptor 1 (TNFR1) in *E. coli*

Derya Hatipoğlu¹, Gizem Dinler Doganay^{1,2}

¹Molecular Biology, Genetics-Biotechnology, Graduate School of Science, Engineering and Technology, Istanbul Technical University, 34469 Istanbul, Turkey

²Department of Molecular Biology and Genetics, Istanbul Technical University, 34469 Istanbul, Turkey

*Correspondence: gddoganay@itu.edu.tr

Abstract

Tumor Necrosis Factor Receptor Superfamily (TNFRs) is a group of transmembrane glycoproteins that plays critical roles in the activation of signaling pathways including host defence, inflammation, apoptosis, autoimmunity and organogenesis. Tumor necrosis factor (TNF) is a member of cytokines having soluble and membrane bound forms. When TNF molecules bind to its receptor, TNFR1, activation of the signaling mechanism occurs, stating the importance of relationship between TNF and TNFR for the homeostasis of cells.

TNF amount increase is observed in some diseases such as cancer, osteoporosis, autoimmune. For that reason, TNF receptors and antibody-based drugs have been developed to neutralize TNF. In particular, soluble TNFRs are critical modulators of the bioactivity of TNF.

Because TNFRs have a common cysteine-rich domain in their extracellular domain, expression of a soluble form of this protein is difficult in *E. coli*. To express the soluble form of our recombinant proteins in *E. coli*, we tried different parameters like variation of growth conditions, usage of different strains and fusion tags.

Fusion tags could be used to increase solubility and native folding of recombinant proteins and also facilitate purification. Recently, a lot of fusion tags have been developed for different purposes. Distinct tags such as MBP, GST, Trx, DsbA and DsbC could be used to express proteins of interest as soluble. DsbC tag is particularly useful to express proteins in bacteria and DsbC co-expression with recombinant protein catalyzes disulfide bonds and increases solubilization.

The aim of our study is to develop the functional recombinant form of TNFR. For this purpose, recombinant TNFR protein was produced with the DsbC tag.

To achieve the expression of the soluble form of TNFR1 in *E. coli*, several parameters, such as different strains, growth medium, temperature, inducer concentration, and induction time were tested. In addition, divergent detergent treatment was performed to increase the amount of soluble membrane protein during cell disruption. *E. coli* cells were disrupted by sonication and the lysate was centrifuged. Supernatant fraction and cell pellet were controlled whether or not to include the desired protein after running SDS-PAGE and immunoblotting, revealing the changes between different treatment.

Key words: TNFR1, Disulfide bond, Soluble protein, DsbC, Fusion tags

A novel approach of polyclonal antibody purification based on affinity chromatography

Ozge Aksoy¹, Furkan Sahin², Seyma Aydinlik Sanli³, Arzu Ekiz³, Fatih Karakaya³,
Hasan Umit Ozturk³, Saban Tekin³

¹Department of Molecular Biology and Genetics, Institute of Natural and Applied Sciences, Gebze Technical University, Kocaeli, Turkey

²Department of Molecular Biology and Genetics, Faculty of Science, Tokat Gaziosmanpaşa University, Tokat, Turkey

³The Scientific and Technological Research Council of Turkey (TUBITAK) Marmara Research Center (MAM), Genetic Engineering and Biotechnology Institute, 41470 Gebze Kocaeli, Turkey

Passive immunity is gained by the administration of immunoglobulins from a particular source. Immunoglobulin G (IgG) developed against a certain disease is known to have a significant effect on the treatment of patients. From the past to the present, people who were exposed to animal bites, poisons, or disease factors, have been treated by polyclonal antibodies until now.

Purification procedures have been applied to ensure that antibodies are successful in poison and disease treatments. The main reason for performing the purification step is to prevent adverse effects including anaphylactic shock in individuals against impurities. Hence, antibodies were first purified by the precipitation process such as caprylic acid or ammonium sulfate precipitation and then purified using a newly improved protocol with the prepacked protein-A column -Hi Trap mAb Select Sure- using the AKTA-Avant 25 purification system. In this method, albumin residues and other small impurities were eliminated and improvements were made by optimizing the sample quantity, flow rate, salt concentration, and pH values in the prepared buffers to achieve the highest purity. All optimization values were compared with SDS-PAGE, western blot, and ELISA results.

Consequently, the yield of the antibody was determined as 81% after caprylic acid or ammonium sulfate precipitation. After precipitation process, antibodies were purified using affinity chromatography (Hi Trap mAb Select Sure) and a high recovery yield (97 %) was achieved. It is concluded that this study provides new methods and different perspectives on the antibody purification process.

Keywords: Immunoglobulin G (IgG), Protein-A Chromatography, Polyclonal Antibodies

Studies on development of lipid nanoparticle formulation containing vitexin and pDNA

Hazal Eken¹, Behiye Şenel², Nurcan Bektaş¹, Rana Arslan¹

Anadolu University Faculty of Pharmacy, Department of Pharmacology¹

Anadolu University Faculty of Pharmacy, Department of Pharmaceutical Biotechnology²

Vitexin, a flavone glycoside, which found in various medicinal plants has various pharmacological effect such as antinociceptive, anti-oxidant, antispasmodic, anti-inflammatory, antiviral, antibacterial. Nowadays, flavonoids such as quercetin, apigenin, and vitexin are frequently studied because of their pharmacological effects and potential to be developed as medicine. However, there are difficulties in their use due to their low solubility, instability in aqueous media, poor absorption, photodegradation and rapid metabolization. In recent years, research in the field of nanotechnology has increased, especially in the pharmaceutical industry. Solid lipid nanoparticles (SLN) and nanostructured lipid carriers (NLC) are used as important materials for oral administration of natural phenolic compounds, improving their bioavailability and stability. In this study, the SLN formulation containing vitexin and pDNA was developed. Characterization studies, *in vitro* release analyzes and cytotoxicity analyzes of the developed formulation were performed. According to NMR and FTIR analyzes, it is thought that the chemical structures of the substances used during formulation preparation and vitexin are preserved and there is no chemical interaction between them and also vitexin can be successfully loaded into SLNs. In the *in vitro* release analysis, %98 release was observed in the first 4 hours for pure vitexin, while time-dependent release was observed in the formulation. As a result of cytotoxicity tests on the normal cell line NIH-3T3 and cancer cell line A549, it was determined that the formulation showed concentration-dependent cytotoxicity. In addition, the GFP plasmid was loaded as genetic material to determine whether the formulation can carry DNA. According to agarose gel electrophoresis method, it is thought that the formulation is able to successfully retain genetic material and also protect the DNA in the presence of serum and DNase. This study provides data that will contribute to the literature and new drug development. However, the effects of SLNs on vitexin activity need to be tested by *in vivo* experiments.

Keywords: Vitexin, Solid lipid nanoparticles, GFP plasmid.

Production and Characterization of SARS-CoV-2 Spike and S1 from Mammalian Cells

Miray Turk¹, Baran Dingiloglu¹, Gizem Dinler Doganay^{1,2}

¹Molecular Biology, Genetics-Biotechnology, Graduate School of Science, Engineering and Technology, Istanbul Technical University, 34469 Istanbul, Turkey

²Department of Molecular Biology and Genetics, Istanbul Technical University, 34469 Istanbul, Turkey

Correspondence: gddoganay@itu.edu.tr

Approximately 200 million people in the world and five and a half million people in Turkey have been infected as of today, and approximately five million people have died in the world due to the new type of coronavirus (SARS-CoV-2), which is the causative agent of COVID-19. Studies demonstrated that SARS-CoV-2 virus attaches to ACE2 receptors on the host cell surface by using the viral cell surface glycoprotein Spike to infect the host cell. S1 subunit of Spike protein possesses critical function in this interaction. In this project, we aimed recombinant production of SARS-CoV-2 Spike ecto-domain and its S1 subunit, which can be used for determination of Spike/ACE2 interaction dynamics in short term. In long term, these results obtained from this project and further studies will exhibit a guiding effect on the vaccine and drug development processes and thus will make a great contribution to the production of effective vaccines and drugs.

There are different types of post-translational modifications identified on Spike protein, which are also critical for its interaction with ACE2. For this reason, we produced Spike ecto-domain and S1 subunit in transiently transfected HEK293 suspension cells to best mimic their 3D structure. Spike and S1 subunit were purified through affinity chromatography via FPLC system and their purity was determined via SDS-PAGE (>90%). The primary structures of the purified proteins were determined by peptide mapping analysis in mass spectrometry and secondary structure analysis was performed via circular dichroism (CD) spectroscopy. Additionally, activity of Spike and S1 was analyzed by their interaction property to ACE2 receptor *in vitro*. In conclusion, SARS-CoV-2 Spike protein and its S1 subunit were produced in mammalian cells, purified and characterized in our laboratory successfully. This project allowed us to study Spike/ACE2 interaction in detail to struggle against COVID-19. Also, these experiments constituted the first step of recombinant drug and/or vaccine development.

This study was supported by TUBITAK 120Z305 and TUSEB 7162/8972 projects.

Key words: Spike, S1, COVID-19, SARS-CoV-2

PP-16

Development of Anti-human Secondary Antibodies for Serological Tests

Gökçe Kaymaz, Göknur Gizem Dinç, İlkay Göksu Polat, Gamze Kılıç, Fatıma Yücel, Esin Akçael

Genetic Engineering and Biotechnology Institute, TUBITAK MAM, Gebze, Kocaeli, Turkey

Secondary antibodies are used for the indirect detection of the primary antibody which directly binds to the specific antigen in serological tests. They are polyclonal or monoclonal antibodies that bind to primary antibodies or antibody fragments, such as the Fc or Fab regions. Not only easy and fast to produce, also polyclonal antibodies (pAbs) are favored as secondary antibodies as they bind multiple epitopes of primary antibody. They are also conjugated to labels with enzyme, biotin or gold etc. Anti-human secondary antibodies for serological testing should be developed to minimize non-specific binding that can lead to high background signals and false positives.

In our study, New Zealand White rabbit was immunized with the Fc fragment (Sigma, AG714) of heavy chains on human immunoglobulin G (IgG), and their immune response was controlled by enzyme-linked immunosorbent assay (ELISA). After immunizations, anti-human Fc immunoglobulins were purified from the serum by affinity chromatography when the immune response reached a high level. After the purification and characterization, anti-human Fc pAb was labeled with Horseradish Peroxidase (HRP) for use in serological tests. Optimal concentration of HRP labeled antibody was determined to use as the secondary antibody in ELISA diagnostic tests for the detection of human IgG.

Anti-Fc secondary antibodies only react with heavy chains of the primary antibody and also class-specific. This makes our antibody more specific to bind primary antibodies and helps to prevent false-positive results in antibody detection tests. Therefore, in our study only the Fc region was selected, not the whole IgG molecule.

During the ongoing global COVID-19 pandemic, it is important to detect the specific IgGs against Severe Acute Respiratory Syndrome Coronavirus 2 (SARS CoV-2) developed in the serum of people who had the disease and have been vaccinated. In this study, it has been shown that our secondary antibody can be successfully used for the sensitive detection of IgG developed against SARS-CoV-2 proteins in human serum samples in serological tests.

Process development of Pfu DNA Polymerase production by using GroEL/GroES co-expression method

Kubra Turk¹, Gizem Dinler Doganay^{1,2}

¹Molecular Biology, Genetics-Biotechnology, Graduate School of Science, Engineering and Technology, Istanbul Technical University, 34469 Istanbul, Turkey

²Department of Molecular Biology and Genetics, Istanbul Technical University, 34469 Istanbul, Turkey

Correspondence: gddoganay@itu.edu.tr

PCR technique is accepted as one of the most popular molecular biology experiments since its invention due to its wide application usage. High fidelity property of DNA polymerase II made it suitable for variable PCR applications and it is widely used by researchers around the world. For this reason, it is established as commercially important. Pfu DNA polymerase is DNA polymerase II which was initially isolated from an anaerobic archimycetes called *Pyrococcus furiosus*. But, obtaining large quantities of the enzyme was a challenge due to its difficult culturing conditions. This problem directed researchers to produce Pfu polymerase in bacterial cultures. Recombinant protein production in *E. coli* is carried out by induction with IPTG conventionally. However, researches have shown that to enhance soluble protein production, using IPTG may have a negative effect, may not have an effect or its effect may not be sufficient depending on process conditions or protein being produced.

In this study, our aim is to develop a process for production of Pfu polymerase with high efficiency in *E. coli*. For this purpose, we applied different production methodologies including conventional production in LB medium, co-expression with GroEL/GroES chaperonin and auto-induction. Purification of all proteins were performed via affinity purification. Although co-expression approach resulted in higher soluble protein yield, purification of co-expressed Pfu was more challenging than purification of Pfu produced in other conditions.

In conclusion, although its purification step requires improvement, production process of Pfu polymerase was developed in our laboratory successfully. In the near future, our own-produced Pfu polymerase will be ready to use in our laboratory. Also, experience we obtained from this project will give us more detailed know-how of enzyme production.

Key words: DNA polymerase, Pfu, enzyme production

Microbiota: A Potential Therapy for Autism

Berna Özdem

bernaozdem@gmail.com

Department of Medical Biology and Genetics

İnönü University Malatya

Autism is a developmental disorder that affects a large number of individuals. Its incidence is increasing in our country and around the world. Autism is a spectrum disorder, meaning there is a wide degree of variation in the way it affects people. Every child on the autism spectrum has unique abilities, symptoms, and challenges. Autism may occur due to genetic and environmental factors. However, the actual mechanism that plays a role in the etiology of autism is not clearly known. Human intestinal microbiota is a complex ecosystem with various functions integrated in the host organism (metabolic, immunity, nutrient absorption, etc.). Human microbiota is formed by viruses, bacteria, yeasts, fungi, and last but not least, viruses, whose composition has not been completely described.

Human microbial populations include populations of microbial species that live on or in human body - commensal bacteria, viruses, and fungi (and other single-celled animals such as protists) that call our bodies home.

Gastrointestinal symptoms appear in ASD individuals. They have more GI syndromes, including constipation (20%) and diarrhea (19%), than in their unaffected siblings (42 vs. 23%, respectively). ASD patients with symptoms of GI may exhibit significant behavioral symptoms such as anxiety, self-harm, and aggression. Many evidence suggests that the intestinal microbiota is directly or indirectly associated with ASD symptoms, in part by influencing the immune system and metabolism. A higher percentage of abnormal intestinal permeability has been observed in 36.7% of patients with ASD and their relatives (21.2%) compared with control children (4.8%). An increased intestinal permeability has been resulted in a higher antigenic load from the gastrointestinal tract.

Current data show that intestinal microbiota is associated with autism. To date, scientists have tried methods such as rehabilitation and drug therapy for the treatment of this disease. However, it is now thought that autism symptoms can be reduced by a simple method such as changing the diet. There is a lot of research for the treatment of autism with Bacterial Transmission.

It has also been observed that intestinal microbiota of autistic children has markedly decreased species of Prevotella, Coprococcus, and Veillonellaceae. These changes were found to be closely related to the specific diets, additional diets, and severity of gastrointestinal symptoms. These findings support the idea that "certain bacterium of intestinal microbiology affects autism" rather than the idea that dietary differences or eating behaviors affect the microbiota in autistic individuals. Another species that differs in autistic individuals and healthy individuals is gram-negative and anaerobic bacteria *Desulfovibrio* spp.

3 strains of *Lactobacillus* (60%), 2 strains of *Bifidumbacteria* (25%) and 1 strain of *Streptococcus* (15%) were injected for 3 months in a study consisting of 10 autistic children, 9 non-autistic siblings and 10 healthy non-autistic individuals.

When fecal specimens were examined before probiotic reinforcement, Bacteroidetes / Firmicutes rate were found to be significantly lower compared to the control group in autistic children. Clostridia and *Desulfovibrio* concentrations in autistic children have been observed significantly higher than control groups.

When fecal samples were examined after probiotic treatment, that have been observed Bacteroidetes / Firmicutes rates increase and the concentration of *Desulfovibrio* that were decreased. In autistic children, a reduction in TNF- α levels, an indicator of inflammation after probiotic therapy, has also been observed. *Sutterella* spp. is another type of bacteria found to play a role in autism. In a study of fecal specimens of 9 control groups with 20 autistic children, 22 siblings and no autism in their family, *Sutterella* spp. and *Ruminococcus torques* were found to be high. There is no definite evidence between *Sutterella* and autism. It is stated that *Sutterella* spp. May be an indicator of infection with gastrointestinal symptoms of autistic children. Although the role of the *Sutterella* strain in autism is not as clear as Clostridia, His presence in the class of Betaproteobacteria and showing similar associations with *Neisseria gonorrhoeae* and *Neisseria meningitidis*, *Bordetella pertussis* and *Burkholderia cepacia* make it more likely to play a role in autism.

Current studies show a strong relationship between changes in the intestinal microbiota and autism symptoms. Intestinal microbiota composition can control autistic behaviors by various mechanisms. In addition, probiotic supplements have been found to reduce autism symptoms.

This study provides data that will contribute to the literature. Based on these results, new treatments can be developed.

Key Words: Autism; Microbiota; Bacteria; Gaita transplantation

PP-19

Profiling the mutational spectrum of hereditary breast cancers in Turkey using multi-gene panel testing

Nisan Denizce Can^{1,5}, Jale Yıldız^{1,5}, Izzet Akcay^{1,5}, Tugba Kizilboga^{1,5}, Gizem Alkurt^{1,5}, Elifnaz Celik^{1,5}, Fikret Ezberci², Ebru Zemheri³, Levent Doganay^{4,5}, Gizem Dinler Doganay^{1,5}

¹ Istanbul Technical University, Department of Molecular Biology and Genetics, Maslak, Istanbul, Turkey

² University of Health Sciences, Umraniye Teaching and Research Hospital, Department of General Surgery, Umraniye, Istanbul, Turkey

³ University of Health Sciences, Umraniye Teaching and Research Hospital, Department of Pathology, Umraniye, Istanbul, Turkey

⁴ University of Health Sciences, Umraniye Teaching and Research Hospital, Department of Gastroenterology and Hepatology, Umraniye, Istanbul, Turkey

⁵ GLAB (Genomic Laboratory), Istanbul Association of Northern Anatolian Public Hospitals, Umraniye, Istanbul, Turkey

Breast cancer is the most common cancer and the second leading cause of death in women worldwide. Approximately 10% of all breast cancers are hereditary, clustering in families and occurring at an earlier age than sporadic cancers. Pathogenic germline variants in *BRCA1* and *BRCA2* account for the majority of hereditary breast cancers. Other cancer susceptibility genes such as *CHEK2*, *TP53*, *PTEN*, *PALB2*, and *CDH1* are also responsible for a considerable fraction of hereditary breast cancers, too. By using next generation sequencing technology, variant screening for multiple genes in a single run is possible and routinely applied in a cost-effective manner. To determine the mutation profile of hereditary breast cancer in the Turkish population, we screened pathogenic mutations in a panel of 27 cancer susceptibility genes in 939 breast cancer patients. We investigated the relationships between the pathogenic variants and the clinical/epidemiologic data. We also examined the penetrance of cancer susceptibility genes in our dataset and compare to the dataset of sequenced 490 healthy individuals with no personal or familial cancer history. We detected pathogenic variants in 14.9% of all breast cancer patients and 2.4% for healthy controls. 52.1% of all pathogenic germline variants were found in *BRCA1* and *BRCA2* genes. *CHEK2* pathogenic variants were also prevalent (11.4%). VUS were detected in 33.8% of all subjects and *CHEK2* had the highest VUS (variant of unknown significance) density. These findings will help us to better understand the genetic basis of hereditary breast cancer and we will achieve to characterize the mutational landscape of hereditary breast cancer in Turkish population.

Keywords: hereditary breast cancer; next generation sequencing; multi-gene panel testing

* This project is funded by Istanbul Development Agency projects TR10/15/YNK/0085 and TR10/16/YNY0144, and by The Scientific and Technological Research Council of Turkey project 318S127.

PP-25

Development of an immunoassay for detection of soluble programmed death-ligand 1 in serum of patients with non-small cell lung cancer

Dilek Çeker¹, Sinem Nalbantoglu¹, Nilufer Kara², Nilgun Algan², Hatice Aslanoglu², Abdurrahim Gordebil², Serdar Evman², Volkan Baysungur^{2,3}, Abidin Sehitogullari⁴, Mahmut Gumus⁵, Ihsan Boyaci⁶, and Abdullah Karadag¹

¹TUBITAK Marmara Research Center, Genetic Engineering and Biotechnology Institute, Kocaeli, Turkey

²Ministry of Health, İstanbul Sureyyapasa Chest Diseases and Thoracic Surgery Research and Training Hospital, İstanbul, Turkey

³University of Health Sciences, Department of Thoracic Surgery, İstanbul, Turkey

⁴Sakarya University Medical School, Department of Thoracic Surgery, Sakarya, Turkey

⁵İstanbul Medeniyet University Medical School, Department of Internal Medicine, İstanbul, Turkey

⁶İstanbul Medipol University Medical School, Department of Internal Medicine, İstanbul, Turkey

Lung cancer leads incidence and death rates among all cancers worldwide when both men and women accounts. Disease is characterized with a poor prognosis since 75% of patients are metastatic at the diagnosis when primary treatment option surgery, is no longer available. Alternative treatments include chemoradiotherapy, targeted therapy, and immunotherapy. Although development of the resistance is the major determinant factor in lung cancer prognosis, immunotherapy among alternative therapies is particularly efficient if a candidate patient is treated with. Therefore, identification of candidate patients for immunotherapy is a hot field in the research and management of lung cancer. Tumor cells escape from immune system by manipulating immune checkpoints such as, cytotoxic T-lymphocyte-associated antigen 4 (CTLA-4,) and programmed cell death protein 1 (PD-1) / programmed death-ligand 1 (PD-L1) axes. Overexpression of PD-L1 protein by tumor cells and/or tumor microenvironment cells may result in immunotolerance through interaction with PD-1 protein on the membrane of the T cells via inactivation of CD4⁺ and CD8⁺ T cells. A number of monoclonal antibody (mAb)-based immunotherapeutics targeting PD-1 / PD-L1 axis have been developed. Candidate patients with lung cancer are identified through immunohistochemistry of biopsy samples. If at least 50% of the sample is PD-L1 positive, patient is a candidate for the immunotherapy, which costs about 1 million USD per patient. However, method has limitations: i) biopsy is an invasive procedure and cannot be repeated, ii) histological section may not represent tumor microenvironment properly, and iii) detection margin in immunohistochemistry is limited. Therefore, we propose development of an antibody-based immunoassay as a minimally invasive or non-invasive system both to identify candidate patients and to monitor prognosis and the effect of the treatment. We have developed three monoclonal antibodies against PD-L1 protein through hybridoma technology. We envisage developing an immunoassay system using these antibodies and validate through serum/plasma samples and other body fluids taken from patients with lung cancer and normal control individuals. Preliminary results indicate that levels of the soluble PD-L1 in samples from the serum of the patients with lung cancer may differ from the control individuals.

Research Topic: Lung cancer, programmed cell death protein 1, programmed death-ligand 1, monoclonal antibody, immunoassay.

Preparation, Characterization, and Cell Culture Studies of Herbal Emulgel Formulations for Topical Administrations

Emre Şefik Çağlar¹, Ayşe Esra Karadağ^{2,3}, Sevde Nur Biltekin^{4,5}, Neslihan Üstündağ Okur¹

¹University of Health Sciences, Faculty of Pharmacy, Department of Pharmaceutical Technology, Istanbul, Turkey

²Istanbul Medipol University, School of Pharmacy, Department of Pharmacognosy, 34810- Beykoz, Istanbul, Turkey

³Anadolu University, Graduate School of Health Sciences, 26470-Eskişehir, Turkey

⁴Istanbul Medipol University, Department of Pharmaceutical Microbiology, School of Pharmacy, 34810- Beykoz, Istanbul, Turkey

⁵Istanbul University, Institute of Sciences, 34116-Istanbul, Turkey

Myrtle (*Myrtus communis* L.) is a medicinal and aromatic plant that its leaves and fruits can be used in various conditions such as cough, mouth sores, constipation, improving appetite, wound healing, and due to hypoglycemic and antimicrobial effects¹. Phenolic compounds such as quercetin 3-O-galactoside, quercetin 3-O-rhamnoside, myricetin 3-O-rhamnoside, quercetin 3-O-glucoside, ellagic acid and myricetin and anthocyanins, which are found in high amounts in myrtle fruits, are extremely important for human health². Emulgels are the combination of emulsion and gel formulations with different ratios. Emulgels have several advantages for topical administration such as being thixotropic, greaseless, easily spreadable, easily removable, emollient, water-soluble, longer shelf life³. In this study, *Myrtus communis* L. fruit extract was identified by using an HPLC method and antioxidant activity studies of the extract was performed. Later, *Myrtus communis* L. fruit extract loaded emulgel formulations were prepared, characterized, and evaluated for antibacterial activity and cell culture studies. In addition, textural and rheological analysis, and spreadability studies of the formulations were performed. Results of the characterization studies showed that pH value of the formulations was in between 5.37 ± 0.02 and 6.60 ± 0.01 , viscosity of the formulations was in between 1264.00 ± 21.91 and 10044.00 ± 29.66 cP. Addition of plant extract decreased the viscosity. The results of textural analysis and spreadability studies showed that decreased viscosity changed the mechanical properties and spreadability of the formulations. Rheological behaviors of all formulations were Non-Newtonian as expected. Cell culture studies indicated that the cell viability of formulations was more than 80%. In conclusion, the prepared formulations are promising preparations for cosmetic usages.

References

1. Aydin, C. & Özcan, M. M. Determination of nutritional and physical properties of myrtle (*Myrtus communis* L.) fruits growing wild in Turkey. *J. Food Eng.* **79**, 453–458 (2007).
2. Sarais, G. *et al.* Targeted and untargeted mass spectrometric approaches in discrimination between *Myrtus communis* cultivars from Sardinia region. *J. Mass Spectrom.* **51**, 704–715 (2016).
3. Mohammed Haneefa, K. P., Abid, Shahima Hanan, K., Mohanta, G. P. & Nayar, C. Formulation and evaluation of herbal emulgel of *Pothos scandens* linn for burn wound healing activity. *J. Pharm. Sci. Res.* **6**, 63–67 (2014).

PP-30

Osteogenic Differentiation of Human Amniotic Membrane Stem Cells on Bone ECM Biological Scaffolds

Melisa BAŞTUĞ,¹ Murat Taner VURAT,¹ Rahmi Sinan KARADENİZ,² Yaprak ENGİN-ÜSTÜN,²
Ayşe Eser ELÇİN,¹ Yaşar Murat ELÇİN^{1,3}

- 1 Tissue Engineering, Biomaterials and Nanobiotechnology Laboratory, Ankara University Biotechnology Institute, Ankara University Faculty of Science, Ankara University Stem Cell Institute, Ankara, Turkey
- 2 Ankara Etlik Zübeyde Hanım Women's Health and Research Center, University of Health Sciences, Ankara, Turkey
- 3 Biovalda Health Technologies, Inc., Ankara, Turkey

melissabastug@gmail.com

Introduction

The low regeneration potential of the human body hinders proper regeneration of tissues or organs that have lost their function due to disease or trauma. Regenerative medicine encompasses approaches to replacing or regenerating human cells, tissues, or organs to restore normal function or rebuild healthy tissue [1,2]. The combined use of stem cell and tissue engineering (TE) technologies has gained importance, especially in the last decade. Studies with stem cells obtained from well-known sources such as bone marrow, adipose tissue and placenta continue at full speed [2-4]. The placenta is a reservoir of progenitors and stem cells that can differentiate into different lineages and cell types [5]. In particular, human amniotic membrane-derived stem cells (hAMSCs) are of interest for TE related to their high regenerative potential and ease of propagation. TE focuses on combining stem cells with extracellular matrix (ECM)-like biomaterials possessing biological, mechanical and architectural properties suitable for functional tissue reconstruction [3].

In this study, an *in vitro* bone TE approach was developed by utilizing the known osteogenic differentiation properties of hAMSCs and bone-derived ECM-based biological scaffolds.

Materials and Methods

Bone-derived ECM was obtained from bovine tibia heads. Cancellous tissue was processed; demineralization and decellularization protocols were applied. Decellularization efficiency was evaluated by DNA and histochemical analyses. Bioactive content of bone ECM was investigated by assays for sulfated glycosaminoglycans and collagen [6]. Two types of scaffolds were used as cell substrates. First, enzymatically-digested ECM was neutralized, gelled at physiological temperature and freeze-dried. Secondly, this construct was kept in simulated body fluid (SBF) to form a mineralized layer on the scaffold surface. Single cell suspensions of hAMSCs were isolated by enzymatic digestion from three human placentas with ethical approval (I7-410-20). hAMSCs were expanded in culture in α -MEM (with 10% FBS, penicillin-streptomycin, fungizone). The immunophenotype of hAMSCs at P-3 was characterized by flow

cytometry. Tri-lineage and colony-forming potentials, doubling-time of cells were evaluated. hAMSCs were seeded on two types of constructs; cultured either under standard expansion or osteogenic culture conditions. The osteogenic differentiation status of hAMSCs cultured on both types of substrates was examined comparatively using biochemical methods.

Results and Discussion

Single cell suspensions of hAMSCs were successfully proliferated in culture. These cells were able to form colonies in extended culture and were able to differentiate into three distinct lineages. Immunophenotypical characterizations revealed the dominant mesenchymal stem cell character of the hAMSCs.

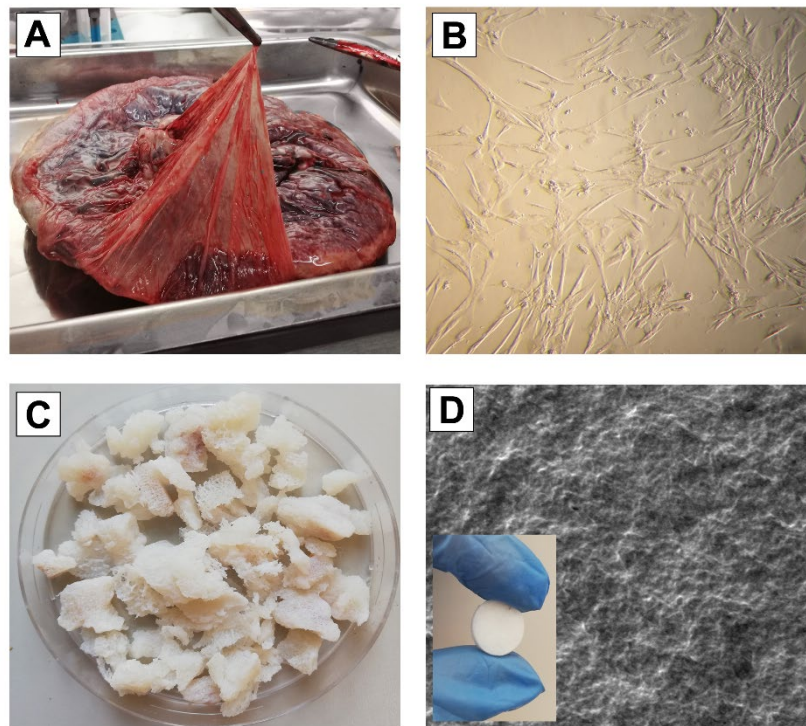


Figure 1. (A) Isolation of amniotic membrane from the placenta. (B) Phase-contrast image of hAMSC culture. (C) Demineralized and decellularized bone cancellous tissue. (D) SEM image demonstrating the surface morphology of the biological scaffold.

DNA and histochemical analyses demonstrated the successful obtainment of bone-derived decellularized ECM. Biochemical assays indicated the product was rich in collagen and glycosaminoglycans. The cell substrates were successfully created as a result of enzymatic digestion, neutralization, gelation and lyophilization steps. Composite mineralized substrates were successfully formed by incubation in SBF.

hAMSCs seeded on both type of scaffolds survived *in vitro*. Biochemical findings indicated that the constructs supported the osteogenic differentiation of hAMSCs. Findings support the notion that human amniotic membrane-derived stem cell-laden bone ECM-derived scaffolds have the potential for use in bone regenerative applications in the future.

References

- [1] Yamada S., Behfar A., Terzic A., "Regenerative medicine clinical readiness", *Regen. Med.* 16(3), 309-322, 2021.
- [2] Elçin Y.M., "Kök hücre ve rejeneratif tıp alanında dünya ve Türkiye'deki gelişmeler", *Anahtar Dergisi*, T.C. Bilim, Sanayi ve Teknoloji Bakanlığı, 328, Ankara, 2016.
- [3] Elçin Y.M. (Ed.), "Tissue Engineering, Stem Cells and Gene Therapies", Kluwer Academic-Plenum Publishers, New York and London, 2003.
- [4] Elçin Y.M. (Ed.), "Kök Hücre Araştırmaları ve Biyoetik", *Raporlar No.20*, Türkiye Bilimler Akademisi, Ankara, 2016.
- [5] Sibiak R., Jaworski M., Dorna Z., "Human placenta-derived stem cells - recent findings based on the molecular science", *Med. J. Cell Biol.* 8(4), 164-169, 2020.
- [6] Parmaksiz M., Dogan A., Elçin A.E., Elçin Y.M., "Clinical applications of decellularized extracellular matrices for tissue engineering and regenerative medicine", *Biomed. Mater.* 11(2), 022003, 2016.



International
Biotechnology Congress

StartHUB

BIOSphere